FACULDADE DE ENGENHARIA DA UNIVERSIDADE DO PORTO

# Preliminary validation of a hybrid polymer gear concept


**James Duncan Sinclair Hooton**


Mestrado Integrado em Engenharia Mecânica

Supervisor: Carlos M.C.G. Fernandes

Co-Supervisor: David E.P. Gonçalves

Co-Supervisor: Professor Jorge H.O. Seabra

July 21, 2021

# Preliminary validation of a hybrid polymer gear concept

**James Duncan Sinclair Hooton**

Mestrado Integrado em Engenharia Mecânica

July 21, 2021

# Abstract

In recent years, the use of polymer gears has grown quickly due to their economic potential and technical advantages over metallic gears. The main advantages of polymer gears are their light weight, corrosion resistance, possibility of dry running, good damping resistance and low cost. However, polymer gears have some disadvantages compared to metal gears, for instance they have inferior mechanical properties, poor thermal conductivity and thermal resistance. Polymer materials also have strong dependence on their mechanical properties in relation to the operating temperature. For these reasons, many techniques have been studied in order to improve the mechanical and thermal properties of polymer gears. The concept of a hybrid polymer gear is one of the possible solution.

In previous works, a concept for a hybrid polymer gear was developed and a thermo-mechanical study was performed. For this dissertation, a hybrid polymer gear was manufactured based on the findings of the previous works. Additionally, a heating system was conceptualized, developed and manufactured in order to study the themo-mechanical behaviour of the hybrid polymer tooth and validate a pre-existing FEM model.

For the experimental work of this dissertation, thermal tests were performed for a standard rack tooth (*STD*), a hybrid rack tooth with no insert (*HT1*), a hybrid rack tooth with an aluminum insert (*HT2*) and finally, for a hybrid rack tooth with an epoxy insert (*HT3*). The results from the *STD* were then used as a reference for the remainder of the tests. The thermal results indicated that the polymer hybrid gear design was capable of improving the thermal behaviour of polymer gears, but only if the thermal conductivity of the insert material is sufficiently high.

The second phase of the experimental work consisted of a DIC test performed for the *STD* and *HT1*, using the heating system. The DIC test aimed to analyze the surface displacements caused by the thermal expansion. The DIC measurements showed a significant displacement field for the insert region, which could reveal a possible source of stress in this region. Afterwards, the FEM model was validated by comparing the results from the thermal and DIC tests. The FEM models showed accurate thermal results for the standard and the hybrid rack tooth models. The thermo-mechanical results were accurate for the $y$ displacements, whereas the $x$ displacement showed an offset of the values.

Once the FEM model was validated, a comparison of the thermal behaviour of the *STD*, *HT2* (aluminum) and *HT3* (epoxy) was performed. The purpose of the simulation was to identify the necessary heat flux to increase the minimum temperature of the tooth to $T_{min}$ = 50°C. The results showed that the hybrid teeth required significantly less power to increase the minimum body temperature

**Keywords:** Polymer Gears, Hybrid Polymer Gears, FEM, Thermo-Mechanical Model, DIC

# Resumo

Recentemente, e sobretudo devido ao seu potencial económico e vantagens técnicas sobre as engrenagens metálicas, a utilização de engrenagens poliméricas tem aumentado. As suas principais vantagens são: reduzida massa, boa resistência à corrosão e amortecimento, possibilidade de trabalharem a seco e baixo custo. No entanto, possuem também desvantagens como as inferiores propriedades mecânicas, reduzidas condutividade e resistência térmica. Os matérias poliméricos apresentam, ainda, uma elevada dependência entre a sua temperatura de funcionamento e propriedades mecânicas. Por estas razões, várias técnicas foram estudadas para melhorar as propriedades térmicas e mecânicas de engrenagens poliméricas. Uma possível solução é o uso de engrenagens híbridas.

Na presente dissertação, uma engrenagem híbrida polimérica foi fabricada, tendo por base trabalhos anteriores. Para além disso, um sistema de aquecimento foi desenvolvido e produzido, com o objetivo de estudar o comportamento termomecânico de um dente híbrida polimérico e, posteriormente, validar um modelo FEM previamente formulado.

Para o trabalho experimental da corrente dissertação, ensaios térmicos foram realizados para diversos dentes de cremalheira: standard (*STD*), híbrido sem inserto (*HT1*), híbrido com inserto de alumínio (*HT2*) e híbrido com inserto epóxi (*HT3*). Os resultados obtidos para o *STD* foram posteriormente usados como controlo para os restantes ensaios. Os resultados dos ensaios térmicos indicam que a engrenagem polimérica híbrida foi capaz de um melhor desempenho térmico face a engrenagens poliméricas, mas apenas se a condutividade térmica do material do inserto for suficientemente alta.

A segunda fase do trabalho experimental consistiu em ensaios DIC para o *STD* e *HT1*, usando o sistema de aquecimento desenvolvido, com o propósito de analisar os deslocamentos na superfície do dente causados pela expansão térmica. As medições DIC revelaram um campo de deslocamentos significativo na região do inserto, o que indicará uma possível fonte de tensões nessa região. Posteriormente, o modelo FEM foi validado pela comparação entre os ensaios térmicos e de DIC. Os resultados térmicos para o modelo de FEM foram consistentes tanto para o dente standard como para os dentes híbridos. Os resultados termomecânicos obtidos foram coerentes para os deslocamentos em $y$, mas revelaram um offset para os deslocamentos em $x$.

Uma vez que o modelo FEM foi validado, uma comparação do comportamento térmico do *STD*, *HT2* (alumínio) e *HT3* (epóxi) foi realizada. O objetivo da simulação foi identificar o fluxo de calor necessário para aumentar a temperatura mínima do dente para $T_{min}$ = 50 °C. Os resultados mostraram que os dentes híbridos requeriam significativamente menos energia para aumentar a temperatura corporal mínima.

**Palavras Chave:** Engrenagens poliméricas, Engrenagens híbridas poliméricas, FEM, Modelo Termomecânico, DIC

# Acknowledgments

I would like to acknowledge and thank the following important people who have supported me during the course of this dissertation.

Foremost, I would like to express my sincere gratitude to my supervisor Professor Carlos Fernandes for the continuous support, enthusiasm and knowledge during these last few months. A special thanks to Professor David Gonçalves and to Professor Jorge Seabra for their help, insightful comments and suggestions throughout this dissertation.

To the people working at CETRIB, who provided the means for this research and allowed me to experience an idea of real life work environment and leading to a continuous learning opportunity.

And finally, I would like to thank my friends and family who have supported me for as long as I can remember.

*"A common mistake that people make when trying to design something completely foolproof is to underestimate the ingenuity of complete fools."*

Douglas Adams

# Contents

# List of Figures

# List of Tables

# List of Symbols

| | | |
|---|---|---|
| $a$ | Hertzian contact semi-width | mm |
| $\alpha$ | Thermal expansion coefficient | $°C^{-1}$ |
| $\alpha_n$ | Gear pressure angle | $^{o}$ |
| $b$ | Gear face width | mm |
| $c_p$ | Heat capacity | $J/(kgK)$ |
| $d_h$ | Distance of insert to | mm |
| $d_t$ | Distance of insert to rack tooth tip | mm |
| $E$ | Elastic Young's Modulus | Pa |
| $e$ | Gap of the insert from the gear faces | mm |
| $\varepsilon$ | Emissivity coefficient | |
| $F_r$ | Radial force | N |
| $F_t$ | Tangential force | N |
| $h_{aP}$ | Gear addendum coefficient | |
| $h_{contact}$ | Point of contact of the rack tooth from the tip | mm |
| $h_{fP}$ | Gear deddendum coefficient | |
| $h_n$ | Heat transfer coefficient | $W/(m^2K)$ |
| $h_{rack}$ | Height of the rack tooth model body | mm |
| $j_c$ | Circumferential backlash | mm |
| $j_n$ | Normal backlash | mm |
| $j_r$ | Radial backlash | mm |
| $k$ | Wear coefficient | $m^3/(Nm)$ |
| $\kappa$ | Thermal conductivity | $W/(mK)$ |
| $l_{heater}$ | Distance between the two heaters | mm |
| $l_{rack}$ | Length of the rack tooth model | mm |
| $l_{insert}$ | Length of the insert | mm |
| $m$ | Module | mm |
| $\mu$ | Coefficient of friction | |
| Nu | Nusselt number | |
| $\nu$ | Poisson's ratio | |
| $\omega$ | Rotational speed | rad/s |
| $P$ | Static Load | N |
| $p$ | Gear pitch | mm |
| Pr | Prandtl number | |
| $\rho$ | Density | $kg/m^3$ |
| $\rho_r$ | Root radius coefficient | |
| Ra | Rayleigh number | |
| $\sigma$ | Stefan-Boltzmann Constant | |
| $r_d$ | Gear root radius | mm |

| | | |
|---|---|---|
| $r_f$ | Gear fillet radius | mm |
| $r_0$ | Gear reference radius | mm |
| $\sigma_H$ | Hertz contact pressure | Pa |
| $t$ | Gap of the insert from the tooth tip | mm |
| $T_B$ | Absolute bulk temperature | mm |
| $t_c$ | Cooling duration of the thermal test | min |
| $t_h$ | Heating duration of the thermal test | min |
| $T_{Heaters}$ | Temperature of the cartridge heaters | °C |
| $t_{total}$ | Total heating duration of the DIC test | min |
| $w_x$ | Insert width | mm |
| $\phi_{shaft}$ | Shaft bore hole | mm |
| $x_1$ | Profile shift coefficient of the pinion | |
| $x_2$ | Profile shift coefficient of the wheel | |
| $z_1$ | Number of teeth of the pinion | |
| $z_2$ | Number of teeth of the wheel | |

# List of Abbreviations

| | |
|---|---|
| DIC | Digital Image Correlation |
| FEM | Finite Element Method |
| HDPE | High-density polyethylene |
| HT | Hybrid rack tooth |
| PA | Polyamide |
| PBT | Polybutylene terephthalate |
| PE | Polyethylene |
| PEEK | Polyether ether ketone |
| PI | polyimides |
| PTFE | Polytetrafluoroethylene |
| POM | Polyacetal |
| STD | Standard rack tooth |

# Chapter 1

# Introduction

Polymer materials have been used for many gear applications due to several advantages over metal gears. The main advantages for polymer gears are their light weight, corrosion resistance, possibility of dry running, good damping resistance and low cost. However, polymer gears have some disadvantages compared to metal gears, for instance they have inferior mechanical properties, poor thermal conductivity and thermal resistance. In fact, the mechanical properties of polymer materials are highly dependent on temperature, which makes these gears very susceptible to gear failure with the rise in operating temperature.

With the purpose of improving the mechanical and thermal properties of polymer gears new techniques have been developed to enhance their performance. These techniques include modification to gear tooth geometry, adding cooling holes, combining different materials for the gear pair, or a hybrid gear designs. Some of these ideas have been shown to increase the gear life cycle, reduce wear, increase durability and increase thermal behaviour.

A hybrid polymer gear concept was previously studied [1; 2] with the purpose of improving the thermal behaviour and heat evacuation of these gears. Working upon this new concept, a more recent thermo-mechanical study was performed and a hybrid geometry was suggested [3]. However, the hybrid gear design still lacks experimental validation.

The purpose of this dissertation is to verify the feasibility of the hybrid polymer gear and validate its concept. That being said, a hybrid polymer gear will be manufactured and a heating system will be developed in order to verify the thermal capabilities of this concept. Additionally, the surface temperature and thermal expansion of the hybrid gear geometry will be analyzed in order to characterize the thermo-mechanical behavior and validate a pre-existing FEM model.

## 1.1 Thesis Outline

Chapter 1, entitled **Introduction**, provides a brief introduction of polymer gears, summarizes the most commonly used polymer materials, the advantages and disadvantages of using polymer gears, and their manufacturing process. Additionally, the types of failure mechanism associated with these gears are studied, as well as subsequent methods of improving polymer gear performance.

Chapter 2, entitled **Hybrid Polymer Gear**, studies a solution for a hybrid polymer gear developed in previous works, and adapts their findings for the purpose of this dissertation.

Chapter 3, entitled **Development of a Gear Tooth Heating System**, covers the development process of a gear tooth Heating System.

Chapter 4, entitled **Thermo-Mechanical Finite Element Model**, describes the FEM model of the hybrid gear tooth used to simulate the conditions of the Heating System, the software necessary for its development and its implementation.

Chapter 5, entitled **Experimental Procedure**, covers the procedure for the thermal test and the DIC test, the preparation of the test specimens, and the post processing method for the test data.

Chapter 6, entitled **Experimental Results**, presents the results collected from the thermal and DIC tests. In this chapter, the results are briefly analyzed and commented on. Additionally, the FEM model is validated using the results thermal and DIC tests.

Chapter 7, entitled **Conclusion and Future Work**, presents the final conclusions of the thesis and suggests possible future work.

## 1.2 Literature Review on Polymer Gears

In recent years, the use of polymer gears has grown quickly due to their economic potential and technical advantages over metallic gears. Polymer gears have a low production cost and are able to operate without grease or oil lubrication, which makes them perfect for non lubricated applications, such as medical or laboratory devices, the food industry and household appliances. Additionally, due to their low density, polymer gears are lighter than steel, and thus can significantly reduce power consumption and noise level in gearboxes [4–6].

A major limitation common to several polymer materials is their low thermal conductivity and the strong dependence of their mechanical properties in relation to the operating temperature. For these reasons, polymer gears are typically used in low load transmission applications [2].

This first chapter summarizes the most commonly used polymer materials, the advantages and disadvantages of using polymer gears over metallic gears and their manufacturing process. Furthermore, the types of failure mechanism associated with these gears were studied, as well as subsequent methods of improving polymer gear performance.

## 1.3 Polymer Materials

There are many different types of polymers on the market for a wide range of applications, among them engineering polymers. These polymers are plastics with superior structure-property correlation, which guaranties exceptional mechanical and thermal properties such as strength, stiffness, creep, dimensional stability and thermal stability. Therefore, engineering polymers are typically used in specific, high-end mechanical components such as gears [7].

Engineering polymers can be divided into three subgroups according to the type of monomers used to build the polymeric chain and the links between them. Polymers used in industrial applications such as structural and mechanical components are called "general-purpose engineering plastics". Generally, these polymers have a minimum heat-resistance of 100 °C, tensile strength of at least 49 MPa, and Young modulus of at least 2.4 GPa. Polymers suitable for temperatures of at least 150 °C are called "super-engineering plastics". Finally, "quasi-super-engineering plastics" are polymers with intermediate characteristics between the previous two subgroups.

"General-purpose engineering plastics" can be characterized as thermosetting resin or thermoplastic resin. Both are generally used for manufacturing polymer gears due to their comparatively low price whilst maintaining a decent strength and heat resistance. In fact, thermoplastic resins, such as polyamide (PA) and polyacetal (POM), account for 85% of materials used for manufacturing gears [8].

## 1.4 Polymer Gear Materials

As mentioned above, advanced polymer materials are typically used in engineering applications, due to their improved mechanical, thermal and electrical characteristics. The most common materials for gears are polyamides (PA46, PA66, PA12, and PA6), polyacetal (POM), polybutylene terephthalate (PBT), and high-density polyethylene (HDPE). Some high-performance, heat resistant and high temperature stable materials are polyether ether ketone (PEEK), and polyimides (PI) [9; 10]. Mechanical and thermal properties for some of the thermoplastics mentioned above can be found in Table 1.1. The tribological properties for different material combinations for the pinion and wheel can be analyzed in Figure 1.1. The properties of these materials were obtained from VDI 2736 Part 1 [9].

Table 1.1: Mechanical and thermal properties of thermoplastic polymers [9].

| | POM | PA 6 | PA 12 | PA 46 | PA 66 | PEEK |
|---|---|---|---|---|---|---|
| Young's Modulus at 23°C, $E$ / GPa | 2.6-3.2 | 2.8 | 1.1 | 3.3 | 3.0 | 3.5-3.7 |
| Poisson's ratio at 23°C, $\nu$ | 0.42-0.45 | 0.38-0.42 | 0.38-0.42 | 0.37 | 0.38-0.42 | 0.4 |
| Density, $\rho$ / $\mathrm{kg/m^3}$ | 1390-1430 | 1120-1150 | 1010 | 1180-1210 | 1130-1160 | 1260-1300 |
| Thermal conductivity, $\kappa$ / $\mathrm{W/(m \cdot K)}$ | 0.25-0.3 | 0.29 | 0.23 | - | 0.23 | 0.29 |
| Working thermal limits, short term, °C | 110-140 | 140-160 | 140 | 180 | 140-170 | 300 |
| Working thermal limits, continuous,°C | 90-100 | 80-100 | 70-80 | 140 | 80-100 | 250 |
| Price range, €/kg | 1.8-3.0 | 2.6-3.1 | 8-12 | 7-12 | 3.1-3.6 | 80-100 |

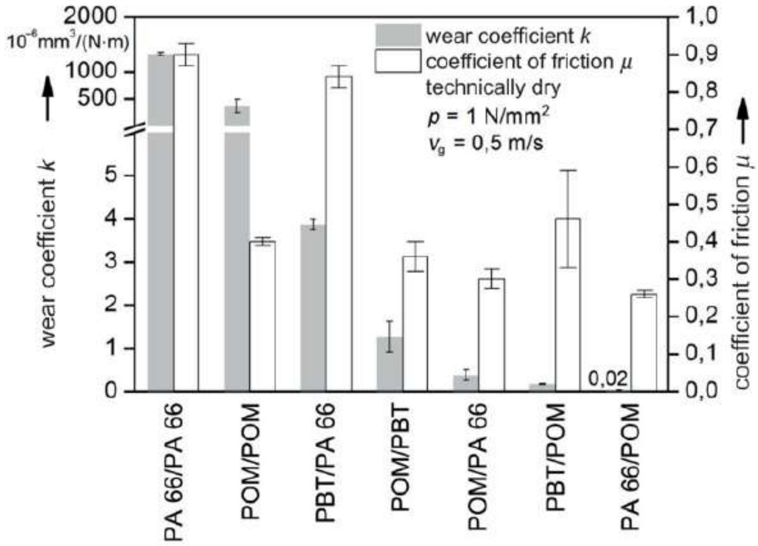


Figure 1.1: Wear and friction coefficients for different pairing materials [9].

In order to improve the physical properties of polymer gears, additives and reinforcing materials can be used for a variety of purposes. These additives can influence mechanical properties, thermal properties and even tribological properties. Although these fillers can have a positive impact, they can also have a negative influence [9]. The most common fillers used for polymer gears can be found in Table 1.2.

Table 1.2: Properties of filler and reinforcing materials [9].

| **Filler or Reinforcing Material** | **Positive Influence** | **Negative Influence** |
|---|---|---|
| Glass, carbon or aramid fibers | increase of stiffness, tensile strength, flexural fatigue strength and heat distortion resistance | reduction of impact strength |
| PTFE | reduction of friction and wear | reduction of impact strength and flexural fatigue strength |
| PE | reduction of friction | reduction of impact strength |
| Graphite, Boron Nitride | reduction of friction and wear, increase of thermal conductivity | reduction of impact strength |
| Silicone oil | reduction of friction and wear, increase of toughness | - |
| Mineral fillers | increase of heat distortion resistance | - |

## 1.5 Manufacture of Polymer Gears

Thermoplastic gears are typically manufactured by injection molding, casting or machining. The method used for this process will depend on the gear material, the required surface quality, the quantity, form and size of the gear wheels [9].

Injection molding is the most common manufacturing process and the most economically viable option for gears made of thermoplastic, provided that production quantities are sufficient.

This process allows for a greater variety in gear design. In situations with particularly demanding requirements for the tooth quality, secondary finishing by machining may be necessary [9].

Gears manufactured by casting are typically of large dimensions and a minimum weight of 1 kg. Due to the characteristics of this material, the gear wheel is cast with rough toothing and the final tooth shape is finished by machining [9].

Finally, manufacturing plastic gears by machining is done using the same method as metal gears, usually by gear forming (by milling or broaching) and gear generation process (hobbing). When machining in small and medium scale production, this method is advantageous since tooling costs are lower than injection molding. In large scale production, this method is used as a secondary finishing operation [9].

## 1.6 Advantages and Disadvantages of Polymer Gears

As mentioned above, the use of polymer gears is growing fast and even replacing metallic gears used in low and medium power transmissions. The mechanical and tribological properties of the polymer material grants these type of gears with characteristics not found in standard steel gears. These type of gears can be used without lubrication due to there low frictional properties. Because of their lower density than steel, polymer gear can weigh up to seven times less than a steel gear. In addition to the previous properties, plastic gears are able to reduce vibrations and noise due to their internal damping and resilience [4; 8]. The main advantages for polymer gears are:

- Good noise dampening properties;
- Possibility of dry running;
- Chemical inertness, good resistance to corrosion;
- Low density and inertia, leading to better dynamic response;
- Low cost on mass production.

Despite having all these advantages, polymer gears also have many demerits in regards to their mechanical and thermal properties compared to metallic gears. For instance, polymers typically have a tensile strength of about $1/7$, Young's modulus of about $1/75$, thermal conductivity of about $1/80$ and coefficient of linear expansion about 11 times those of steel. As a result of plastics having poor thermal properties, the working conditions become a major factor, because the temperature can drastically change the mechanical properties: elastic modulus, tensile strength and even water absorption rate [8]. The main disadvantages for polymer gears are:

- Low mechanical resistance;
- Poor thermal conductivity;
- Low heat resistance;
- High hygroscopicity;
- Limited load capacity and maximum running temperature.

## 1.7 Modes of Failure and Causes

The main modes of failure for polymer gears, which are distinct from their metal counterparts, are typically related to melting due to thermal overload, wear of the gear surface resulting in tooth thickness reduction, tooth root and pitch fracture caused by mechanical overload [5; 8–10].

In fact, the material properties of the polymer gears can drastically influence the modes of failure. For example, applying a load above the materials' specific load can cause instances of melting during gearing. Consequently, this will damage the tooth flanks and may lead to tooth fractures and wear. Tooth fracture can originate from the active flank and outside face of the same flank. Wear leads to a change in the tooth surface and simultaneously to a reduction in the tooth cross section, especially in dry running conditions. In the event of external lubrication, tooth fracture and pitting become more predominant [9; 10]. A visual representation for each mode of failure can be seen in Figure 1.2.

(a) Melting

(b) Tooth root fracture

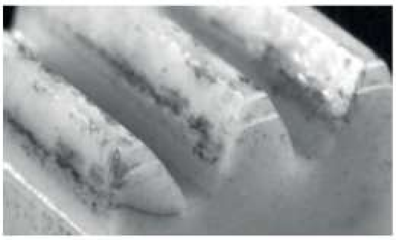

(c) Tooth flank fracture

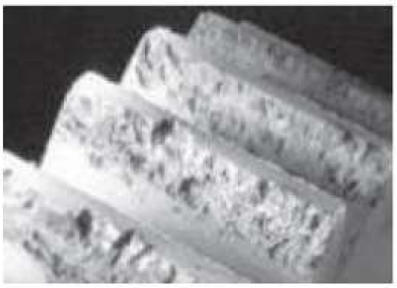

(d) Pitting

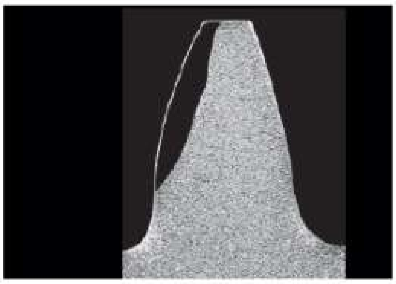

(e) Tooth Wear

(f) Plastic Deformation

Figure 1.2: Modes of failure for polymer gears [9].

### 1.7.1 Tooth Temperature

Tooth temperature is a fundamental parameter for polymer gears. The increased temperature is mainly caused by heat generated from the friction between meshing gear teeth. The temperature field of meshing gears can be divided in two parts: the bulk temperature and transient temperature of gear surface (flash temperature). Bulk and flash temperature are crucial parameters for polymers selection as their load-carrying capacity is much lower than the ones allowed for steel and are strongly dependent on the operating temperature [2].

As mentioned above, with the rise in tooth temperature the mechanical and tribological properties of polymer material tend to worsen and, consequently, these gears become more susceptible to different modes of failure. For instance, contact of two meshing surfaces could lead to the degradation of the polymer's mechanical properties, such as stiffness, as well as the reduction of the load capacity. Thermal expansion could also modify the tooth dimensions to the extent that meshing might become impossible, causing tooth failure [4; 9]. Furthermore, the poor thermal properties of polymers can aggravate the previously mentioned modes of failure, due to their low thermal conductivity, which makes it harder to evacuate the heat.

Even though temperature distribution of polymer gears varies with the type of material and operating conditions, the temperature tends to be higher at pitch point, where rolling contact occurs, than at the tip or root of the tooth, where sliding occurs. That is to say, during the meshing phase of two teeth the temperature is lower for the tip and root of the tooth because the heat dissipation occurs more easily than near the pitch point [5; 11].

### 1.7.2 Wear on Plastic Gears

For acetal gears wear appears to be the prevailing mode of gear failure, especially in dry running applications. Many different factors can influence wear propagation, for instance the meshing gear material and their additives, load, operating speed, ambient temperature, and gear geometry [10].

Typically a polymer gear can be used as the pinion as well as the wheel, or it can be used in combination with a metal gear, in which case either one can be used as the pinion. Any one of these combination has advantages and disadvantages [8]. However, when combining different materials, the one with the lower wear resistance should be placed as the driven wheel.

Tests made by Mao et al. [5] with POM, PA and steel gears indicate that the wear behaves differently for each material and for each combination of materials used for the pinion and wheel. Mao also stated that in the cases of POM/POM and PA/PA the wear could be divided into three phases: the "initial running in", a "nearly linear" and a "final fracture" phase. During the "initial running in" phase the wear is considerable, but only for a short period. During the "nearly linear" phase, the wear increases progressively until it reaches a critical value. For the last period, after reaching the critical value, the wear rate increases drastically leading to failure ("final fracture").

Mao et al. [5] testing revealed a disparity in wear performance with polyacetal against nylon in comparison with the results for PA/PA and POM/POM. When nylon is used as the driver, the polyacetal gear fails due to thermal wear, similar to that observed with POM/POM case. However, when polyacetal is used as the driver, a significant increase in wear performance is observed compared to all other combinations.

### 1.7.3 Tooth Deflection

Given that the stiffness of polymers is much lower when compared to steel, the tooth deflection must be taken into account. For materials which have small stiffness, the tooth deflection can lead to major failure in gear meshing. The deflection of spur gears can be influenced by the applied load, the width of the tooth face and by the material stiffness [8; 12].

Polymers have different stress-strain behaviors in tensile and compression regions that can lead to an inconsistency of the Young's modulus value in each region. Furthermore, polymers can show nonlinear behavior in elastic regions which can not be described with a Young's modulus [12]. The deflection of the tooth varies with the kind of polymer. Since POM has a lower rigidity in comparison with PA, the POM gear tooth undergoes a greater deflection than PA. However, since POM has a lower viscosity than PA, after a certain amount of time, the POM gear tooth exhibits a smaller deflection than the PA gear tooth under the same conditions [8].

## 1.8 Methods of Improving Polymer Gears Performance

As mentioned before, the performance and durability of polymer gears is an important aspect of their application. For this reason, many techniques have been employed in order to enhance the performance of polymer gears. These techniques include modification to gear tooth geometry, adding cooling holes, combining different materials for the gear pair, adding fillers or reinforcing materials and, finally, creating new hybrid gear designs. These techniques have been shown to increase the life cycle of these gears, reduce wear, increase durability and increase thermal behavior [13].

### 1.8.1 Gear Geometry

Several methods have been implemented to reach the best gear geometry for a certain application, keeping in mind life span, temperature, load and tangential speed. Typically, polymer gears are designed in the same way as metal gears, using the same specifications because there is no unique standard that would account for polymer material properties. Hribersek *et al.* [10] suggests that specific design rules need to be developed for polymer gear features, including failure modes of these gears which are not the same as their metal counterparts.

Imrek *et al.* [14] proposed a new design for gear teeth, Figure 1.3b, and subsequently studied the performance of the modified and unmodified gears. For gears to be continuously in mesh, two gear teeth pairs should be in contact at the same instant, dividing the total tooth load into two parts. However, in actual practice, double tooth and single tooth contacts take place alternately, Figure

1.3a. In order to correct the load sharing ratio, this new design increased the width of the teeth in the precise region where single tooth contact occurs.

For the experiments three different types of gears were manufactured. Two gears were made of Nylon 6 and the other from an AISI 1045 steel alloy. The tooth width of a Nylon 6 gear was modified while the other was unmodified. Fatigue testing of the gear pairs was performed on FZG test machine. Imrek *et al.* [14] test concluded that the tooth width modifications contributed in the reduction of wear rates of the tooth profile and a reduction of 10–15 °C of the surface temperature when compared to the unmodified gears. The reduction of heat generation and the increase of heat dissipation for the modified gears prevented premature failures and increased the gear life.

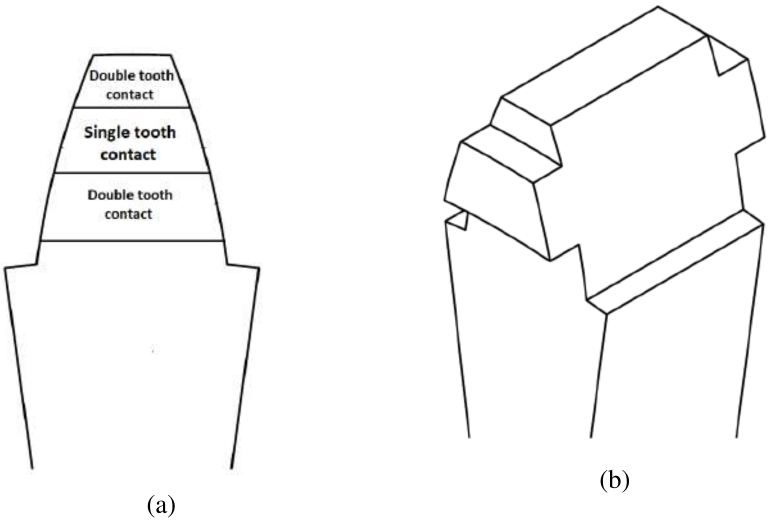


Figure 1.3: Tooth contact area (a) and modified gear tooth model (b).

### 1.8.2 Cooling Holes

This method consists in drilling small holes at the pitch diameter and along the top land surface, Figure 1.4, in order to decrease the amount of thermal damage by reducing the heat accumulated in the tooth. The accumulated heat in this region would be expelled by air circulation generated as a consequence of the gears rotation [13].

The load-carrying capacity of the gear pairs was tested on an FZG machine. The experiments were performed under dry conditions with initial pinion rotational speed of 200 rpm and a low load of 2 N · mm. During the experiments an increase in heat transfer and a reduced body temperature compared to the original gear design was observed. However, once a higher tooth load was applied, the pitch region of some of the teeth started to show some initial thermal damage [13].

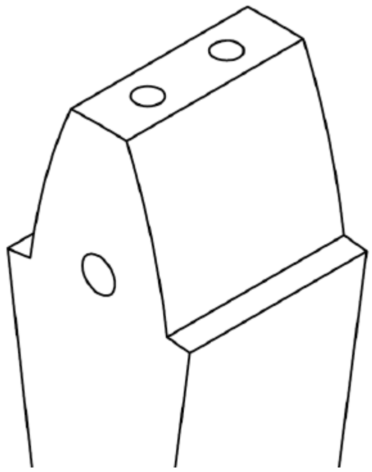

Figure 1.4: Model of gear tooth with cooling holes.

### 1.8.3 Hybrid Gears

This solution generally consists of a polymer gear which can house a metallic insert, or any other candidate material with good thermal conductivity and adequate mechanical properties, with the purpose of improving heat conduction, mechanical resistance and increased gear life.

A hybrid gear design was proposed by Kim *et al.* [15], in order to improve the durability of polymer gears. With this new design, an experimental investigation of power-transmission plastic spur gears was performed by inspecting both the characteristics of wear and durability.

For the purpose of the experiment, three types of plastic pinion were manufactured: a solid-type, a hole-type, and an insert type. For the solid-type, the pinion was manufactured without any modifications. A hole-type pinion was obtained by drilling a hole of 0.5 mm radius at the intersection of the base circle and the tooth centerline of the pinion as shown in Figure 1.5. For the insert-type pinion, a steel-pin was inserted after drilling.

A power circulation test rig was used for the experiments with the nylon and acetal pinion. Each plastic pinion was meshed with an S45C steel gear, tested with a load of 9.8, 19.6 and 29.4 N/mm, a rotational speed of 1273 rpm, and operated up to the total revolution of $1 \times 10^7$ or until it revealed breakage. The wear loss of the plastic pinion was evaluated by weighing it just before and after each test. The temperature of the tooth surface was measured using a non-contact type temperature sensor.

Kim *et al.* [15] testing showed that the surface of the nylon tooth decreased by a range of 3–10 °C by drilling a hole or inserting a steel-pin in the tooth body. This led to a reduction in wear rate by over 30% and greatly increased the service life by up to 415%. Kim *et al.* [15] explained that lowering the surface temperature of the nylon tooth below its glass transition temperature, prevented the deterioration of the mechanical properties, which leads to a decrease in wear rate and a delay in crack initiation. In conclusion, these results showed that this design can increase the durability of visco-elastic materials, such as nylon.

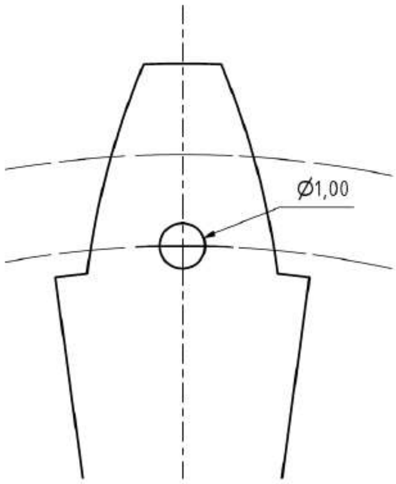


Figure 1.5: Model of a plastic pinion tooth.

Fernandes *et al.* [6] proposed four different designs with a metallic insert impregnated in the polymer matrix, which can be seen in Figure 1.6, that would promote better heat conduction, decreasing the operating temperature and increasing the load carrying capacity. This design also aims to improve the gear tooth geometry, which could decrease the power loss and the heat generation between the contacting teeth. The author was also able to predict bulk and flash temperature for both lubricated and dry conditions with different gear materials (steel, polymer) using FEM [6]. The model was later used to study the influence of different metallic inserts, as well as its geometry, on the thermal behavior of a non lubricated hybrid polymer gear.

For the FEM analysis, the insert implied a new boundary condition between metal and plastic. The study of heat transfer mechanisms between the two bodies became one of the main focuses of the study. Only the bulk temperature was considered critical for the analysis and a steady-state model was used. The bulk temperature, for a point far away from the thermal skin, was assumed to remain constant at any point of the gear, as the time required for one revolution of a gear is shorter than the time needed for any change in the gear bulk temperature [6]. The author initially compared the thermal effects of different insert materials, at maximum bulk temperature, for a polymer gear. The metallic inserts were made out of aluminum, copper and steel. The metallic insert promoted a decrease of the maximum temperature for all materials, but implied an increment of approximately 3% of tooth model weight if aluminum was used, 17% for steel and 14% for copper. The FEM analysis results showed that the metallic insert could in fact increase the heat flux and, therefore, reduce the maximum temperature. However, the insert directs the heat flux to the colder part of the tooth, and consequently, the minimum temperature rises.

Fernandes *et al.* [6] concluded that a metallic insert is effective in decreasing the bulk temperature of polymer gears. When comparing the different materials, aluminum presented the best compromise between thermal behavior, weight and manufacturing possibilities. The aluminum insert increased the mass of the original gear by 9% and it also decreased the maximum operating temperatures by 28%.

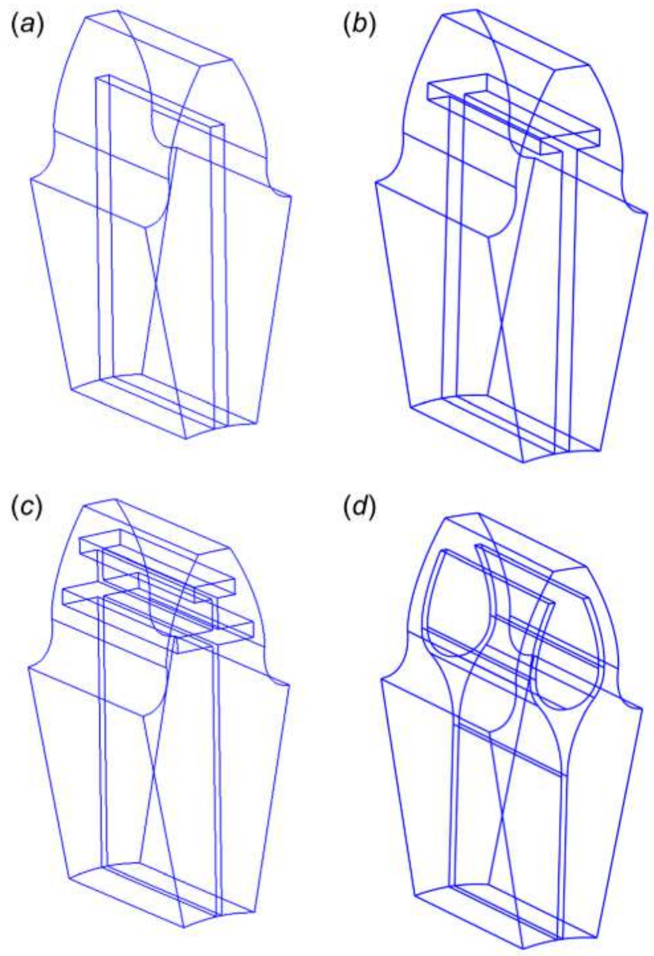


Figure 1.6: Different insert geometries: (a) plate, (b) T-profile, (c) doubleT-profile, and (d) involute.

# Chapter 2

# Hybrid Polymer Gear

## 2.1 Hybrid Gear Concept

### 2.1.1 Introduction

The first chapter summarized the most common types of materials used for polymer gears, their advantages, disadvantages and their modes of failure. The final part of the chapter showcased a few techniques that try to enhance the performance and durability of polymer gears.

As mentioned previously, this dissertation will focus mainly on the hybrid gear solution proposed by Fernandes *et al.* [6]. Previous works by Rocha [1] and by Moutinho [3] were focused on different geometries for the metallic insert and their impact was analyzed an compared using a FEM model. Rocha's work [1] explored different designs and materials for the insert and the influence of the contact pressure on the gradient of bulk temperature for the gear and the insert, whereas Moutinho's work [3] focused on a single design for the insert and tried to find the ideal dimensions and position for the hybrid gear model.

This chapter will explore some of the solutions proposed by Rocha and Moutinho [1; 3] and adapt them for this dissertation.

### 2.1.2 Rocha's Dissertation [1]

For polymer gears, the mechanical resistance properties are highly dependent on the imposed temperature of the gear, so it becomes crucial to control the maximum temperature during gear meshing. For this reason, Rocha's work studied how the bulk temperature is influenced by the implementation of a metallic insert inside the gear tooth.

For the initial design, Rocha started of with a CAD model of a C14 gear with a simple insert in the shape of a rectangular cuboid positioned in the middle of each gear tooth, Figure 2.1a. Once this initial design was implemented using a FEM model, Rocha studied the influence of different insert materials (copper, aluminum and steel), the contact pressure, and the influence of the insert's width, gap from the insert to the tooth tip and sides, Figure 2.1b. After optimizing the dimensions of a simple insert, Rocha also studied different insert geometries made out of aluminum, Figure 1.6.

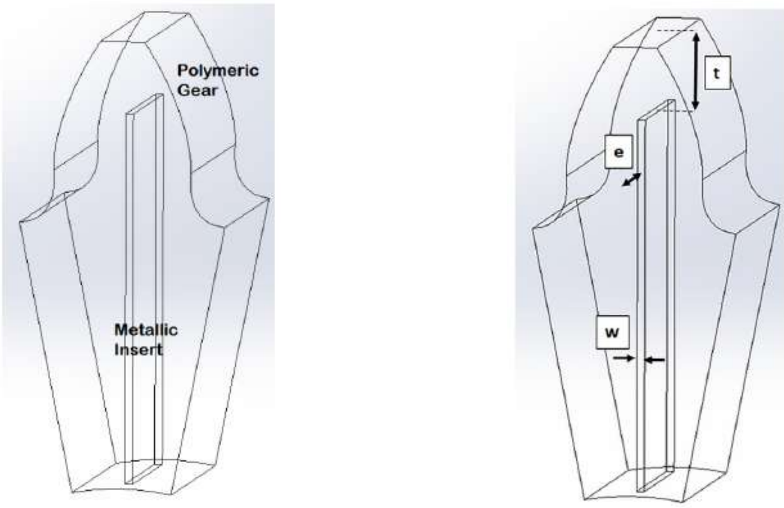


(a) (b)

Figure 2.1: (a) First iteration of a hybrid gear model and (b) the geometric parameters [1].

Using the FEM model, Rocha chose an acetal polymer for the hybrid gear and compared the influence of a copper, aluminum and steel insert.The FEM results showed that the copper insert provoked the largest temperature change in relation to the standard C14 POM gear, with a surface temperature reduction of 8.13%.

However, the weight increment using copper is higher than with the aluminum insert and the aluminum insert also had a similar decrease in maximum temperature.

For these reasons, aluminum was chosen as the best option for the insert material.

Afterwards, Rocha studied the influence of the insert dimensions, Figure 2.1b. The dimensions of the insert width ($w_x$) was tested using 10%, 25% and 50% of the gear module (m=4.5 mm), respectively 0.45 mm, 1.125 mm and 2.25 mm. The gap of the insert from the tooth tip ($t$) was tested with 4.50 mm, 2.25 mm and 0.00 mm. Finally, the gap of the insert distance from the side faces of the gear ($e$) was tested with 50% and 0% of the gear module, that is, 2.25 mm and 0 mm. Rocha concluded that the ideal dimensions for a rectangular cuboid insert was $w_x$=1.125 mm, $e$=0 mm and $t$=4.5 mm.

Once again, Rocha analyzed the impact of three new geometries for the insert and compared them with the original cuboid insert. As mentioned previously, a T-Profile, a Double T-Profile and a Involute-Profile were created to increase the heat transfer, Figure 1.6. All three profiles showed positive results in increasing heat dissipation, leading to a decrease of the maximum temperature of 28% using the double T-profile. However, the intricate design of these inserts would be challenging to manufacture in comparison to a simple cuboid insert.

### 2.1.3 Moutinho's Dissertation [3]

Similar to the previous work, Moutinho tried to determine the ideal geometry and material for the insert by comparing the thermal and mechanical behavior of the hybrid gear. Moutinho compared inserts with three different characteristics: a simple cuboid design, a rounded edges design and a T-Profile design. In addition to these combinations, some of the inserts could be attached to a fixed ring around the bore hole or simply inserted in the matrix of the gear, Figure 2.2.

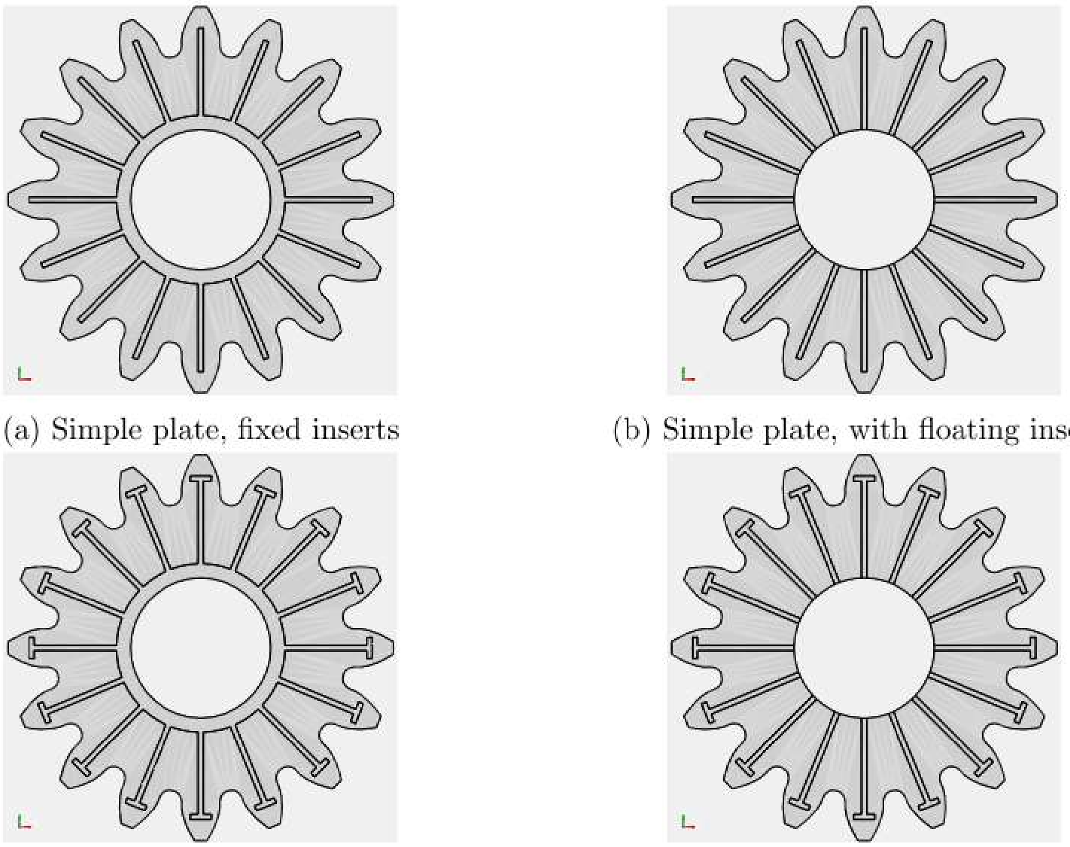

(a) Simple plate, fixed inserts

(b) Simple plate, with floating inserts

(c) T plate, with fixed inserts

(d) T plate, with floating inserts

Figure 2.2: Example of different combination for the insert [3].

In order to determine the ideal geometry for the insert, Moutinho developed a FEM model to compare the impact of the following geometric parameters for a C14 gear: distance ($t$) between the tooth tip and the insert, the width ($w$) of the insert, the length ($L$) of the horizontal plate for the T shaped inserts, filleted or rectangular corners for the insert in contact with the polymer, fillet radius ($Rd$) equal to 1mm or 0.5mm, and finally a simple or T-profile for the insert, Figure 2.3.

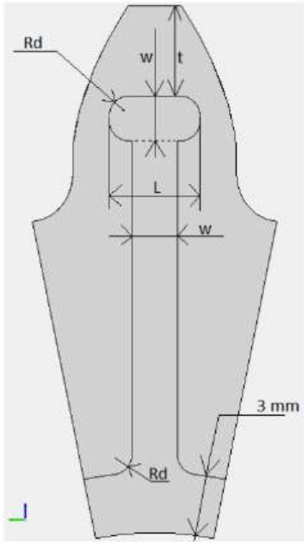


Figure 2.3: Geometric values for the insert.

The FEM results showed that the temperature value for all the geometry combinations were lower than the temperature for the standard polymer tooth. The FEM results also indicated that there was a significant increase in tooth root stress for polymer gears with a simple plate insert. In spite of this fact, the simple plate design can not be ruled out since a lower temperature at maximum tooth root stress could still improve the durability of polymer gears. The T-profile insert showed the lowest tooth root stress, on the other hand, lead to a weight increase of 25% compared to the standard gear. From these initial results, Moutinho concluded that simpler design and lower weight increase of the simple plate insert would be the best option for the hybrid gear design. Nonetheless, the analysis also concluded that the geometry with a simple plate needed some improvements to the stress and decreased load carrying capacity caused by the proximity of the insert to the hub.

After concluding that the floating insert was causing extra stress, Moutinho decided to shorten the length of the insert and compare the temperature and stress value with different value for the insert distance from the hub, Figure 2.4. The distance of the insert to the tooth tip (t) and the width (w) would be equal to the value of the gear module. The results showed that by increasing the distance from the hub to the base of the inserts would decrease the tooth root stress but also increase tooth root temperature. The analysis showed that the distance equal to the the module of the gear resulted in a low enough value for the tooth root stress without compromising the tooth root temperature.

Finally, Moutinho concluded that the ideal geometry for the insert would be a simple plate design, width equal to half the value of the module, straight corners and a distance from the hub and the tip equal to the value of the module.

Once the design of the hybrid gear was optimized, Moutinho chose an acetal polymer gear and compared the influence of different materials for the insert. The initial phase compared three metallic inserts: aluminum, copper and steel. The FEM analysis showed that the tooth root stress was higher for the aluminum, followed by copper and then steel. It also showed that the temperature at maximum tooth root stress conditions was lowest for the aluminum, followed by copper and then steel. Moutinho concluded that the aluminum would be the best choice for the insert. However, FEM analysis showed that there was an elevated stress concentration at the interface of the hybrid tooth and the metallic insert due to the thermal expansion of the polymer material. For this reason, Moutinho's final solution consisted of an acetal gear with a silver filled epoxy for the insert material. In terms of thermal expansion the silver filled epoxy was more compatible with the acetal gear, and the thermal conductivity and the Young's Modulus was higher than the gear material.

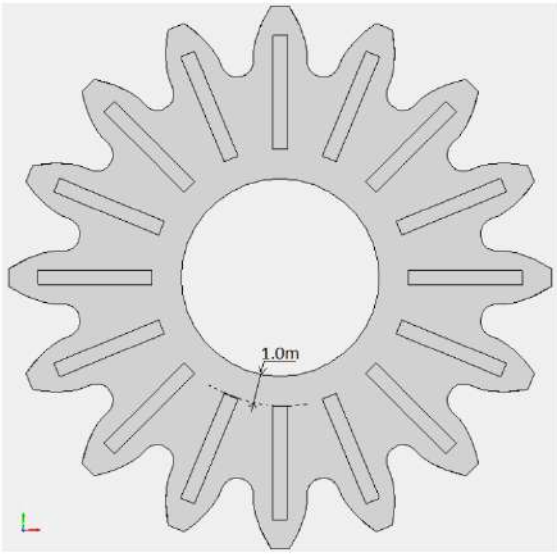


Figure 2.4: Insert distance from hub equal to 100% of the module.

## 2.2 Hybrid Gear Geometry

For this dissertation, the gear geometry chosen for the hybrid gear design was the C14 standard gear. The gear geometry properties were obtained from the KISSsoft software based on the gear parameters and the 3D model can be exported to the Autodesk Inventor software.

For the purpose of the thermal tests, only a single gear tooth was used as a test sample. For this reason, a pinion and rack system was chosen as the test specimen in order to simplify the geometry design and the manufacturing process.

### 2.2.1 KISSsoft

The KISSsoft software enables the selection of several different standards that are then used for the calculation of the machine element's geometry. It also offers the possibility to export to any 3D CAD software to easily integrate them into Autodesk Inventor with a STEP file.

As mentioned before, the model for the hybrid gear was based on the C14 standard gear. The gear geometry properties were generated by KISSsoft and are listed in Table 2.1. Next, by using the pinion and rack generator from KISSsoft and inputting the values from the C14 gear pinion, such as the module ($m$ = 4.5 mm), number of teeth ($z_1 = 16$), normal pressure angle ($\alpha = 20^{\circ}$), face width ($b = 14$ mm) and profile shift coefficient ($x_1 = +0.1817$), it was possible to obtain the geometric properties for a rack tooth, Table 2.2. Finally, the 3D model for the pinion and rack system generated by the KISSsoft program was exported to a STEP file as seen in Figure 2.5 and the KISSsoft report can be found in Appendix A.

Table 2.1: C14 standard gear geometry properties.

| | Pinion | Wheel |
|---|---|---|
| Number of Teeth, z | 16 | 24 |
| Module, $m_n$ / mm | 4.5 | |
| Center Distance, a / mm | 91.5 | |
| Pressure angle, $\alpha_n$ / ° | 20 | |
| Pitch, p / mm | 14.137 | |
| Root Radius Coefficient, $\rho_r$ | 0.38 | |
| Fillet Radius, $r_f$ / mm | 1.71 | |
| Face Width, b / mm | 14 | |
| Profile Shift Coef., x | +0.1817 | +0.1715 |
| Addendum Coef., $h_{aP}$ | 1 | |
| Deddendum Coef., $h_{fP}$ | 1.25 | |
| Shaft Bore Hole, $\phi_{shaft}$ / mm | 30 | |
| Normal Backlash, $j_n$ | 0.224 | |
| Material | 16MnCr5 | |

Table 2.2: Pinion rack system gear geometry properties.

| Rack | Pinion | Rack |
|---|---|---|
| Number of Teeth, $z$ | 16 | - |
| Module, $m$ / mm | 4.5 | |
| Center Distance, a / mm | 82.318 | |
| Pressure angle, $\alpha_n$ / ° | 20 | |
| Root Radius Coeficient, $\rho$ | 0.38 | |
| Fillet Radius, $r_f$ / mm | 1.71 | |
| Face Width, b / mm | 14 | |
| Addendum Mod., $x$ | +0.1817 | 0 |
| Radial Backlash, $j_r$ / mm | 0.320 | 0.175 |
| Normal Backlash, $j_n$ / mm | 0.219 | 0.12 |
| Circunferential Backlash, $j_c$ / mm | 0.233 | 0.127 |
| Addendum Coef., $h_{aP}$ | 1 | |
| Deddendum Coef., $h_{fP}$ | 1.25 | |

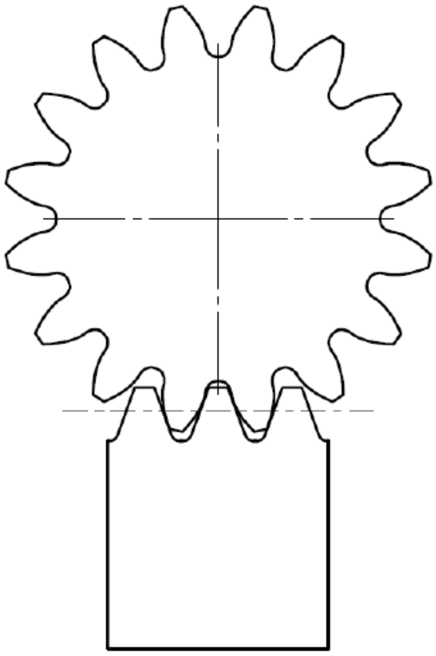

Figure 2.5: Model of the pinion and rack system.

### 2.2.2 Autodesk Inventor

#### 2.2.2.1 Standard Rack Tooth Model

Afterwards, using the Autodesk Inventor software it was possible to edit the rack tooth STEP file. The first stage consisted of determining the length and height of the rack. The total length of the rack was defined as the length of three individual teeth, that is, the equivalent of three times the value of the circle pitch ($p = m \cdot \pi$), Equation 2.1. The height of rack body should be equal to the distance of the pinion root radius ($r_d$) to the shaft radius ($r_{shaft}$ = 15mm), and taking into account the value of the pinion tooth profile shift coefficient ($x_1 = +0.1817$), Equation 2.4. Once these values were calculated, the *Extrude Cut* tool of Autodesk Inventor was used to remove the excess volume from the original STEP file, Figure 2.6.

$$l_{Rack} = 3 \cdot p = 3 \cdot \pi \cdot m = 42.41\text{mm} \tag{2.1}$$

The reference radius for the pinion ($r_0$) can be calculated with the following Equation 2.2.

$$r_0 = \frac{z_1 \cdot m}{2} = 36.0\text{mm} \tag{2.2}$$

$$r_d = r_0 - h_{fP} \cdot m = 30.19\text{mm} \tag{2.3}$$

$$h_{Rack} = \frac{z_1 \cdot m}{2} + x_1 \cdot m - h_{fP} \cdot m - \frac{\phi_{shaft}}{2} = 16.19\text{mm} \tag{2.4}$$

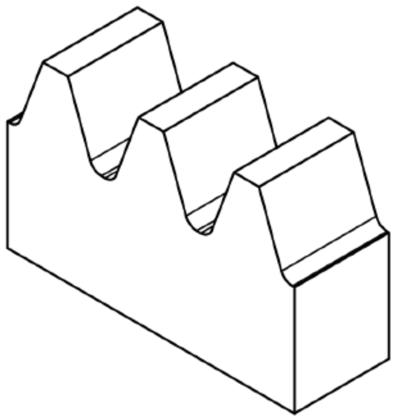

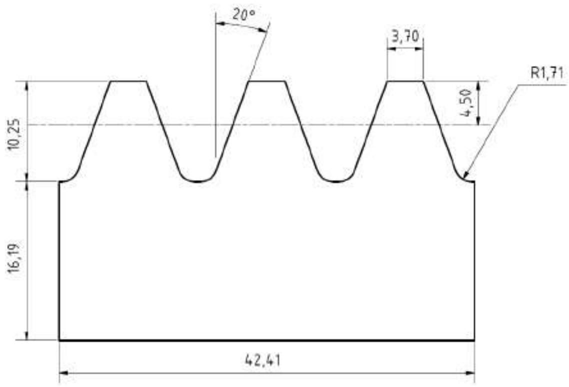


(a) (b)

Figure 2.6: Rack with modified dimensions for the height and length.

The following step was to remove the two extra teeth from the rack body without modifying the global dimensions. Once again, the *Extrude Cut* tool of Autodesk Inventor was used to remove the excess teeth, Figure 2.7. This final design for the standard rack tooth will be used as a reference for the tests. The final manufacturing drawings can be found in Appendix B. The general geometrical tolerances ISO 2768-fH was defined for the manufacturing drawings.

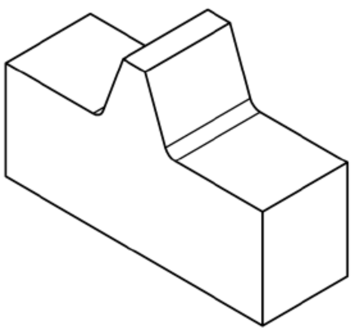

(a)

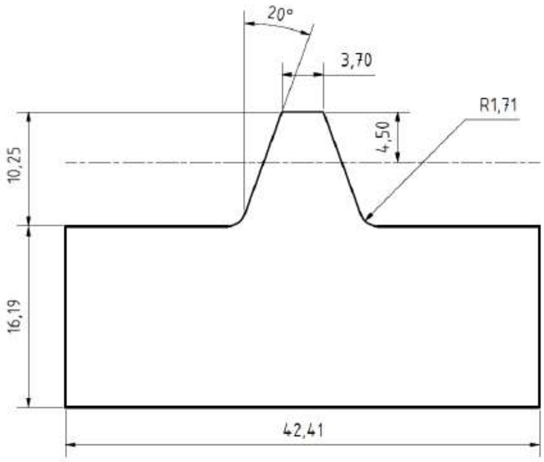


(b)

Figure 2.7: Modified rack with one tooth.

#### 2.2.2.2 Hybrid Rack Tooth Model

The dimensions of the insert for the hybrid tooth were based on the final conclusions of Moutinho's [3] work. Even though Moutinho [3] concluded that a straight corner cuboid design was ideal, a rounded corner geometry was chosen for the final solution in order to simplify the manufacturing process.

The geometry of the insert consists of a simple cuboid design with rounded corners, width equal to half the gear module, distance from hub and tooth tip equal to the module. The total length of the insert can be determined by Equation 2.5. The following Table 2.3 summarizes the dimensions of the insert. Once the final dimensions of the insert were determined, a hollow cavity for the insert was created using the *Extrude Cut* tool of Autodesk Inventor, Figure 2.8. The final manufacturing drawings can be found in Appendix B. The general geometrical tolerances ISO 2768-fH was defined for the manufacturing drawings.

Table 2.3: Dimensions for the insert based on previous works [1; 3].

| Insert Dimensions | |
|---|---|
| Module, $m$ / mm | 4.50 |
| Width, $w$ / mm | 2.25 |
| Distance Hub, $d_h$ / mm | 4.50 |
| Distance Tip, $d_t$ / mm | 4.50 |
| Length, $l$ / mm | 17.44 |

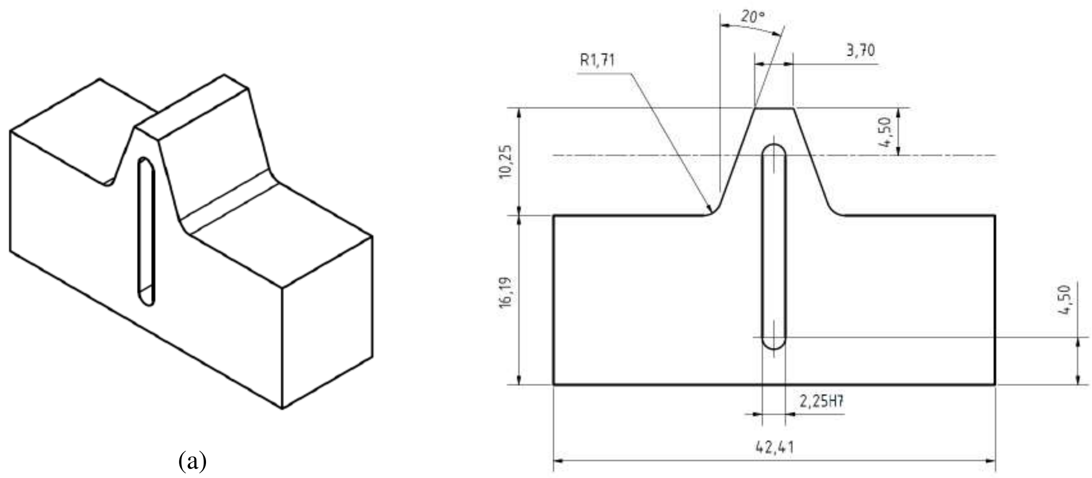


(a)

(b)

Figure 2.8: Final design for the hybrid rack tooth.

The length of the insert was determined with the following Equation 2.5.

$$l_{insert} = h_{rack} - 2 \cdot m = 17.44\text{mm} \tag{2.5}$$

## 2.3 Proposed Solution

Based on the findings of the previous two works [1; 3], it was possible to arrive at a final solution for the hybrid gear. For the purpose of the thermal test, a simpler rack design with a single tooth was developed, figure 2.7 and 2.8. The material for the polymer gear was based on the VDI 2736 guidelines [9] and also followed the suggested materials from the two previous works. The material for the insert took into account the findings of the previous FEM analysis and the availability of different products in the domestic market.

The polymer material chosen for the standard and hybrid gear was ERTACETAL C ® (PolyLanema Lda., Portugal), which is a type c acetal. The mechanical and thermal properties provided by the suppliers can be found in Table 2.4. The final manufactured solution for the standard rack tooth and hybrid tooth can be seen in Figure 2.9.

Table 2.4: Mechanical and thermal properties of ERTACETAL C ®.

| ERTACETAL C® [PolyLanema] | |
|---|---|
| Density, $\rho$ / $\mathrm{kg/m^3}$ | 1410 |
| Melt Temperature, $T_f$ / °C | 165 |
| Thermal conductivity coef., $\kappa$ / $\mathrm{W/(m \cdot K)}$ | 0.31 |
| Thermal expansion coeff. [23-100°C], $\alpha$ / °C$^{-1}$ | 1.25E-04 |
| Young's Modulus, $E$ / GPa | 2.80E+09 |
| Max. Service Temperature, °C | 140 |
| Max. Continuous Service Temperature, °C | 100 |

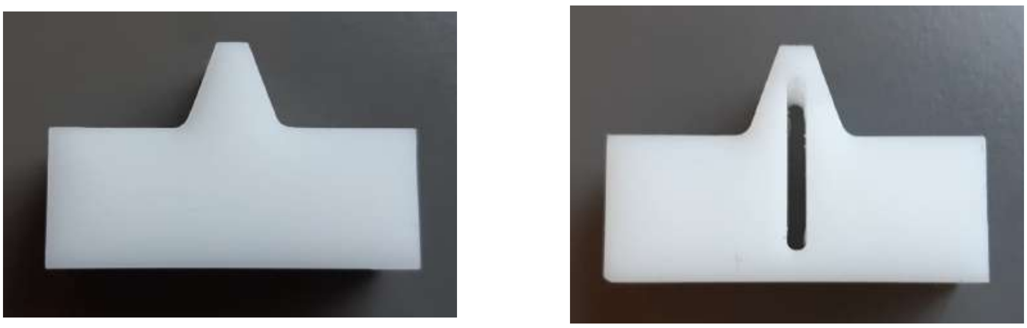

(a) (b)

Figure 2.9: Proposed solution for the (a) standard and (b) hybrid tooth

One of the objectives of this dissertation is to compare the impact and viability of different materials for the insert. Therefore, two different materials were selected. As mentioned before, in both works [1; 3] steel, copper and aluminum inserts were compared using FEM analysis and the aluminum insert was chosen as the best option. Moutinho [3] final solution also suggested the use of a silver filled epoxy resin. So, the proposed solution will use an acetal gear with an aluminum insert and also a highly conductive epoxy resin ER2220® (Electrolube, United Kingdom). The cured resin properties can be found in Table 2.5. The aluminum alloy properties can be found in table 2.6.

Table 2.5: Mechanical and thermal properties of ER2220®.

| ER2220® [Electrolube] | |
|---|---|
| Thermal conductivity, $\kappa$ / W/(mK) | 1.54 |
| Cured Density, $\rho$ / kg/m$^3$ | 2.22 |
| Temperature range, °C | -40º to +130º |
| Max. Service Temperature, °C | 150 |
| Tensile Strength, MPa | 60 |
| Compressive Strength, MPa | 120 |
| Thermal expansion coeff., $\alpha$ / °C$^{-1}$ | 3.00E-05 |

Table 2.6: Mechanical and thermal properties of aluminum 6061.

| Aluminum 6061 alloy | |
|---|---|
| Density, $\rho$ / kg/m$^3$ | 2700.0 |
| Young's Modulus, E / GPa | 69.0 |
| Poisson's Ratio, $\nu$ | 0.33 |
| Thermal expansion coeff, $\alpha$ / °C$^{-1}$ | 2.31E-05 |
| Thermal conductivity, $\kappa$ / W/(mK) | 170-200 |

# Chapter 3

# Development of a Gear Tooth Heating System

## 3.1 Introduction

For the experimental work of this dissertation, a gear tooth heating system was conceptualized, developed and manufactured. The purpose of the heating system is to apply concentrated heat, from a controlled source, on each side of the gear tooth flank and, at the same time, be able to measure the temperature of different sections of the tooth.

The heating system went through many different iterations. The first step was to design a mechanism which could hold two cartridge heaters and apply heat to the flank of the tooth. Once the heating mechanism design was finalized, the objective was to apply pressure as well as heat to the tooth, to better simulate the conditions of gear meshing. This would imply a system which could hold a gear tooth in place, apply controlled heat, a structure to support weights and be able to apply both pressure and heat in a controlled environment. For the first few iterations, the tooth was fixed to the table support and the pressure was applied in a vertical direction using a separate mechanism. The final iterations, inverted the orientation of the system, that is to say that the heaters were placed on the table support and the tooth was fixed to the plate which also supported the weights.

Once the general structure of the heating system were defined, all the different standardized components were chosen, as well as the materials for the different parts of the Heating System. The technical drawings were finalized and sent to the workshop to be manufactured.

## 3.2 Objectives and Specifications

As mentioned before, the heating system was developed for the experimental work of this work. To be able to control the conditions of the experiments and be able to measure precisely the temperature of different sections of the tooth, the following requirements were imposed for the heating system:

- Apply heat on both flanks of the gear tooth using a cartridge heater;
- Control the temperature of the cartridge heaters;
- Apply pressure on both flanks of the gear tooth;
- Control the load being applied on the tooth;
- Control the point of contact on the tooth flank;
- Fix the position of the gear tooth so it does not move;
- Include a Pt100 sensor to control the temperature of the cartridge heater;
- Include type K thermocouple to measure the surface temperature of the tooth.

## 3.3 Development of a Heating System

### 3.3.1 Initial Development

The first step in developing the heating system was to design a component which could hold two cartridge heaters and transfer the heat to the flank of the tooth. This component will be referred to as "heaters" for the remainder of the dissertation. Initially the heater was composed of a single body, two holes for the two cartridge heaters and rounded corners for the contact point with the tooth, Figure 3.1. However, this design would not allow for an adjustable point of contact, so the heaters became two separate bodies connected by a shaft that extruded from one of the heaters, Figure 3.2. In order to better calibrate the distance between the two bodies, a Hexagon Socket Head Cap Screw (ISO 4762) was used to connect the heater on the left to the heater on the right, Figure 3.2b. The head of the screw would lean against the surface of the heater on the left and be bolted to the right one, so whenever the screw was tightened it would bring both heaters closer. Additionally, two hexagon socket set screws (ISO 4026) were added to the top section of the heaters to fix their position in relation to one another, and another two socket set screws were added to each side of the heater to fix in place the cartridge heaters. A single hole was also added to the heater on the left, in between the two socket set screws, for the Pt100 temperature sensor.

After finalizing the workings of the heaters, the next step consisted in defining the remainder of the heating system components, creating a work space for the heaters and fixing them in place, a mechanism to hold the a polymer tooth and be able to apply pressure to the flank. One of the main difficulties developing this mechanism was guaranteeing the correct position of the tooth on the two heaters. In order to adjust the point of contact, the heaters would need to move horizontally to increase the distance between them and at the same time vertically to maintain contact with the tooth. Therefore, the system of the heaters and gear tooth has two possible degrees of freedom.

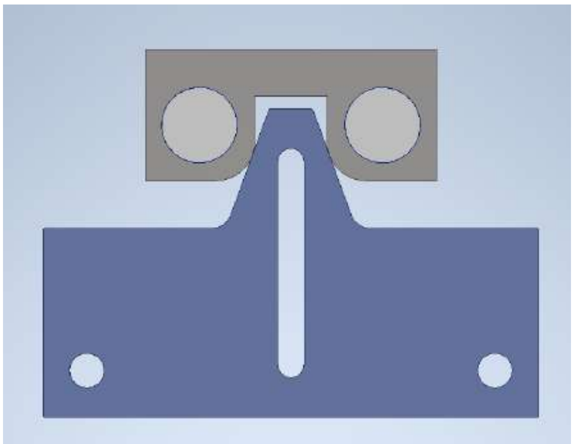

Figure 3.1: First iteration of the heater and hybrid gear tooth assembly

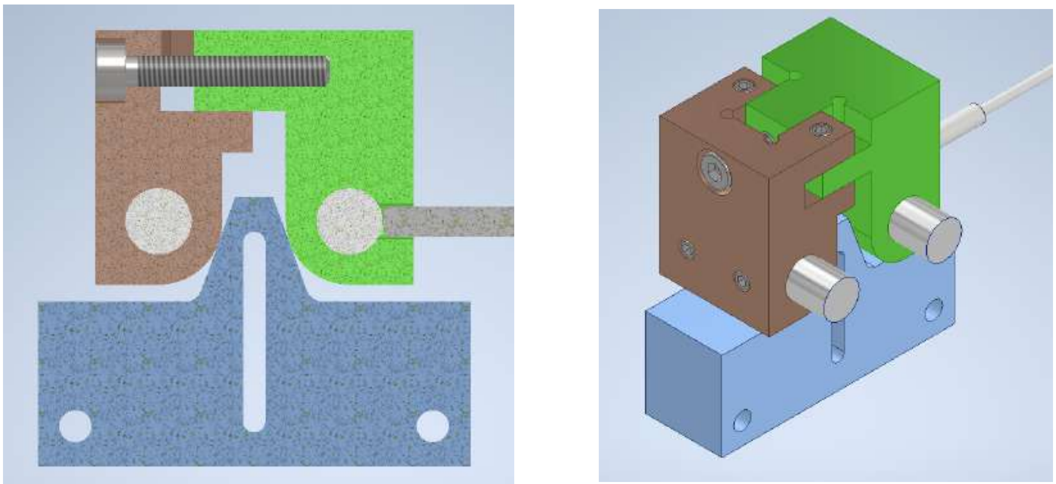

(a) (b)

Figure 3.2: Second iteration of the two heaters and hybrid gear tooth assembly

### 3.3.2 First Design

For the first design of the Heating System, the polymer tooth was fixed to a metal frame which could slide on the table support, and the heaters would sit on top of the tooth, Figure 3.3. The system also includes an arm which guides a shaft with a block at the end to apply pressure on the base of the heaters. The pressure is transferred to the flank of the tooth in order to simulate the contact pressure of two meshing gears.

This first design still showed some flaws, but it contributed to understanding what needed to be improved. For instance, the heaters were being balanced by the pressure of the block and the flank of the tooth, the arm which holds the shaft would be impractical to manufacture and its height would limit the number of weights which could be applied.

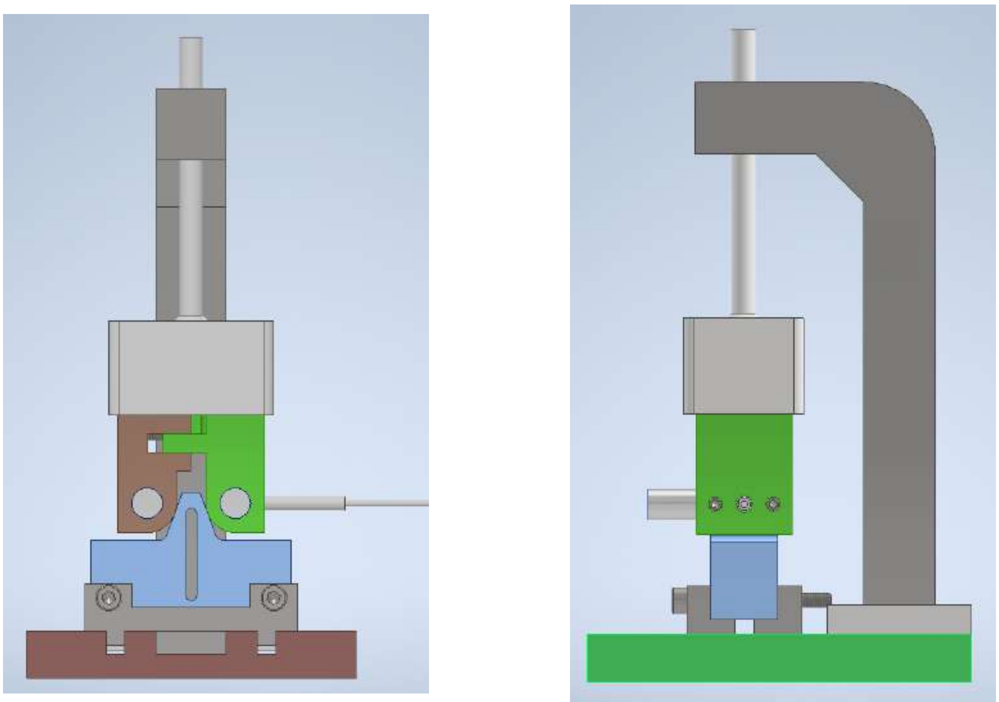

(a) (b)

Figure 3.3: First design with tooth fixed to table support and heater on top: (a) front view and (b) side view.

### 3.3.3 Second Design

For the following two iterations the system underwent many changes, Figure 3.4. The position of the heaters and the tooth were inverted and the connection of the two heaters was also adjusted. The heaters were placed on a polymer base and bolted to the metal table support. The material chosen for the support plate was polymer, in order to reduce the conduction of heat from the heaters to the table support. The base of the tooth was fixed by two dowel pins (ISO 8734) to the plate that supports the weights. A circular shaft was also screwed to the plate using a hexagon socket Head Cap Screws (ISO 4762). The function of the arm structure was to guarantee the perpendicular position of the shaft in relation to the table support whilst maintaining both vertical and horizontal degrees of freedom. The arm design included a horizontal groove and the shaft's a vertical groove. A dowel pin (ISO 8734) connected the shaft to the arm via the grooves, and helped stabilize the structure.

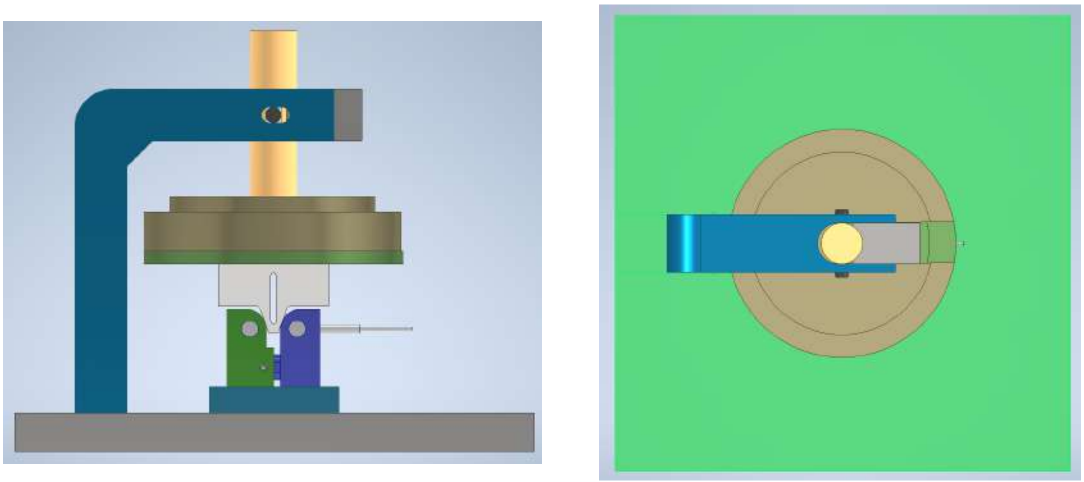

(a) (b)

Figure 3.4: Second design with a arm supporting the weight plate: (a) front view and (b) top view.

The heater with the female connection (left side) was fixed to the polymer base by two dowel pins, Figure 3.4a. The mechanism to adjust the position of one heater relative to the other was improved by simplifying the shape of the two connecting shafts and having the bolt pass through the very same extruded shape, Figure 3.5. The same as before, the head of the Head Cap Screw (ISO 4762) leans on the outer surface of the heater with a female connection, Figure 3.5a, and connects to the shaft of the male connection heater, Figure 3.5b. An additional two holes were added on each side of the female connection heater and fixes the shaft of the male heater in place using two hexagon socket set screws (ISO 4026).

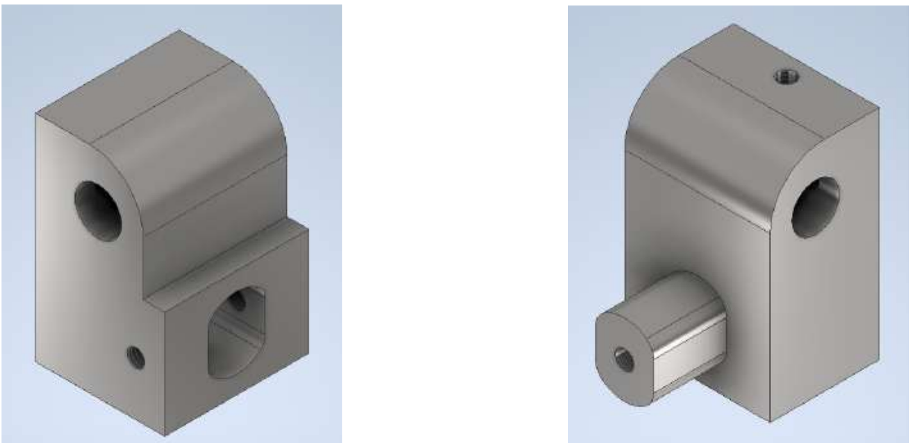

(a) (b)

Figure 3.5: Final design for the heaters: (a) heater female connection (M) and (b) heater male connection (F).

In this version, the mechanism used to guarantee the perpendicular position of the shaft in relation to the table support was improved, based on designs of tensile testing machines, Figure 3.6. The mechanism consists of two vertical shafts and one horizontal beam with a fixed position,

Figure 3.6b. The beam's midsection has a rectangular groove with rounded corners so that the shaft can vary its horizontal and vertical position. The shaft's position is kept stable by means of a dowel pin which is also connected to the horizontal beam. The remainder of the components did not suffer any modifications. Compared to the previous version this one improved the positioning of the shaft and simplified the machining process in developing these components. However, this mechanism still does not guarantee precise positioning.

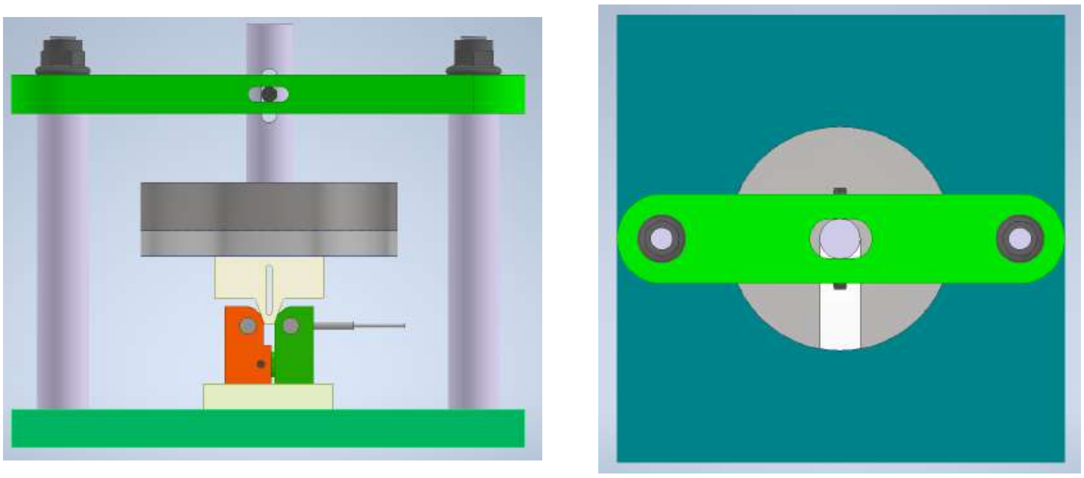

(a)

(b)

Figure 3.6: Second design with shafts and a horizontal beam support: (a) front view and (b) top view.

### 3.3.4 Final Design

The main goal of the final design was to improve the precise positioning and stability of the gear tooth (*ITEM 15*) and the remainder of the connected components (plate(*ITEM 8*), shaft (*ITEM 13*) and weights(*ITEM 12*)). In order to achieve this, the new design was based on a cylinder and piston mechanism. The tooth and heaters (*ITEM 1 and 4*) did not suffer any modification. The new system consists of a hollow cylinder (*ITEM 11*) that guides the plate which holds the tooth and the weights, Figure 3.7. The system also has two rectangular columns (*ITEM 10*) on either side. The cylinder is held up by four dowel pins (ISO 8734) (*ITEM 7*) connected to the two columns. The cylinder has two vertical drilled section opposite each other with the same dimension as the pins. Two of the pins to hold up cylinder body and two more pins are used to guarantee its vertical stability. This solution still allows the cylinder to adjust its horizontal position as well as the vertical position of the tooth when calibrating the relative position of the heaters. This means that this solution can guarantee a precise positioning of the tooth whilst maintaining the two degrees of freedom of the system.

Once the 3D modeling of the system was finalized, the materials for each of the components had to be defined. The plate support which sits on the table, the plate that connects to the tooth, the shaft and the cylinder were manufactured using carbon steel due to its higher density which would increase the weight and the stability of the components. The polymer plate connected to the heaters and the gear tooth were manufactured using POM C (table 2.4), in order to reduce the thermal loss of the heaters. The material chosen for the heaters was aluminum, because of their small dimensions and complex geometry. Aluminum is a softer which makes it easier to machine complex components. Aluminum dissipates heat at a very even rate, which allows for great dimensional stability due to less distortion.

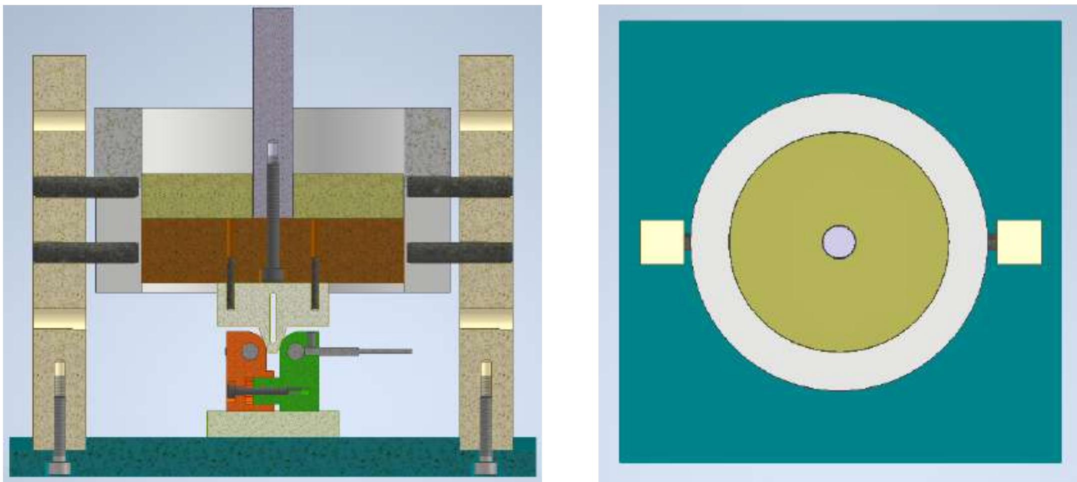

(a) (b)

Figure 3.7: Final design for the heating system: (a) Section view and (b) top view.

## 3.4 Final Technical Drawings

The technical drawings were developed for the assembly of the heating system as well as the manufacturing drawing for each component. The assembly drawing can be found below and the manufacturing drawings of each component can be found in Appendix B.

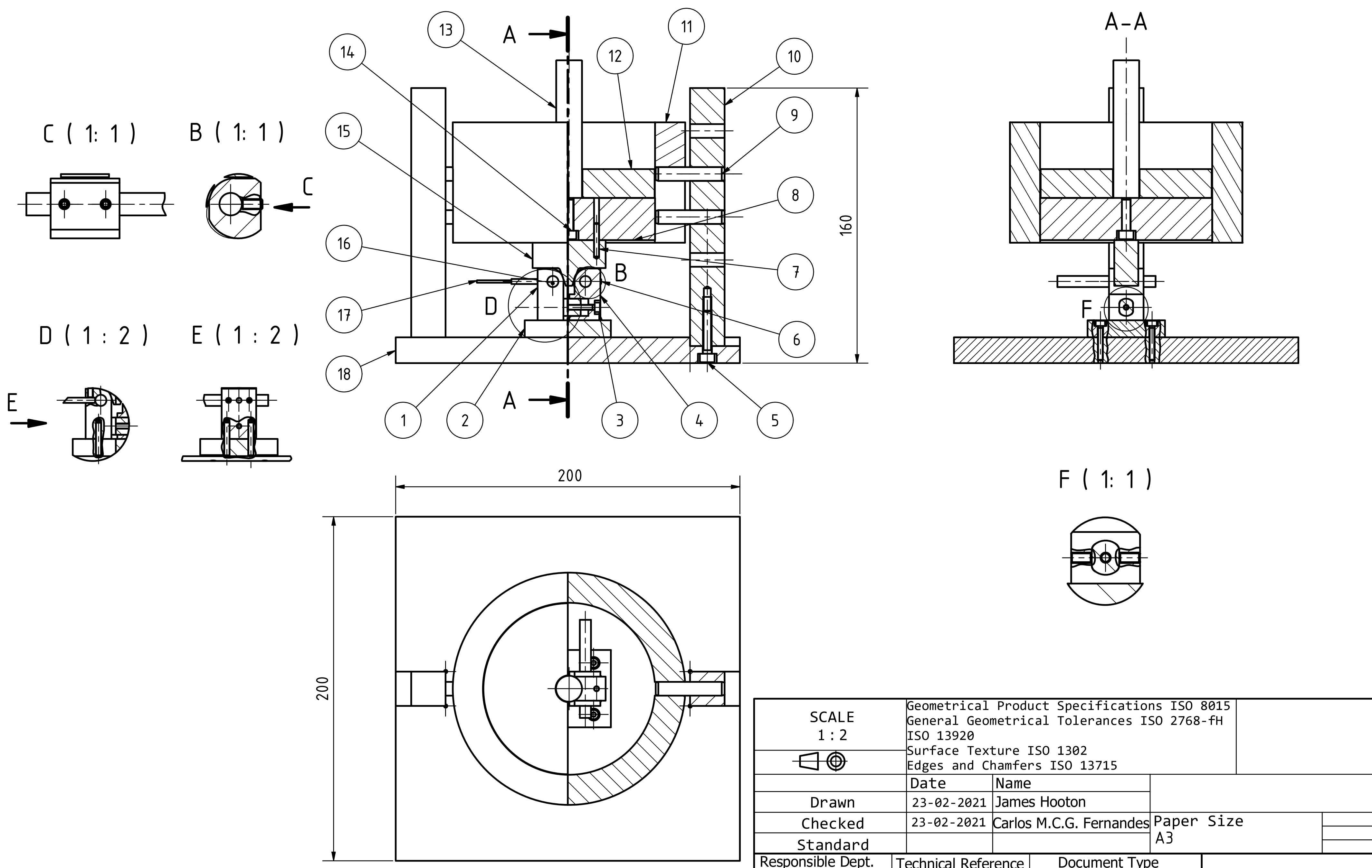


| | | | | |
|---|---|---|---|---|
| SCALE 1 : 2 | Geometrical Product Specifications ISO 8015<br>General Geometrical Tolerances ISO 2768-fH<br>ISO 13920<br>Surface Texture ISO 1302<br>Edges and Chamfers ISO 13715 | | | |
| | Date | Name | | |
| Drawn | 23-02-2021 | James Hooton | | |
| Checked | 23-02-2021 | Carlos M.C.G. Fernandes | Paper Size<br>A3 | |
| Standard | | | | |
| Responsible Dept.<br>DEMec | Technical Reference | Document Type<br>Assembly Drawing | | |
| Legal Owner | DEMec<br>CETRIB<br>James D.S. Hooton | Title<br>Gear Tooth Heating System | | Sheet Number<br>1/1 |

## 3.5 Parts List

The parts list for the assembly drawing of the Heating System can be found below.

| PARTS LIST | | | | |
|---|---|---|---|---|
| ITEM | QTY | DESCRIPTION | PART NUMBER | MATERIAL |
| 1 | 1 | Gear Tooth Heater (M) | | Aluminum 6061 |
| 2 | 1 | Polymer Support Plate | | Acetal (POM) |
| 3 | 5 | Hexagon Socket Head Cap Screw | ISO 4762 - M3 x 20(1) | |
| 4 | 1 | Gear Tooth Heater (F) | | Aluminum 6061 |
| 6 | 7 | Hexagon socket set screws with flat point | ISO 4026 - M3 x 6(1) | |
| 7 | 4 | Parallel Dowel Pins | ISO 8734 - 3 x 20 - A(1)(4) | |
| 8 | 1 | Platform | | 34 CrNiMo 6 |
| 9 | 4 | Parallel Dowel Pins | ISO 8734 - 8 x 40 - A(1)(4) | |
| 10 | 2 | Support Column | | Aluminum 6061 |
| 11 | 1 | Cylinder | | 34 CrNiMo 6 |
| 12 | 1 | Weight 1 kg | | 34 CrNiMo 6 |
| 13 | 1 | Shaft | | 34 CrNiMo 6 |
| 14 | 1 | Hexagon Socket Head Cap Screw | ISO 4762 - M5 x 40(1) | |
| 15 | 1 | Rack Tooth | | Acetal (POM) |
| 16 | 2 | Cartridge Heater | CAR.03.05 | |
| 17 | 1 | RTD Pt-100 | | |
| 18 | 1 | Table Support Plate | | 34 CrNiMo 6 |

Figure 3.8: Parts list of the gear tooth Heating System.

## 3.6 Heating System Assembly Procedure

The assembly process for the heating system ir relatively simple and only requires three different sized hex key wrenches. The following images demonstrate how to proceed with the assembly.

**Step 1 and 2:**

The first step is to place the table support plate on the workbench, Figure 3.9a. Next bolt in the polymer support plate with four screws (ISO 4762 - M3x20) and also place two dowel pins (ISO 8734 - 3x20) as seen in Figure 3.9b.

(a) (b)

Figure 3.9: Step 1 and 2: placing the table (a) and polymer support plate(b).

**Step 3 and 4:**

The third step is to bolt in the two support columns with one screw each (ISO 4762 - M5x30) to the table support plate, Figure 3.10a. Each column also needs two dowel pins (ISO 8734 - 8x40) to be placed in the holes with the desired height. The fourth step consists of assembling the two heaters, Figure 3.10b. The heater (F) holds the screw (ISO 4762 - M3x20) which is then bolted to the shaft of the heater (M). Next, four screws (ISO 4026 - M3x6) need to be placed in the heater (F) and three screws (ISO 4026 - M3x6) in heater (M). These screws were designed to fix the cartridge heaters in place as well as the Pt100 sensor.

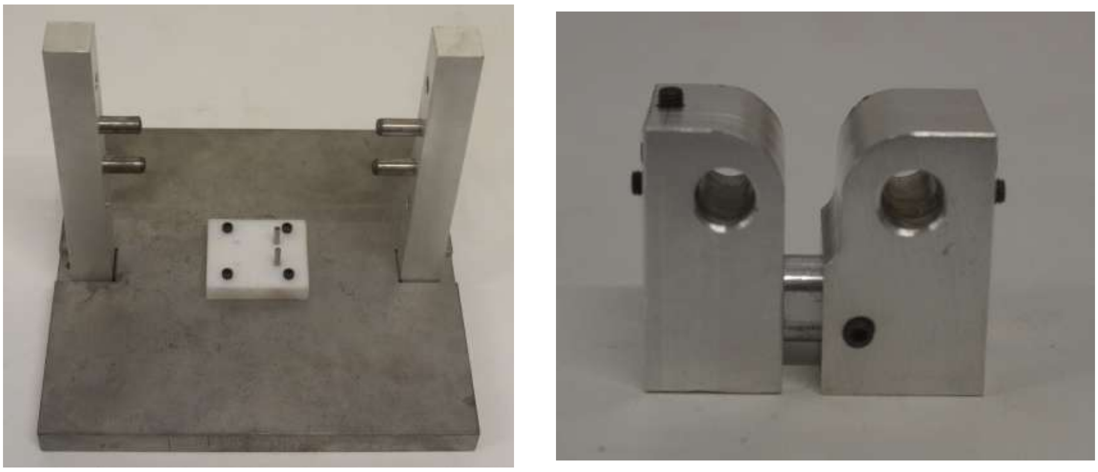

(a) (b)

Figure 3.10: Step 3 and 4: attaching the columns (a) and connecting the heaters (b).

**Step 5 and 6:**

The fifth step consists in placing the heater on the polymer support plate by connecting the two dowel pins to the two holes in the male heater, Figure 3.11a. The next step is to place the cylinder by guiding the pins through the grooves on each side of the cylinder, Figure 3.11b

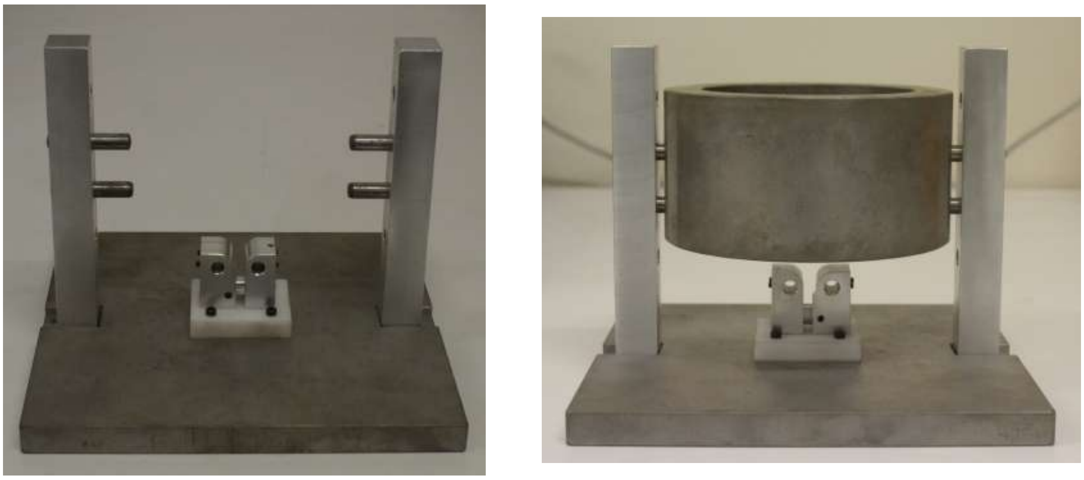

(a) (b)

Figure 3.11: Step 5 and 6: placing the heaters (a) and the cylinder (b).

**Step 7 and 8:**

The seventh step consists in placing a screw (ISO 4762 - M5 x 40) to the base of the platform and bolt it to the circular shaft, Figure 3.12a. After placing the two dowel pins (ISO 8734 - 8x40) to the two holes on the base of the platform, the next step is to attach the polymer tooth to the pins on the platform, Figure 3.12b.

(a)

(b)

Figure 3.12: Step 7 and 8: attaching the shaft (a) and tooth (b) to the platform.

**Step 9:**

The final step of the assembly process is to place the platform with the gear tooth on the circular surface of the heaters by guiding it through the cylinder. Now that the assembly process is complete, the weights can be placed on top of the platform and the cartridge heaters with the Pt100 can be placed in their respective holes.

Figure 3.13: Final assembly of the Heating System.

## 3.7 Heating System Operating Procedure

In order to run a thermal measurement of a gear tooth using the heating system, four additional steps must be taken before proceeding with the test. The following images demonstrate the additional steps.

**Step 1 and 2:**

Just before finalizing the assembly process, the distance in between the two heaters needs to be calibrated, Figure 3.14a. The two screws (ISO 4026 - M3x6) on each side of the heater (F) and the screw (ISO 4762 - M3x20) connecting the two heaters need to be loosened. Using a feeler gauge tool it is possible to measure the desired distance of the heaters, and afterwards tighten the three screws in place so that the heaters stay in place. Equation 3.1 calculates the distance of the heaters ($l_{heater}$) in relation to the point of contact of the tooth flank ($h_{contact}$) from the tooth tip. For example, with a distance of $l_{heater} = 6.05$ mm the point of contact will be equivalent to $h_{contact} = 4.47$ mm.

$$l_{heater} = 2.794 + h_{contact} \cdot 0.728\text{mm} \tag{3.1}$$

The following step consists in placing one or two cartridge heaters, depending on the testing conditions, and tightening the two screws (ISO 4026 - M3x6) on the side of the heater. Next, the Pt100 sensor is placed in the middle hole on the side of the heater and tighten the screw (ISO 4026 - M3x6) in the hole placed on the top side of the heater. For safety measures, a ground wire is attached to one of the screws which is in contact with the cartridge heater.

(a)

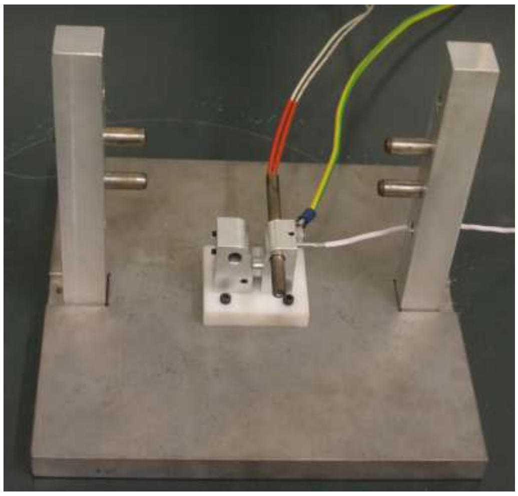

(b)

Figure 3.14: Step 1 and 2 of operating procedure.

**Step 3 and 4:**

The third step is to place the cylinder and the platform that holds the tooth in place. The final step is to turn on the heat source and choose the desired temperature for the cartridge heater. The cartridge heater and the Pt100 form a closed loop system. The Pt100 sensor that was previously placed in the heater, is in contact with the surface of the cartridge heater and measures its temperature. The Pt100 sensor returns the temperature data to the power source, which in turn calibrates the output power to the cartridge heater. Basically, this system automatically achieves and maintains the desired output temperature by comparing it with the actual temperature.

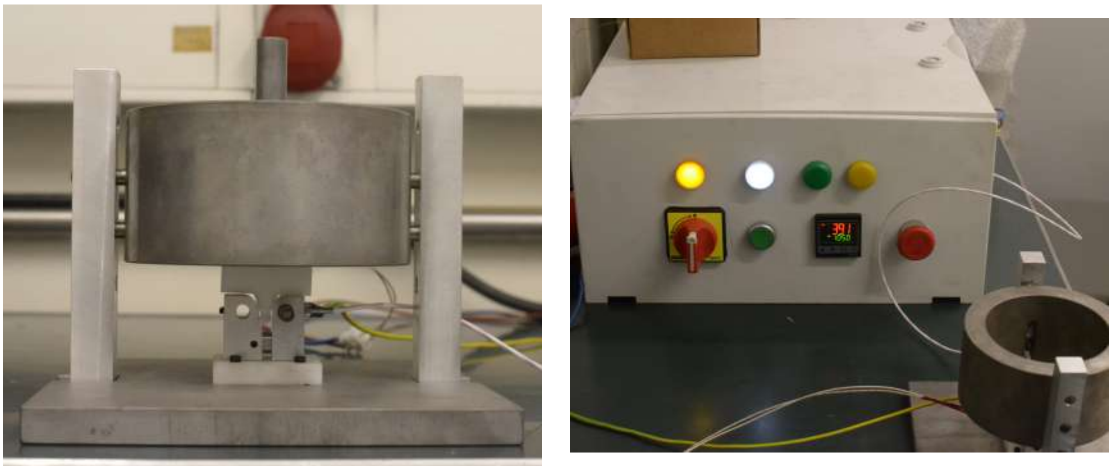

(a) (b)

Figure 3.15: Step 3 and 4 of operating procedure.

# Chapter 4

# Thermo-Mechanical Finite Element Model

## 4.1 Introduction

The previous chapters focused on the study of a rack tooth and hybrid tooth design, and the development of a gear tooth Heating System. Both the standard rack tooth and hybrid tooth were used as test specimens for the Heating System. In order to simulate and help to understand the results from the experiments, a FEM model of the tooth was developed. First of all, a mesh for the rack tooth and hybrid tooth was generated using Gmsh program. Afterwards, a thermal model and a thermo-mechanical model were developed to simulate the exact condition of the Heating System. Finally, the mesh for both teeth was refined using the h-refinement method to assure a convergence of the results.

## 4.2 Mesh Generation

Gmsh is an open source software for three-dimensional finite element mesh generation with a built-in CAD engine and post-processor. The program can be used either by interacting with the graphical user interface or using Gmsh's own programming language similar to C++. Gmsh uses the boundary representation to describe geometries, where the models are created in the following order: points, oriented lines, oriented surfaces and volumes [16].

The finite element mesh is generated by dividing a subset of the three-dimensional space by elementary geometrical elements (lines, triangles, quadrangles, tetrahedra and hexahedra). In order to guarantee the conformity of the mesh, mesh generation is performed in a bottom-up flow: curves are discretized first; the discretization of the curves is then used to mesh the surfaces; then the mesh of the surfaces is used to mesh the volumes [16].

Gmsh's mesh module reorganizes several 1D, 2D and 3D meshing algorithms, all of them producing mesh conforming to the two main algorithms: unstructured (spawning triangle and quadrangles in 2D and tetrahedra in 3D) and structured (originating triangle in 2D and tetrahedra and hexahedra in 3D) [16].

Once the mesh has been optimized, it can be exported in the desired format with the mesh properties, and imported to a FEM solver program.

### 4.2.1 Standard Rack Tooth Model

The mesh for the rack tooth model was generated automatically by inputting the coordinates for the 2D geometry which was defined in chapter 2.2.2.1. The coordinates for this model were generated parametrically in function of the gear module ($\alpha_n$). A few additional nodes were defined in order to create a smaller quadrilateral regions for a more organized mesh generation. Next, the points were connected with individual lines to define the general outline of the tooth. An 1D transfinite algorithm was applied to the lines, which defines the number of nodes that characterize the curve, in order to create a structured mesh. The different surfaces were defined by selecting the lines which surround the desired geometry, Figure 4.1a. A 2D transfinite algorithm was applied to the 2D geometry and later recombined. Finally, the geometry was extruded and a 3D mesh was generated, figure 4.1b and 4.2.

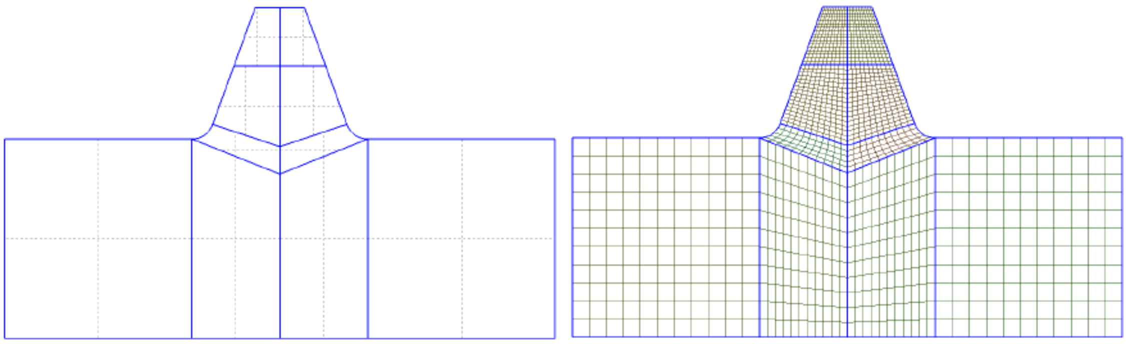

(a) (b)

Figure 4.1: Rack Tooth model: (a) 2D geometry and (b) 2D model with mesh generation.

The Gmsh program generates the line elements as a two-node 3D truss element (T3D2), the surface elements as a four-node plane stress element (CPS4) and the volume elements as an eight-node brick element (C3D8). The element generated by the Gmsh program are also used by the Abaqus software. For the thermal model a first-order element was chosen.

When the mesh is created, the Gmsh program exports the mesh properties in the desired format. The GEO file with the geometrical properties from which the mesh was created can be found in Appendix C.1. The final GEO file that was imported to the FEM solver only contained the 3D eight-node brick elements (C3D8).

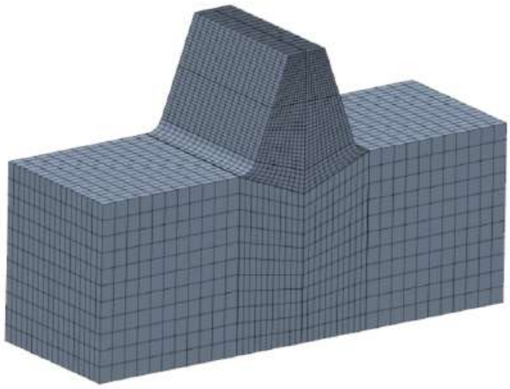

Figure 4.2: 3D mesh of the standard rack tooth.

### 4.2.2 Hybrid Gear Tooth Model

The hybrid gear tooth model went through the same process as the standard rack tooth. First of all, the mesh was generated automatically by inputting the coordinates for the 2D geometry which was defined in chapter 2.2.2.2. The coordinates for this model were generated parametrically in function of the gear module. Once the nodes were created, they were connected with individual lines to define the general outline of the hybrid gear tooth. An 1D transfinite algorithm was applied to the lines, in order to create a structured mesh. The different surfaces are defined by selecting the lines which surround the desired geometry, Figure 4.3a. A 2D transfinite algorithm was applied to the 2D geometry and later recombined. Finally, the geometry was extruded and a 3D mesh was generated, figure 4.3b and 4.4.

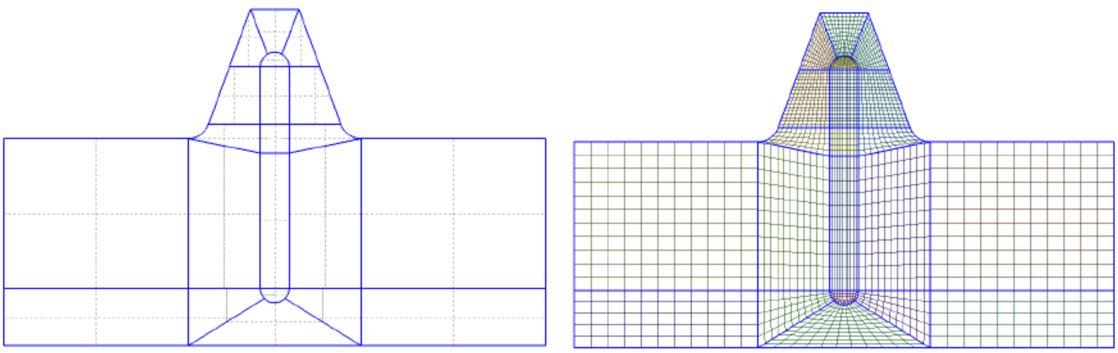

(a) (b)

Figure 4.3: Hybrid gear tooth model: (a) 2D geometry and (b) 2D model with mesh generation.

Just like before, the Gmsh program generates the line elements as a two-node 3D truss element (T3D2), the surface elements as a four-node plane stress element (CPS4) and the volume elements as an eight-node brick element (C3D8). For the thermal model a first-order element was chosen. The GEO file with the geometrical properties of the hybrid gear from which the mesh was created can be found in Appendix C.2. The final GEO file that was imported to the FEM solver only contained the 3D eight-node brick elements (C3D8).

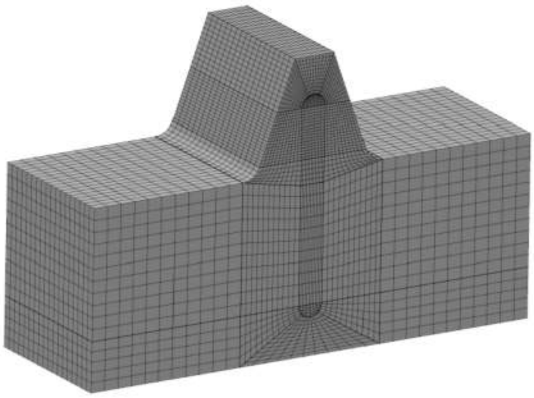

Figure 4.4: 3D mesh of the hybrid rack tooth with an insert.

## 4.3 Thermal Model

The thermal model was developed to simulate the conditions of the rack tooth during the heating process of the thermal tests. The boundary conditions were based on the design of the Heating System and procedure used for the thermal tests.

### 4.3.1 Transient State

According to energy conservation, Fourier's law and the transient differential equation, the distribution of the three dimensional temperature within the meshing gear is governed by equation 4.1. The transient term is only observed on the meshing tooth flank. Bellow the surface of the meshing teeth the transient effects are negligible. After a sufficiently long time elapsed from the action of the heat source, the temperature solution within the body will be quasi-steady [2].

$$\underbrace{k \cdot \left( \frac{\partial^2 T}{\partial x^2} + \frac{\partial^2 T}{\partial y^2} + \frac{\partial^2 T}{\partial z^2} \right)}_{\text{heat conduction}} = \underbrace{\rho \cdot c_p \cdot \left( \frac{\partial T}{\partial t} \right)}_{\text{transient term}} \tag{4.1}$$

### 4.3.2 Steady State

The bulk temperature of a point distant from the heat source is assumed to remain constant at any point of the gear. That being said, the transient term of equation 4.1 is equal to zero $\partial T / \partial t = 0$. The differential equation that describes the steady state is given by equation 4.2 [2].

$$k \cdot \left( \frac{\partial^2 T_B}{\partial x^2} + \frac{\partial^2 T_B}{\partial y^2} + \frac{\partial^2 T_B}{\partial z^2} \right) = 0 \tag{4.2}$$

### 4.3.3 Boundary Conditions

In order to solve the steady state differential equation, it is necessary to describe the boundary conditions for the different surfaces of the rack tooth attached to the Heating System. The nomenclature used to describe the different surfaces of the tooth can be seen in Figure 4.5.

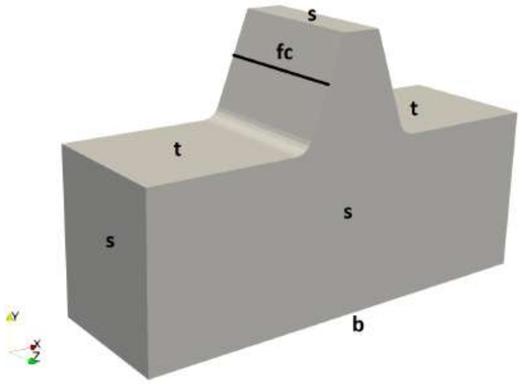


Figure 4.5: Surfaces used as boundary conditions for the thermal model.

**Gear Sides**

For the gear sides (s), which include all the surfaces except the bottom surface (b), the boundary condition is dependent on the ambient temperature surrounding the tooth and the convective heat transfer coefficient of the gear sides ($h_s$). The boundary condition is given by equation 4.3.

$$-k \cdot \left. \frac{\partial T}{\partial n} \right|_s = h_s \cdot (T - T_{air}) \tag{4.3}$$

The heat transfer coefficient for the sides of the tooth was determined by considering the surface of the tooth equivalent to a vertical plate and calculating the value of the natural convection over the surface of the tooth. The natural convection heat transfer on a surface depends on the geometry of the surface as well as its orientation. It also depends on the variation of temperature on the surface and the thermophysical properties of the fluid involved [17].

The natural convection heat transfer ($h$) is given by equation 4.4. The empirical correlation for the average Nusselt number ($Nu$) for natural convection over surface is given by equation 4.5. The Rayleigh number ($Ra_L$) was calculated with equation 4.6 [17].

$$h = \frac{k \cdot Nu}{L_c} \tag{4.4}$$

$$Nu = \left\{ 0.825 + \frac{0.387 \cdot Ra_L^{1/6}}{[1 + (0.492/Pr)^{9/16}]^{8/27}} \right\}^2 \tag{4.5}$$

$$Ra_L = \frac{g \cdot \beta \cdot (T_s - T_\infty) \cdot L_c^3}{\nu^2} Pr \tag{4.6}$$

**Tooth Flank Surface**

For the flank of the tooth, the contact of the heaters with the flank of the tooth creates a boundary condition which is dependent on the temperature of the cartridge heaters. The contact of the circular surface of the heater with the flank can be approximated to a horizontal line. The temperature of the contact line ($T_{fc}$) with the heater is equal to the temperature of the heaters ($T_{Heater}$).

$$T_{fc} = T_{Heater} \tag{4.7}$$

**Top Surface**

For the top surface of the tooth (t), the boundary condition is dependent on the temperature of the heat source which is emitting radiation, and the emissivity coefficient of the gear material ($\varepsilon$), the boundary condition is given by equation 4.8.

$$-k \cdot \left.\frac{\partial T}{\partial n}\right|_t = \varepsilon \cdot \sigma \cdot \left(T_{Heaters}^4 - T_{air}^4\right) + h_t \cdot (T - T_{air}) \tag{4.8}$$

**Bottom Surface**

For the bottom surface of the tooth (b), which is in contact with the platform that supports the tooth and the weights of the Heating System, the effects of the heat conduction will be neglected and will be considered an adiabatic surface ($\partial T/\partial t$=0), which was verified experimentally.

### 4.3.4 Heat Transfer Coefficient

When studying the temperature distribution of a gear tooth, the convective heat transfer coefficient is fundamental in obtaining an accurate representation of the real condition. As mentioned above, the heat transfer coefficient for the surface of the rack tooth when attached to the Heating System is comparable to the natural convection of a vertical plate. That being said, the values for the surface temperature ($T_s$) and the ambient temperature ($T_\infty$) were determined in order to calculate an accurate value for the heat transfer coefficient when heat is being applied to the rack tooth.

A thermal test was performed with a thermocouple sensor measuring the surface temperature near the heat source and a second thermocouple sensor measuring the ambient temperature near the surface of the tooth. With the temperature of the heaters set to $T_{Heaters}$=100 °C, the surface temperature near the heat source was equal to $T_s$=87.5 °C and the ambient temperature near the tooth surface was equal to $T_\infty$=33.8 °C. Next, using equations 4.4 to 4.6 the convective heat transfer coefficient was calculated using a range of temperature from [$T_\infty$ ; $T_s$]. The total height of the rack tooth ($h_{tooth}$=26.44 mm) was used for the length of the surface ($L_c$). That being said, the heat transfer coefficient along the surface of the tooth can be seen in Figure 4.6.

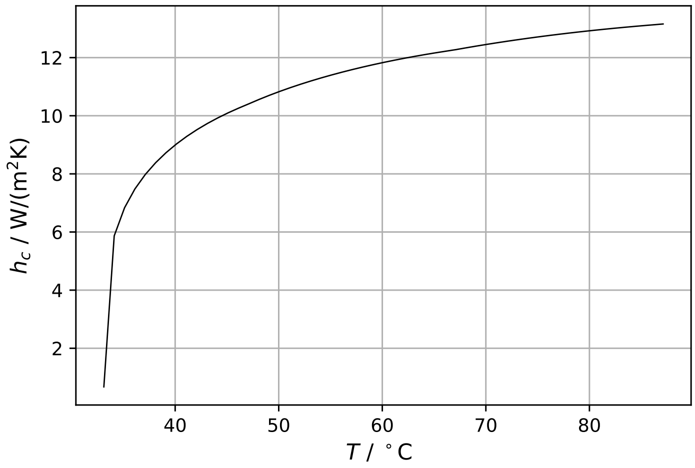


Figure 4.6: Heat transfer coefficient of the tooth surface for $T_{Heater}$=100 °C.

## 4.4 Mechanical Model

The mechanical model was developed to better simulate the conditions of the rack tooth under the conditions of the thermal tests performed with the Heating System. The boundary conditions for the tooth were based on the design of the Heating System. The pressure of the rack tooth flank in contact with the circular surface of the heaters was determined with the Hertzian contact theory.

### 4.4.1 Hertz Contact Theory

The Hertzian contact theory describes the contact problem of two elastic bodies with curved surfaces. Therefore, using the Hertz Contact Theory it is possible to determine the contact pressure generated by the rack tooth and the heaters of the Heating System. Figure 4.7 illustrate the conditions for the Hertzian Contact Theory [18].

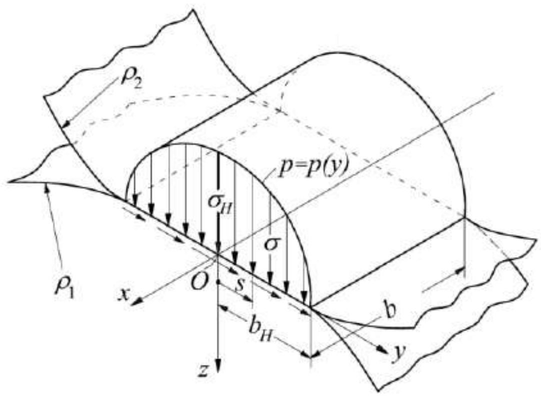


Figure 4.7: Hertzian Contact Theory illustration [18].

The Hertzian contact stress is given by equation 4.9. The equivalent elastic modulus ($E^*$) is dependent on the mechanical properties of the acetal tooth and the aluminum heaters, equation 4.10. The equivalent contact radius ($R^*$) is dependent on the the radius of the heater surface ($\rho_1$) and the rack tooth ($\rho_2$), equation 4.11. Since the rack tooth does not have a circular geometry, the value for $\rho_2$ is equal to infinity for the purpose of the equation. The applied force ($F_n$) is equivalent to the contact force perpendicular to the surface of the tooth flank generated by the weight of the mass being applied during the thermal tests. The radial force generated by the weight is given by equation 4.12 and the contact force perpendicular to the surface is given by equation 4.13. The thickness of the Hertzian contact region is given by equation 4.14, which refers to the Hertzian contact semi-width.

$$\sigma_H = \sqrt{\frac{F_n \cdot E^*}{\pi \cdot b \cdot R}} \tag{4.9}$$

$$\frac{1}{E^*} = \left(\frac{1-\nu_1^2}{E_1} + \frac{1-\nu_2^2}{E_2}\right) \tag{4.10}$$

$$\frac{1}{R^*} = \left(\frac{1}{\rho_1} + \frac{1}{\rho_2}\right) \tag{4.11}$$

$$F_r = \frac{m_w \cdot g}{2} \tag{4.12}$$

$$F_n = \frac{F_r}{\sin \alpha_n} \tag{4.13}$$

$$a = \frac{2 \cdot R^* \cdot \sigma_H}{E^*} \tag{4.14}$$

A FEM model for the rack tooth was developed with a Hertzian contact region equivalent to the conditions of the thermal tests, Figure 4.8. This model was developed to more accurately predict the effects of the applied weights on the flank of the tooth.

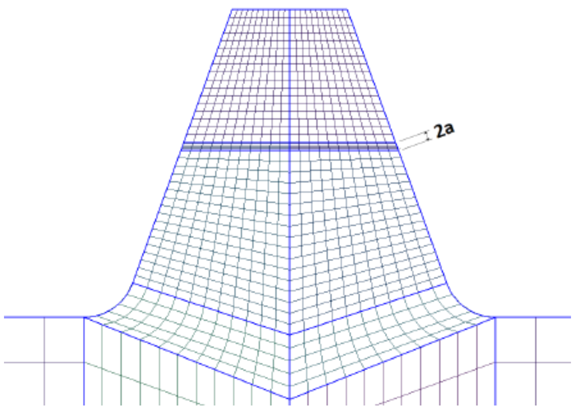


Figure 4.8: Representation of the Hertz semi width.

### 4.4.2 Boundary Conditions

The boundary conditions for the mechanical model are directly influenced by the design of the Heating System. The gear was attached to a platform that slides inside a cylinder, which restricts the axial movement of the platform. The platform also supports a group of weights that try to simulate the contact pressure during meshing. The system of the cylinder and weights also has a secondary function of restricting the vertical movement of the rack tooth. Therefore, the bottom surface of the tooth has a fixed boundary condition for x and y axis. In order to reduce the computational power required to solve the mechanical model, the mesh of the rack tooth was extruded with half of the width (b = 7 mm). By only generating half of the mesh of the tooth, a boundary condition was imposed on the face of the tooth (*xy*-plane), in order to guarantee a symmetrical result in relation to that plane.

So a fixed boundary condition for the $x$ and $y$ axis was imposed for the bottom surface and a fixed boundary condition for the $z$ axis was imposed for the surface of the tooth (*xy*-plane). Due to the vertical force from the weights, contact pressure will also be applied to the pitch point axis on each flank of the tooth. The boundary conditions can be seen in Figure 4.9, with the two triangles located on the bottom surface illustrating the $x$ and $y$ axis constraint and the triangle located near the tooth region illustrating the $z$ axis constraint. The arrows on either side of the flank illustrate the normal contact force (F) generated by the pressure of the heaters in contact with the tooth flank.

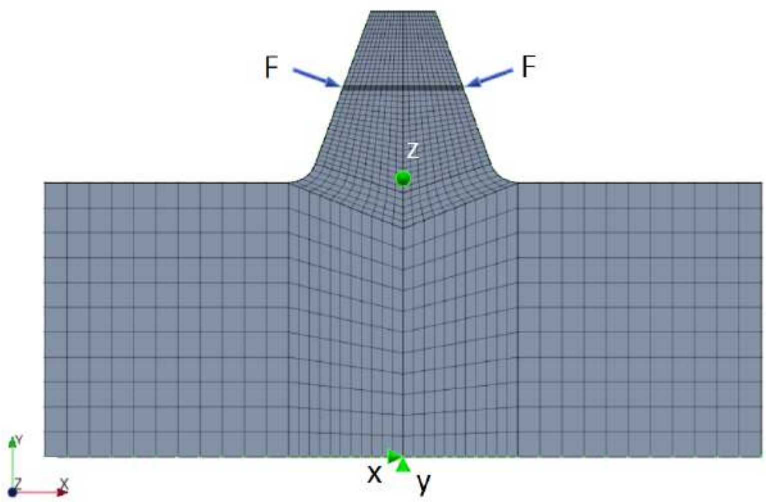


Figure 4.9: Boundary conditions for the mechanical model.

## 4.5 Thermo-Mechanical Model

The thermo-mechanical model couples the thermal model and mechanical models previously discussed. This model combines the effects of the heating process of the flank of the tooth and the contact pressure during the thermal tests. The thermo-mechanical model also determines the thermal expansion of the polymer material under these conditions.

## 4.6 Implementation of the FEM Models

In order to simulate and predict the conditions of the rack tooth during the thermal tests, a FEM model was developed. The first step was to generate a mesh for both standard and hybrid tooth. Next, the thermal and mechanical aspects of the Heating System were studied and translated to a thermo-mechanical model. The final step was to implement the FEM model into a finite element method solver. The solver chosen for this task was the CalculiX software, which is capable of solving contact and thermo-mechanical problems. The mesh files were imported to the CalculiX software and the boundary conditions of the thermo-mechanical model were adapted to an INP file that could be read by the program [16].

The INP file of the FEM models contains the mesh properties of the rack tooth, the properties of the different materials, the initial boundary conditions, the step definition for the simulation, the definition of the variables that are exported by the software. The INP files for the thermal and thermo-mechanical model are included in Appendix D.

The results of the simulation from the CalculiX software were exported to a DAT file that can be read as a text file, or as a FRD binary file that works with a 3D visualization tool. The DAT file was used with the Python programming language to process its information and create the plots. The FRD file is used for a preliminary analysis of the FEM simulation results. In order to view the FRD file using the Paraview software, the file was converted to a VTU file using the CCX2PARAVIEW converter program. Figure 4.10 illustrates the the different stages necessary to implement the FEM model.

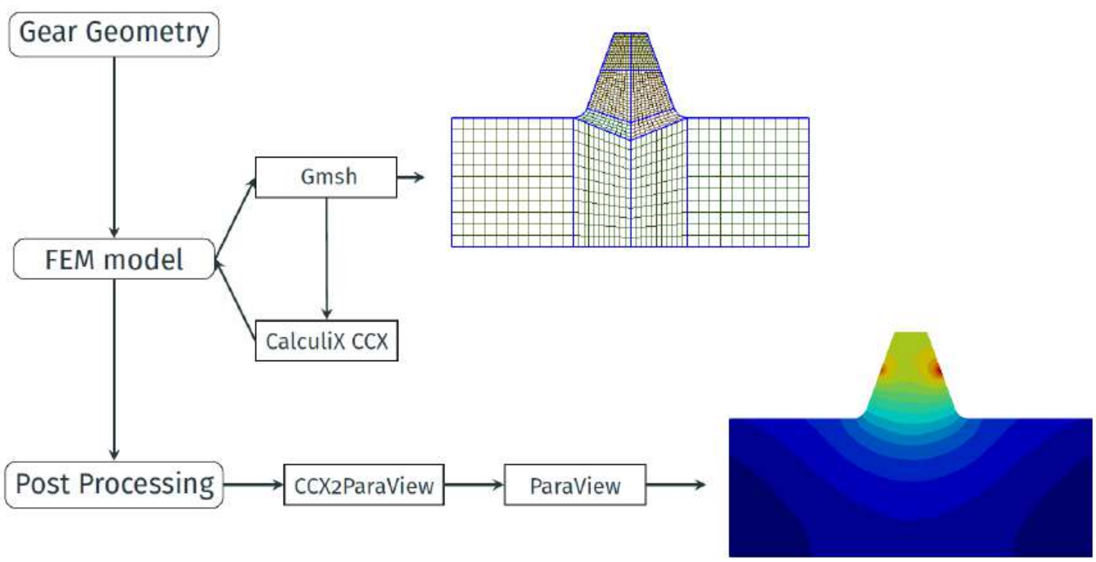


Figure 4.10: Graphic representation of the FEM model implementation.

## 4.7 Mesh h-Refinement

A mesh refinement study was performed for the standard rack tooth model and the hybrid tooth model, where the total number of elements was successively increased until the results of the simulation converged.

The density of the rack tooth mesh ($n_M$) was generated as a function of the gear modulus ($n_M = N \cdot m$) as seen in Figure 4.11. A python script was developed for the h-refinement that would increase the density of the mesh in each cycle ($N = N + 0.5$) and run a thermal model with the new mesh. With the results of each cycle it was possible to quantify the convergence of results. For each cycle, the results of the node temperature of the denser mesh was compared with the courser mesh of the precious cycle and the relative error was calculated. The graph in Figure 4.12 illustrates the relative error for the node temperature for each increment of the mesh refinement. The mesh convergence occurs for $N$ equal to 5, with a relative error of 0.10%.

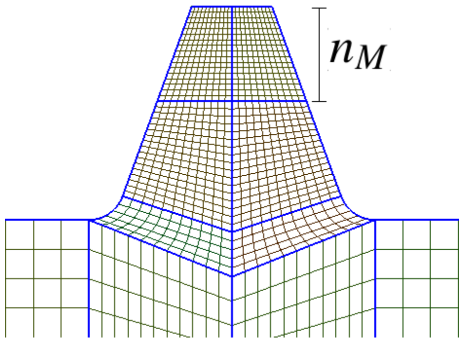


Figure 4.11: Standard rack tooth with illustration of the $n_M$ mesh density.

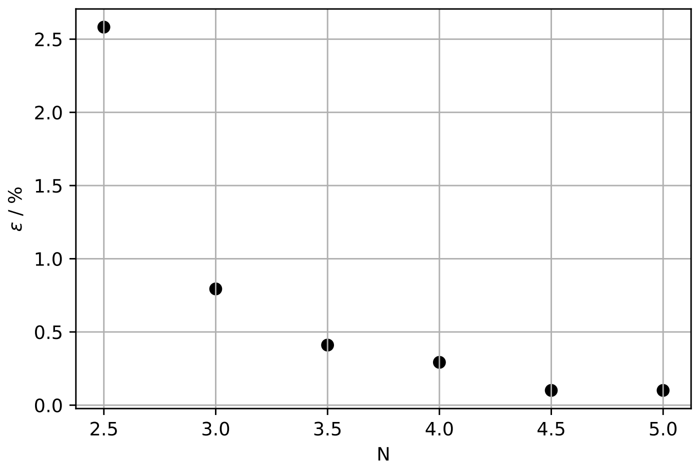


Figure 4.12: Graphic demonstrating the h-refinement mesh convergence.

# Chapter 5

# Experimental Procedure

## 5.1 Introduction

In this chapter, the experimental procedure for the thermal test and digital image correlation (DIC) tests were explained. For the thermal test, heat was applied to the flank of the tooth and the surface temperature were measured. For the DIC tests, heat was applied to the flank of the tooth and the thermal expansion was measured with a DSLR camera. For both of the experiments some preparation was necessary in preparing the tests specimens, attaching the thermocouple sensors to the surface of the tooth and setting up the Heating System. Once the tests were performed, the thermal data and the images captured during the DIC tests were collected and analyzed.

## 5.2 Thermal Experiment Procedure

The purpose of the thermal experiments was to validate the hybrid gear concept and study the impact of different materials for the insert by applying heat to the flank of the tooth. The thermal experiment consisted of a series of tests for the standard tooth and the hybrid tooth under different conditions. For the duration of the experiment, four k-type thermocouple sensors were attached to the surface of the tooth in different positions.

Taking into account the design of the Heating System, it is possible to apply heat using one or two cartridge heaters, apply pressure and adjust the point of contact. To know the applied load on the flank of the tooth, the mass of the platform and the mass of the shaft that supports the weights have to be taken into account. During the experiment, it is possible to control the temperature of the cartridge heaters and the duration of the heating and the cooling.

The operating variables related to this experiment can be found in Table 5.1 and the factors with which it is possible to vary the condition of the experiment can be found in Table 5.2.

Table 5.1: Thermal experiment operating variables.

| Thermal Experiment Variables | |
|---|---|
| **Purpose:** | Preliminary validation of a hybrid polymer gear concept and of the FEM thermal model |
| **Response Variable:** | Surface temperature of the tooth / °C |
| **Fixed Variable:** | Polymer Gear Material: POM |
| | Weight of the Platform: m = 1.483 kg |
| | Weight of the Shaft: m = 0.104 kg |
| **Independent Variable:** | Ambient Temperature °C |

Table 5.2: Thermal Experiment factors.

| Thermal Experiment Factors: |
|---|
| Insert Material |
| Cartridge Heater Temperature / °C |
| Applied Weight / kg |
| Point of Contact / mm |
| Heating duration / min |
| Cooling duration / min |

### 5.2.1 Thermal Experiment Factors

The first phase of the thermal test measured the surface temperature of the standard tooth (*STD*). Afterwards the same test was performed for the hybrid tooth without a filler for the insert *HT1*, the hybrid tooth with a aluminum insert *HT2* and finally the hybrid tooth with an epoxy insert *HT3*. A list of the tests specimens can be seen in Table 5.3.

Table 5.3: Abbreviations for the test specimens.

| Tests Specimens | |
|---|---|
| *STD* | Standard Rack Tooth |
| *HT1* | Hybrid Rack Tooth with no Insert (air) |
| *HT2* | Hybrid Rack Tooth with an Aluminum Insert |
| *HT3* | Hybrid Rack Tooth with an Epoxy Insert |

In order to better study the thermal capabilities of the standard tooth and hybrid tooth, the thermal test objective was to push the limits of the polymer material. The maximum continuous service temperature for ERTACETAL C ® is 100 °C, Table 2.4. Therefore, the temperature range of the cartridge heater were between 40 °C and 110 °C. A test with was set conditions was performed in order to determine the necessary duration for the heating and cooling steps. The test showed that a 45 minute heating period would be sufficient for the temperature of the tooth to stabilize. The test also revealed that a cooling duration of 45 minutes would also be sufficient.

The point of contact chosen for the heaters was set to the pitch point ($h_{contact} = 4.5$ mm) as seen in Figure 5.1. The applied pressure was limited by the available weights and their compatibility to the dimensions of the Heating System. Hence, the applied weight was reduced to 4.6 kg plus the mass of the platform and the shaft (1.588 kg), which is a total of (6.188 kg). The contact pressure generated by the applied load is equal to 29.138 $N^2/mm$. Table 5.4 contains the geometric and mechanical properties for the POM rack tooth and aluminum insert, which were used to calculate the values in Table 5.5 with the equations from Chapter 4.4.1.

Table 5.4: Geometric and mechanical properties of the rack tooth and aluminum heaters.

| Geometric and Mechanical Properties | | |
|---|---|---|
| $R_I$ | 7.5 | mm |
| Pressure angle, $\alpha_n$ | 0.349 | rad |
| b | 14 | mm |
| $E_1$ (POM) | 2.80x$10^3$ | MPa |
| $E_2$ (Al) | 6.90x$10^4$ | MPa |
| $\nu_1$ (POM) | 0.386 | - |
| $\nu_2$ (Al) | 0.33 | - |
| E* | 3156.12 | MPa |

Table 5.5: Hertzian contact pressure for the rack tooth and aluminum heater.

| Hertzian Contact Pressure | | |
|---|---|---|
| $m$ | 6.188 | kg |
| $F_{weights}$ | 60.699 | N |
| $F_r$ | 30.350 | N |
| $F_n$ | 88.737 | N |
| $\sigma_H$ | 29.138 | $N/mm^2$ |
| $a$ | 0.138 | mm |

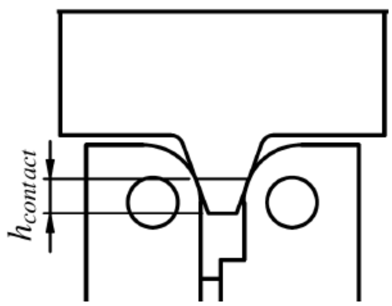


Figure 5.1: Graphic representation of the contact point.

Finally, for the thermal experiments a tooth was attached to the platform and pressed against the two heaters. Only one cartridge heater was used for the duration of the tests. The tests started by turning on the power source that controls the cartridge heaters and choosing the desired temperature, for example $T_{Heater} = 100$ °C. The heating process lasted a total of 45 minutes. Afterwards, the power source was turned off and the system was let to cool off at ambient temperature for 45 minutes. During the whole process the surface temperature was measured with four thermocouple sensors and saved on to a Datalogger.

The operating conditions for the thermal test are summarized in Table 5.6. A graphical representation of the heating procedure can be seen in Figure 5.2.

Table 5.6: Test conditions for the thermal tests.

| **Thermal Experiment Factors:** | |
|---|---|
| Type of Tooth: | Standard and Hybrid |
| Insert Material: | Air, Aluminum and Epoxy |
| Temperature Range, °C: | $T_{Heater}$=[40, 50, 60, 70, 80, 90, 100, 110] |
| Applied Weight, kg: | $m = 4.6$ |
| Point of Contact, mm: | $h_{Heater} = 4.6$ |
| Heating duration, min: | $t_h = 45$ |
| Cooling duration, min: | $t_c = 45$ |

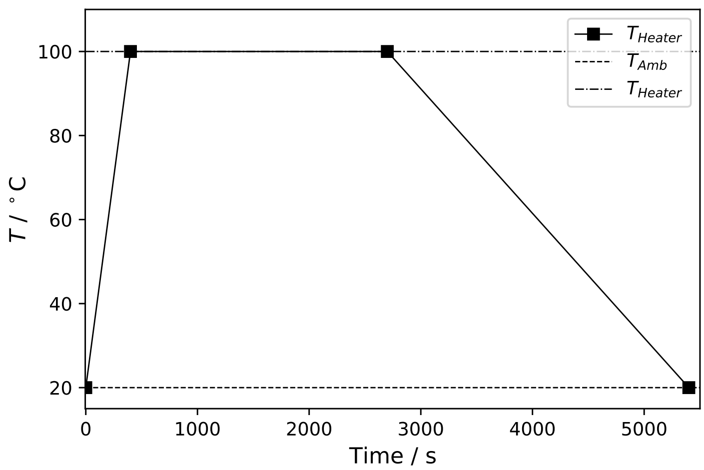


Figure 5.2: Graphic representation of the thermal test procedure.

### 5.2.2 Experimental Procedure

For the experimental procedure of the thermal test a certain amount of preparation was necessary. First of all, the test specimens were prepared and the thermocouple sensors were attached to the surface of the teeth. For instance, the insert material for *HT2* (aluminum) and *HT3* (epoxy) was also prepared. Afterwards, the heating system was prepared, taking in to account the predefined factors, and the test specimen was attached. Once the thermal test was performed, the temperature data was collected and processed. A graphic representation of the test procedure can be seen in Figure 5.3.

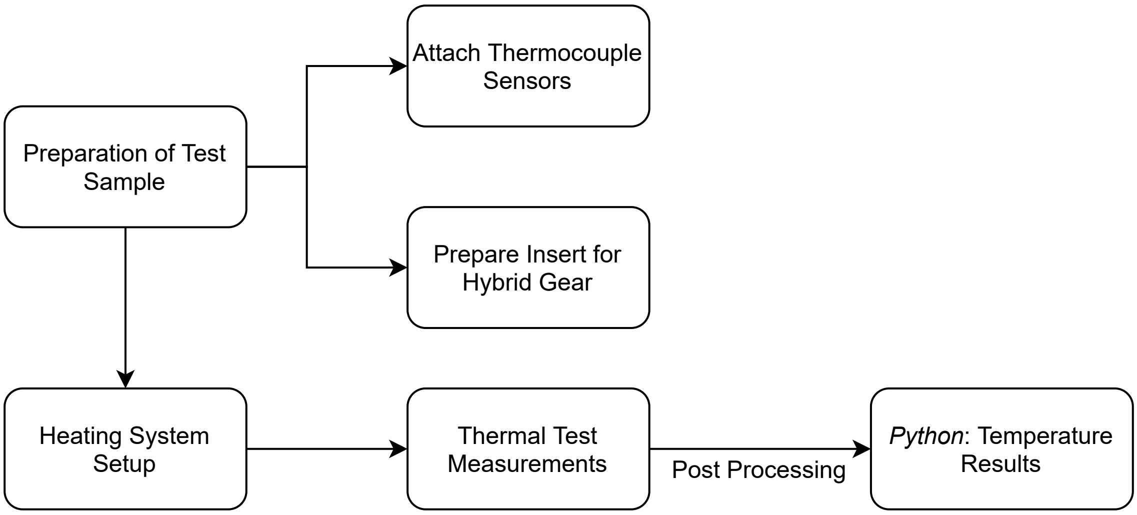


Figure 5.3: Graphic representation of the thermal test experimental procedure.

#### 5.2.2.1 Preparing the Hybrid Tooth with Aluminum Insert (*HT2*)

An aluminum insert was manufactured and inserted inside the cavity of a hybrid tooth. The assembly drawing for the hybrid tooth with an aluminum insert can be seen in Figure 5.4, and a detail drawing for the insert in Figure 5.5. Both original drawings can be found in Appendix B. The final tooth with the aluminum insert used in the thermal tests can be seen in Figure 5.6. The thermal and mechanical properties can be found in Chapter 2.3.

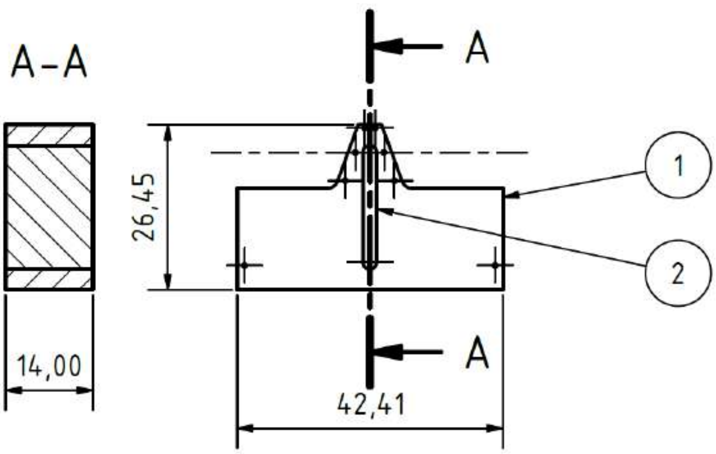


Figure 5.4: Assembly drawing of the hybrid tooth (1) and aluminum insert (2).

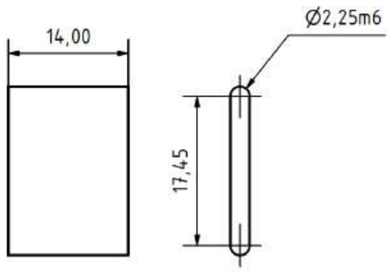


Figure 5.5: Detail drawing of the aluminum insert.

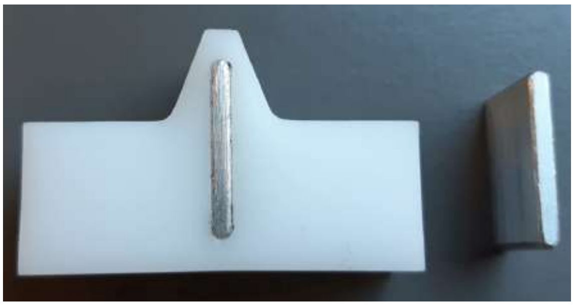

Figure 5.6: Hybrid tooth with an aluminum insert (left) and an aluminum insert (right).

#### 5.2.2.2 Preparing the Hybrid Tooth with Epoxy Insert (*HT3*)

For the hybrid tooth with epoxy insert, the ER2220® epoxy had to be treated before pouring the resin into the insert cavity. The ER2220® epoxy packaging had two components, a silver colored epoxy resin and a hardener, Figure 5.7. When in resin pack form, the resin and hardener were mixed by removing the clip and moving the contents around inside the pack until thoroughly mixed. Once the resin and the hardener were mixed together, the mixture had a lifespan of only 120 minutes before the epoxy solidified.Two curing procedures were possible: at room temperature (23 °C) with a cure time of 24 hours, or it could be cured in an oven at 100 °C with a cure time of 1 hour. The thermal and mechanical properties can be found in Chapter 2.3.

Figure 5.7: ER2220®: epoxy resin (silver) and hardener (black).

A total of three hybrid teeth were prepared using the resin mixture described above.. The teeth were placed on a flat surface and the resin mix was poured in the tooth insert. Two of the teeth were cured at room temperature and the third was cured in an oven at 100 °C. The hybrid tooth with ER2220® epoxy insert with a cure at ambient temperature can be seen in Figure 5.8.

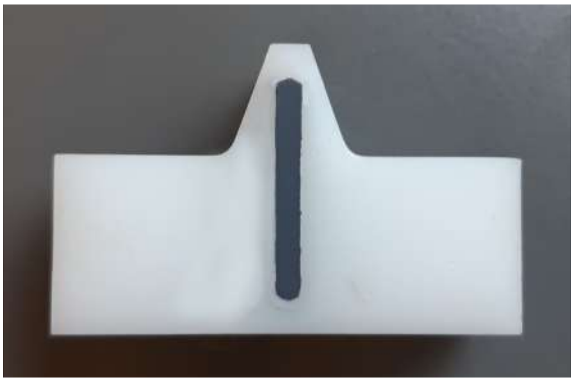

Figure 5.8: Hybrid tooth with ER2220® insert.

#### 5.2.2.3 Preparing the Thermocouple Sensors

In order to measure the surface temperature of the standard rack tooth and hybrid tooth during the tests, four thermocouple sensors need to be attached to the surface. For this reason, small bore holes ($\phi$=0.60 mm and $depth$=0.50 mm) were machined on the surface of the tooth to guarantee the same positioning of the thermocouple for all the tests. The detail drawing of these teeth can be found in Appendix B. The positions of the holes chosen for the thermal test can be seen in Figure 5.9. The pitch point region ($T_{1a}$ and $T_{2a}$) was chosen for its proximity to the contact point of the heaters. The tooth root region ($T_{2b}$) was chosen because it is typically associated with different modes of failure. The insert region ($T_{2a}$) was chosen to analyze the effects of different insert material. To attach the thermocouple to the face of the tooth, an Araldite® epoxy glue was applied on the desired bore holes with the thermocouple, Figure 5.10.

The surface temperature of the tooth was measured using four k-type thermocouple sensors. The coordinates of the holes of the four thermocouple sensors in relation to the reference point in the lower left corner of the tooth, Figure 5.9a, can be found in Table 5.7. The setup of the Heating System with a standard tooth and the four thermocouple attached to the surface can be seen in Figure 5.11.

Table 5.7: Coordinates and dimensions of the bore holes for thermal test.

| Hole | $x$ mm | $y$ mm | Dimensions mm |
|---|---|---|---|
| T1a | 18.92 | 21.95 | $\phi$0.60x0.50 |
| T2a | 21.21 | 12.95 | $\phi$0.60x0.50 |
| T1b | 23.49 | 21.95 | $\phi$0.60x0.50 |
| T2b | 25.13 | 17.45 | $\phi$0.60x0.50 |

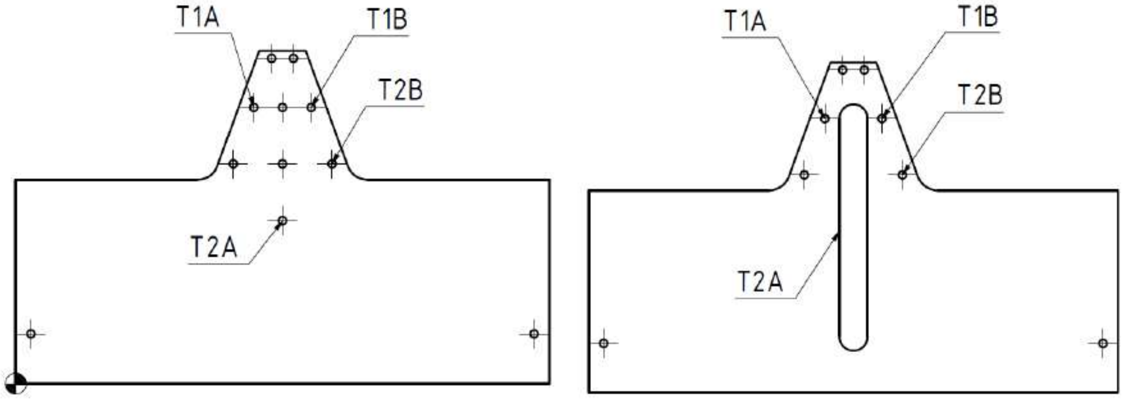


(a) (b)

Figure 5.9: Drawings of (a) standard tooth (b) and hybrid Tooth with bore holes for thermocouple.


(a) (b)

Figure 5.10: Araldite® epoxy glue (a) and a hybrid tooth with glued thermocouple (b)

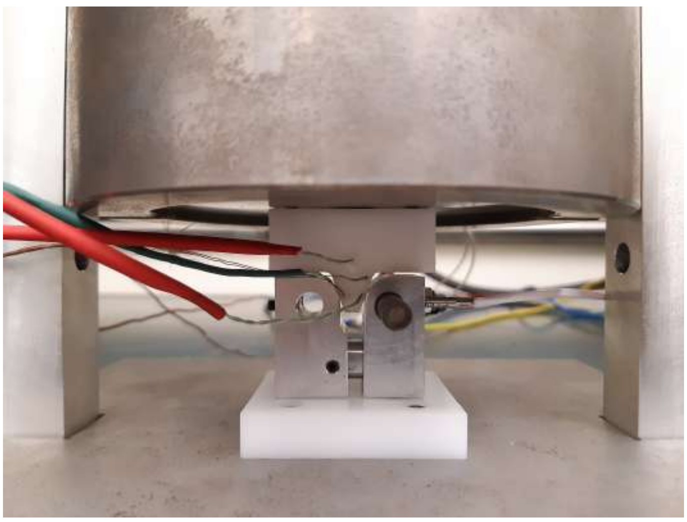

Figure 5.11: Heating System setup with a standard tooth with thermocouple.

#### 5.2.2.4 Processing Data from DataLogger

The k-type thermocouple sensors measured the surface temperature of the tooth and were connected to a two channel k-type thermocouple Datalogger. Two different dataloggers were used for the four thermocouple sensors. The HH306 Datalogger recorded the temperature every 20 seconds with an accuracy of ± 1 °C and resolution of 0.1 °C.

For the duration of the thermal tests, the Datalogger recorded the surface temperature measured by the thermocouple sensors. Afterwards, the recorded data from the Datalogger was exported using their proprietary software and saved as text file. A script was developed in Python to read and interpret the data. The script would imported the data from the thermal test and generated a graph of the temperature over time for each of the four thermocouple measurements. An example of this plot can be seen in Figure 5.12.

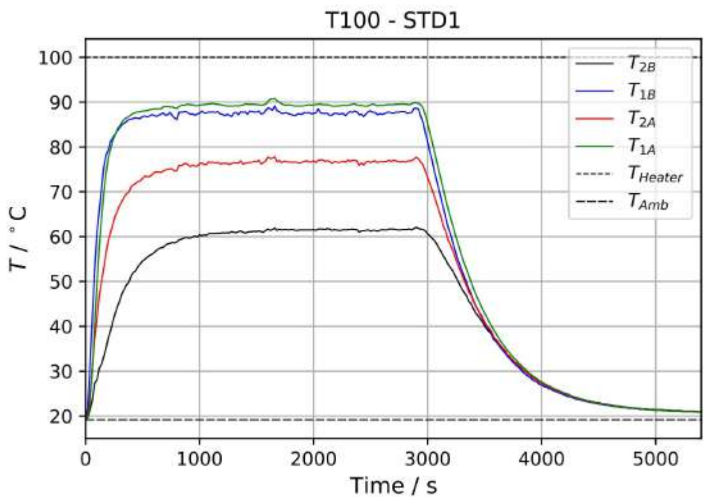


Figure 5.12: Temperature measurement of a standard tooth and $T_{heater} = 100$ °C.

## 5.3 DIC Experiment Procedure

Digital Image Correlation (DIC) is a surface displacement measuring technique that can captures the shape, motion and deformation of solid objects. DIC is performed by processing a series of images captured during the deformation process of an object, tracking the displacements of unique patterns on the surface and comparing the coordinates of the reference image with the deformed image. In most cases, a speckle pattern is applied on the surface of the object being deformed in order to facilitate the tracking process. The pattern moves and deforms with the sample, but does not exert a significant mechanical stress on the sample [19].

The Digital Image Correlation technique can be performed in two or three dimensions. The 2D DIC employs a single fixed camera and estimates displacements and deformations in a selected plane. For a 3D DIC measurement, at least two fixed cameras are needed to determine the whole 3D deformation field [20].

The basic operation of DIC is based on tracking a speckle pattern in a sequence of images. The process of a DIC experiment can be divided into three steps: obtain a pattern on the sample for tracking, capture images of the sample during motion/deformation, and analyze the images to compute the sample surface's displacements [21].

Owing to the growing popularity of this technique, several research DIC software are now made freely available to the scientific community, with *Ncorr*, *DICe* and *YaDICs* being the most popular [20]. After a quick comparison of the different programs, the *DICe* software was chosen because it allows easy access of the results, which can be post-processed and analyzed using different programs.

The purpose of the DIC experiments was to validate the FEM thermo-mechanical model and study the thermal expansion of the acetal material when applying heat to the flank of the tooth. The DIC tests consisted of a single test for the standard rack tooth and a single test for the hybrid tooth without an insert. For the duration of the experiment, a Nikon D3200 DSLR was used to take pictures of the tooth speckle pattern and four k-type thermocouple sensors measured the surface temperature.

The operating variables and the experimental factors related to the experiment were similar to the thermal tests, due to the fact that the experiment were executed using the Heating System under similar conditions. The operating variables can be found in Table 5.8 and the experiment factors can be seen in Table 5.9.

Table 5.8: DIC experiment operating variables.

| **DIC Experiment Variables** | |
|---|---|
| **Purpose:** | Preliminary validation of a hybrid polymer gear concept and of the FEM thermo-mechanical model |
| **Response Variable:** | Surface displacement of the tooth / mm |
| | Surface temperature of the tooth / °C |
| **Fixed Variable:** | Polymer Gear Material: POM |
| | Weigh of the Platform: m=1.483 kg |
| | Weigh of the Shaft: m=0.104 kg |
| **Independent Variable:** | Ambient Temperature °C |

Table 5.9: DIC experiment factors.

| **DIC Experiment Factors:** |
|---|
| Cartridge Heater Temperature / °C |
| Applied Weight / kg |
| Point of Contact / mm |
| Heating duration / min |
| Cooling duration / min |

### 5.3.1 DIC Experiment Factors

The different factors for the digital image correlation (DIC) experiment were studied and an experimental procedure was defined for the standard and hybrid tooth. The first test measured the displacements and surface temperature of the standard tooth, and afterwards the same tests was performed for the hybrid tooth without an insert. Once both tests were performed, it was possible to compare the data collected of the surface displacement under different temperature conditions.

The setup of the Heating System were under the same conditions as the thermal tests. Therefore, the point of contact of the heaters was equal to the pitch point ($h_{contact} = 4.5$ mm) and the applied weight was equal to 4.6 kg.

Finally, for the DIC experiments a tooth with a speckle pattern was attached to the the platform and placed on the two heaters. The weights were placed on top of the platform inside the cylinder. Only one cartridge heater was used for the duration of the tests. The test started by turning on the power source that controls the heaters and choosing the desired temperature. For the first stage of the test the temperature of the heater was set to $T_{Heaters} = 40$ °C with a heating duration of 30 minutes. The second stage the temperature was increased to $T_{Heaters} = 70$ °C with a heating duration of 30 minutes. The third phase increased the temperature to $T_{Heaters} = 100$ °C with a heating duration of 30 minutes. For the final phase, the power source was turned off and the cooling duration lasted 45 minutes. During this process the surface temperatures was measured with four thermocouple sensors and saved on to a Datalogger. The displacements were measured by a Nikon D3200 DSLR which took a picture of the surface of the tooth, with the speckle pattern, every 15 minutes.

The conditions of the operating procedure for the DIC experiment are summarized in Table 5.10 and a graphic representation of the heating process can be seen in Figure 5.13. The setup of the Heating System with the Nikon D3200 DSLR camera can be seen in Figure 5.14.

Table 5.10: Test conditions for the DIC tests.

| **DIC Experiment Factors:** |
|---|
| Type of Tooth: Standard and Hybrid |
| Temperature Range, °C: $T_{Heater}$ = [40, 70, 100] |
| Applied Weight, kg: $m = 4.6$ |
| Point of Contact, mm: $h_{Heater} = 4.5$ |
| Heating duration, min: $t_h = 30$ & $t_{total} = 90$ |
| Cooling duration, min: $t_c = 45$ |

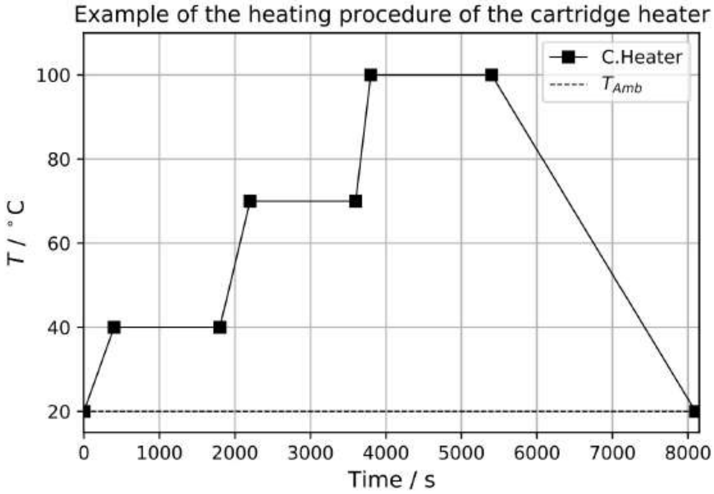


Figure 5.13: Graphic representation of the DIC test procedure.

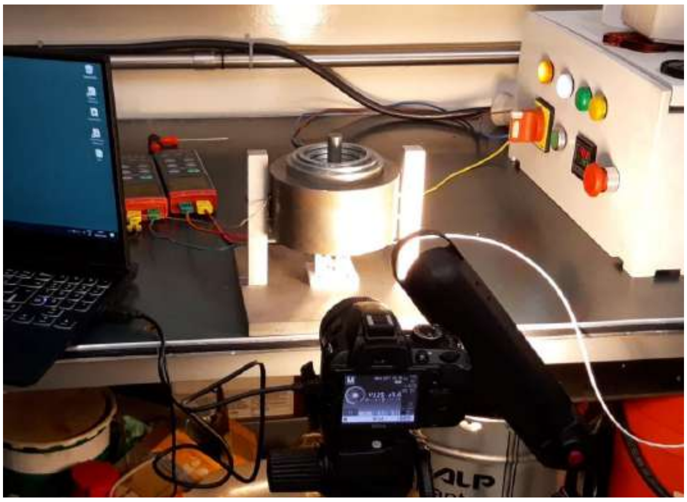

Figure 5.14: DIC experiment test setup.

### 5.3.2 Experimental Procedure

For the experimental procedure of the thermal test a certain amount of preparation was necessary. First of all, the speckle pattern for the test specimens were prepared (*STD* and *HT1*) and the thermocouple sensors were attached to the surface of the teeth. Afterwards, the heating system was prepared, taking in to account the predefined factors, and the test specimen was attached. Once the DIC test was performed, the temperature data was collected and processed, as well as the displacement measurements. A graphic representation of the test procedure can be seen in Figure 5.15.

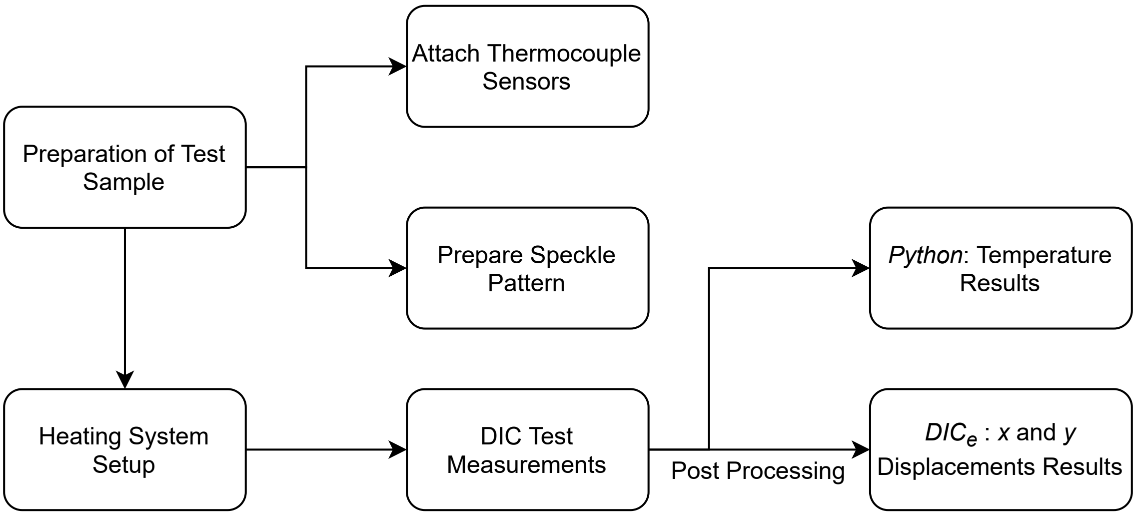


Figure 5.15: Graphic representation of the DIC test experimental procedure.

#### 5.3.2.1 Preparing the Speckle Pattern

For the DIC experiment, a speckle pattern needed to be applied on the surface of the standard and hybrid tooth. The methodology of DIC is based on tracking the unique pattern of the speckle in a sequence of images. For this reason, the quality of the speckle pattern affects the accuracy and precision of the displacement results.

A painted speckle pattern is the most popular technique for creating a pattern, because paint is relatively compliant to most engineering materials, and high-quality speckle patterns can be applied quickly with spray paint at a low cost. Typically, painting directly on the test sample's natural surface does not produce the best pattern possible. For this reason, a initial base-coat of white paint is applied on the surface, followed by a black speckle pattern [21]. Therefore, the first step to create a speckle pattern on the surface of the standard tooth and hybrid tooth was to apply a initial layer of white paint using RIVELEX 200 crack detector, Figure 5.16. Once the white layer had dried, a speckle pattern was created with a matt black spray, Figure 5.16. The speckle pattern for the standard tooth and hybrid tooth can be seen in Figure 5.17.


Figure 5.16: Spray used for the speckle pattern: (a) RIVELEX 200 and (b) LUXENS matt black.

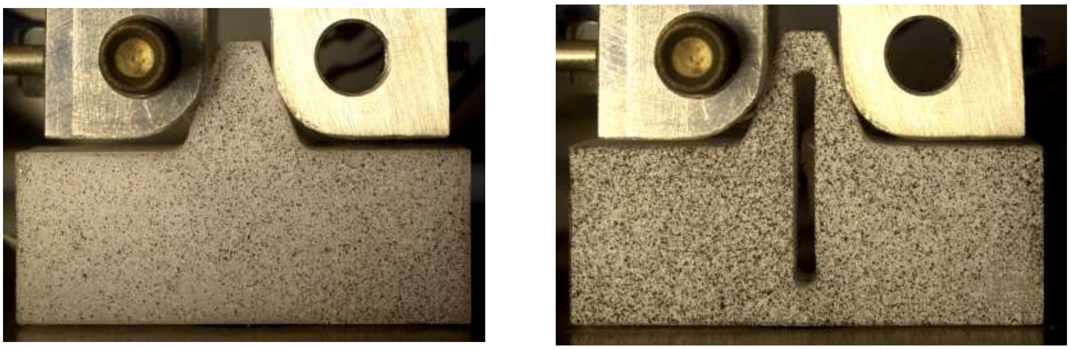

(a) (b)

Figure 5.17: DIC speckle pattern: (a) standard tooth and (b) hybrid tooth.

#### 5.3.2.2 Preparing the Thermocouple Sensors

For the DIC experiments, the surface temperature was measured using four k-type thermocouple sensors and the positions chosen for the test can be seen in Figure 5.18. The coordinates of the holes of the four thermocouple sensor in relation to the reference point in the lower left corner of the tooth, Figure 5.9a, can be found in Table 5.7. The pitch point ($T_{2b}$) was chosen for its proximity with the contact point of the heaters. The tooth root region ($T_{2b}$) was chosen because this region is typically associated with different modes of failure. The insert region ($T_{2a}$) was chosen to study the impact of the thermal expansion of different insert materials. The base of the tooth ($T_{1a}$) was chosen in order to study the temperature change near the extremities of the tooth.

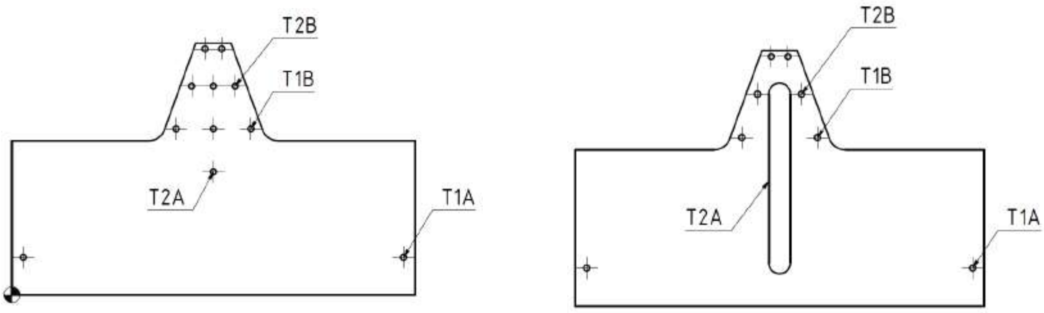


(a) (b)

Figure 5.18: DIC: Standard tooth (a) and hybrid tooth (b) with bore holes for thermocouple.

Table 5.11: Coordinates and dimensions of the bore holes for DIC test.

| Hole | $x$ mm | $y$ mm | Dimensions mm |
|---|---|---|---|
| T1a | 41.21 | 3.95 | $\phi$0.60x0.50 |
| T2a | 21.21 | 12.95 | $\phi$0.60x0.50 |
| T1b | 25.13 | 17.45 | $\phi$0.60x0.50 |
| T2b | 23.49 | 21.95 | $\phi$0.60x0.50 |

#### 5.3.2.3 Processing the Data From DataLogger and DICe

During the DIC test, four thermocouple sensors were used to measure the surface temperature and a DSLR camera was used to track the displacement of the speckle during the heating process. The surface temperature data was exported from the Dataloggers and a script would read and was used to plot the data. The images captured during the DIC test were exported to a processing software to compute the displacements of the tooth surface.

As was mentioned above, *DICe* software was chosen to compute the displacements field. The first step when using the *DICe* software was to choose a reference image, which in this case was the first picture taken at ambient temperature. The deformed images that were analyzed by the program were taken for each one of the temperature increments. That is, the first picture for $T_{Heaters} = 40$ °C, the second for $T_{Heaters} = 70$ °C, and the third picture for $T_{Heaters} = 100$ °C. Next, the region of interest of the reference image was selected, which allowed the software to create a matrix with the speckle pattern, Figure 5.19. Once the matrix was created, the program was ready to compute the displacements. The results from the *DICe* software were saved as a text file.

Figure 5.19: Digital Image Correlation Engine (DICe): region of interest and matrix.

A script was developed in Python in order to read the results from the *DICe* software. The text file from the *DICe* software contained the node coordinates and their displacements in pixels. So, the script would initially read the data and then convert the units to millimeters using the known dimensions of the length of the rack tooth ($L_{\mathrm{mm}}$=42.41 mm) and the total length of the rack matrix in pixels ($L_{pixel}$), Equation 5.1.

$$data_{\mathrm{mm}} = data_{pixel} \cdot \frac{L_{\mathrm{mm}}}{L_{pixel}} \tag{5.1}$$

Next, the script would plot the matrix created by the *DICe* software and create a mesh using a 2D Delaunay Triangulation. The mesh for the standard tooth and hybrid tooth created by the script can be seen in Figure 5.20. Finally, the scrip would read the displacement data and plot the $x$ and $y$ displacements with the mesh. An example of the $y$ displacement for the standard tooth can be seen in Figure 5.21.

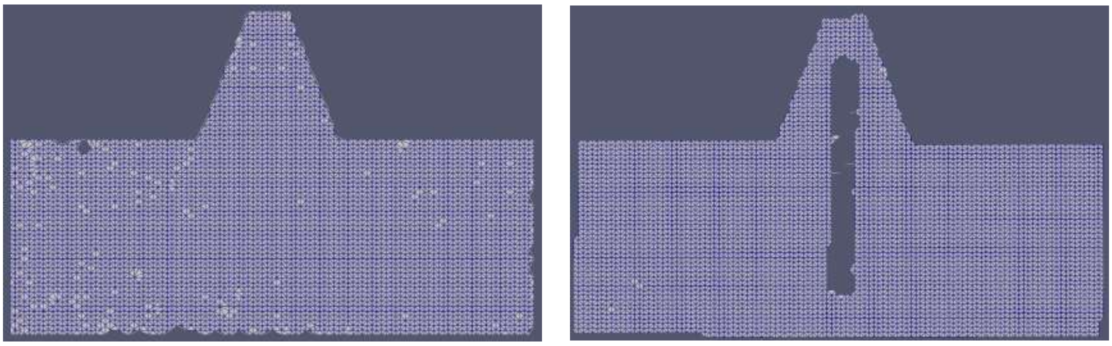

(a) (b)

Figure 5.20: Mesh generated for the (a) standard tooth and (b) hybrid tooth.

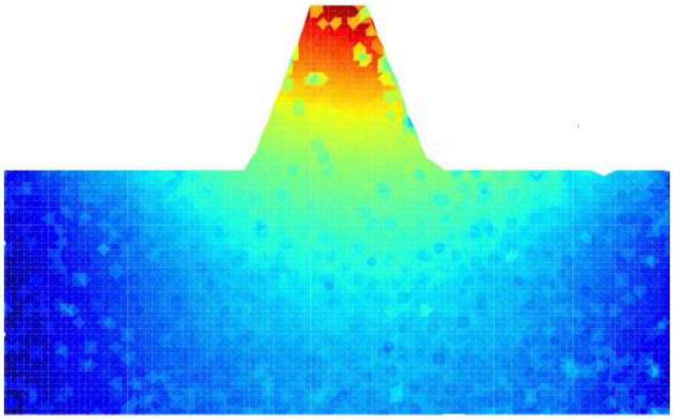

Figure 5.21: Example of the processed data from Python: y displacements for the standard tooth.

# Chapter 6

# Experimental Results

## 6.1 Thermal Experiment Measurements

### 6.1.1 Summary of the Results

The thermal tests were performed for the standard rack tooth (*STD*), the hybrid rack tooth without an insert (*HT1*), the hybrid rack tooth with an aluminum insert (*HT2*) and the hybrid rack tooth with an epoxy filled insert (*HT3*). The thermal tests were performed for each tooth with a heater temperature of $T_{Heater}$=[40, 50, 60, 70, 80, 90, 100, 110]°C. During the tests only one of the cartridge heaters was used, which was located on the right side of the tooth ($T_{1b}$). The surface temperature was measured with four thermocouple sensors as seen in Figure 5.9, and later exported to a Python script to be processed. The ambient temperature of each test was measured with a mercury thermometer. The average ambient temperature for each tooth can be found in Table 6.1. The test report for each of the teeth can be found from Appendix E.1 to E.4.

Table 6.1: Average ambient temperature / °C (for each test specimen).

| | Average ambient temperature / °C |
|---|---|
| *STD* | 19.5 |
| *HT1* | 20.3 |
| *HT2* | 21.1 |
| *HT3* | 24.1 |

The stabilization temperature temperature ($T_{stabilized} = T - T_{amb}$) was calculated for each of the thermocouple sensors, Figure 5.9. The relative change of temperature was calculated for the stabilized temperatures of each hybrid tooth in relation to the standard tooth, in order to measure the impact of the hybrid tooth design under similar conditions. These results can be found in table 6.2 to 6.5.

The thermocouple sensor $T_{1b}$ measured the temperature near the point of contact of the heater that contained the cartridge heaters. The $T_{1a}$ sensor measured the temperature near the point of contact of the second heater. The heat source would transfer heat to the first heater and since both aluminum heaters were in contact, the temperature of the two heaters would stabilize. For this reason, the temperatures for $T_{1a}$ for the *STD* and *HT1* were very similar to $T_{1b}$.

The temperatures of $T_{1a}$ for the *STD* and *HT1* (air) were very similar with an average temperature change of 1.9%. The temperature of the point of contact for hybrid teeth with an insert were significantly higher. The *HT3* (epoxy) showed an average temperature change of 6.7% and the *HT2* (aluminum) a change of 12.6%. These results clearly show than in the presence of an insert, the hybrid teeth were able to absorb more heat. The values for the stabilized temperature of $T_{1a}$ can be found in Table 6.2 and the graphic representation can be seen in Figure 6.1.

Table 6.2: Average stabilized temperature for $T_{1a}$ and relative change.

| $T_{Heater}$ | $T_{STD}$ | $T_{HT1}$ | % | $T_{HT2}$ | % | $T_{HT3}$ | % |
|---|---|---|---|---|---|---|---|
| 40 | 19.1 | 19.0 | -0.8 | 20.1 | 4.8 | 15.9 | -16.8 |
| 50 | 27.5 | 26.9 | -2.4 | 31.2 | 13.3 | 26.8 | -2.6 |
| 60 | 34.9 | 34.8 | -0.1 | 41.4 | 18.9 | 38.2 | 9.5 |
| 70 | 44.3 | 43.5 | -1.7 | 48.6 | 9.7 | 48.2 | 8.9 |
| 80 | 53.5 | 52.3 | -2.3 | 59.6 | 11.4 | 61.7 | 15.3 |
| 90 | 61.3 | 60.9 | -0.8 | 67.3 | 9.8 | 70.1 | 14.4 |
| 100 | 70.3 | 67.2 | -4.5 | 82.1 | 16.8 | 79.6 | 13.1 |
| 110 | 79.2 | 77.0 | -2.7 | 92.1 | 16.3 | 88.9 | 12.2 |
| Avg | - | - | -1.9 | - | 12.6 | - | 6.7 |

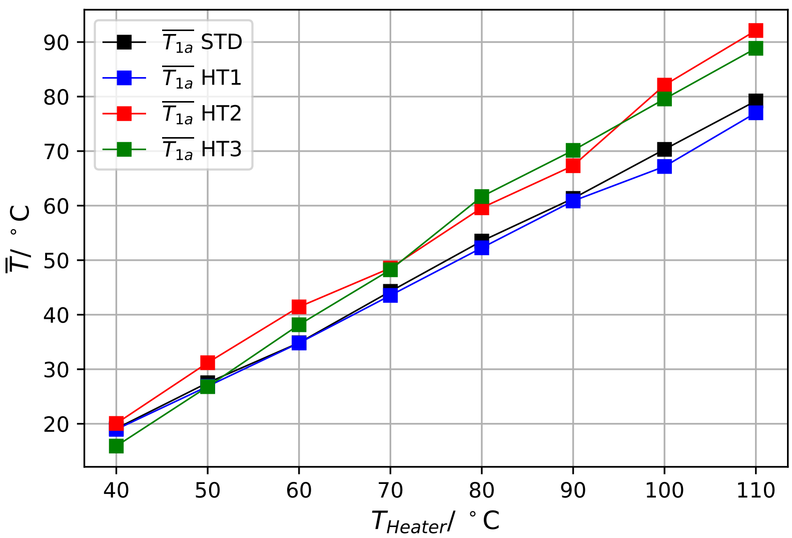


Figure 6.1: Average stabilized temperature for $T_{1a}$.

The temperature of $T_{1b}$ for the *HT1* (air) was 5.2% lower than the *STD*. The lower temperature for the *HT1* could be a result of convective heat transfer inside the region of the insert, instead of conduction to the remainder of the body. Once again, the temperature of the point of contact for hybrid teeth with an insert were significantly higher. The *HT2* showed the highest temperature change, with an average of 27.9%. The *HT3* also showed a significant temperature change of 19.6%. The values for the stabilized temperature of $T_{1b}$ can be found in Table 6.3 and the graphic representation can be seen in Figure 6.2.

Table 6.3: Average stabilized temperature for $T_{1b}$ and relative change.

| $T_{Heater}$ | $T_{STD}$ | $T_{HT1}$ | % | $T_{HT2}$ | % | $T_{HT3}$ | % |
|---|---|---|---|---|---|---|---|
| 40 | 19.1 | 17.7 | -7.2 | 21.7 | 13.6 | 18.0 | -5.6 |
| 50 | 26.6 | 25.4 | -4.7 | 34.1 | 28.2 | 30.2 | 13.5 |
| 60 | 35.1 | 32.8 | -6.7 | 46.0 | 30.9 | 41.8 | 18.9 |
| 70 | 43.7 | 41.1 | -6.0 | 54.5 | 24.7 | 53.3 | 21.9 |
| 80 | 52.5 | 49.7 | -5.3 | 66.3 | 26.1 | 67.9 | 29.3 |
| 90 | 60.3 | 58.7 | -2.6 | 75.7 | 25.5 | 76.8 | 27.3 |
| 100 | 68.5 | 66.0 | -3.7 | 93.2 | 36.0 | 86.7 | 26.6 |
| 110 | 77.4 | 73.5 | -5.1 | 106.9 | 38.1 | 96.8 | 25.1 |
| Avg | - | - | -5.2 | - | 27.9 | - | 19.6 |

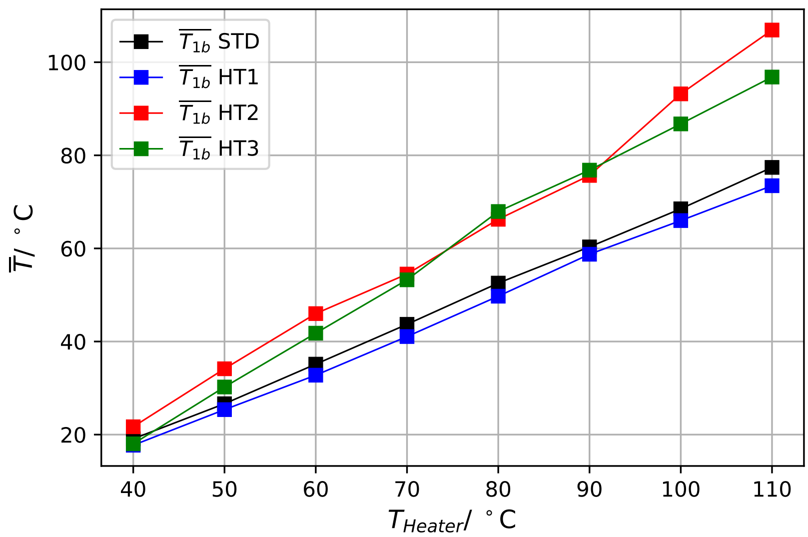


Figure 6.2: Average stabilized temperature for $T_{1b}$.

The $T_{2a}$ measured the surface temperature of the region where the insert would be located. For the *HT1* the thermocouple was placed on the surface of the inner wall of the insert cavity. The temperature for *HT1* followed a similar pattern to the previous measurements. The *HT3* did not reveal a significant impact, with an average temperature change of 1.1%. In contrast, the *HT2* showed an average temperature change of 30.4% and a maximum temperature change of 43.3% for $T_{Heater}$=100°C. The disparity of the results from the *HT2* and *HT3* could be related to the difference in thermal conductivity of the two materials used for the insert. The thermal conductivity of aluminum material is 500-600 times superior to POM material, whereas the ER2220® epoxy is 5 times superior. The values for the stabilized temperature of $T_{2a}$ can be found in Table 6.4 and the graphic representation can be seen in Figure 6.3.

Table 6.4: Average stabilized temperature for $T_{2a}$ and relative change.

| $T_{Heater}$ | $T_{STD}$ | $T_{HT1}$ | % | $T_{HT2}$ | % | $T_{HT3}$ | % |
|---|---|---|---|---|---|---|---|
| 40 | 11.8 | 10.5 | -10.7 | 13.4 | 13.6 | 10.8 | -8.4 |
| 50 | 15.9 | 15.2 | -4.7 | 21.3 | 33.8 | 19.7 | 23.7 |
| 60 | 20.5 | 19.9 | -2.7 | 28.9 | 40.9 | 19.4 | -5.1 |
| 70 | 26.4 | 25.1 | -4.9 | 32.3 | 22.2 | 25.3 | -4.2 |
| 80 | 32.5 | 30.3 | -6.8 | 40.7 | 25.1 | 33.1 | 1.9 |
| 90 | 36.7 | 35.8 | -2.2 | 45.7 | 24.5 | 37.5 | 2.3 |
| 100 | 42.4 | 41.1 | -2.9 | 60.7 | 43.3 | 42.5 | 0.2 |
| 110 | 48.5 | 48.4 | -0.2 | 67.7 | 39.6 | 47.6 | -1.9 |
| Avg | - | - | -4.4 | - | 30.4 | - | 1.1 |

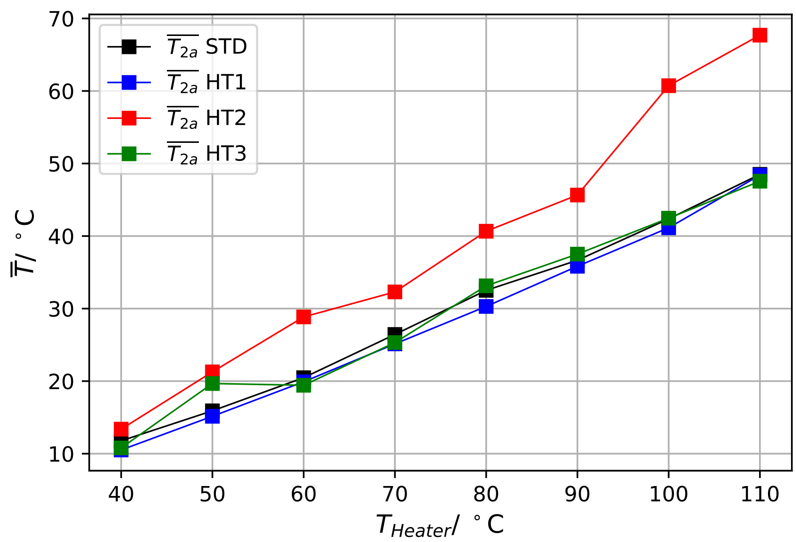


Figure 6.3: Average stabilized temperature for $T_{2a}$.

The $T_{2b}$ thermocouple sensor measured the surface temperature of the tooth root region. All three of the hybrid teeth showed a significant increase in temperature. The *HT1* and *HT3* showed a similar increase of 13.7% and 19.2%, and the *HT2* showed an average temperature change of 30.4%. These results showed that the hybrid gear design had a tendency to increase the temperature of the tooth root region. Given that the tooth root region is is generally associated with different modes of failure for gears, a future study should be done to verify if this design could lead to an increase of tooth root failure. The values for the stabilized temperature of $T_{2b}$ can be found in Table 6.5 and the graphic representation can be seen in Figure 6.4.

Table 6.5: Average stabilized temperature for $T_{2b}$ and relative change.

| $T_{Heater}$ | $T_{STD}$ | $T_{HT1}$ | % | $T_{HT2}$ | % | $T_{HT3}$ | % |
|---|---|---|---|---|---|---|---|
| 40 | 15.6 | 17.8 | 13.8 | 18.6 | 19.1 | 15.0 | -3.9 |
| 50 | 22.0 | 25.5 | 15.8 | 29.2 | 32.4 | 25.4 | 15.3 |
| 60 | 28.6 | 33.3 | 16.4 | 39.5 | 38.3 | 34.6 | 20.9 |
| 70 | 36.0 | 41.6 | 15.6 | 46.3 | 28.7 | 43.6 | 21.3 |
| 80 | 43.6 | 49.7 | 13.9 | 57.1 | 30.8 | 55.5 | 27.1 |
| 90 | 50.6 | 59.1 | 16.8 | 65.2 | 28.8 | 63.3 | 25.1 |
| 100 | 57.7 | 62.2 | 7.8 | 81.5 | 41.4 | 72.0 | 24.9 |
| 110 | 65.5 | 71.7 | 9.5 | 92.9 | 41.8 | 80.5 | 22.9 |
| Avg | - | - | 13.7 | - | 32.7 | - | 19.2 |

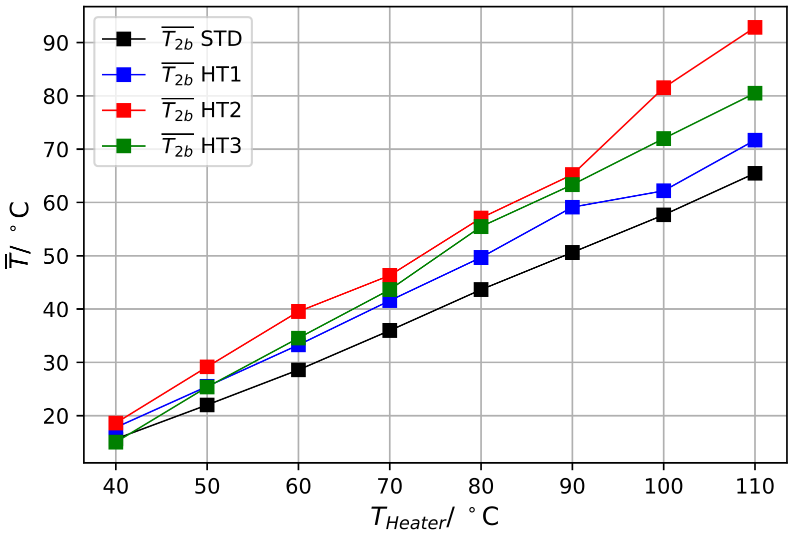


Figure 6.4: Average stabilized temperature for $T_{2b}$.

With the temperature measurements for $T_{1a}$ and $T_{1b}$, it is important to note that the *HT2* and *HT3* showed a surface temperature measurement greater than the imposed cartridge heater temperature. For instance, for $T_{Heater}$=110°C the *HT2* showed a surface temperature of 127.5 °C. These results show a potential a potential flaw with this test procedure. During the thermal tests, a Pt100 sensor measured the temperature of the cartridge heater and returned the temperature data to the power source, which in turn calibrated the output power to the cartridge heater. That being said, the test procedure could be improved by changing the location of the Pt100 sensor to a bore hole located on the rack tooth body. Instead of applying a controlled temperature to the surface of the tooth, the purpose of the test would be to increase the body temperature to a predefined value and measure the output power necessary to raise the body temperature of each test specimen.

### 6.1.2 Comparison of the Natural Cooling Curve

Newton's law of cooling states that the rate of heat loss of a body is directly proportional to the difference in the temperatures between the body and its surroundings. During the cooling phase, the temperature of a body approaches the ambient temperature ($T_\infty$) at an exponential rate. The temperature of the body changes rapidly at the beginning, but rather slowly later on. equation 6.1 describes the exponential cooling curve for a body as a function of time. It is possible to determine the temperature T($t$) of a body at time $t$, or alternatively, the time $t$ required for the temperature to reach a specified value T($t$) [17].

$$\frac{T(t) - T_\infty}{T_i - T_\infty} = e^{-b \cdot t} \tag{6.1}$$

$$b = \frac{h \cdot A_s}{\rho \cdot V \cdot c_p} \tag{6.2}$$

The constant $b$ referred to in the literature as the Biot number, is a positive quantity whose dimension is (time)$^{-1}$ and is given by equation 6.2. A larger value for $b$ indicates that the body approaches the environment temperature in a shorter time, which means that the body has a higher rate of decay in temperature. The value of $b$ is proportional to the surface area, but inversely proportional to the mass and the specific heat of the body [17].

The value of $b$ was calculated for each of the teeth from the surface temperature measurements for $T_{Heater}$=100°C. The value of $b$ was calculated for each tooth using the same value for the initial temperature $T_i$, which was defined as the average stabilized temperature for the *STD* tooth. Using a Python script, the temperature values for each tooth from $T_i$ to $T_\infty$ were exported and used for equation 6.1. The temperature measurements of $T_{1b}$ for each of the teeth and the value of the initial temperature $T_i$ can be seen in Figure 6.5. The Biot time constant $b$ was calculated for $T_{1b}$ and a plot was generated, Figure 6.6, in order to compare the results for each of the teeth.

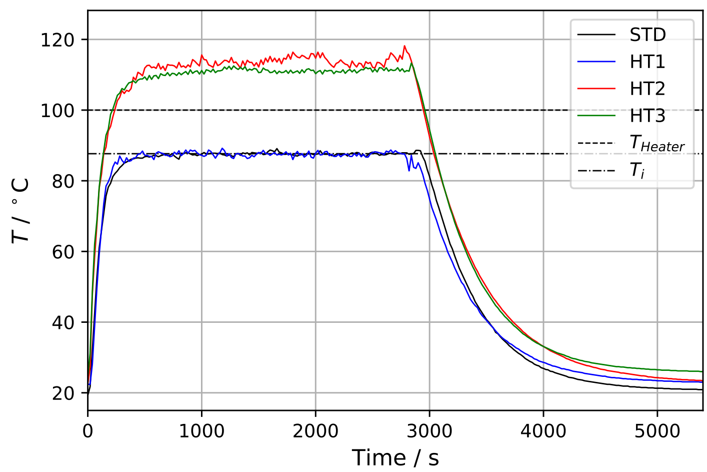


Figure 6.5: Thermocouple measurements of $T_{1b}$ for $T_{Heater}$=100°C.

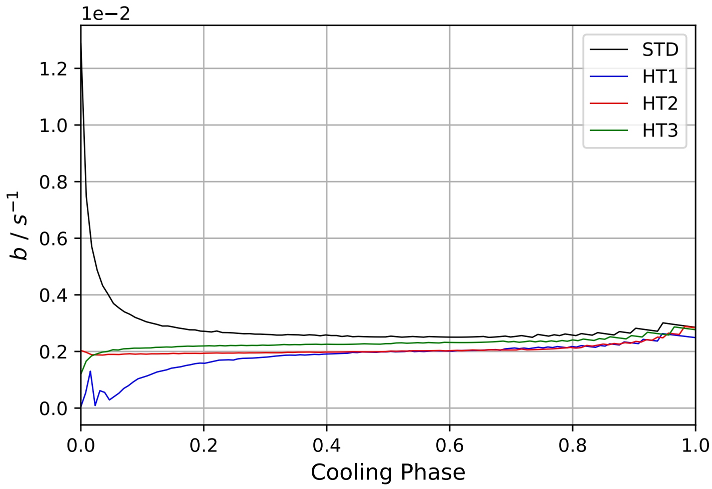


Figure 6.6: Biot time constant $b$ of $T_{1b}$ for $T_{Heater}$=100°C.

The value of $b$ and the relative change in relation to the standard rack tooth was calculated for each of the four thermocouple sensors measurements and can be found in Table 6.6. The average value of $b$ was calculated from [0.4 ; 0.6] of the cooling phase. The *HT2* (aluminum) and *HT3* (epoxy) than the *STD* showed a higher value of $b$ for the for the insert region ($T_{2a}$) in comparison to the *STD*, because the specific heat value ($c_p$) of the insert materials is lower than the polymer material. Equation 6.2 demonstrates that the time constant $b$ is inversely proportional to the specific heat. The *STD* showed a higher average value of $b$ in comparison to the hybrid rack teeth, which reveals that the standard rack tooth has a higher rate of decay in temperature.

Table 6.6: Biot time constant $s^{-1}$ and relative change for $T_{Heater}$=100°C.

| | $T_{1a}$ | $T_{1b}$ | $T_{2a}$ | $T_{2b}$ | Avg | % |
|---|---|---|---|---|---|---|
| *STD* | 0.00246 | 0.00253 | 0.00203 | 0.00231 | 0.00233 | - |
| *HT1* | 0.00185 | 0.00198 | 0.00221 | 0.00181 | 0.00196 | -15.9 |
| *HT2* | 0.00196 | 0.00200 | 0.00226 | 0.00162 | 0.00196 | -15.9 |
| *HT3* | 0.00229 | 0.00228 | 0.00226 | 0.00187 | 0.00217 | -6.8 |

## 6.2 DIC Experiment Measurements

The DIC test was performed for the standard rack tooth and for the hybrid rack tooth. The test was performed for $T_{Heater}$=[40, 70, 100]°C with a heating duration of $t_{heating}$=30 min. The *DICe* software determined the displacements in $x$ and $y$ direction as well as the strain for $x$ and $y$ direction. The ambient temperature during the tests was also measured using a mercury-filled glass thermometer. The test report with the temperature measurements and the results for each instance can be found in Appendix E.5 and E.6.

### 6.2.1 Standard Rack Tooth Measurements

The average ambient temperature during the test was measured at $T_{amb}$=20.1°C. The results for the stabilization temperature ($T_{stabilized} = T - T_{amb}$) for each thermocouple sensor and the maximum displacement for $x$ and $y$ direction can be found in Table 6.7.

During the DIC test for the standard rack tooth, the thermocouple that was placed on the node $T_{1B}$ malfunctioned, Figure 5.18. Since the main purpose of the DIC test was to analyze the displacements of the polymer teeth, it was not deemed necessary to repeat the measurements of the surface temperature.

The results from Table 6.7 showed a clear increase in the $x$ and $y$ displacements with the rise of the heater temperature ($T_{Heater}$), which was in accordance with the equation of linear thermal expansion, shown in equation 6.3. This equation demonstrates that for a change in temperature ($\Delta T$), an object will also expand in all dimensions if it is not restricted. The thermal expansion is also highly dependent on the coefficient of thermal expansion of the objects' material. The coefficient of thermal expansion for ERTACETAL C® is equal to $\alpha$=0.000125 °C$^{-1}$, as shown before in Table 2.4.

$$\Delta L = \alpha \cdot L_0 \cdot \Delta T \tag{6.3}$$

Table 6.7: DIC results for *STD*: stabilization temperature (°C) and maximum displacement (mm).

| $T_{Heater}$ | $T_{1a}$ | $T_{2a}$ | $T_{2b}$ | Max $d_x$ | Max $d_y$ |
|---|---|---|---|---|---|
| 40 | 5.8 | 13.1 | 22.7 | 0.067 | 0.050 |
| 70 | 15.5 | 29.2 | 50.2 | 0.111 | 0.090 |
| 100 | 24.1 | 46.7 | 73.4 | 0.255 | 0.183 |

The standard rack tooth showed the largest thermal expansion for $T_{Heater}$=100 °C, which allowed for a better visualization of the displacement field. The displacements field for $x$ and $y$ directions for $T_{Heater}$=100 °C can be seen in figures 6.7 and 6.8, respectively.

The displacement field for the $x$ direction showed a greater thermal expansion for the horizontal extremities of the tooth, which coincides with the largest value for $L_{x_0}$ in relation to the middle axis of the rack tooth. The thermal expansion was greater for the right side of the tooth compared to the left, as a result of the cartridge heater having been powered only on the right side. Although the temperature at pitch point ($T_{2b}$) was more elevated than the rest of the body, the tooth's expansion in $x$ direction was restricted by the heaters on either side.

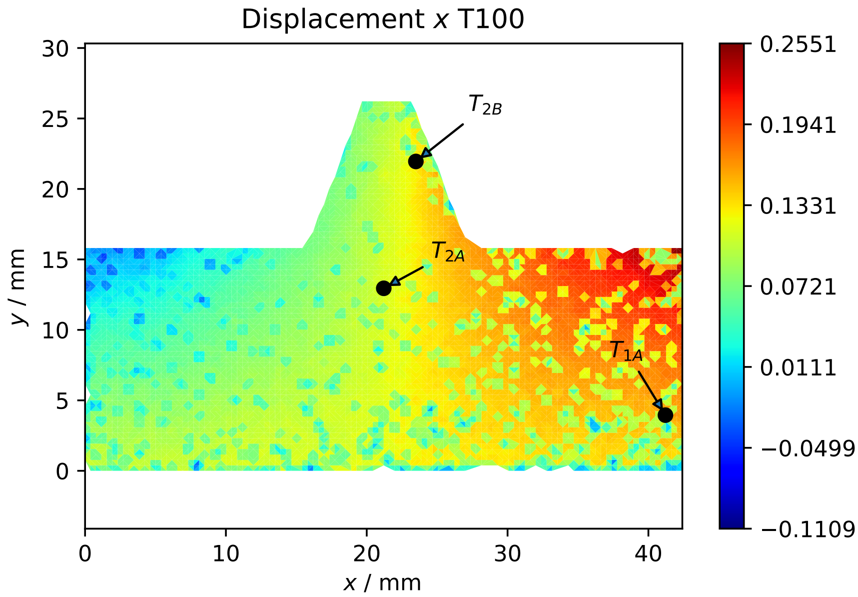


Figure 6.7: DIC standard rack tooth: $x$ displacements for $T_{Heater}$=100 °C.

The displacement field for the $y$ direction demonstrated a greater thermal expansion for the gear tip and a lower thermal expansion for the base of the tooth ($y$ = 0 mm). That being said, the maximum $y$ direction displacement overlapped with the contact point of the cartridge heater, that is, the region of the tooth with the largest change in temperature ($\Delta T$). The base of the tooth is attached to the support platform of the Heating System, which restricts the vertical movement of the tooth. The base of the tooth suffered the smallest temperature change ($T_{1a}$) and $y$ displacement.

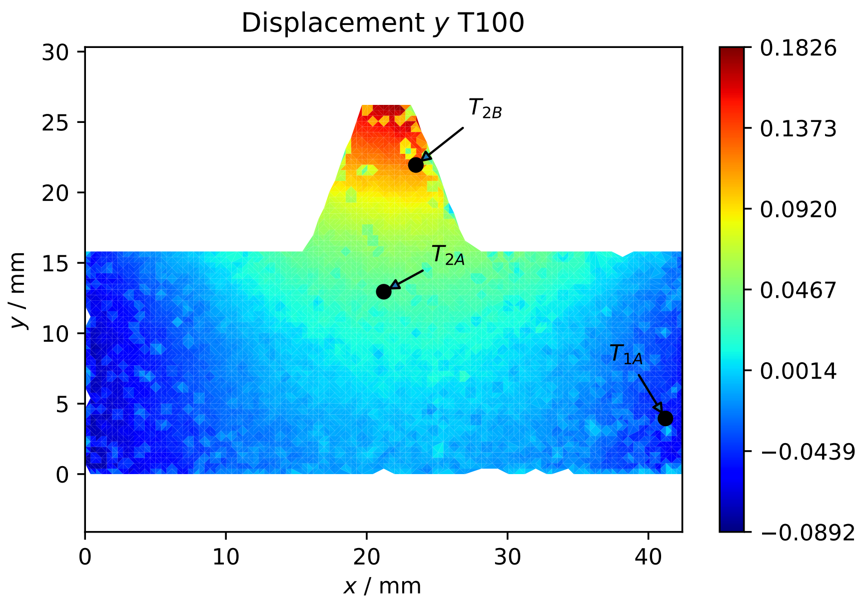


Figure 6.8: DIC standard rack tooth: $y$ displacements for $T_{Heater}$=100 °C.

### 6.2.2 Hybrid Rack Tooth Measurements

The data for the *HT1* DIC test went through the same process as the standard rack tooth. The average ambient temperature during the test was measured at $T_{amb}$ = 21.7°C. The results for the stabilized temperature for each thermocouple sensor and the maximum displacement for $x$ and $y$ direction can be found in Table 6.8. The average stabilized temperatures for the hybrid tooth were in the same range as the standard rack tooth.

The results from Table 6.8 showed that the displacement value for $x$ for $T_{Heater}$ = 40°C were 125% larger than the standard tooth, and yet the displacement in $x$ did not change significantly with the increase of temperature, which showed a clear difference from the *STD* displacement results progression. Consequently, for $T_{Heater}$=100°C the value for the maximum $x$ displacements was 33.7% lower than the standard tooth.

The values for the maximum $y$ displacements increased with each increment of the heater temperature. For $T_{Heater}$= 40 °C the value for $y$ displacements was already 125% larger than the standard tooth. As the heater temperature increased, the difference of $y$ displacements for the two teeth decreased to 33%.

Table 6.8: DIC results for *HT1*: stabilized temperature (°C) and maximum displacement (mm).

| $T_{Heater}$ | $T_{1A}$ | $T_{2A}$ | $T_{1B}$ | $T_{2B}$ | Max $d_x$ | Max $d_y$ |
|---|---|---|---|---|---|---|
| 40 | 4.8 | 9.6 | 14.4 | 17.1 | 0.152 | 0.116 |
| 70 | 15.62 | 26.2 | 38.6 | 45.8 | 0.143 | 0.193 |
| 100 | 30.3 | 46.9 | 64.7 | 75.9 | 0.169 | 0.243 |

The displacement field for $x$ and $y$ directions for $T_{Heater}$ = 100°C can be seen in figures 6.9 and 6.10, respectively. The $x$ displacements results for the hybrid tooth revealed a very distinct displacement field in comparison with the standard rack tooth. While the horizontal extremities of the rack body followed a similar displacement field as the rack tooth. The insert showed a tendency to contract due to thermal expansion. The combination of the thermal expansion of the extremities and the contraction of the insert region, led to a lower maximum $x$ displacement value compared to the standard rack tooth. However, this could become problematic if a rigid insert had been had been used for the hybrid rack tooth, because the contraction of the insert region could cause a significant amount of stress.

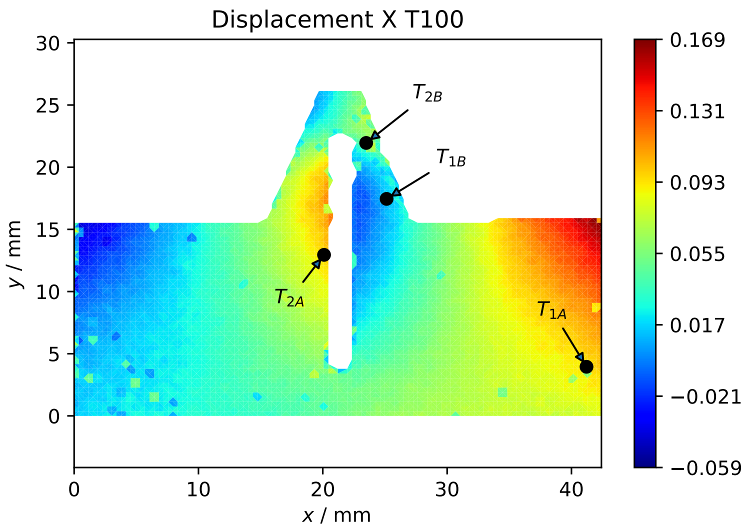


Figure 6.9: DIC hybrid rack tooth: $x$ displacements for $T_{Heater}$=100°C.

The displacement field for the $y$ direction showed a greater thermal expansion for the gear tip and a lower thermal expansion for the base of the tooth, similar to the standard rack tooth. As mentioned before, the maximum $y$ displacement for $T_{Heater}$ = 100°C was 30% larger than the standard tooth. Additionally, the region near the pitch point also revealed a larger displacement value than the standard tooth. The increase of thermal expansion for the tooth tip could have been caused by a lower heat dissipation of the tooth region, due to the missing mass. The temperature measurements for $T_{2b}$ for the *HT1* was 2.49°C higher than the *STD* for $T_{Heater}$ = 100°C. The increase in displacements for the tooth tip could also have been influenced by the contraction of insert region.

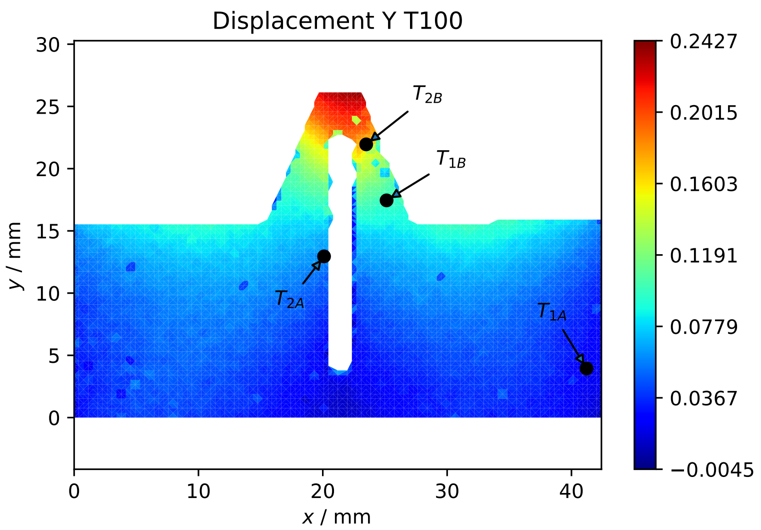


Figure 6.10: DIC hybrid rack tooth: $y$ displacements for $T_{Heater}$=100°C.

## 6.3 FEM Model Validation

### 6.3.1 Thermal Model Validation

The thermal model was validated for the standard tooth and the hybrid tooth, by comparing the temperature measured of the four thermocouple sensors for $T_{Heater}$=100°C with the FEM thermal model. As mentioned previously in Chapter 4.3.4, the heat transfer coefficient for the rack tooth, when attached to the Heating System, can range between $h_c$=[0.6 ; 13.2] $W/(^2mK)$ with an ambient temperature near the surface of the tooth equal to $T_{amb}$=33.8°C. That being said, the accuracy of the thermal model was calculated taking into account the range of the heat transfer coefficient.

#### 6.3.1.1 Standard Rack Tooth (*STD*) Thermal Results

The thermal model for the standard rack tooth was adapted for the test conditions of $T_{Heater}$=100°C and an ambient temperature of $T_{amb}$=33.8°C. The thermal results from the Chapter 6.1.1 for $T_{1a}$ and $T_{1b}$ were adapted for the thermal model boundary conditions. The FEM results for the nodal temperature can be seen in Figure 6.11.

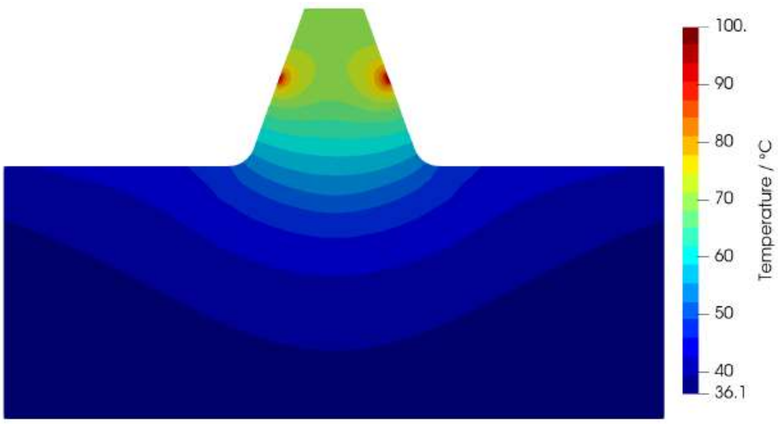


Figure 6.11: Thermal model standard rack tooth and $T_{Heater}$=100°C.

The temperature of the thermocouple sensors was compared with the node temperature of the FEM model. The temperature difference was calculated taking into account the range of the heat transfer coefficient, which can be seen in Figure 6.12. The results showed that the thermal model could accurately predict the surface temperature for a heat transfer coefficient of $h_c$=5 $W/(m^2K)$. With these results, the average relative error of the FEM analysis for each thermocouple node was calculated and can be seen in Figure 6.13. The thermal model for the standard tooth showed a minimum relative error of 6.1% for the contact point with the heaters ($T_{1b}$), and a maximum relative error of 14.8% for the tooth root region ($T_{2b}$).

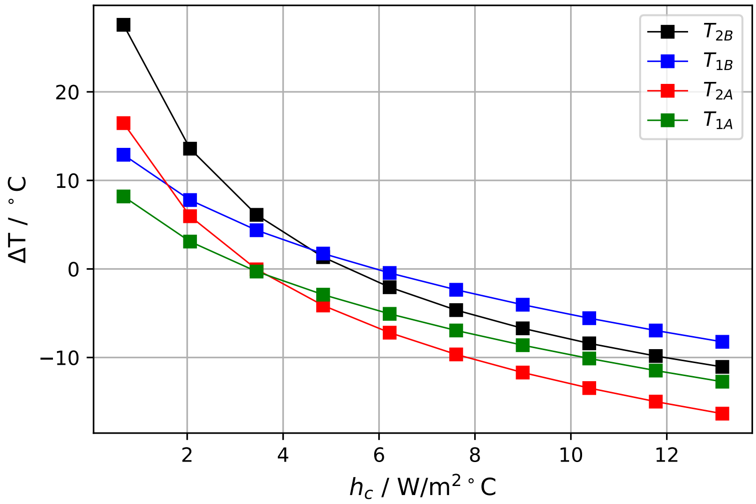


Figure 6.12: Comparison of the temperature results of the *STD* measurements with the FEM analysis for $T_{Heater}$=100°C.

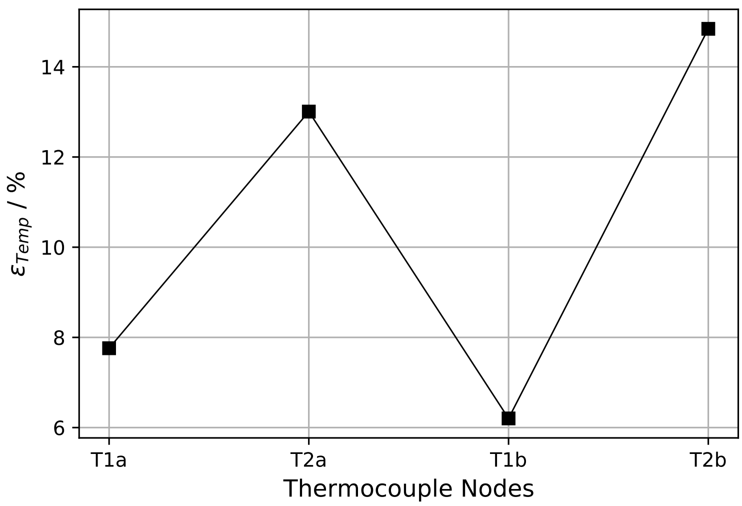


Figure 6.13: Relative error % of the FEM analysis for *STD*.

The results from Figure 6.12 showed that the temperature change varies drastically with the convective heat transfer. In Chapter 4.3.3, the natural convective heat transfer ($h$) was calculated by considering the surface of the tooth equivalent to a vertical plate, and its value was determined with the Nusselt number given by equation 4.5, and considering the length of the plate $L_c$ equal to the height of the tooth. That being said, if the natural heat transfer equations were implemented in the FEM model and it could calculate the heat transfer as a function of the tooth height ($L_c$), which would increase the accuracy of the temperature results along the height of the tooth.

#### 6.3.1.2 Hybrid Rack Tooth (*HT1*) Thermal Results

The thermal model for the hybrid rack tooth with no insert was adapted for the test conditions of $T_{Heater}$=100°C and an ambient temperature of $T_{amb}$=33.8°C. The thermal measurements of $T_{1a}$ and $T_{1b}$ from chapter 6.1.1 were used for the boundary conditions of the thermal model. The FEM results can be seen in Figure 6.14. The relative error was also calculated for the hybrid rack tooth using the same process as before. The results can be seen in Figure 6.15. The thermal model showed a minimum error of 12.5% for the contact region ($T_{1b}$) and a maximum error of 29.5% for the tooth root region ($T_{2b}$).

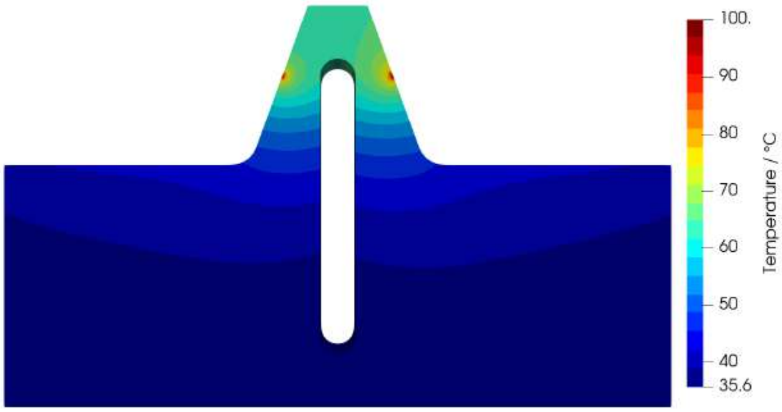


Figure 6.14: Thermal model *HT1* and $T_{Heater}$=100°C.

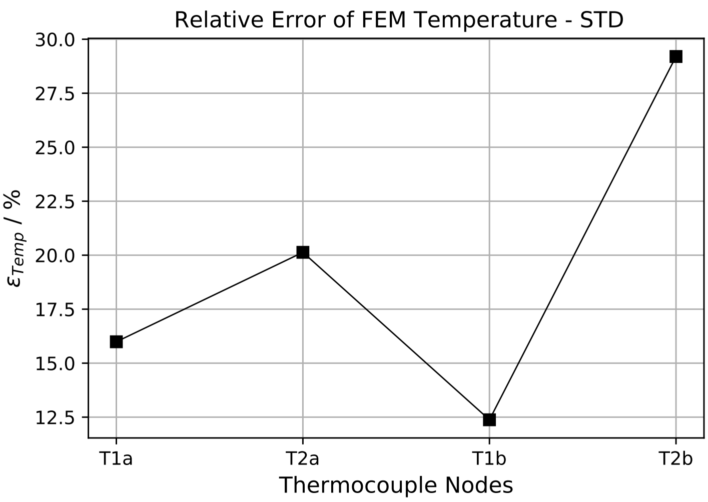


Figure 6.15: Relative error % of the FEM analysis for *HT1*.

#### 6.3.1.3 Hybrid Rack Tooth (*HT2*) Thermal Results

The thermal model for the hybrid rack tooth with an aluminum insert was adapted for the test conditions of $T_{Heater}$=100°C and an ambient temperature of $T_{amb}$=33.8°C. The thermal measurements of $T_{1a}$ and $T_{1b}$ from chapter 6.1.1 were used for the boundary conditions of the thermal model. The FEM results can be seen in Figure 6.16, with a visible outline of the temperature field of the aluminum insert. The relative error was also calculated for the hybrid rack tooth using the same process as before. The results can be seen in Figure 6.17. The thermal model showed a minimum error of 12.3% for the insert region ($T_{2a}$) and a maximum error of 39.4% for the contact point with the heater ($T_{1b}$).

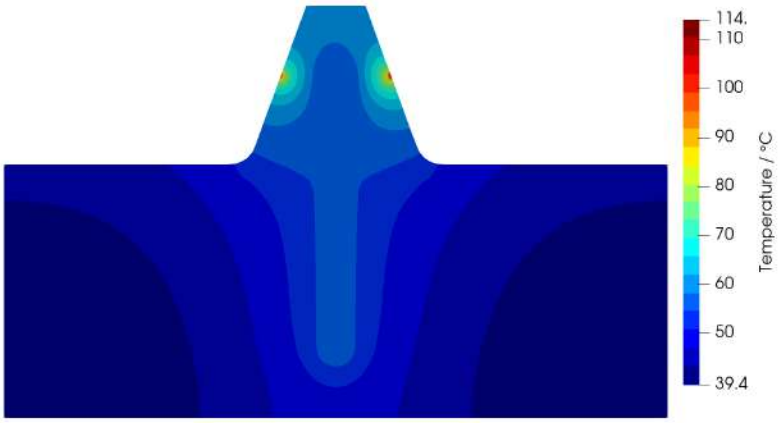


Figure 6.16: Thermal model *HT2* and $T_{Heater}$=100°C.

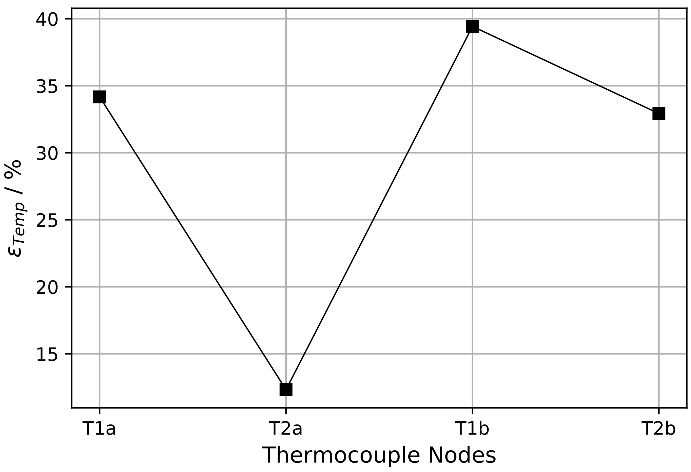


Figure 6.17: Relative error % of the FEM analysis for *HT2*.

### 6.3.2 Thermo-Mechanical Model Validation

The thermo-mechanical model was validated for the standard rack tooth and for the hybrid rack tooth, by comparing the $x$ and $y$ displacement fields from the FEM model with the DIC results. The values of the displacements were also plotted over a line in order to compare the absolute value of the FEM and DIC results.

### 6.3.3 Standard Rack Tooth Comparison

The displacement field for $x$ direction can be seen in Figure 6.18 and the $y$ direction can be seen in Figure 6.19. The displacement field of the FEM model for both $x$ and $y$ directions are visibly similar to the displacement field measured with the DIC tests. This indicates that the boundary conditions of the mechanical model that were imposed on the rack tooth FEM model were accurate.

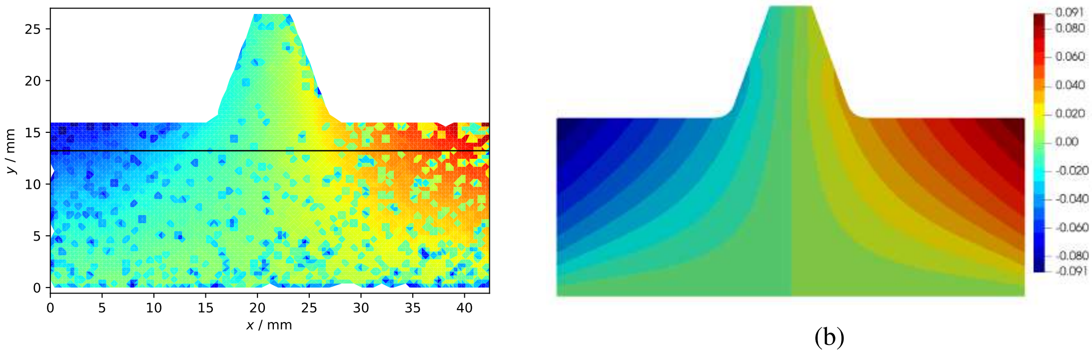


(a) (b)

Figure 6.18: Comparison of $x$ displacements results for *STD*: (a) DIC and (b) FEM.

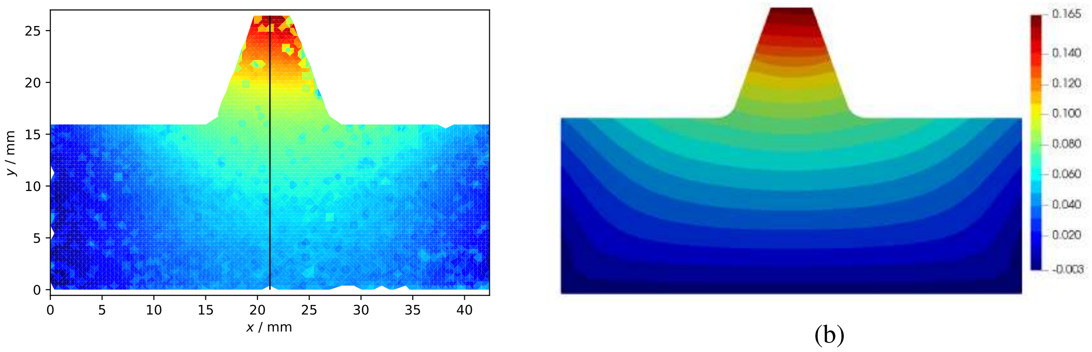


(a) (b)

Figure 6.19: Comparison of $y$ displacements results for *STD*: (a) DIC and (b) FEM.

In order to compare the absolute values of the FEM and DIC results, the $x$ direction displacement values were exported for $y$=13.22 mm, Figure 6.18a, and the $y$ direction displacement values for $x$=21.21 mm, Figure 6.19a. Afterwards, the values were analyzed with a Python script and a plot was created with DIC and FEM results. The $x$ direction displacements can be found in Figure 6.20 and the $y$ direction in Figure 6.21. The FEM results for the $x$ displacements showed a similar progression along the length of the tooth. However, DIC $x$ displacements results showed a offset of the values, which was caused by rigid body motion of the heaters due to the thermal expansion of the tooth. Whereas, the $y$ displacements showed an accurate result for the FEM model along the length of the tooth. These results reveal that the FEM model was able to accurately simulate the thermal expansion of the *STD* with a offset for the $x$ displacements.

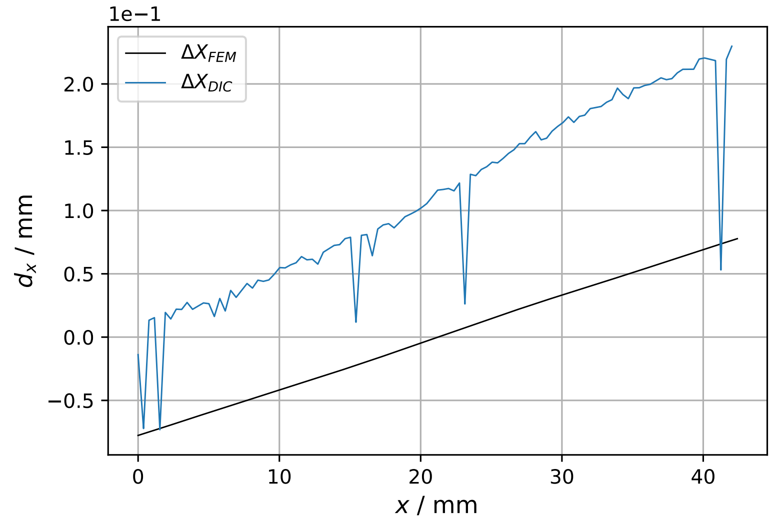


Figure 6.20: Plot of $d_x$ for DIC and FEM results for the *STD*.

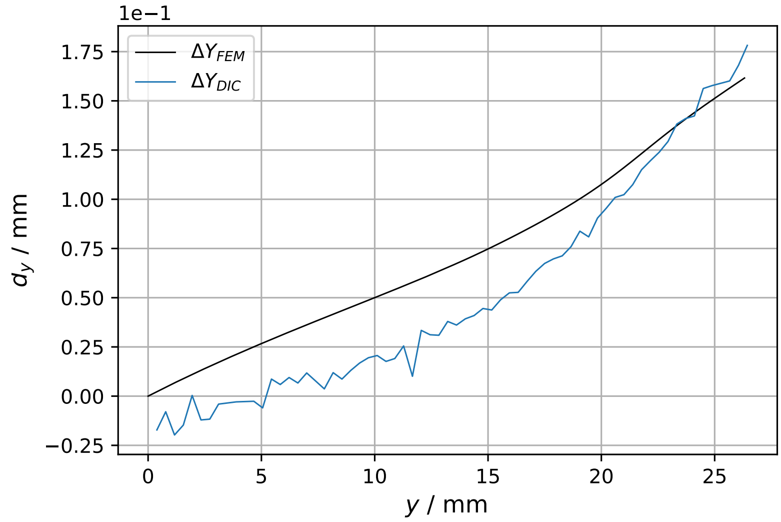


Figure 6.21: Plot of $d_y$ for DIC and FEM results for the *STD*.

### 6.3.4 Hybrid Rack Tooth Comparison

The same process for the standard rack tooth was applied for the hybrid rack tooth. The displacement fields for the $x$ and $y$ directions can be seen in figures 6.22 and 6.23, respectively. Once again, the displacement field for the $x$ and $y$ direction for the FEM model were visibly similar to the DIC results.

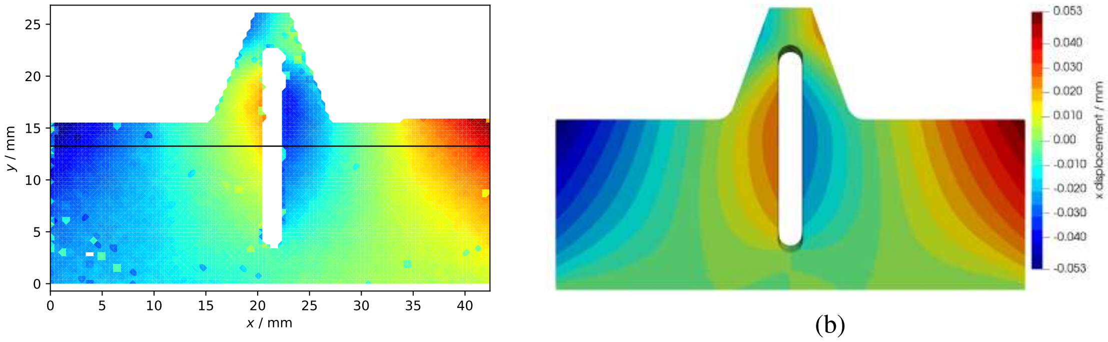


(a) (b)

Figure 6.22: Comparison of $x$ displacements results for *HT1*: (a) DIC and (b) FEM.

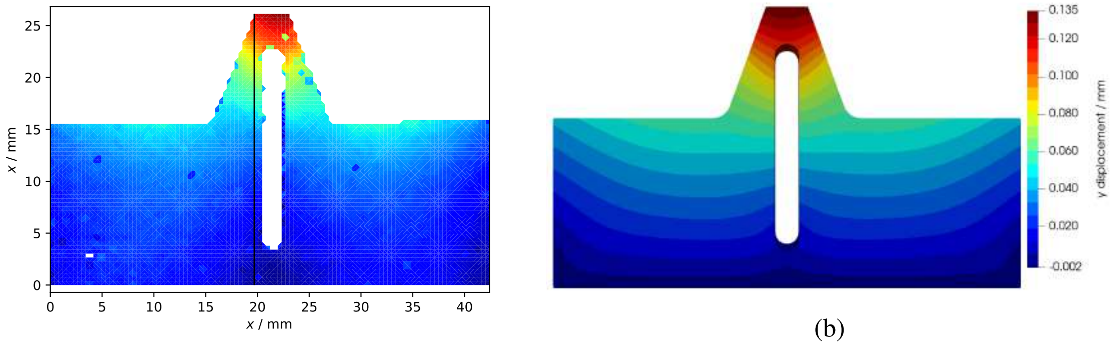


(a) (b)

Figure 6.23: Comparison of $y$ displacements results for *HT1*: (a) DIC and (b) FEM.

In order to compare the absolute values of the FEM and DIC results, the same method as the standard tooth was applied for the hybrid tooth results. The $x$ displacement values were exported for $y$=13.22 mm, Figure 6.22a, and the $y$ direction values were exported for $x$=19.71mm, Figure 6.23a. The $x$ displacements for the DIC and FEM can be seen in Figure 6.24 and the $y$ displacements in Figure 6.25. The $x$ and $y$ displacements showed a similar progression, but the FEM model results were not very accurate. Once again, the $x$ displacements showed a similar progression along the length of the tooth with an offset of the DIC values due to the rigid body motion of the heaters. That being said, the maximum displacement for the $x$ direction for the DIC test were significantly higher than the FEM results. The $y$ displacements for the FEM model were accurate up to $y$=15mm, and then the maximum value of $y$ displacements for the DIC test were significantly higher than the FEM analysis. These results reveal that the FEM model was able to predict the thermal expansion of the hybrid tooth with, with an offset of the displacement values for the insert region and tooth tip.

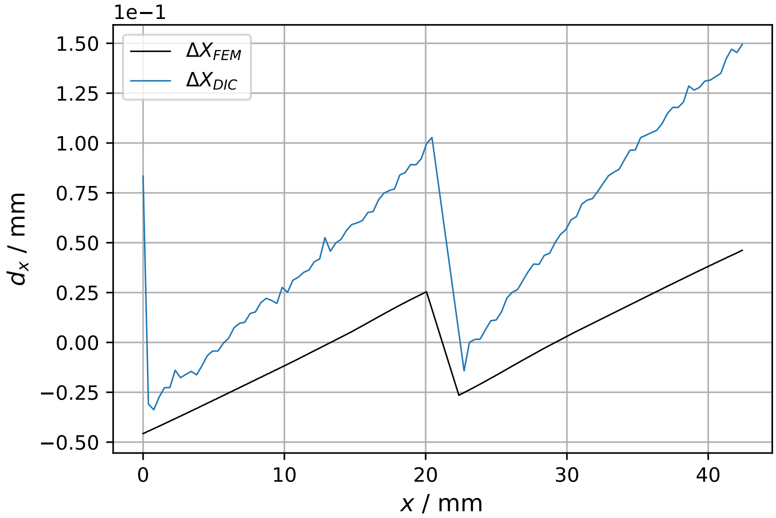


Figure 6.24: Plot of $d_x$ for DIC and FEM results for the *HT1*.

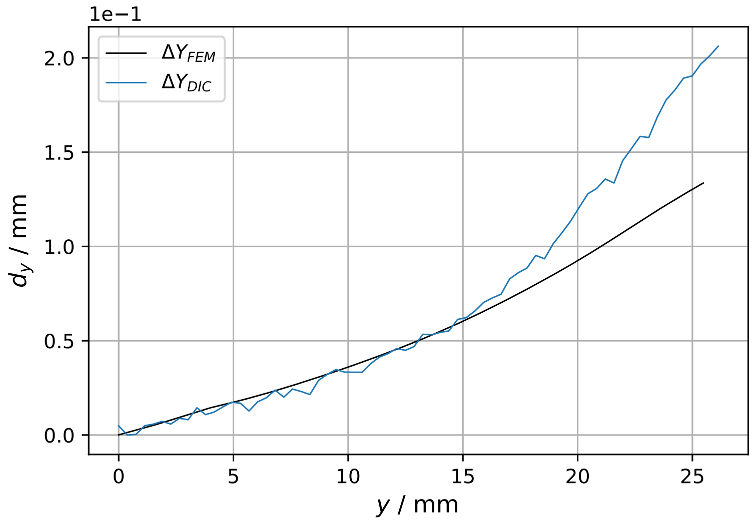


Figure 6.25: Plot of $d_y$ for DIC and FEM results for the *HT1*.

### 6.3.5 Calibration of the DIC Results and FEM Model

The FEM and DIC displacement results showed a similar progression with an offset of the values for the *STD* and *HT1*. The offset of the values was caused by the rigid body motion of the heaters during the thermal expansion of the tooth. For this reason, a script was developed which would offset the values of the DIC results taking in to account the boundary and symmetry conditions of the gear tooth. During the tests, the base of the tooth was attached to the support platform of the Heating System, which restricted the vertical movement. For the mechanical model, the base of the tooth was considered a fixed boundary condition for the $x$ and $y$ axis. The

FEM results show that the $x$ displacement was symmetrical for $x = L_{rack}/2$, which means that the displacement along the axis of symmetry was equal to $d_x \approx 0\,\mathrm{mm}$. Therefore, the DIC result was adjusted so that the $y$ displacement value for $y = 0\,\mathrm{mm}$ was equal to $d_y = 0\,\mathrm{mm}$, and the $x$ displacement value for $x \approx 21.21\,\mathrm{mm}$ was equal to $d_x = 0\,\mathrm{mm}$. The displacement results for the *STD* and *HT1* can be seen in figures 6.26 and 6.27.

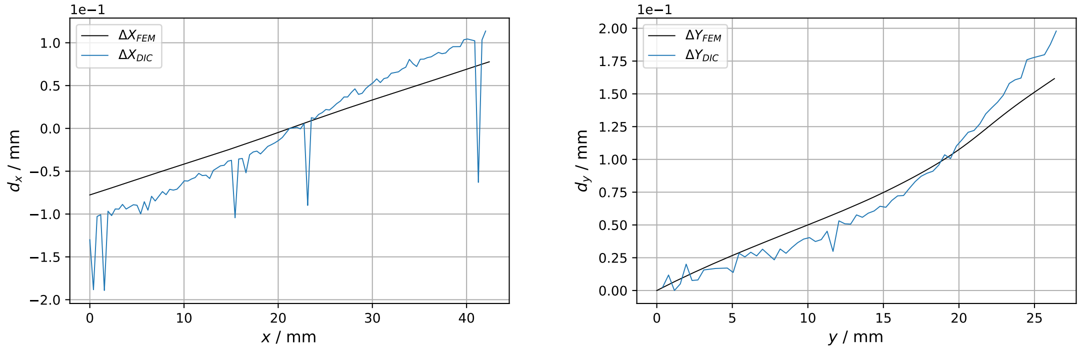


(a) (b)

Figure 6.26: Offset of the DIC results for the *STD*: (a) $d_x$ and (b) $d_y$.

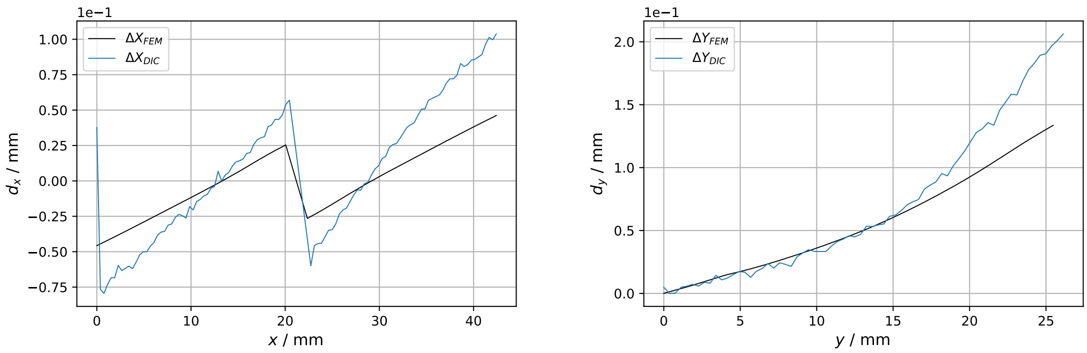


(a) (b)

Figure 6.27: Offset of the DIC results for the *HT1*: (a) $d_x$ and (b) $d_y$.

Once the rigid body motion was corrected, the DIC results showed that the FEM model could accurately predict the thermal expansion for the *STD*. However, the FEM results for the *HT1* still showed a significant displacement difference for the insert region. Figure 6.12 from Chapter 6.3.1.1 showed that the temperature difference for the tooth insert region ($T_{2a}$) was close to zero for $h = 3\,\mathrm{W}/(\mathrm{m}^2\,{}^\circ\mathrm{C})$. Therefore, the convective heat transfer for the surface of the tooth was calibrated and a new FEM analysis was performed. The new displacement results for the FEM model and the DIC measurements can be seen in figures 6.28 and 6.29. If the convective heat transfer equation were implemented in the FEM model as a function of the tooth height, the $y$ displacement results would also follow the same progression as the DIC results. These results showed that a correct calibration of the thermal model directly affects the accuracy of the thermo-mechanical results.

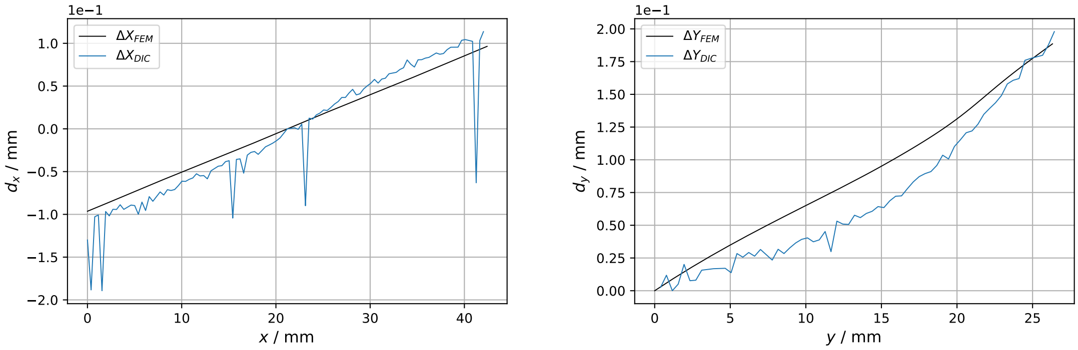


(a) (b)

Figure 6.28: FEM model calibration for the *STD*: (a) $d_x$ and (b) $d_y$.

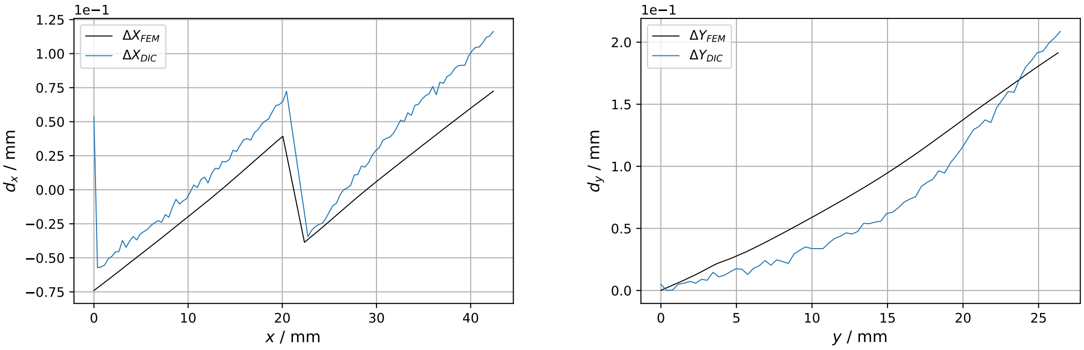


(a) (b)

Figure 6.29: FEM model calibration for the *HT1*: (a) $d_x$ and (b) $d_y$.

### 6.3.6 Comparison of the Thermal Behaviour using FEM Model

Once the FEM model was validated, a comparison of the thermal behaviour of the *STD*, *HT2* (aluminum) and *HT3* (epoxy) was performed. The boundary condition of the thermal model related to the tooth flank surface was adapted for this purpose. For the simulation, a concentrated heat flux ($q_{cf}$) was applied over a line along the tooth flank for $h_{contact}$ = 4.5 mm, which coincided with the positions of the heaters during the thermal tests. The boundary condition for the tooth flank surface is given by Equation 6.4.

$$-k \cdot \frac{\partial T}{\partial n}\bigg|_s = h_s \cdot (T - T_{air}) - q_{cf} \tag{6.4}$$

The purpose of the simulation was to identify the required heat flux to increase the minimum temperature of the tooth to $T_{min}$ = 50°C. A script was developed which would increase the value of the concentrated heat flux until the minimum temperature of the body coincided with $T_{min}$. The results for the necessary power for each tooth, maximum surface temperature and relative change can be found in Table 6.9. The results showed that both hybrid teeth with an insert needed less power than the *STD* to increase the minimum body temperature. The *HT2* (aluminum) required 85.9% less power than the *STD*, and the *HT3* (epoxy) required 63.8% less power. The maximum surface temperature results showed that the *HT2* suffered the lowest temperature increase, followed by the *HT3*. The *STD* showed a maximum surface temperature of $T_{max}$ = 276.5 °C is significantly higher than the melting point of the ER2220®($T_f$ = 165 °C), which means that the tooth can not realistically increase the body temperature to $T_{min}$. These results showed that the hybrid polymer gear design can increase the heat distribution from the tooth to the remainder of the body. The temperature fields from the FEM analysis for the *STD*, *HT2* (aluminum) and *HT3* (epoxy) can be seen in figures 6.30, 6.31 and 6.32, receptively.

Table 6.9: Power output (W), maximum surface temperature (°C) and relative change (%) in relation to *STD*.

| | Power / W | % | $T_{max}$ / °C |
|---|---|---|---|
| *STD* | 0.3306 | - | 276.5 |
| *HT2* | 0.0466 | 85.9 | 88.3 |
| *HT3* | 0.1197 | 63.8 | 139.0 |

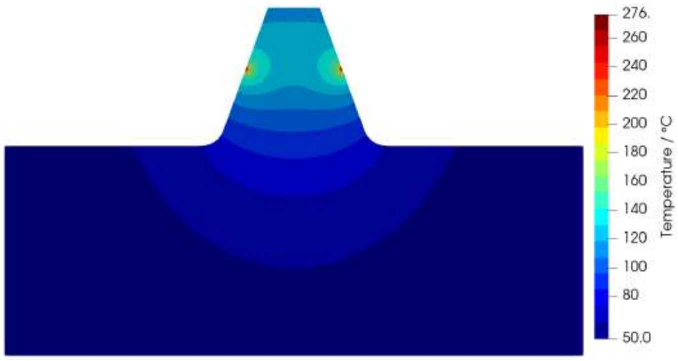


Figure 6.30: Thermal model of *STD* with $q_{cf}$ = 0.3306 W.

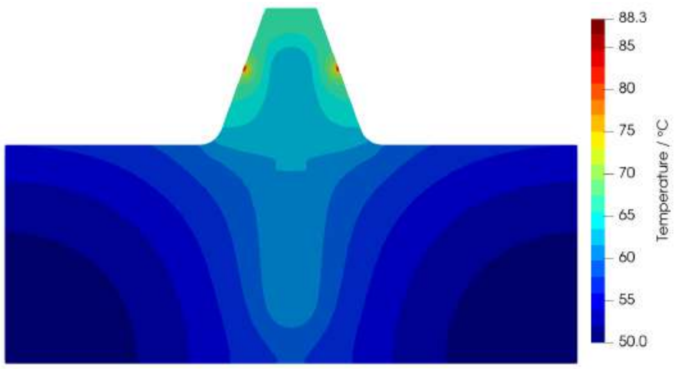


Figure 6.31: Thermal model of *HT2* with $q_{cf}$ = 0.0466 W.

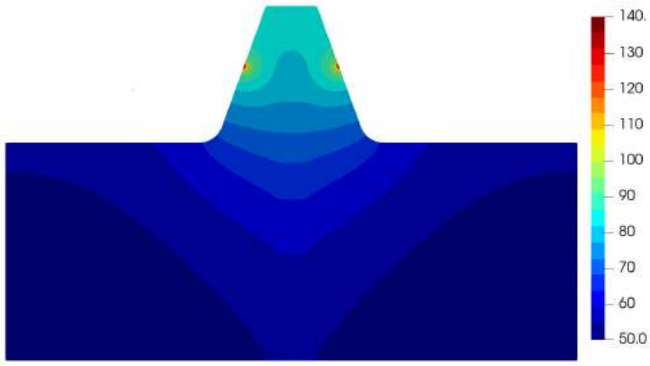


Figure 6.32: Thermal model of *HT3* with $q_{cf}$ = 0.1197 W.

# Chapter 7

# Conclusion and Future Work

## 7.1 Conclusion

This dissertation aimed to study the feasibility of a hybrid polymer gear and validate its concept by developing a heating system capable of simulating the gearing conditions. Additionally, the heating system was used to study the thermo-mechanical behavior of the hybrid gear and validate a pre-existing FEM model. Overall, the key objectives were achieved and the results from the heating system experiments indicated that the hybrid gear design can increase the thermal capabilities of polymer gears.

The thermal tests using the heating system were performed for the standard rack tooth (*STD*), the hybrid rack tooth with no insert (*HT1*), the hybrid rack tooth with an aluminum insert (*HT2*) and finally, for the hybrid rack tooth with an epoxy insert (*HT3*). The results from the *STD* were then used as a reference for the remainder of the tests. The tests were performed with a temperature range of [40; 110] °C and the surface temperature was measured in four predetermined locations.

The results of the pitch point region ($T_{1a}$ and $T_{1b}$) showed an increase in temperature for both *HT2* and *HT3*, which reveal that the hybrid teeth were able to absorb more heat. The tooth root region ($T_{2b}$) suffered a significant temperature increase for the three hybrid teeth. The results of this region showed an average temperature change of 13.7% for the *HT1*, 32.7% for the *HT2* and 19.2% for the *HT3*, indicating that a hybrid polymer gear could be more susceptible to different modes of failure related to the tooth root region. For the insert region ($T_{2a}$), the *HT2* showed a substantial temperature increase of 30.4%, whereas the *HT3* only showed a temperature change of 1.1%. This result indicates that the epoxy insert did not have a significant impact in transferring heat to the remainder of the polymer tooth.

In order to study the cooling phase of the temperature measurements, the Biot number time constant ($b$) was calculated for each experiment. The results showed that the *STD* had a higher rate of decay in temperature compared to the hybrid teeth. Admittedly, considering that the average body temperature of the *STD* was lower than the hybrid teeth, it would take a shorter amount of time to cool down.

In conclusion, the thermal tests revealed that the polymer hybrid gear design is capable of increasing the thermal capabilities of a polymer gear, but only if the thermal conductivity of the insert material is sufficiently high. In order to validate the results, the tests for the *HT2* and *HT3* should be repeated in a second phase.

The DIC tests were performed for the *STD* and *HT1*, with the purpose of measuring the surface displacement caused by thermal expansion. The test was performed once for each tooth and consisted of three temperature stages [40; 70; 100] °C. The displacement field for the $x$ and $y$ direction was more predominant for the $T_{Heater}$=100°C, which allowed for a better comparison of results. That being said, for *HT1* the value for the maximum $x$ displacement was 33.7% lower than the standard tooth, and the value for $y$ displacement was 125% higher. The $x$ displacement field for the *HT1* revealed a significant contraction of the insert region, which could have caused the reduced maximum $x$ displacement value. As a result of the thermal expansion of the insert region, it is plausible to assume that a hybrid tooth with a rigid insert, for example *HT2*, would demonstrate a significant amount of stress for the insert region. Therefore, in a future work a DIC test should be performed for the *HT2* and *HT3* to fully understand the thermo-mechanical behaviour of a hybrid polymer gear.

Finally, the existing FEM model was validated by comparing the results from the thermal and DIC tests. The FEM model showed accurate thermal results for the *STD*, with a maximum relative error of 14.8%, whereas the results for the *HT2* showed a minimum error of 12.3% for the insert region ($T_{2a}$), and a maximum error of 39.4% for the pitch point region ($T_{1b}$). The thermo-mechanical results for the *STD* and *HT* showed accurate results for the $y$ displacements. The $x$ displacement showed a accurate progression along the tooth length, but with a significant offset of the values. When analyzing the images captured during the DIC tests, it is possible to identify a rigid body motion of the heaters due to the thermal expansion. For this reason, the $x$ displacement results of the DIC tests suffered an offset of the values. Therefore, the FEM model can accurately simulate the thermo-mechanical behavior of the hybrid gear when attached to the heating system.

Once the FEM model was validated, a comparison of the thermal behaviour of the *STD*, *HT2* (aluminum) and *HT3* (epoxy) was performed. The purpose of the simulation was to identify the required heat flux to increase the minimum temperature of the tooth to $T_{min}$ = 50°C. The heat flux was applied to the tooth flank in the same location of the heaters during the thermal tests. The results showed that the hybrid teeth with an insert required significantly less power to increase the minimum body temperature. The *HT2* required 85.9% less power than the *STD*, and the *HT3* required 63.8% less power. These results showed that the hybrid polymer gear design can increase the heat distribution.

## 7.2 Future Works

Several topics addressed in this dissertation require further analysis and development:

- Validate the thermal results of the hybrid polymer tooth with a second phase of testing;

- Develop a new test procedure where the Pt100 sensor would measure the body temperature of the base of the tooth, instead of the temperature of the cartridge heater. With this setup it would be possible to quantify and compare the power necessary to raise the body temperature of a hybrid polymer tooth with different insert materials;
- Improve the heating system by reducing the rigid body motion of the heaters caused by thermal expansion;
- Perform the DIC tests for the hybrid polymer gear with the aluminum insert (*HT2*) and the epoxy insert (*HT3*);
- Perform a 3D DIC tests with two cameras to accurately measure the displacements, strain and stress fields for the hybrid polymer gear [20];
- Implement the natural convective heat transfer ($h$) equation as a function of the tooth height ($L_c$) to the FEM model.

# Bibliography


[1] Rocha, Diogo M. P. Bulk Temperature in Polymer-Metal Hybrid Gears, MSc dissertation, Faculdade de Engenharia da Universidade do Porto, 2017.

[2] Carlos M.C.G. Fernandes, Diogo M. P. Rocha, Ramiro C. Martins, Luis Magalhães, and Jorge H.O. Seabra. Finite element method model to predict bulk and flash temperatures on polymer gears. *Tribology International*, 120:255–268, apr 2018.

[3] Moutinho, Mário R. C. Load carrying capacity of polymer-metal hybrid gears, MSc dissertation, Faculdade de Engenharia da Universidade do Porto, 2020.

[4] Khalid Abdulkhaliq M. Alharbi. *The Mechanical Contact Behaviour and Tribology of Polymer Gears*. PhD thesis, The University of Warwick, 2018.

[5] K. Mao, W. Li, C. J. Hooke, and D. Walton. Friction and wear behaviour of acetal and nylon gears. *Wear*, 267(1-4):639–645, 2009.

[6] Carlos M.C.G. Fernandes, Diogo M.P. P. Rocha, Ramiro C. Martins, Luís Magalhães, and Jorge H.O. Seabra. Hybrid Polymer Gear Concepts to Improve Thermal Behavior. *Journal of Tribology*, 141(3):032201, mar 2019.

[7] Vikas Mittal. *Advances in synthesis and properties of engineering polymers*. Number 2003. Elsevier Ltd., 2015.

[8] Kaneda Tanaka. NII-Electronic Library Service. *Chemical Pharmaceutical Bulletin*, 57(534):364–370, 1977.

[9] Verein Deutscher Ingenieure. *VDI 2736 - Part 1*. 2013.

[10] M. Hribersek, M. Erjavec, Gorazd Hlebanja, and Simon Kulovec. Durability testing and characterization of POM gears. *Engineering Failure Analysis*, 124(December 2020):105377, 2021.

[11] Kaneda Tanaka. NII-Electronic Library Service. *Chemical Pharmaceutical Bulletin*, 57(534):364–370, 1977.

[12] B. Trobentar, S. Glodež, and B. Zafošnik. *Gear tooth deflection of spur polymer gears*. Woodhead Publishing Limited, 2014.

[13] Prashant Kumar Singh, Siddhartha, and Akant Kumar Singh. An investigation on the effects of the various techniques over the performance and durability of polymer gears. *Materials Today: Proceedings*, 4(2, Part A):1606–1614, 2017. 5th International Conference of Materials Processing and Characterization (ICMPC 2016).

[14] Hüseyin İmrek. Performance improvement method for nylon 6 spur gears. *Tribology International*, 42(3):503–510, 2009.

[15] Choong Hyun Kim. Durability improvement method for plastic spur gears. *Tribology International*, 39(11):1454–1461, 2006.

[16] Christophe Geuzaine and Jean François Remacle. Gmsh: A 3-D finite element mesh generator with built-in pre- and post-processing facilities. *International Journal for Numerical Methods in Engineering*, 79(11):1309–1331, 2009.

[17] Y.A. Çengel and A.J. Ghajar. *Heat and Mass Transfer: Fundamentals & Applications*. Asia Higher Education Engineering/Computer Science Mechanical Engineering. McGraw Hill Education, 2015.

[18] Vincenzo Vullo. *Gears*, volume 10 of *Springer Series in Solid and Structural Mechanics*. Springer International Publishing, Cham, 2020.

[19] Sindre Nordmark Olufsen, Marius Endre Andersen, and Egil Fagerholt. $\mu$DIC: An open-source toolkit for digital image correlation. *SoftwareX*, 11:100391, 2020.

[20] Valeria Belloni, Roberta Ravanelli, Andrea Nascetti, Martina Di Rita, Domitilla Mattei, and Mattia Crespi. Py2dic: A new free and open source software for displacement and strain measurements in the field of experimental mechanics. *Sensors (Switzerland)*, 19(18):1–19, 2019.

[21] W. S. LePage, J. A. Shaw, and S. H. Daly. Optimum Paint Sequence for Speckle Patterns in Digital Image Correlation. *Experimental Techniques*, 41(5):557–563, 2017.

## Appendix A

# KISSsoft Report Document

File

Name : Rack
Changed by: jamie on: 05.02.2021 at: 17:00:01

**Important hint: At least one warning has occurred during the calculation:**

1-> Gear 1:
The specific sliding at the root [zetaf] is less than -3.00.

2-> The speed is 0.
The predefined service life is not taken into account.
The calculation is performed with a load cycle.

3-> Small line loads [w]:
The calculation of tooth contact stiffness [cg] is very uncertain.
It could result inaccurate, high values for dynamic factor [Kv],
face load factor [KHβ] and transverse load factor [KHα].
We recommend to enter these values directly
(for example Kv=1.0, KHβ=1.5, KHα=1.0)
and to use a more accurate method for the calculation of cg
(see 'Tooth contact stifness' in 'Details' of resistance window).

4-> Mesh gear 1 - 2:
The face load coefficient is very high.
The formulas for the calculation according ISO or DIN sometimes results
in values that are too high. We recommend that you use the
KISSsoft shaft module to calculate KHβ more accurate.

5-> The circumferential speed is very low!
This causes the following:
The lubrication is no longer guaranteed.
Long term wear can occur.
The calculation is not intended for this case!

6-> Calculation of scuffing:
The entered gear pair data is outside the boundary of the calculation method!

The application of ISO/TS 6336-21 has following limitations:
wBt (=109.1 N/mm) >= 150.0 N/mm
1.0 m/s <= v(=0.0 m/s) <= 50.0 m/s

## Rack calculation (cylindrical gear)

Drawing or article number:
Gear 1: 0.000.0
Gear 2: 0.000.0

Calculation method ISO 6336:2019

| | | ---- Pinion ---------- Rack - |
|---|---|---|
| Power (W) | [P] | 0.000 |
| Speed (1/min) | [n] | 0.0 |
| Torque (Nm) | [T] | 10.0 |
| Application factor | [KA] | 1.25 |
| Required service life (h) | [H] | 20000.00 |
| Gear driving (+) / driven (-) | | + - |
| Working flank gear 1: | Right flank | |
| Gear 1 direction of rotation: | Clockwise | |

**Tooth geometry and material**

Geometry calculation according to ISO 21771:2007

| | | ---- Pinion | ---------- Rack - |
|---|---|---|---|
| Running center distance (mm) | [a] | 82.318 | |
| Center distance tolerance | ISO 286:2010 Measure js7 | | |
| Rack height (mm) | [Hz] | 50.000 | |
| Normal module (mm) | [mn] | 4.5000 | |
| Normal pressure angle (°) | [αn] | 20.0000 | |
| Helix angle at reference circle (°) | [β] | 0.0000 | |
| Number of teeth | [z] | 16 | 2.9790 |
| Rack length (mm) | [l] | 42.111 | |
| Facewidth (mm) | [b] | 14.00 | 14.00 |
| Hand of gear | Spur gear | | |
| Accuracy grade | [Q-ISO 1328:2013] | A6 | A6 |
| Inner diameter (mm) | [di] | 0.00 | |
| Inner diameter of gear rim (mm) | [dbi] | 0.00 | |

Material

Gear1
18CrNiMo7-6, Case-carburized steel, case-hardened
ISO 6336-5 Figure 9/10 (MQ), Core hardness >=25HRC Jominy J=12mm<HRC28

Gear2
18CrNiMo7-6, Case-carburized steel, case-hardened
ISO 6336-5 Figure 9/10 (MQ), Core hardness >=25HRC Jominy J=12mm<HRC28

| | | ------- Gear 1 | -------- Gear 2 -- |
|---|---|---|---|
| Surface hardness | | HRC 61 | HRC 61 |
| Material treatment according to ISO 6336:2006 Normal, life factors ZNT and YNT >=0.85 | | | |
| Fatigue strength. tooth root stress (N/mm²) | [σFlim] | 430.00 | 430.00 |
| Fatigue strength for Hertzian pressure (N/mm²) | [σHlim] | 1500.00 | 1500.00 |
| Tensile strength (N/mm²) | [σB] | 1200.00 | 1200.00 |
| Yield point (N/mm²) | [σS] | 850.00 | 850.00 |
| Young's modulus (N/mm²) | [E] | 206000 | 206000 |
| Poisson's ratio | [ν] | 0.300 | 0.300 |
| Roughness average value DS, flank (µm) | [RAH] | 0.60 | 0.60 |
| Roughness average value DS, root (µm) | [RAF] | 3.00 | 3.00 |
| Mean roughness height, Rz, flank (µm) | [RZH] | 4.80 | 4.80 |
| Mean roughness height, Rz, root (µm) | [RZF] | 20.00 | 20.00 |

Gear reference profile
1:

| | | |
|---|---|---|
| Reference profile | 1.25 / 0.38 / 1.0 ISO 53:1998 Profil A | |
| Dedendum coefficient | [hfP*] | 1.250 |
| Root radius factor | [ρfP*] | 0.380 (ρfPmax*=0.472) |
| Addendum coefficient | [haP*] | 1.000 |
| Tip radius factor | [ρaP*] | 0.000 |
| Protuberance height coefficient | [hprP*] | 0.000 |
| Protuberance angle | [αprP] | 0.000 |
| Tip form height coefficient | [hFaP*] | 0.000 |
| Ramp angle | [αKP] | 0.000 |
| | not topping | |

Gear reference profile
2:

| | | |
|---|---|---|
| Reference profile | 1.25 / 0.38 / 1.0 ISO 53:1998 Profil A | |
| Dedendum coefficient | [hfP*] | 1.250 |
| Root radius factor | [ρfP*] | 0.380 (ρfPmax*=0.472) |
| Addendum coefficient | [haP*] | 1.000 |
| Tip radius factor | [ρaP*] | 0.000 |
| Protuberance height coefficient | [hprP*] | 0.000 |
| Protuberance angle | [αprP] | 0.000 |
| Tip form height coefficient | [hFaP*] | 0.000 |
| Ramp angle | [αKP] | 0.000 |
| | not topping | |

**Information on final machining**

| | | | |
|---|---|---|---|
| Dedendum reference profile | [hfP*] | 1.250 | 1.250 |
| Tooth root radius Refer. profile | [ρfP*] | 0.380 | 0.380 |

| | | | |
|---|---|---|---|
| Addendum Reference profile | [haP*] | 1.000 | 1.000 |
| Protuberance height coefficient | [hprP*] | 0.000 | 0.000 |
| Protuberance angle (°) | [αprP] | 0.000 | 0.000 |
| Tip form height coefficient | [hFaP*] | 0.000 | 0.000 |
| Ramp angle (°) | [αKP] | 0.000 | 0.000 |

| | | |
|---|---|---|
| Type of profile modification: | none (only running-in) | |
| Tip relief by running in (μm) | [Ca L/R] | 2.0 / 2.0 2.0 / 2.0 |

| | | |
|---|---|---|
| Lubrication type | Oil bath lubrication | |
| Type of oil | ISO-VG 220 | |
| Lubricant base | Mineral-oil base | |
| Oil nominal kinematic viscosity at 40°C (mm²/s) | [ν40] | 220.00 |
| Oil nominal kinematic viscosity at 100°C (mm²/s) | [ν100] | 17.50 |
| Specific density at 15°C (kg/dm³) | [ρ] | 0.895 |
| Oil temperature (°C) | [TS] | 70.000 |

| | | ---- Pinion ---------- | Rack - |
|---|---|---|---|
| Transverse module (mm) | [mt] | 4.500 | |
| Transverse pressure angle (°) | [αt] | 20.000 | |
| Working pressure angle (°) | [αwt] | 20.000 | |
| Working pressure angle at normal section (°) | [αwn] | 20.000 | |
| Helix angle at operating pitch circle (°) | [βw] | 0.000 | |
| Base helix angle (°) | [βb] | 0.000 | |
| Sum of profile shift coefficients | [Σxi] | 0.1817 | |
| Profile shift coefficient | [x] | 0.1817 | 0.0000 |
| Tooth thickness, arc, in module | [sn*] | 1.7031 | 1.5708 |
| | | | |
| Tip alteration (mm) | [k*mn] | 0.000 | 0.000 |
| Reference diameter (mm) | [d] | 72.000 | 45.500 |
| Base diameter (mm) | [db] | 67.658 | |
| Tip diameter (mm) | [da,Hz] | 82.635 | 50.000 |
| (mm) | [da,Hz.e/i] | 82.635 / 82.600 | |
| (mm) | [da,Hz.e/i] | | 50.000 / 50.000 |
| Tip diameter allowances (mm) | [Ada,AHz.e/i] | 0.000 / -0.035 | |
| Tip diameter allowances (mm) | [Ada,AHz.e/i] | | 0.000 / 0.000 |
| Tip form diameter (mm) | [dFa] | 82.635 | 50.000 |
| (mm) | [dFa.e/i] | 82.635 / 82.600 | |
| (mm) | [dFa.e/i] | | 50.000 / 50.000 |
| Active tip diameter (mm) | [dNa.e/i] | 82.635 / 82.600 | |
| Active tip diameter (mm) | [dNa.e/i] | | 50.000 / 50.000 |
| Operating pitch diameter (mm) | [dw] | 72.000 | 46.319 |
| Root diameter (mm) | [df] | 62.385 | 39.875 |
| Generating Profile shift coefficient | [xE.e/i] | 0.1603/ 0.1481 | |
| Generating Profile shift coefficient | [xE.e/i] | | -0.0214/ -0.0336 |
| Generated root diameter with xE (mm) | [df.e/i] | 62.193 / 62.083 | |
| Generated root diameter with xE (mm) | [df.e/i] | | 39.779 / 39.724 |
| Theoretical tip clearance (mm) | [c] | 1.125 | 1.125 |
| Effective tip clearance (mm) | [c.e/i] | 1.311 / 1.204 | |
| Effective tip clearance (mm) | [c.e/i] | | 1.294 / 1.204 |
| Active root diameter (mm) | [dNf] | 67.727 | 42.414 |
| (mm) | [dNf.e/i] | 67.732 / 67.723 | |
| (mm) | [dNf.e/i] | | 42.442 / 42.396 |
| Root form diameter (mm) | [dFf] | 67.729 | 41.398 |
| (mm) | [dFf.e/i] | 67.705 / 67.694 | |
| (mm) | [dFf.e/i] | | 41.301 / 41.246 |
| Reserve (dNf-dFf)/2 (mm) | [cF.e/i] | 0.019 / 0.009 | |
| Reserve (dNf-dFf)/2 (mm) | [cF.e/i] | | 1.195 / 1.095 |
| Addendum, mn * (haP*+x)(mm) | [ha] | 5.318 | 4.500 |
| (mm) | [ha.e/i] | 5.318 / 5.300 | |
| (mm) | [ha.e/i] | | 4.500 / 4.500 |
| Dedendum mn * (hfP*-x) (mm) | [hf] | 4.807 | 5.625 |
| (mm) | [hf.e/i] | 4.904 / 4.958 | |
| (mm) | [hf.e/i] | | 5.721 / 5.776 |
| Roll angle at dFa (°) | [ξdFa.e/i] | 40.178 / 40.127 | |
| Roll angle to dNa (°) | [ξdNa.e/i] | 40.178 / 40.127 | |
| Roll angle to dNf (°) | [ξdNf.e/i] | 2.686 / 2.513 | |
| Roll angle at dFf (°) | [ξdFf.e/i] | 2.144 / 1.872 | |
| Tooth height (mm) | [h] | 10.125 | 10.125 |
| Virtual gear no. of teeth | [zn] | 16.000 | |
| Normal tooth thickness at tip circle (mm) | [san] | 2.616 | 3.793 |
| (mm) | [san.e/i] | 2.559 / 2.490 | |

| | | | |
|---|---|---|---|
| (mm) | [san.e/i] | | 3.723 / 3.683 |
| Normal space width at root circle (mm) | [efn] | 0.000 | 2.974 |
| (mm) | [efn.e/i] | 0.000 / 0.000 | |
| (mm) | [efn.e/i] | | 2.958 / 2.949 |
| Max. sliding velocity at tip (m/s) | [vga] | 0.000 | 0.000 |
| Specific sliding at the tip | [ζa] | 0.480 | 0.875 |
| Specific sliding at the root | [ζf] | -7.006 | -0.924 |
| Sliding factor on tip | [Kga] | 0.316 | 0.299 |
| Sliding factor on root | [Kgf] | -0.299 | -0.316 |
| Pitch on reference circle (mm) | [pt] | 14.137 | |
| Base pitch (mm) | [pbt] | 13.285 | |
| Transverse pitch on contact-path (mm) | [pet] | 13.285 | |
| Length of path of contact (mm) | [ga, e/i] | 22.188 ( 22.239 / 22.106 ) | |
| Length T1-A (mm) | [T1A] | 1.535 ( 1.483 / 1.586 ) | |
| Length T1-B (mm) | [T1B] | 10.438 ( 10.438 / 10.407 ) | |
| Length T1-C (mm) | [T1C] | 12.308 ( 12.308 / 12.308 ) | |
| Length T1-D (mm) | [T1D] | 14.819 ( 14.768 / 14.870 ) | |
| Length T1-E (mm) | [T1E] | 23.722 ( 23.722 / 23.692 ) | |
| Diameter of single contact point B (mm) | [d-B] | 70.805 ( 70.805 / 70.787 ) | |
| Diameter of single contact point D (mm) | [d-D] | 73.865 ( 73.824 / 73.906 ) | |

| | | |
|---|---|---|
| Transverse contact ratio | [εα] | 1.670 |
| Transverse contact ratio with allowances | [εα.e/m/i] | 1.674 /1.669 /1.664 |
| Overlap ratio | [εβ] | 0.000 |
| Total contact ratio | [εγ] | 1.670 |
| Total contact ratio with allowances | [εγ.e/m/i] | 1.674 /1.669 /1.664 |

**General influence factors**

| | | ---- Pinion ---------- Rack - |
|---|---|---|
| Nominal circum. force at pitch circle (N) | [Ft] | 277.8 |
| Axial force (N) | [Fa] | 0.0 |
| Radial force (N) | [Fr] | 101.1 |
| Normal force (N) | [Fnorm] | 295.6 |
| Nominal circumferential force per mm (N/mm) | [w] | 19.84 |
| Only as information: Forces at operating pitch circle: | | |
| Nominal circumferential force (N) | [Ftw] | 277.8 |
| Axial force (N) | [Faw] | 0.0 |
| Radial force (N) | [Frw] | 101.1 |
| Circumferential speed reference circle (m/s) | [v] | 0.00 |
| Circumferential speed operating pitch circle (m/s) | [v(dw)] | 0.00 |

| | | |
|---|---|---|
| Running-in value (μm) | [yp] | 0.7 |
| Running-in value (μm) | [yf] | 0.8 |
| Correction factor | [CM] | 0.800 |
| Gear blank factor | [CR] | 1.000 |
| Basic rack factor | [CBS] | 0.975 |
| Material coefficient | [E/Est] | 1.000 |
| Singular tooth stiffness (N/mm/μm) | [c'] | 10.093 |
| Meshing stiffness (N/mm/μm) | [cγα] | 15.166 |
| Meshing stiffness (N/mm/μm) | [cγβ] | 12.891 |
| The formula for c' and cγ at w*KA < 25 N/mm is imprecise! | | |
| c' and cγ are calculated using w*KA = 25 N/mm. | | |
| Reduced mass (kg/mm) | [mRed] | 0.01856 |
| Resonance speed (min-1) | [nE1] | 17060 |
| Resonance ratio (-) | [N] | 0.000 |
| Subcritical range | | |
| Running-in value (μm) | [yα] | 0.7 |
| Bearing distance l of pinion shaft (mm) | [l] | 28.000 |
| Distance s of pinion shaft (mm) | [s] | 2.800 |
| Outside diameter of pinion shaft (mm) | [dsh] | 14.000 |
| Load in accordance with Figure 13, ISO 6336-1:2006 | [-] | 4 |
| 0:a), 1:b), 2:c), 3:d), 4:e) | | |
| Coefficient K' according to Figure 13, ISO 6336-1:2006 | [K'] | -1.00 |
| Without stiffening | | |
| Tooth trace deviation (active) (μm) | [Fβy] | 9.10 |
| from deformation of shaft (μm) | [fsh*B1] | 0.22 |
| fsh (μm) =0.22, B1= 1.00, fHβ5 (μm) = 11.00 | | |
| Tooth without tooth trace modification | | |
| Position of contact pattern: | | favorable |
| from production tolerances (μm) | [fma*B2] | 11.31 |

102
B2=
1.00

| | | | |
|---|---|---|---|
| Tooth trace deviation, theoretical (µm) | [Fβx] | 10.71 | |
| Running-in value (µm) | [yβ] | 1.61 | |
| Dynamic factor | [Kv] | 1.000 | |
| Face load factor - flank | [KHβ] | 3.076 | |
| - Tooth root | [KFβ] | 2.177 | |
| - Scuffing | [KBβ] | 3.076 | |
| Transverse load factor - flank | [KHα] | 1.288 | |
| - Tooth root | [KFα] | 1.431 | |
| - Scuffing | [KBα] | 1.431 | |
| Number of load cycles (in mio.) | [NL] | 0.000 | 0.000 |
| Rack length (mm) | [l] | 42.111 | |

**Tooth root load capacity**

Calculation of Tooth form coefficients according method: B
Internal toothing: Calculation of ρF and sFn according to ISO 6336-3:2007-04-01
Internal toothing: Calculation of YF, YS with pinion type cutter, z0= 50 , x0=0.000 , ρaP0*= 0.380

| | | ---- Pinion | ---------- Rack - |
|---|---|---|---|
| Calculated with generating profile shift coefficient | [xE.i] | 0.1481 | -0.0336 |
| Tooth form factor | [YF] | 1.44 | 1.27 |
| Stress correction factor | [YS] | 1.94 | 2.36 |
| Load application angle (°) | [αFen] | 18.23 | 20.00 |
| Coefficient | [fε] | 1.000 | |
| Diameter, height at point of load application (mm) | [den(hen)] | 73.865 | 46.959 |
| Bending moment arm (mm) | [hF] | 4.10 | 5.29 |
| Tooth thickness at root (mm) | [sFn] | 8.81 | 10.61 |
| Tooth root radius (mm) | [ρF] | 2.39 | 1.71 |
| Bending moment arm (-) | [hF/mn] | 0.911 | 1.175 |
| Tooth thickness at root (-) | [sFn/mn] | 1.958 | 2.357 |
| Tooth root radius (-) | [ρF/mn] | 0.530 | 0.380 |
| Calculation cross section diameter (mm) | [$d_{sFn}$/$h_{sFn}$] | 63.648 | 40.579 |
| Tangents on calculation cross section (°) | [$α_{sFn}$] | 30.000 | 30.000 |
| Notch parameter | [$q_s$] | 1.847 | 3.102 |
| Helix angle factor | [Yβ] | 1.000 | |
| Deep tooth factor | [YDT] | 1.000 | |
| Gear rim factor | [YB] | 1.00 | 1.00 |
| Effective facewidth (mm) | [beff] | 14.00 | 14.00 |
| Nominal stress at tooth root (N/mm²) | [σF0] | 12.30 | 13.21 |
| Tooth root stress (N/mm²) | [σF] | 47.87 | 51.42 |
| Permissible bending stress at root of Test-gear | | | |
| Notch sensitivity factor | [YdrelT] | 0.972 | 1.159 |
| Surface factor | [YRrelT] | 1.000 | 1.000 |
| Size factor, tooth root | [YX] | 1.000 | 1.000 |
| Finite life factor | [YNT] | 2.500 | 2.500 |
| $Y_C*Y_{drelT}*Y_{RrelT}*Y_X*Y_{NT}$ | | 2.430 | 2.898 |
| Alternating bending factor, mean stress influence coefficient | [YM] | 1.000 | 1.000 |
| Stress correction factor | [Yst] | 2.00 | |
| Yst*σFlim (N/mm²) | [σFE] | 860.00 | 860.00 |
| Permissible tooth root stress σFG/SFmin (N/mm²) | [σFP] | 1492.54 | 1780.19 |
| Limit strength tooth root (N/mm²) | [σFG] | 2089.56 | 2492.27 |
| Required safety | [SFmin] | 1.40 | 1.40 |
| Safety for tooth root stress | [SF=σFG/σF] | 43.65 | 48.47 |
| Transmittable power (W) | [WRating] | 0.00 | 0.00 |

**Flank safety**

| | | ---- Pinion | ---------- Rack - |
|---|---|---|---|
| Zone factor | [ZH] | 2.495 | |

| | | | |
|---|---|---|---|
| Elasticity factor ($\sqrt{N/mm^2}$) | [ZE] | 189.812 | |
| Contact ratio factor | [Zε] | 0.881 | |
| Helix angle factor | [Zβ] | 1.000 | |
| Effective facewidth (mm) | [beff] | 14.00 | |
| Nominal contact stress (N/mm$^2$) | [σH0] | 218.87 | |
| Contact stress at operating pitch circle (N/mm$^2$) | [σHw] | 487.01 | |
| Single tooth contact factor | [ZB,ZD] | 1.09 | 1.00 |
| Contact stress (N/mm$^2$) | [σHB, σHD] | 528.92 | 487.01 |

| | | | |
|---|---|---|---|
| Lubrication factor for NL | [ZL] | 1.000 | 1.000 |
| Speed factor for NL | [ZV] | 1.000 | 1.000 |
| Roughness factor for NL | [ZR] | 1.000 | 1.000 |
| Material hardening factor for NL | [ZW] | 1.000 | 1.000 |
| Finite life factor | [ZNT] | 1.600 | 1.600 |
| | [ZL*ZV*ZR*ZNT] | 1.600 | 1.600 |
| Limited pitting is permitted: No | | | |
| Size factor (flank) | [ZX] | 1.000 | 1.000 |
| Permissible contact stress, σHG/SHmin (N/mm$^2$) | [σHP] | 2400.00 | 2400.00 |
| Pitting stress limit (N/mm$^2$) | [σHG] | 2400.00 | 2400.00 |
| Required safety | [SHmin] | 1.00 | 1.00 |
| Safety factor for contact stress at operating pitch circle | [SHw] | 4.93 | 4.93 |
| Safety against pressure, σHG/σHBD Single contact | [SHBD] | 4.54 | 4.93 |
| Safety regarding transmittable torque | [(SHBD)^2] | 20.59 | 24.29 |
| Transmittable power (W) | [WRating] | 0.00 | 0.00 |

**Micropitting according to** **ISO/TS 6336-22:2018**

Calculation has not been carried out, lubricant: Load stage micropitting test not known

**Scuffing load capacity**

Calculation method according to ISO/TS 6336-20/21:2017

| | | | |
|---|---|---|---|
| Helical load factor for scuffing | [KBγ] | 1.000 | |
| Lubrication coefficient for lubrication type | [XS] | 1.000 | |
| Scuffing test and load stage | [FZGtest] FZG - Test A / 8.3 / 90 (ISO 14635 - 1) | 12 | |
| Multiple meshing factor | [Xmp] | 1.000 | |
| Relative structural factor, scuffing | [XWrelT] | 1.000 | |
| Thermal contact factor (N/mm/s^.5/K) | [BM] | 13.780 | 13.780 |
| Relevant tip relief (µm) | [Ca] | 2.00 | 2.00 |
| Optimal tip relief (µm) | [Ceff] | 2.46 | |
| Ca taken as optimal in the calculation (0=no, 1=yes) | | 1 | 1 |
| Effective facewidth (mm) | [beff] | 14.000 | |
| Applicable circumferential force/facewidth (N/mm) | [wBt] | 109.132 | |
| KBγ = 1.000 , wBt*KBγ =109.132 | | | |
| Angle factor | [Xαβ] | 0.977 | |
| ε1: 0.859 , ε2: 0.811 | | | |

Flash temperature-criteria

| | | | |
|---|---|---|---|
| Lubricant factor | [XL] | 0.830 | |
| Tooth mass temperature (°C) | [θMi] | 70.01 | |
| θMi = θoil + XS*0.47*Xmp*θflm | | | |
| Average flash temperature | (°C) | [θflm] 0.03 | |
| Scuffing temperature (°C) | [θS] | 348.80 | |
| Γ coordinates (point of highest temperature) | [Γ] | -0.548 | |
| [Γ.A]= -0.875 [Γ.E]= 0.927 | | | |
| Highest contact temp. (°C) | [θB] | 70.06 | |
| Flash factor (°K*N^-.75*s^.5*m^-.5*mm) | [XM] | 50.058 | |
| Approach factor | [XJ] | 1.000 | |
| Load sharing factor | [XΓ] | 0.453 | |
| Dynamic viscosity (mPa*s) | [ηM] | 41.90 | ( 70.0 °C) |
| Coefficient of friction | [$\mu_m$] | 1.239 | |
| Required safety | [SBmin] | 2.000 | |
| Margin of safety for scuffing, flash temperature | [SB] | 4689.322 | |

Integral temperature-criteria

| | | |
|---|---|---|
| Lubricant factor | [XL] | 1.000 |
| Tooth mass temperature (°C) | [θMC] | 70.03 |

θMC = θoil + XS*0.70*θflaint

| | | | |
|---|---|---|---|
| Mean flash temperature | (°C) | [θflaint] | 0.05 |
| Integral scuffing temperature (°C) | [θSint] | | 360.78 |
| Flash factor (°K*N^-.75*s^.5*m^-.5*mm) | [XM] | | 50.058 |
| Running-in factor, well run in | [XE] | | 1.000 |
| Contact ratio factor | [Xε] | | 0.248 |
| Dynamic viscosity (mPa*s) | [ηOil] | | 41.90 ( 70.0 °C) |
| Mean coefficient of friction | [μm] | | 1.240 |
| Geometry factor | [XBE] | | 0.792 |
| Meshing factor | [XQ] | | 1.000 |
| Tip relief factor | [XCa] | | 1.730 |
| Integral tooth flank temperature (°C) | [θint] | | 70.11 |
| Required safety | [SSmin] | | 1.800 |
| Safety factor for scuffing (intg.-temp.) | [SSint] | | 5.146 |
| Safety referring to transmittable torque | [SSL] | | 290.776 |

**Measurements for tooth thickness**

| | | ---- Pinion | ---------- Rack - | |
|---|---|---|---|---|
| Tooth thickness tolerance | | DIN 3967 cd25 | DIN 3967 cd25 | |
| Tooth thickness allowance (normal section) (mm) | [As.e/i] | -0.070 / | -0.110-0.070 / | -0.110 |
| | | | | |
| Number of teeth spanned | [k] | 3.000 | | |
| For internal toothing: k = measurement gap number | | | | |
| Base tangent length (no backlash) (mm) | [Wk] | 34.779 | | |
| Base tangent length with allowance (mm) | [Wk.e/i] | 34.713 / | 34.676 | |
| (mm) | [ΔWk.e/i] | -0.066 / | -0.103 | |
| Diameter of measuring circle (mm) | [dMWk.m] | 76.035 | | |
| | | | | |
| Theoretical diameter of ball/pin (mm) | [DM] | 8.300 | 8.749 | |
| Effective diameter of ball/pin (mm) | [DMeff] | 9.000 | 9.000 | |
| Radial single-ball measurement backlash free (mm) | [MrK] | 43.848 | 53.447 | |
| Radial single-ball measurement (mm) | [MrK.e/i] | 43.783 / | 43.746 53.351 / | 53.296 |
| Diameter of measuring circle (mm) | [dMMr.m] | 74.366 | | |
| Diametral measurement over two balls without clearance (mm) | [MdK] | 87.696 | | |
| Diametral two ball measure (mm) | [MdK.e/i] | 87.567 / | 87.493 | |
| Diametral measurement over pins without clearance (mm) | [MdR] | 87.696 | | |
| Measurement over pins according to DIN 3960 (mm) | [MdR.e/i] | 87.567 / | 87.493 | |
| Measurement over 3 pins, axial, according to AGMA 2002 (mm) | | | | |
| | [dk3A.e/i] | 87.567 / | 87.493 | |
| | | | | |
| Chordal tooth thickness (no backlash) (mm) | [sc] | 7.649 | 7.069 | |
| Normal chordal tooth thickness with allowance (mm) | [sc.e/i] | 7.582 / | 7.543 6.999 / | 6.959 |
| Reference chordal height from da.m (mm) | [ha] | 5.513 | 4.500 | |
| Tooth thickness, arc (mm) | [sn] | 7.664 | 7.069 | |
| (mm) | [sn.e/i] | 7.594 / | 7.554 6.999 / | 6.959 |
| | | | | |
| Backlash free center distance (mm) | [aControl.e/i] | 82.125 / | 82.015 | |
| Backlash free center distance, allowances (mm) | [jta] | 0.192 / | 0.302 | |
| Tip clearance (mm) | [c0.i(aControl)] | 0.919 | 0.919 | |
| Center distance allowances (mm) | [Aa.e/i] | -0.018 / | 0.018 | |
| | | | | |
| Circumferential backlash from Aa (mm) | [jtw_Aa.e/i] | 0.013 / | -0.013 | |
| Radial backlash (mm) | [jrw.e/i] | 0.320 / | 0.175 | |
| Circumferential backlash (transverse section) (mm) | [jtw.e/i] | 0.233 / | 0.127 | |
| Normal backlash (mm) | [jn.e/i] | 0.219 / | 0.120 | |
| Torsional angle with rack fixed: | | | | |
| Total torsional angle (°) | [j.tSys] | 0.0007/ | 0.0004 | |

**Toothing tolerances**

---- Pinion ---------- Rack -

According to ISO 1328-1:2013, ISO 1328-2:1997
One or several gear data (mn, b, z or d) lay beyond the limits covered by the standard.
Tolerances are calculated following the formulae of the standard.
The values are outside of the range of validity!

| | | | |
|---|---|---|---|
| Accuracy grade | [Q] | A6 | A6 |
| Single pitch deviation (μm) | [fptT] | 9.50 | 9.50 |
| Base circle pitch deviation (μm) | [fpbT] | 9.10 | 9.10 |
| Sector pitch deviation over k/8 pitches (μm) | [Fpk/8T] | 19.00 | 19.00 |

| | | | | |
|---|---|---|---|---|
| Profile form deviation (μm) | [ffαT] | | 11.00 | 11.00 |
| Profile slope deviation (μm) | [fHαT] | | 8.50 | 8.50 |
| Total profile deviation (μm) | [FαT] | | 13.00 | 13.00 |
| Helix form deviation (μm) | [ffβT] | | 9.00 | 9.00 |
| Helix slope deviation (μm) | [fHβT] | | 8.00 | 8.00 |
| Total helix deviation (μm) | [FβT] | | 12.00 | 12.00 |
| Total cumulative pitch deviation (μm) | [FpT] | | 28.00 | 28.00 |
| Adjacent pitch difference (μm) | [fuT] | | 14.00 | 14.00 |
| Runout (μm) | [FrT] | | 25.00 | 25.00 |
| Single flank composite, total (μm) | [FisT] | | 38.00 | 38.00 |
| Single flank composite, tooth-to-tooth | (μm) | [fisT] | 9.50 | 9.50 |
| Radial composite, total (μm) | [FidT] | | 44.00 | 44.00 |
| Radial composite, tooth-to-tooth (μm) | [fidT] | | 22.00 | 22.00 |

FidT (Fi''), fidT (fi'') according to ISO 1328:1997 calculated with the geometric mean values for mn and d

Rack tolerances calculated according to DIN 3961:1978 with number of teeth and pinion reference circle

Axis alignment tolerances (recommendation acc. to ISO TR 10064-3:1996, Quality)
6

| | | | | | |
|---|---|---|---|---|---|
| Maximum value for deviation error of axis (μm) | [fΣβ] | 34.00 | (Fβ= | 34.00 | ) |
| Maximum value for inclination error of axes (μm) | [fΣδ] | 68.00 | | | |

**Modifying and defining the tooth form**

Data for the tooth form calculation :

**Calculation of Pinion**
Tooth form, Pinion, Step 1: Automatic (final machining)
haP*= 1.026, hfP*= 1.250, ρfP*= 0.380

**Calculation of Rack**
Tooth form, Rack, Step 1: Automatic (final machining)
haP*= 1.027, hfP*= 1.250, ρfP*= 0.380

**Supplementary data**

Torsional stiffness at driving gear with fixed driven gear:

| | | |
|---|---|---|
| Torsional stiffness (MNm/rad) | [cr] | 0.207 |
| Torsion when subjected to nominal torque (°) | [δcr] | 0.003 |
| Mean coefficient of friction (as defined in Niemann) | [$\mu_m$] | 0.080 |
| Wear sliding coef. by Niemann | [ζw] | 1.122 |
| Loss factor | [HV] | 0.142 |
| Gear power loss (W) | [PVZ] | 0.000 |

**Service life, damage**

Could not be calculated.

**Remarks:**
- Specifications with [.e/i] imply: Maximum [e] and minimum value [i] for
  Taking all tolerances into account
  Specifications with [.m] imply: Mean value within tolerance
- For the backlash tolerance, the center distance tolerances and the tooth thickness allowance
are taken into account.
The maximum and minimum clearance according to
the largest or smallest allowances are defined..
  The calculation is performed for the operating pitch circle.
- Details of calculation method:
  cγ according to Method B
  Kv according to Method B
  KHβ and KFβ according to Method C
  fmα according to Equation 64, fsh according to 57/58, Fβx according to 52/53/54
  KHα, KFα according to Method B
- The logarithmically interpolated value taken from the values for the fatigue strength and the static strength, based on the number of load

cycles, is used for coefficients ZL, ZV, ZR, ZW, ZX, YdrelT, YRrelT and YX..

| | | |
|---|---|---|
| End of Report | lines: | 531 |

## Appendix B

# Heating System Technical Drawings

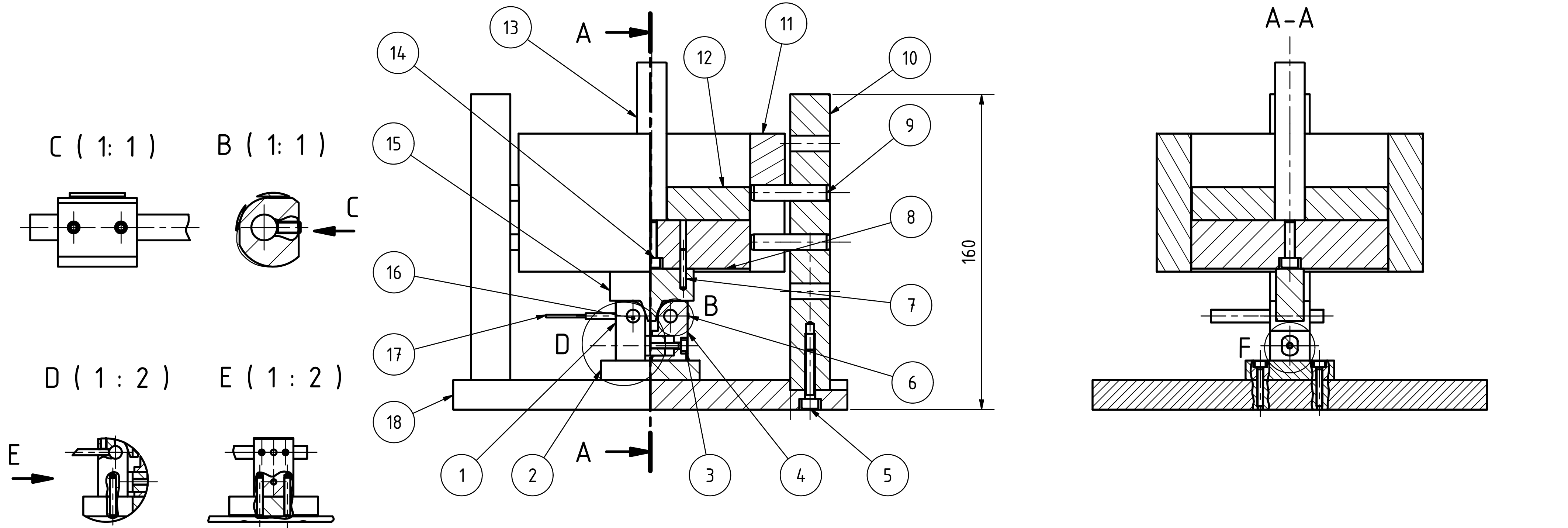


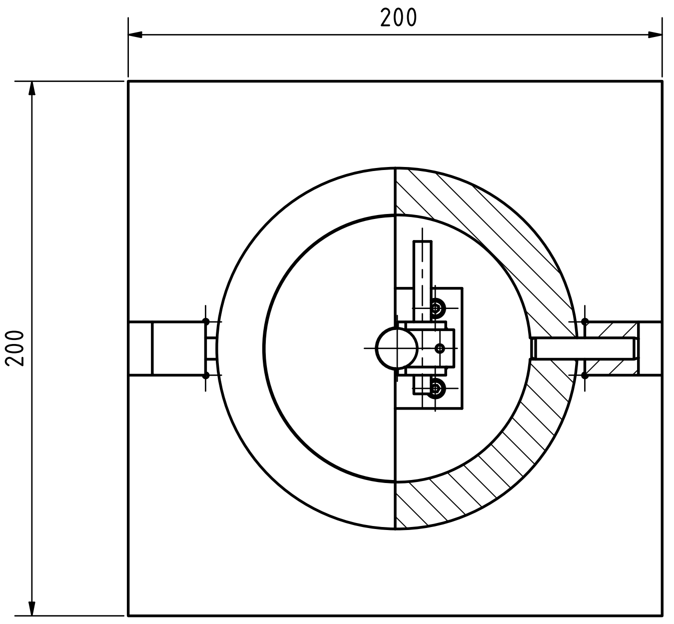


| | | | |
|---|---|---|---|
| SCALE 1 : 2 | Geometrical Product Specifications ISO 8015<br>General Geometrical Tolerances ISO 2768-fH<br>ISO 13920<br>Surface Texture ISO 1302<br>Edges and Chamfers ISO 13715 | | |
| | Date | Name | |
| Drawn | 23-02-2021 | James Hooton | |
| Checked | 23-02-2021 | Carlos M.C.G. Fernandes | Paper Size A3 |
| Standard | | | |

| | | | |
|---|---|---|---|
| Responsible Dept. DEMec | Technical Reference | Document Type Assembly Drawing | |
| Legal Owner | DEMec<br>CETRIB<br>James D.S. Hooton | Title<br>Gear Tooth Heating System | Sheet Number 1/1 |

| PARTS LIST | | | | |
|---|---|---|---|---|
| ITEM | QTY | DESCRIPTION | PART NUMBER | MATERIAL |
| 1 | 1 | Gear Tooth Heater (M) | | Aluminum 6061 |
| 2 | 1 | Polymer Support Plate | | Acetal (POM) |
| 3 | 5 | Hexagon Socket Head Cap Screw | ISO 4762 - M3 x 20(1) | |
| 4 | 1 | Gear Tooth Heater (F) | | Aluminum 6061 |
| 6 | 7 | Hexagon socket set screws with flat point | ISO 4026 - M3 x 6(1) | |
| 7 | 4 | Parallel Dowel Pins | ISO 8734 - 3 x 20 - A(1)(4) | |
| 8 | 1 | Platform | | 34 CrNiMo 6 |
| 9 | 4 | Parallel Dowel Pins | ISO 8734 - 8 x 40 - A(1)(4) | |
| 10 | 2 | Support Column | | Aluminum 6061 |
| 11 | 1 | Cylinder | | 34 CrNiMo 6 |
| 12 | 1 | Weight 1 kg | | 34 CrNiMo 6 |
| 13 | 1 | Shaft | | 34 CrNiMo 6 |
| 14 | 1 | Hexagon Socket Head Cap Screw | ISO 4762 - M5 x 40(1) | |
| 15 | 1 | Rack Tooth | | Acetal (POM) |
| 16 | 2 | Cartridge Heater | CAR.03.05 | |
| 17 | 1 | RTD Pt-100 | | |
| 18 | 1 | Table Support Plate | | 34 CrNiMo 6 |

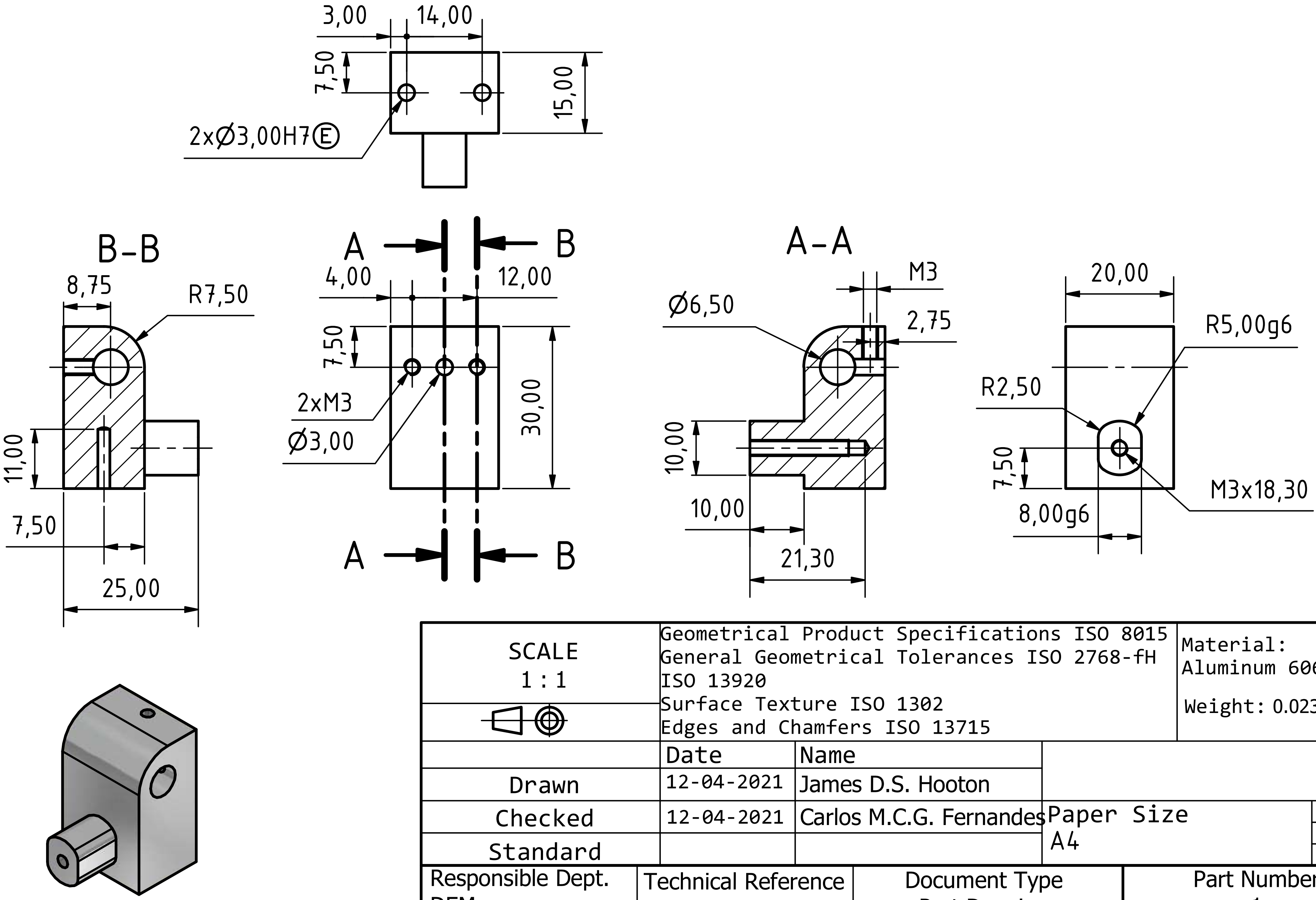


| | | | |
|---|---|---|---|
| SCALE 1 : 1 | Geometrical Product Specifications ISO 8015<br>General Geometrical Tolerances ISO 2768-fH<br>ISO 13920<br>Surface Texture ISO 1302<br>Edges and Chamfers ISO 13715 | | Material: Aluminum 6061<br>Weight: 0.023 kg |
| | Date | Name | |
| Drawn | 12-04-2021 | James D.S. Hooton | |
| Checked | 12-04-2021 | Carlos M.C.G. Fernandes | Paper Size A4 |
| Standard | | | |

| | | | |
|---|---|---|---|
| Responsible Dept. DEMec | Technical Reference | Document Type Part Drawing | Part Number 1 |
| Legal Owner | DEMec<br>CETRIB<br>James D.S. Hooton | Title<br>Gear Tooth Heater (M) | Sheet Number 1/1 |

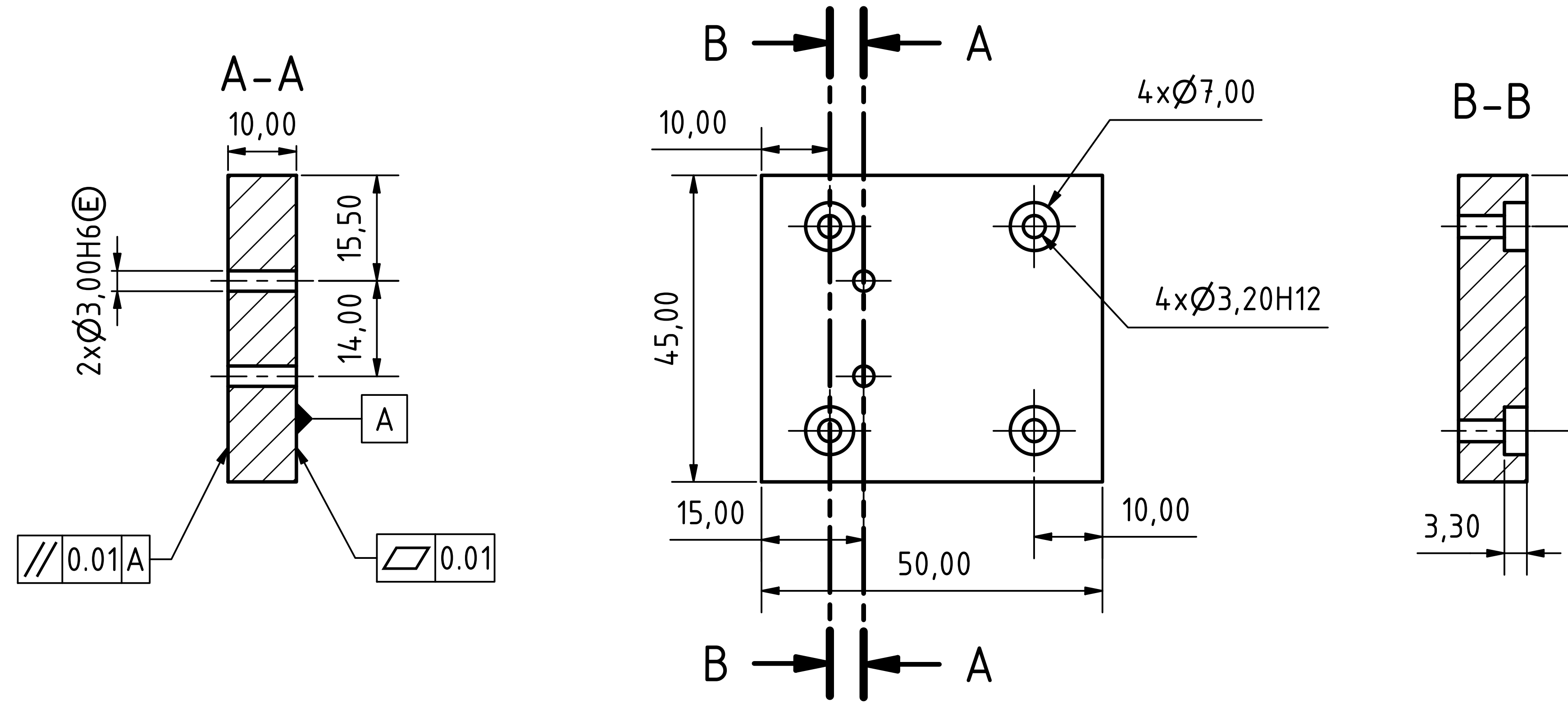


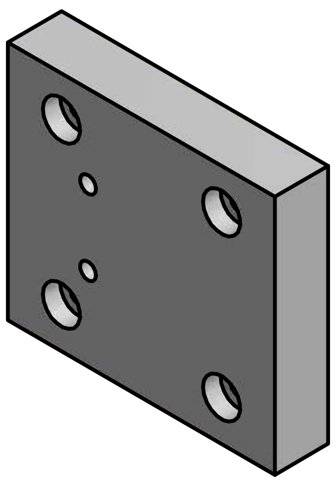

| | | | |
|---|---|---|---|
| SCALE 1 : 1 | Geometrical Product Specifications ISO 8015<br>General Geometrical Tolerances ISO 2768-fH<br>ISO 13920<br>Surface Texture ISO 1302<br>Edges and Chamfers ISO 13715 | | Material:<br>Acetal (POM)<br>Weight: 0.031 kg |
| | Date | Name | |
| Drawn | 12-04-2021 | James D.S. Hooton | |
| Checked | 12-04-2021 | Carlos M.C.G. Fernandes | Paper Size<br>A4 |
| Standard | | | |
| Responsible Dept.<br>DEMec | Technical Reference | Document Type<br>Part Drawing | Part Number<br>2 |
| Legal Owner | DEMec<br>CETRIB<br>James D.S. Hooton | Title<br>Polymer Support Plate | Sheet Number<br>1/1 |

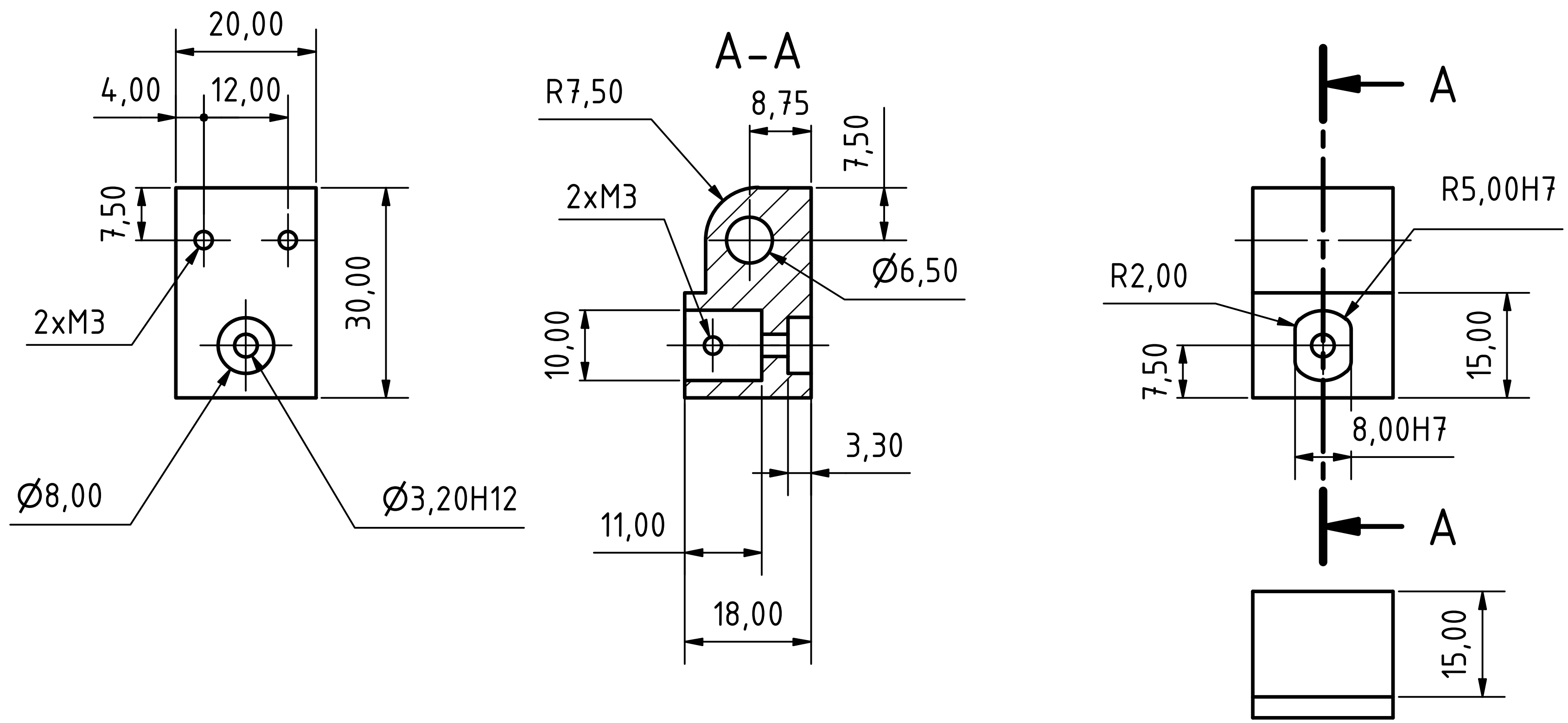


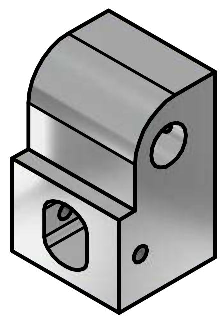

| | | | |
|---|---|---|---|
| SCALE 1 : 1 | Geometrical Product Specifications ISO 8015<br>General Geometrical Tolerances ISO 2768-fH<br>ISO 13920<br>Surface Texture ISO 1302<br>Edges and Chamfers ISO 13715 | | Material: Aluminum 6061<br>Weight: 0.021 kg |
| | Date | Name | |
| Drawn | 12-04-2021 | James D.S. Hooton | |
| Checked | 12-04-2021 | Carlos M.C.G. Fernandes | Paper Size A4 |
| Standard | | | |

| | | | |
|---|---|---|---|
| Responsible Dept.<br>DEMec | Technical Reference | Document Type<br>Part Drawing | Part Number<br>4 |
| Legal Owner | DEMec<br>CETRIB<br>James D.S. Hooton | Title<br>Gear Tooth Heater (F) | Sheet Number<br>1/1 |

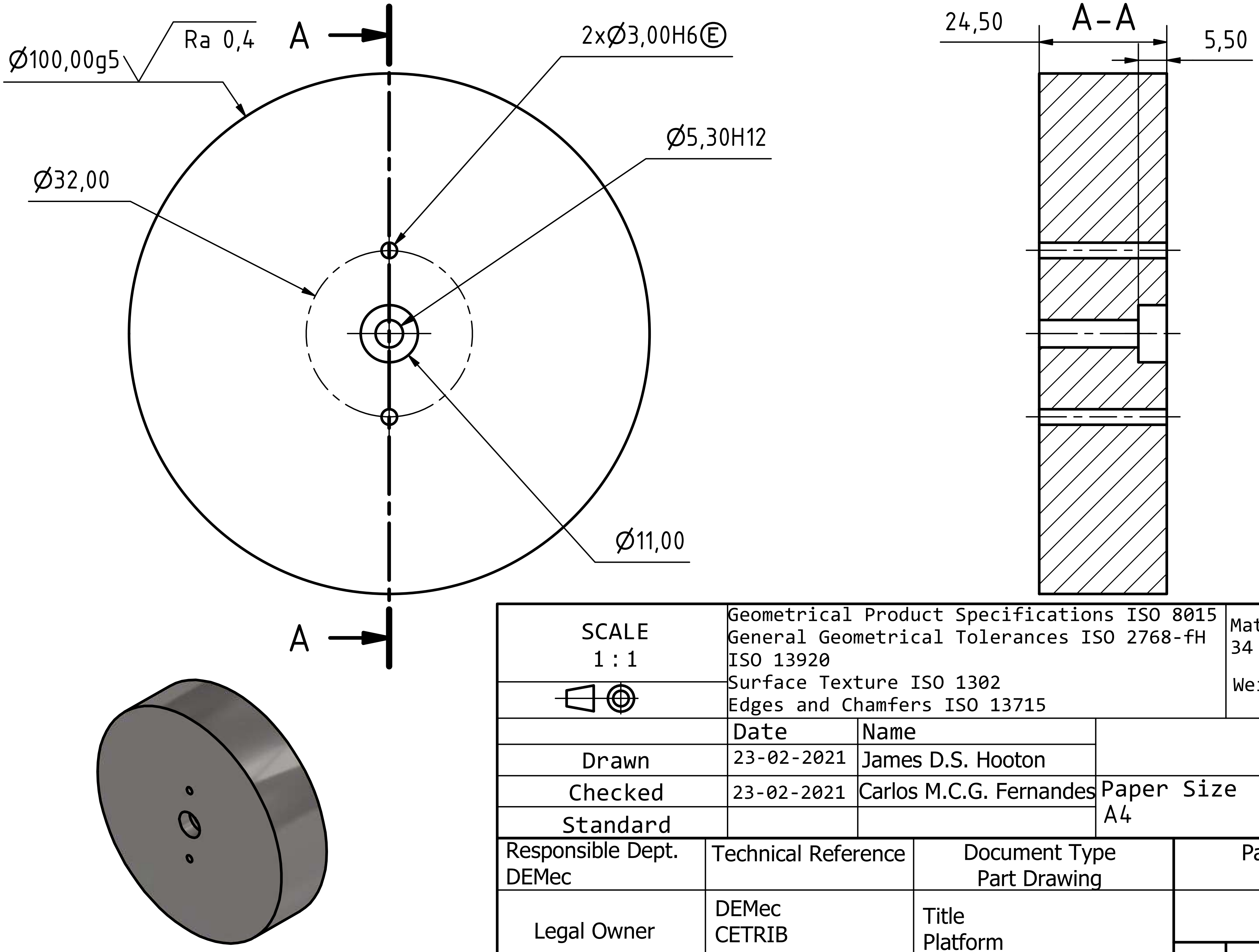


| | | | | |
|---|---|---|---|---|
| SCALE 1 : 1 | Geometrical Product Specifications ISO 8015<br>General Geometrical Tolerances ISO 2768-fH<br>ISO 13920<br>Surface Texture ISO 1302<br>Edges and Chamfers ISO 13715 | | Material:<br>34 CrNiMo 6<br>Weight: 1.500 kg | |
| | Date | Name | | |
| Drawn | 23-02-2021 | James D.S. Hooton | | |
| Checked | 23-02-2021 | Carlos M.C.G. Fernandes | Paper Size<br>A4 | |
| Standard | | | | |
| Responsible Dept.<br>DEMec | Technical Reference | Document Type<br>Part Drawing | Part Number<br>8 | |
| Legal Owner | DEMec<br>CETRIB<br>James D.S. Hooton | Title<br>Platform | Sheet Number<br>1/1 | |

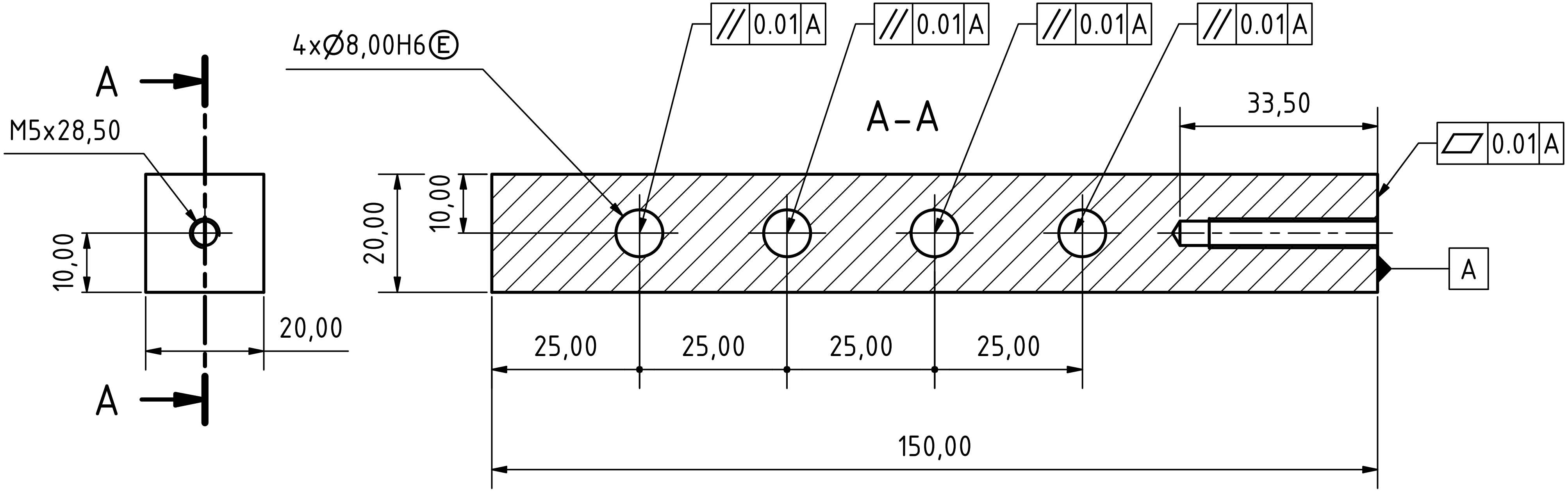


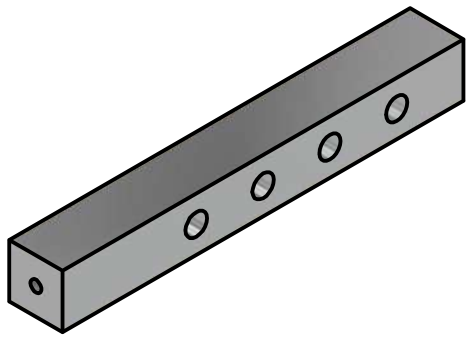

| | | | |
|---|---|---|---|
| SCALE 1 : 1 | Geometrical Product Specifications ISO 8015<br>General Geometrical Tolerances ISO 2768-fH<br>ISO 13920<br>Surface Texture ISO 1302<br>Edges and Chamfers ISO 13715 | | Material: Aluminum 6061<br>Weight: 0.150 kg |
| | Date | Name | |
| Drawn | 23-02-2021 | James D.S. Hooton | |
| Checked | 23-02-2021 | Carlos M.C.G. Fernandes | Paper Size A4 |
| Standard | | | |

| | | | |
|---|---|---|---|
| Responsible Dept. DEMec | Technical Reference | Document Type Part Drawing | Part Number 9 |
| Legal Owner | DEMec<br>CETRIB<br>James D.S. Hooton | Title Support Column | Sheet Number 1/1 |

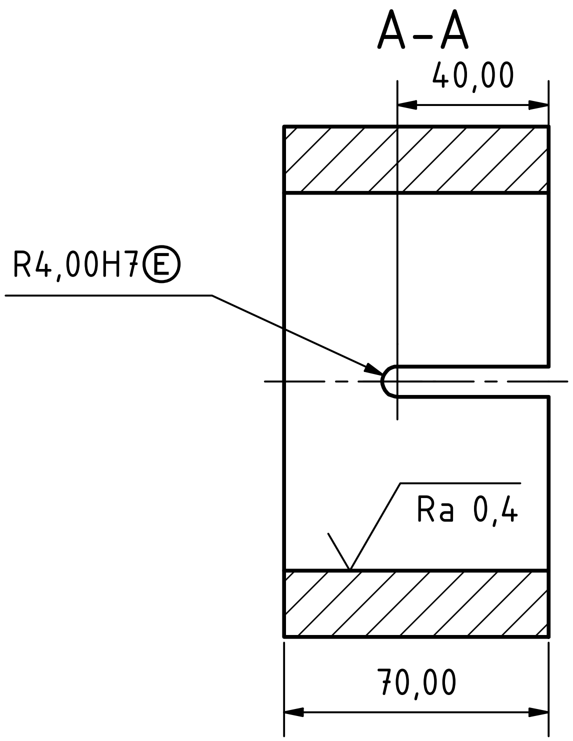


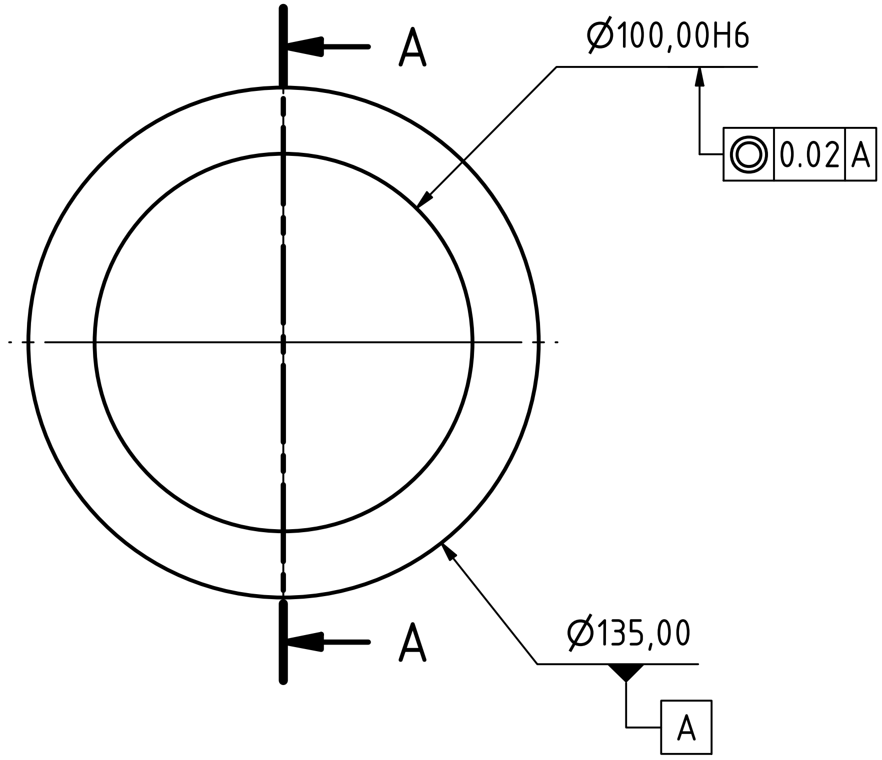


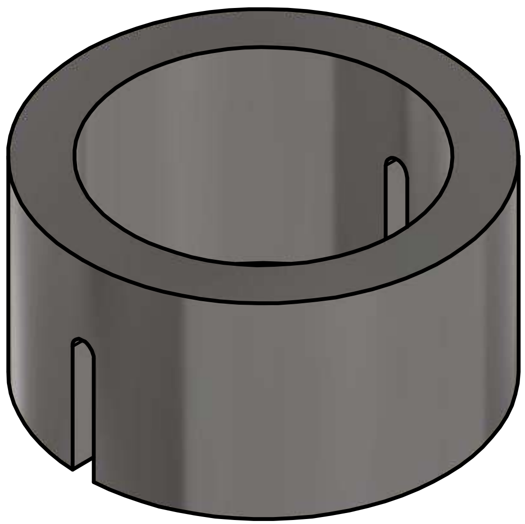

| | | | | |
|---|---|---|---|---|
| SCALE 1 : 2 | Geometrical Product Specifications ISO 8015<br>General Geometrical Tolerances ISO 2768-fH<br>ISO 13920<br>Surface Texture ISO 1302<br>Edges and Chamfers ISO 13715 | | Material:<br>34 CrNiMo 6<br><br>Weight: 3.402 kg | |
| | Date | Name | | |
| Drawn | 23-02-2021 | James D.S. Hooton | | |
| Checked | 23-02-2021 | Carlos M.C.G. Fernandes | Paper Size<br>A4 | |
| Standard | | | | |
| Responsible Dept.<br>DEMec | Technical Reference | Document Type<br>Part Drawing | Part Number<br>10 | |
| Legal Owner | DEMec<br>CETRIB<br>James D.S. Hooton | Title<br>Cylinder | Sheet Number<br>1/1 | |

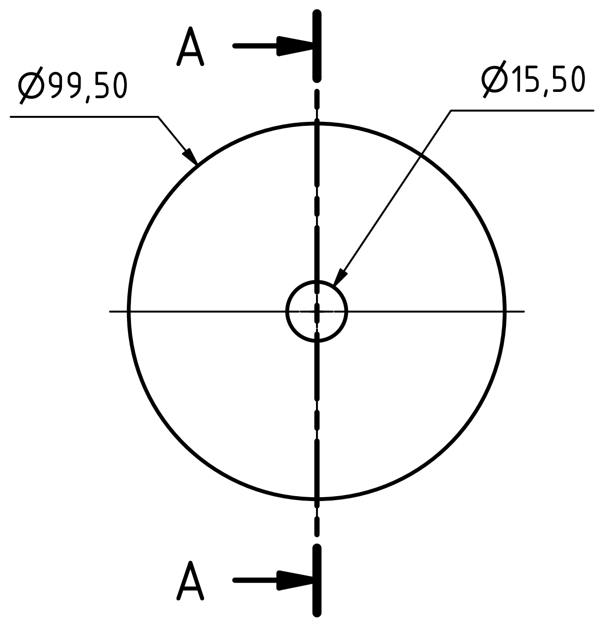


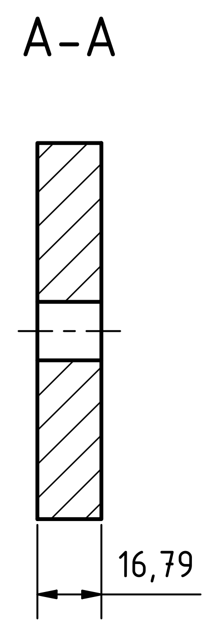


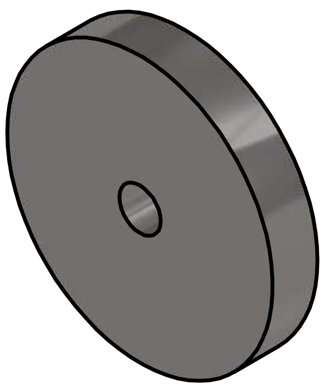

| | | | | |
|---|---|---|---|---|
| SCALE 1 : 2 | Geometrical Product Specifications ISO 8015<br>General Geometrical Tolerances ISO 2768-fH<br>ISO 13920<br>Surface Texture ISO 1302<br>Edges and Chamfers ISO 13715 | | | Material:<br>34 CrNiMo 6<br>Weight: 1.000 kg |
| | Date | Name | | |
| Drawn | 12-04-2021 | James D.S. Hooton | | |
| Checked | 12-04-2021 | Carlos M.C.G. Fernandes | Paper Size<br>A4 | |
| Standard | | | | |
| Responsible Dept.<br>DEMec | Technical Reference | Document Type<br>Part Drawing | Part Number<br>11 | |
| Legal Owner | DEMec<br>CETRIB<br>James D.S. Hooton | Title<br>Weight 1 kg | Sheet Number<br>1/1 | |

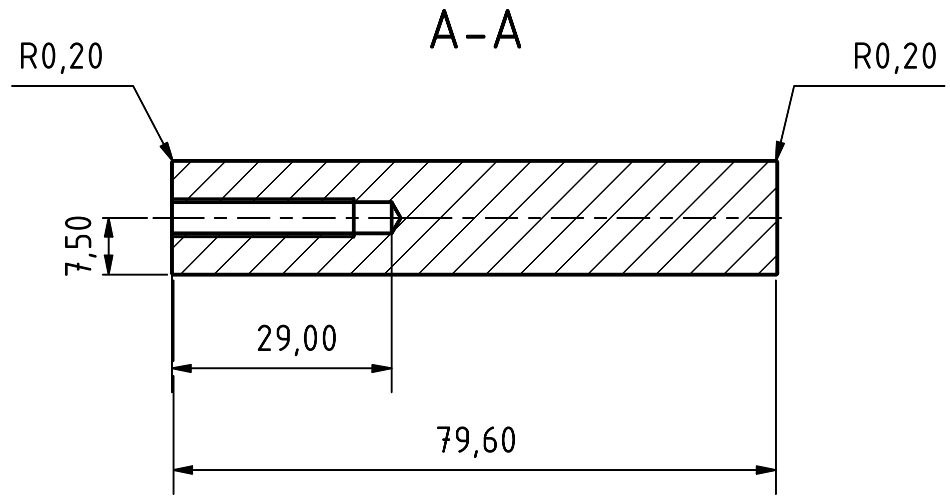


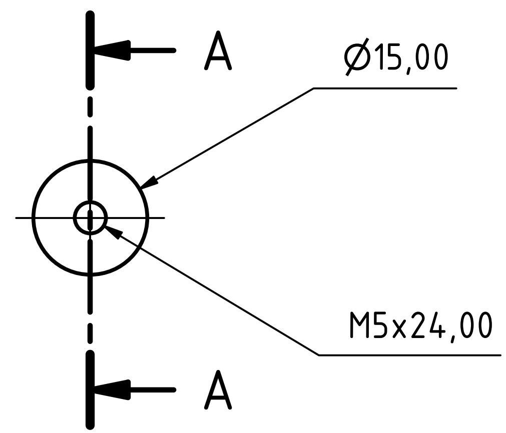


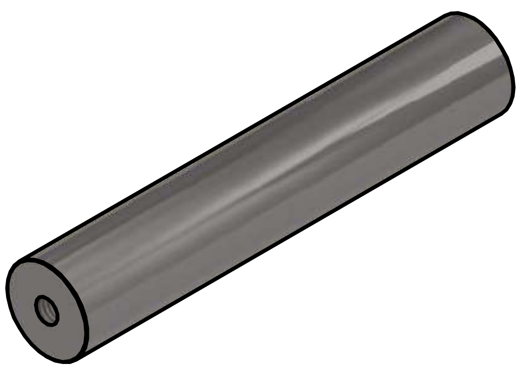

| | | | |
|---|---|---|---|
| SCALE 1:1 | Geometrical Product Specifications ISO 8015<br>General Geometrical Tolerances ISO 2768-fH<br>ISO 13920<br>Surface Texture ISO 1302<br>Edges and Chamfers ISO 13715 | | Material:<br>34 CrNiMo 6<br>Weight: 0.106 kg |
| | Date | Name | |
| Drawn | 23-02-2021 | James D.S. Hooton | |
| Checked | 23-02-2021 | Carlos M.C.G. Fernandes | Paper Size<br>A4 |
| Standard | | | |
| Responsible Dept.<br>DEMec | Technical Reference | Document Type<br>Part Drawing | Part Number<br>12 |
| Legal Owner | DEMec<br>CETRIB<br>James D.S. Hooton | Title<br>Shaft | Sheet Number<br>1/1 |

| HOLE | XDIM | YDIM | DESCRIPTION |
|---|---|---|---|
| 1.1 | -20,01 | -12,25 | Ø0,60-0,50 |
| 1.3 | 20,01 | -12,25 | Ø0,60-0,50 |
| 2.2 | 0,00 | -3,25 | Ø0,60-0,50 |
| 3.1 | -3,92 | 1,25 | Ø0,60-0,50 |
| 3.2 | 0,00 | 1,25 | Ø0,60-0,50 |
| 3.3 | 3,92 | 1,25 | Ø0,60-0,50 |
| 4.1 | -2,29 | 5,75 | Ø0,60-0,50 |
| 4.2 | 0,00 | 5,75 | Ø0,60-0,50 |
| 4.3 | 2,29 | 5,75 | Ø0,60-0,50 |
| 5.1 | -0,87 | 9,65 | Ø0,60-0,50 |
| 5.3 | 0,87 | 9,65 | Ø0,60-0,50 |

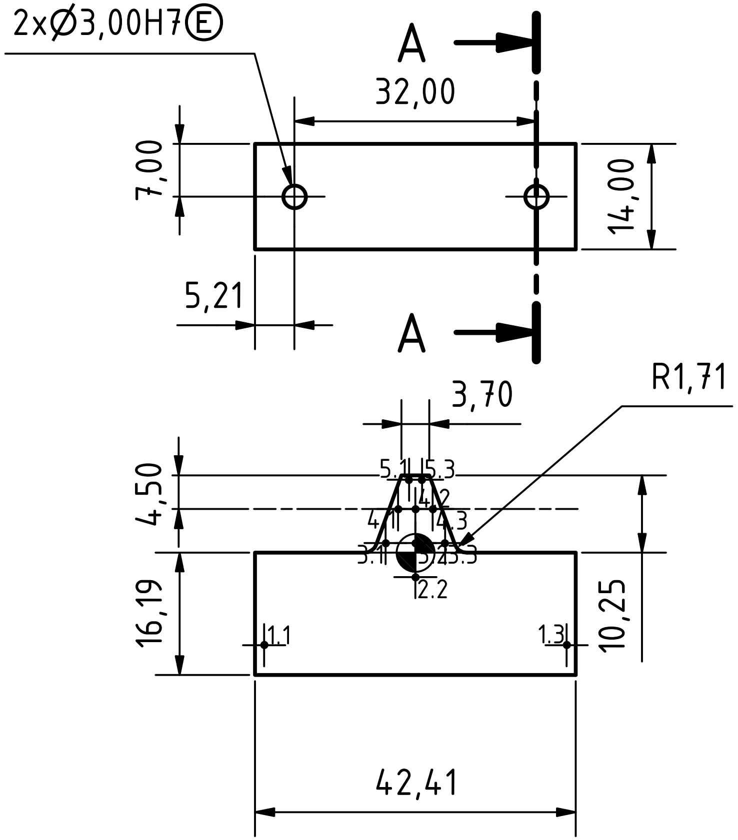


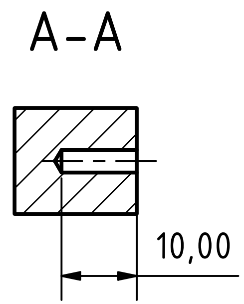


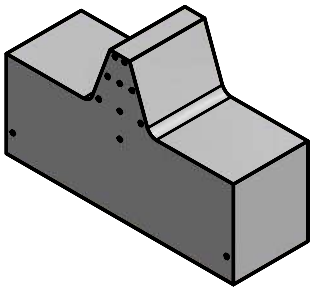

| Geometry | |
|---|---|
| Normal Module [mm], m | 4,5 |
| Normal Pressure Angle, α | 2,0 |
| Root Radius Coefficient, ρ | 0,38 |
| Fillet Radius [mm], rf = ρ x m | 1,71 |

SCALE 1 : 1

Geometrical Product Specifications ISO 8015
General Geometrical Tolerances ISO 2768-fH
ISO 13920
Surface Texture ISO 1302
Edges and Chamfers ISO 13715

Material: Acetal (POM)

Weight: 0.015 kg

| | Date | Name |
|---|---|---|
| Drawn | 12-04-2021 | James D.S. Hooton |
| Checked | 12-04-2021 | Carlos M.C.G. Fernandes |
| Standard | | |

Paper Size A4

| Responsible Dept. | Technical Reference | Document Type | Part Number |
|---|---|---|---|
| DEMec | | Part Drawing | 15 |
| Legal Owner | DEMec<br>CETRIB<br>James D.S. Hooton | Title | Sheet Number 1/1 |

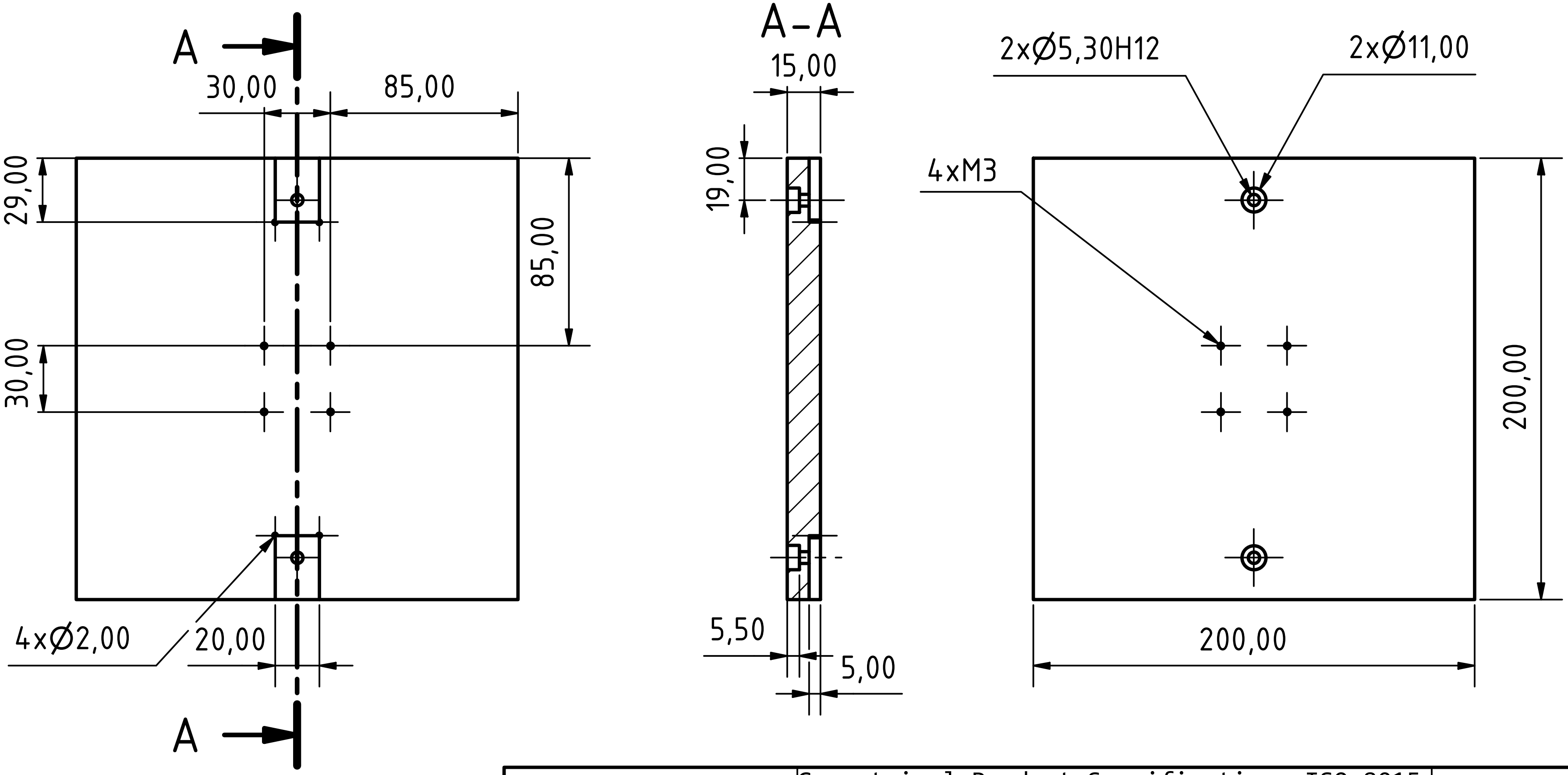


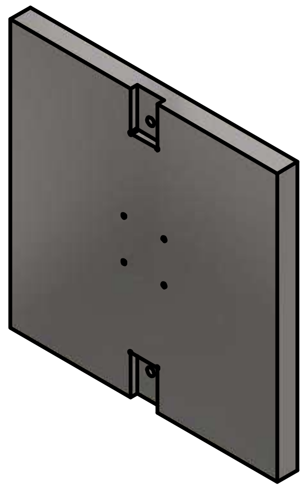

| | | | |
|---|---|---|---|
| SCALE 1 : 3 | Geometrical Product Specifications ISO 8015<br>General Geometrical Tolerances ISO 2768-fH<br>ISO 13920<br>Surface Texture ISO 1302<br>Edges and Chamfers ISO 13715 | | Material:<br>34 CrNiMo 6<br>Weight: 4.581 kg |
| | Date | Name | |
| Drawn | 23-02-2021 | James D.S. Hooton | |
| Checked | 23-02-2021 | Carlos M.C.G. Fernandes | Paper Size<br>A4 |
| Standard | | | |

| | | | |
|---|---|---|---|
| Responsible Dept.<br>DEMec | Technical Reference | Document Type<br>Part Drawing | Part Number<br>18 |
| Legal Owner | DEMec<br>CETRIB<br>James D.S. Hooton | Title<br>Table Support Plate | Sheet Number<br>1/1 |

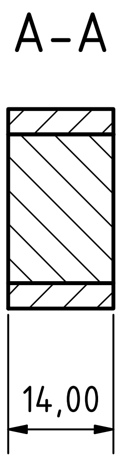


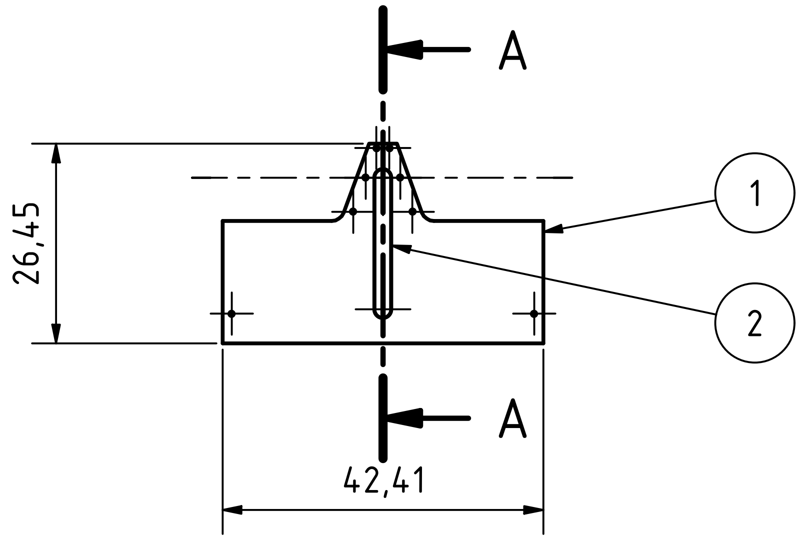


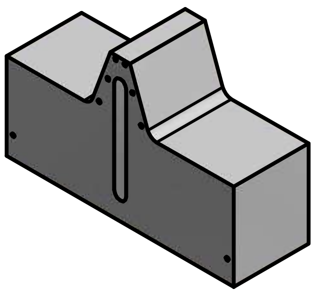

| PARTS LIST | | | |
|---|---|---|---|
| ITEM | QTY | DESCRIPTION | MATERIAL |
| 1 | 1 | Hybrid Gear Tooth | Acetal (POM) |
| 2 | 1 | Insert | Aluminum 6061 |

SCALE
1 : 1

Geometrical Product Specifications ISO 8015
General Geometrical Tolerances ISO 2768-fH
ISO 13920
Surface Texture ISO 1302
Edges and Chamfers ISO 13715

| | Date | Name |
|---|---|---|
| Drawn | 23-02-2021 | James D.S. Hooton |
| Checked | 23-02-2021 | Carlos M.C.G. Fernandes |
| Standard | | |

Paper Size
A4

| Responsible Dept. DEMec | Technical Reference | Document Type Part Drawing | Part Number 15 |
|---|---|---|---|
| Legal Owner | DEMec CETRIB James D.S. Hooton | Title Insert | Sheet Number 1/1 |

| HOLE | XDIM | YDIM | DESCRIPTION |
|---|---|---|---|
| 1.1 | 1,20 | 3,95 | Ø0,60-0,50 |
| 1.2 | 41,21 | 3,95 | Ø0,60-0,50 |
| 2.1 | 17,28 | 17,45 | Ø0,60-0,50 |
| 2.2 | 25,13 | 17,45 | Ø0,60-0,50 |
| 3.1 | 18,92 | 21,95 | Ø0,60-0,50 |
| 3.2 | 23,49 | 21,95 | Ø0,60-0,50 |
| 4.1 | 20,34 | 25,85 | Ø0,60-0,50 |
| 4.2 | 22,07 | 25,85 | Ø0,60-0,50 |

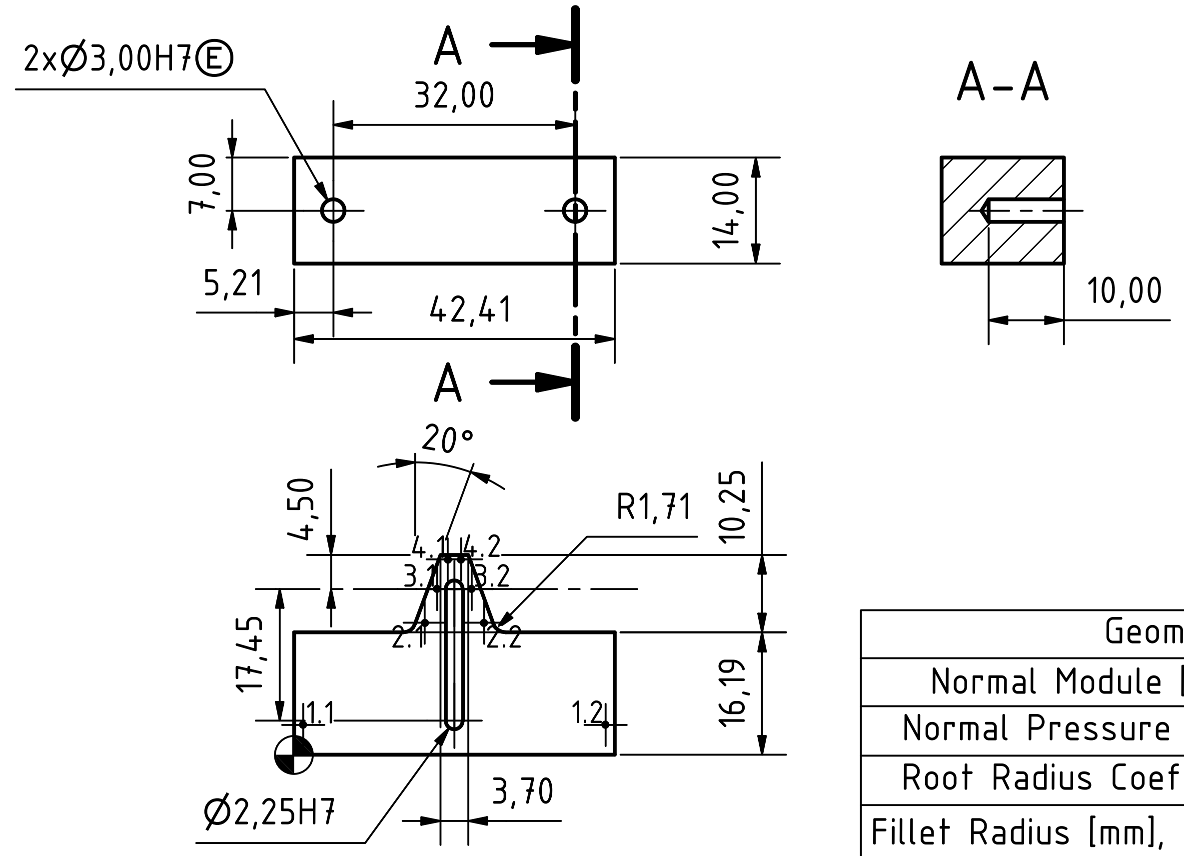


| Geometry | |
|---|---|
| Normal Module [mm], m | 4,5 |
| Normal Pressure Angle, α | 2,0 |
| Root Radius Coefficient, ρ | 0,38 |
| Fillet Radius [mm], rf = ρ x m | 1,71 |

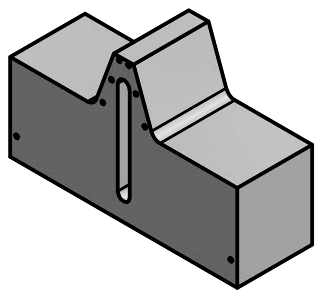

| | | | |
|---|---|---|---|
| SCALE 1 : 1 | Geometrical Product Specifications ISO 8015<br>General Geometrical Tolerances ISO 2768-fH<br>ISO 13920<br>Surface Texture ISO 1302<br>Edges and Chamfers ISO 13715 | | Material: Acetal (POM)<br>Weight: 0.014 kg |
| | Date | Name | |
| Drawn | 12-04-2021 | James D.S. Hooton | |
| Checked | 12-04-2021 | Carlos M.C.G. Fernandes | Paper Size A4 |
| Standard | | | |

| Responsible Dept. DEMec | Technical Reference | Document Type Part Drawing | Part Number 1 |
|---|---|---|---|
| Legal Owner | DEMec<br>CETRIB<br>James D.S. Hooton | Title<br>Hybrid Polymer Gear Tooth | Sheet Number 1/1 |

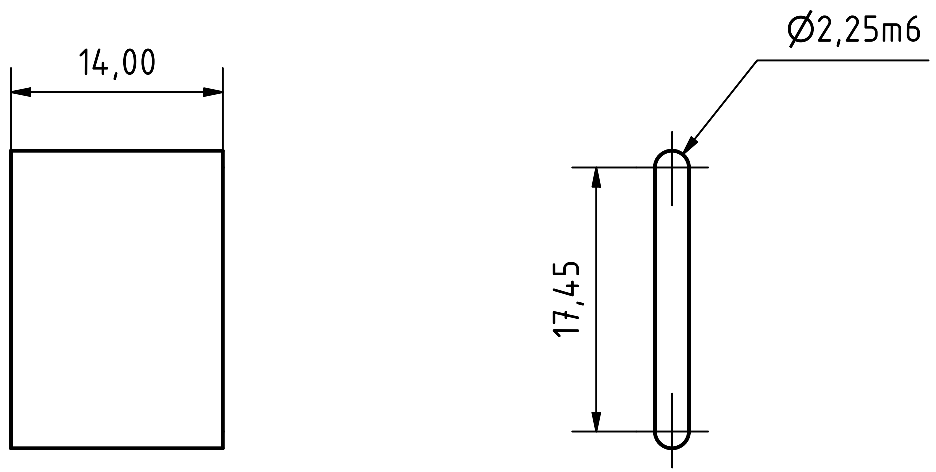


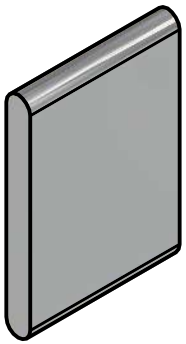

| | | | | |
|---|---|---|---|---|
| SCALE 2:1 | Geometrical Product Specifications ISO 8015<br>General Geometrical Tolerances ISO 2768-fH<br>ISO 13920<br>Surface Texture ISO 1302<br>Edges and Chamfers ISO 13715 | | | Material:<br>Aluminum 6061<br>Weight: 0.002 kg |
| | Date | Name | | |
| Drawn | 23-02-2021 | James D.S. Hooton | | |
| Checked | 23-02-2021 | Carlos M.C.G. Fernandes | Paper Size<br>A4 | |
| Standard | | | | |
| Responsible Dept.<br>DEMec | Technical Reference | Document Type<br>Part Drawing | | Part Number<br>2 |
| Legal Owner | DEMec<br>CETRIB<br>James D.S. Hooton | Title<br>Insert | | QTY. 2<br>Sheet Number<br>1/1 |

# Appendix C

# GMSH GEO File Code

## C.1 Standard Rack Tooth GEO File

```
//
Include "refine.geo";
//Geometry of Rack Tooth
module=4.5;
m=0.0045; //Convert to meters
z=16;
alfa=Pi/9;
rs=0.015;
ro=0.38;
e=0.014;
x=0;
escalar=0.6;
hfP=1.;
haP=1.25;
h=hfP+haP;
rf=m*(z/2-haP+x);
hi=m*(Pi/4+Tan(alfa)*hfP);
hs=m*(Pi/4-Tan(alfa)*hfP);
yc=m*ro*(1-Sin(alfa));
xc=hi+ro*m*Cos(alfa);
gamma=Atan((xc-hi)/(ro*m-yc));
//+
Point(1) = {0, 0, 0, 1.0};
//+
Point(2) = {xc, 0, 0, 1.0};
//+
Point(3) = {hi, yc, 0, 1.0};
//+
Point(4) = {hs, h*m, 0, 1.0};
//+
Point(5) = {0, h*m, 0, 1.0};
//+
Point(6) = {-hs, h*m, 0, 1.0};
//+
Point(7) = {-hi, yc, 0, 1.0};
//+
Point(8) = {-xc, 0, 0, 1.0};
//+
Point(9) = {xc, ro*m, 0, 1.0};
//+
Point(10) = {-xc, ro*m, 0, 1.0};
//+
Point(11) = {0, -rf+rs, 0, 1.0};
//+
Point(12) = {xc, -rf+rs, 0, 1.0};
//+
Point(13) = {-xc, -rf+rs, 0, 1.0};
//+
Point(14) = {0, -m*escalar, 0, 1.0};
//+
```

```
Point(15) = {0, -ro*m*Cos(gamma), 0, 1.0};
//+
Point(16) = {1.5*Pi*m, 0, 0, 1.0};
//+
Point(17) = {-1.5*Pi*m, 0, 0, 1.0};
//+
Point(18) = {1.5*Pi*m, -rf+rs, 0, 1.0};
//+
Point(19) = {-1.5*Pi*m, -rf+rs, 0, 1.0};
//+
Point(20) = {-m*Pi/4, haP*m, 0, 1.0};
//+
Point(21) = {m*Pi/4, haP*m, 0, 1.0};
//+
Point(22) = {0, haP*m, 0, 1.0};
//+
Line(1) = {17, 19};
//+
Line(2) = {19, 13};
//+
Line(3) = {13, 11};
//+
Line(4) = {11, 12};
//+
Line(5) = {12, 18};
//+
Line(6) = {18, 16};
//+
Line(7) = {16, 2};
//+
Line(8) = {2, 12};
//+
Line(9) = {17, 8};
//+
Line(10) = {8, 13};
//+
Line(11) = {11, 14};
//+
Line(12) = {14, 8};
//+
Line(13) = {14, 2};
//+
Line(14) = {7, 15};
//+
Line(15) = {15, 3};
//+
Line(16) = {6, 5};
//+
Line(17) = {5, 4};
//+
```

```
Circle(18) = {8, 10, 7};
//+
Circle(19) = {2, 9, 3};
//+
Line(20) = {14, 15};
//+
Line(21) = {7, 20};
//+
Line(22) = {20, 6};
//+
Line(23) = {4, 21};
//+
Line(24) = {21, 3};
//+
Line(25) = {20, 22};
//+
Line(26) = {22, 21};
//+
Line(27) = {5, 22};
//+
Line(28) = {22, 15};

// TRANSFINITE CUVES
b=1.5; c=1.5; d=3;
nM=module*a; nS=nM/b; nH=nM/c; nR=nM/d; nz=module*a;
//+
Transfinite Curve {1, 10, 11, 8, 6, 9, 2, 7, 5} = nS Using Progression 1;
//+
Transfinite Curve {16, 25, 14, 12, 3, 4, 13, 15, 26, 17} = nH Using Progression 1;
//+
Transfinite Curve {18, 20, 19} = nR Using Progression 1;
//+
Transfinite Curve {21, 28, 24, 22, 27, 23} = nM Using Progression 1;
//+
Curve Loop(1) = {9, 10, -2, -1};
//+
Plane Surface(1) = {1};
//+
Curve Loop(2) = {12, 10, 3, 11};
//+
Plane Surface(2) = {2};
//+
Curve Loop(3) = {11, 13, 8, -4};
//+
Plane Surface(3) = {3};
//+
Curve Loop(4) = {7, 8, 5, 6};
//+
Plane Surface(4) = {4};
//+
```

```
Curve Loop(5) = {12, 18, 14, -20};
//+
Plane Surface(5) = {5};
//+
Curve Loop(6) = {15, -19, -13, 20};
//+
Plane Surface(6) = {6};
//+
Curve Loop(7) = {15, -24, -26, 28};
//+
Plane Surface(7) = {7};
//+
Curve Loop(8) = {25, 28, -14, 21};
//+
Plane Surface(8) = {8};
//+
Curve Loop(9) = {25, -27, -16, -22};
//+
Plane Surface(9) = {9};
//+
Curve Loop(10) = {17, 23, -26, -27};
//+
Plane Surface(10) = {10};
//+
Transfinite Surface {1, 2, 3, 4, 5, 6, 7, 8, 9, 10};
//+
Recombine Surface {1, 2, 3, 4, 5, 6, 7, 8, 9, 10};
//+
Extrude {0, 0, e} {
  Surface{1}; Surface{2}; Surface{3}; Surface{4}; Surface{5}; Surface{6};
Surface{7}; Surface{8}; Surface{9}; Surface{10}; Layers{nz}; Recombine;
}
//+
Physical Volume("BODY") = {1, 2, 3, 4, 5, 6, 8, 7, 9, 10};
//+
Physical Surface("CONVECTION") = {37, 103, 50, 1, 49, 72, 2, 94, 3, 116, 4, 115, 6,
160, 138, 5, 204, 8, 182, 7, 226, 9, 248, 10, 151, 173, 239, 235, 221, 225, 203,
129};
//+
Physical Surface("CONDUCTION") = {111, 93, 67, 45};
//+
Physical Surface("MESH") = {111, 93, 67, 45, 37, 103, 50, 1, 49, 72, 2, 94, 3, 116,
4, 115, 6, 160, 138, 5, 204, 8, 182, 7, 226, 9, 248, 10, 151, 173, 239, 235, 221,
225, 203, 129};
//+
Physical Curve("FLUX") = {189, 172};
//+
Physical Curve("FLUXL") = {189};
//+
Physical Curve("FLUXR") = {172};
```

```
//+
Physical Surface("RADIATION") = {37, 103, 129, 203, 225, 151, 173, 239, 221, 235};
//+
Physical Surface("FRONT") = {50, 72, 94, 116, 160, 138, 182, 204, 248, 226};
//+
Physical Surface("MIDDLE") = {4, 3, 2, 1, 5, 6, 7, 8, 9, 10};
//+
Mesh.SaveGroupsOfNodes = 1;
//+
Mesh.ElementOrder=1;
//+
Mesh 3;
//+
Save 'RackTooth2.inp';
Exit;
```

## C.2 Hybrid Rack Tooth GEO File

```
//
Include "refine.geo";
//Geometry of Rack Tooth
module=4.5;
m=0.0045; //Convert to meters
z=16;
alfa=Pi/9;
rs=0.015;
ro=0.38;
B=0.007;
x=0.1817;
escalar=1;
hfP=1.;
haP=1.25;
h=hfP+haP;
rf=m*(z/2-haP+x);
hi=m*(Pi/4+Tan(alfa)*hfP);
hs=m*(Pi/4-Tan(alfa)*hfP);
yc=m*ro*(1-Sin(alfa));
xc=hi+ro*m*Cos(alfa);
//Geometry of Insert
e=m*1/2;
yt=h*m-m; //Distance from tooth tip
yb=-rf+rs+m; //Distance from shaft bore
Gamma=Pi/3;
Omega=Pi/4;
//+
Point(1) = {0, 0, 0, 1.0};
//+
Point(2) = {xc, 0, 0, 1.0};
//+
Point(3) = {hi, yc, 0, 1.0};
//+
Point(4) = {hs, h*m, 0, 1.0};
//+
Point(5) = {0, h*m, 0, 1.0};
//+
Point(6) = {-hs, h*m, 0, 1.0};
//+
Point(7) = {-hi, yc, 0, 1.0};
//+
Point(8) = {-xc, 0, 0, 1.0};
//+
Point(9) = {xc, ro*m, 0, 1.0};
//+
Point(10) = {-xc, ro*m, 0, 1.0};
//+
Point(11) = {1.5*Pi*m, 0, 0, 1.0};
//+
Point(12) = {-1.5*Pi*m, 0, 0, 1.0};
```

```
//+
Point(13) = {1.5*Pi*m, -rf+rs, 0, 1.0};
//+
Point(14) = {-1.5*Pi*m, -rf+rs, 0, 1.0};
//+
Point(15) = {0, yt, 0, 1.0};
//+
Point(16) = {e/2, yt, 0, 1.0};
//+
Point(17) = {-e/2, yt, 0, 1.0};
//+
Point(18) = {0, yb, 0, 1.0};
//+
Point(19) = {e/2, yb, 0, 1.0};
//+
Point(20) = {-e/2, yb, 0, 1.0};
//+
Point(21) = {-xc, -rf+rs, 0, 1.0};
//+
Point(22) = {xc, -rf+rs, 0, 1.0};
//+
Point(23) = {-e/2, yc, 0, 1.0};
//+
Point(24) = {e/2, yc, 0, 1.0};
//+
Point(25) = {0, yt+e/2, 0, 1.0};
//+
Point(26) = {0, yb-e/2, 0, 1.0};
//+
Point(27) = {0, -rf+rs, 0, 1.0};
//+
Point(28) = {e/2, -e/2*escalar, 0, 1.0};
//+
Point(29) = {-e/2, -e/2*escalar, 0, 1.0};
//+
Point(30) = {m*Pi/4, haP*m, 0, 1.0};
//+
Point(31) = {-m*Pi/4, haP*m, 0, 1.0};
//+
Point(32) = {e/2*Cos(Gamma), yt+e/2*Sin(Gamma), 0, 1.0};
//+
Point(33) = {-e/2*Cos(Gamma), yt+e/2*Sin(Gamma), 0, 1.0};
//+
Point(36) = {xc, yb, 0, 1.0};
//+
Point(37) = {-xc, yb, 0, 1.0};
//+
Point(38) = {e/2*Cos(Omega), yb-e/2*Sin(Omega), 0, 1.0};
//+
Point(39) = {-e/2*Cos(Omega), yb-e/2*Sin(Omega), 0, 1.0};
```

```
//+
Point(40) = {-1.5*Pi*m, yb, 0, 1.0};
//+
Point(41) = {1.5*Pi*m, yb, 0, 1.0};
//+
Line(1) = {6, 4};
//+
Line(2) = {30, 3};
//+
Circle(3) = {32, 15, 33};
//+
Line(4) = {31, 7};
//+
Circle(5) = {7, 10, 8};
//+
Circle(6) = {3, 9, 2};
//+
Line(7) = {8, 12};
//+
Line(8) = {12, 40};
//+
Line(9) = {14, 21};
//+
Line(10) = {41, 11};
//+
Line(11) = {11, 2};
//+
Line(12) = {21, 22};
//+
Line(13) = {22, 13};
//+
Line(14) = {36, 2};
//+
Line(15) = {8, 37};
//+
Line(16) = {17, 23};
//+
Line(17) = {29, 20};
//+
Line(18) = {16, 24};
//+
Line(19) = {28, 19};
//+
Line(20) = {7, 23};
//+
Line(21) = {24, 3};
//+
Circle(22) = {17, 15, 33};
//+
Circle(23) = {32, 15, 16};
```

```
//+
Circle(24) = {19, 18, 38};
//+
Circle(25) = {20, 18, 39};
//+
Line(26) = {21, 39};
//+
Line(27) = {22,38};
//+
Line(28) = {29, 23};
//+
Line(29) = {28, 24};
//+
Line(30) = {29, 8};
//+
Line(31) = {28, 2};
//+
Line(32) = {20, 37};
//+
Line(33) = {19, 36};
//+
Line(34) = {31, 6};
//+
Line(35) = {30, 4};
//+
Line(36) = {16, 30};
//+
Line(37) = {17, 31};
//+
Line(38) = {32, 4};
//+
Line(39) = {33, 6};
//+
Line(40) = {17, 16};
//+
Line(41) = {20, 19};
//+
Line(42) = {23, 24};
//+
Line(43) = {29, 28};
//+
Circle(46) = {39, 18, 38};
//+
Line(47) = {37, 21};
//+
Line(48) = {36, 22};
//+
Line(49) = {40, 37};
//+
Line(50) = {14, 40};
```

```
//+
Line(51) = {36, 41};
//+
Line(52) = {41, 13};

//Transfinite Mesh Density
b=1.5; c=3;
nM=module*a; nb=nM/b; nc=nM/c; nz=nM;
//+
Transfinite Curve {7, 49, 9, 11, 51, 13} = nb Using Progression 1;
//+
Transfinite Curve {8, 15, 17, 19, 14, 10} = nb Using Progression 1;
//+
Transfinite Curve {50, 47, 25, 24, 48, 52} = nc Using Progression 1;
//+
Transfinite Curve {26, 27, 32, 33, 30, 31, 20, 21, 37, 36, 39, 38} = nb Using
Progression 1;
//+
Transfinite Curve {46, 41, 43, 42, 40, 3, 1, 12} = nb Using Progression 1;
//+
Transfinite Curve {5, 28, 29, 6} = nc Using Progression 1;
//+
Transfinite Curve {4, 16, 18, 2} = nM Using Progression 1;
//+
Transfinite Curve {34, 22, 23, 35} = nb Using Progression 1;
//+
Curve Loop(1) = {1, -38, 3, 39};
//+
Plane Surface(1) = {1};
//+
Curve Loop(2) = {34, -39, -22, 37};
//+
Plane Surface(2) = {2};
//+
Curve Loop(3) = {38, -35, -36, -23};
//+
Plane Surface(3) = {3};
//+
Curve Loop(4) = {4, 20, -16, 37};
//+
Plane Surface(4) = {4};
//+
Curve Loop(5) = {36, 2, -21, -18};
//+
Plane Surface(5) = {5};
//+
Curve Loop(6) = {20, -28, 30, -5};
//+
Plane Surface(6) = {6};
//+
```

```
Curve Loop(7) = {21, 6, -31, 29};
//+
Plane Surface(7) = {7};
//+
Curve Loop(8) = {22, -3, 23, -40};
//+
Plane Surface(8) = {8};
//+
Curve Loop(9) = {40, 18, -42, -16};
//+
Plane Surface(9) = {9};
//+
Curve Loop(10) = {42, -29, -43, 28};
//+
Plane Surface(10) = {10};
//+
Curve Loop(11) = {43, 19, -41, -17};
//+
Plane Surface(11) = {11};
//+
Curve Loop(12) = {7, 8, 49, -15};
//+
Plane Surface(12) = {12};
//+
Curve Loop(13) = {50, 49, 47, -9};
//+
Plane Surface(13) = {13};
//+
Curve Loop(14) = {15, -32, -17, 30};
//+
Plane Surface(14) = {14};
//+
Curve Loop(15) = {31, -14, -33, -19};
//+
Plane Surface(15) = {15};
//+
Curve Loop(16) = {32, 47, 26, -25};
//+
Plane Surface(16) = {16};
//+
Curve Loop(17) = {33, 48, 27, -24};
//+
Plane Surface(17) = {17};
//+
Curve Loop(18) = {46, -27, -12, 26};
//+
Plane Surface(18) = {18};
//+
Curve Loop(19) = {41, 24, -46, -25};
//+
```

```
Plane Surface(19) = {19};
//+
Curve Loop(20) = {11, -14, 51, 10};
//+
Plane Surface(20) = {20};
//+
Curve Loop(21) = {48, 13, -52, -51};
//+
Plane Surface(21) = {21};
//+
Transfinite Surface {1, 2, 3, 4, 5, 6, 7, 8, 9, 10, 11, 12, 13, 14, 15, 16, 17, 18,
19, 20, 21};
//+
Recombine Surface {1, 2, 3, 4, 5, 6, 7, 8, 9, 10, 11, 12, 13, 14, 15, 16, 17, 18,
19, 20, 21};
//+
Extrude {0, 0, -B} {
  Surface{1}; Surface{2}; Surface{3}; Surface{4}; Surface{5}; Surface{6};
Surface{7}; Surface{8}; Surface{9}; Surface{10};
  Surface{11}; Surface{12}; Surface{13}; Surface{14}; Surface{15}; Surface{16};
Surface{17}; Surface{18}; Surface{19}; Surface{20}; Surface{21}; Layers{nz};
Recombine;
}
//+
Physical Volume("BODY") = {12, 13, 21, 20, 18, 17, 16, 19, 15, 11, 14, 6, 10, 7, 5,
9, 4, 2, 8, 1, 3};
//+
Physical Volume("BODY1") = {20, 21, 18, 17, 16, 13, 12, 15, 14, 6, 7, 5, 4, 2, 1,
3};
//+
Physical Volume("BODY2") = {8, 9, 10, 11, 19};
//+
Physical Surface("CONVECTION") = {470, 127, 83, 153, 109, 316, 338, 448, 514, 492,
303, 479, 17, 21, 13, 20, 12, 18, 404, 16, 426, 15, 382, 360, 14, 11, 294, 19, 10,
9, 8, 1, 74, 2, 96, 118, 3, 162, 5, 140, 4, 6, 184, 7, 206, 250, 228, 272, 183,
197, 61};
//+
Physical Surface("MASTER") = {316, 360, 12, 303, 307, 325, 337, 13, 338, 505, 21,
514, 509, 491, 20, 492, 479, 443, 448, 404, 426, 17, 16, 18, 382, 184, 206, 162,
140, 96, 74, 118, 15, 14, 6, 7, 197, 183, 5, 4, 2, 1, 3, 127, 153, 83, 109, 61,
285, 293, 425, 403, 435, 205, 175, 161, 135, 91, 117, 69};
//+
Physical Surface("SLAVE") = {19, 470, 435, 425, 403, 293, 285, 11, 294, 10, 272,
205, 175, 9, 250, 135, 161, 8, 228, 117, 91, 69};
//+
Physical Curve("FLUXL") = {81};
//+
Physical Curve("FLUXR") = {108};
//+
Physical Curve("FLUX") = {81, 108};
```

```
//+
Physical Surface("MESH") = {12, 316, 13, 338, 21, 514, 20, 492, 16, 404, 18, 448,
17, 426, 337, 443, 505, 14, 360, 15, 382, 6, 184, 7, 206, 5, 162, 4, 140, 2, 96, 3,
118, 1, 74, 61, 109, 83, 127, 153, 183, 197, 479, 303, 307, 325, 509, 491, 19, 470,
11, 294, 10, 272, 9, 250, 8, 228};
//+
Physical Surface("CONDUCTION") = {337, 443, 505};
//+
Physical Surface("RADIATION") = {303, 183, 127, 83, 61, 109, 153, 197, 479, 6, 184,
10, 272, 7, 206, 9, 250, 4, 140, 5, 162, 8, 228, 2, 96, 1, 74, 3, 118};
//+
Physical Surface("FRONT") = {12, 13, 21, 20, 18, 16, 17, 14, 15, 7, 6, 10, 5, 9, 4,
3, 1, 2, 8, 11, 19};
//+
Physical Surface("MIDDLE") = {228, 514, 338, 448, 426, 404, 492, 316, 382, 360,
470, 294, 206, 184, 272, 162, 250, 140, 118, 74, 96};
//+
Mesh.SaveGroupsOfNodes = 1;
//+
Mesh.ElementOrder=1;
//+
Mesh 3;
//+
Save 'Rack2.inp';
```

# Appendix D

# CalculiX INP File Code

## D.1 Thermal Model INP File for the Hybrid Tooth

```
** mesh file
*INCLUDE, INPUT=mesh.inp
*INCLUDE, INPUT=CONVECTION.sur
*INCLUDE, INPUT=SLAVE.sur
*INCLUDE, INPUT=MASTER.sur
*******************************************************
*MATERIAL,NAME=POM
*ELASTIC
2.80E+09,0.43,21
*EXPANSION
125E-06,21
*SPECIFIC HEAT
1470.0
*DENSITY
1410.0
*CONDUCTIVITY
0.31
*******************************************************
*MATERIAL,NAME=ALUMINUM
*ELASTIC
69.0E09,0.33,0
*EXPANSION
22.50e-06,0
*SPECIFIC HEAT
903.0
*DENSITY
2702.0
*CONDUCTIVITY
237.0
*******************************************************
*MATERIAL,NAME=ER2220
*ELASTIC
2.90E+09,0.42,0
*EXPANSION
60E-06,0
*SPECIFIC HEAT
1240.0
*DENSITY
2220.0
*CONDUCTIVITY
1.54
*******************************************************
*PHYSICAL CONSTANTS, ABSOLUTE ZERO=-273.15, STEFAN BOLTZMANN=5.669E-8
*INITIAL CONDITIONS,TYPE=TEMPERATURE
BODY, 21.5
*******************************************************
*SOLID SECTION, MATERIAL=POM, ELSET=BODY1
*SOLID SECTION, MATERIAL=ALUMINUM, ELSET=BODY2
*CONTACT PAIR,INTERACTION=SI1,TYPE=SURFACE TO SURFACE
SSLAVE, SMASTER
```

```
*SURFACE INTERACTION,NAME=SI1
*SURFACE BEHAVIOR,PRESSURE-OVERCLOSURE=TIED
1000.00E+09
*FRICTION
0.2,5000.
*GAP CONDUCTANCE
17563.08,,0
*******************************************************
*STEP
*HEAT TRANSFER,STEADY STATE
*FILM
SCONVECTION, F0, 33.116, 5
*BOUNDARY
FLUXL,11,11,103
*BOUNDARY
FLUXR,11,11,114
*RADIATE
*INCLUDE, INPUT=RADIATION.rad
*NODE FILE
NT
*EL FILE
HFL
*NODE PRINT,NSET=FRONT
NT
*END STEP
```

## D.2 Thermo-Mechanical Model INP File for the Standard Tooth

```
** mesh file
*INCLUDE, INPUT=mesh.inp
*INCLUDE, INPUT=CONVECTION.sur
*******************************************************
*MATERIAL,NAME=POM
*ELASTIC
3.10E+09,0.43,0
2.90E+09,0.44,20
2.60E+09,0.44,40
2.40E+09,0.45,60
2.10E+09,0.45,80
1.80E+09,0.46,100
1.50E+09,0.47,120
1.10E+09,0.48,140
0.50E+09,0.49,160
*EXPANSION
125E-06,0
*SPECIFIC HEAT
1470.0
*DENSITY
1410
*CONDUCTIVITY
0.31
*******************************************************
*MATERIAL,NAME=ALUMINUM
*ELASTIC
69.0E09,0.33,0
*EXPANSION
22.50e-06,0
*SPECIFIC HEAT
903.0
*DENSITY
2702.0
*CONDUCTIVITY
237.0
*******************************************************
*PHYSICAL CONSTANTS,ABSOLUTE ZERO=-273.15,STEFAN BOLTZMANN=5.669E-8
*INITIAL CONDITIONS,TYPE=TEMPERATURE
BODY, 21.5
*SOLID SECTION,ELSET=BODY,MATERIAL=POM
*******************************************************
*STEP
*UNCOUPLED TEMPERATURE-DISPLACEMENT,STEADY STATE
*FILM
SCONVECTION,F0,33.116,5
*BOUNDARY
FLUXL,11,11,100
*BOUNDARY
FLUXR,11,11,110
*RADIATE
```

```
*INCLUDE, INPUT=RADIATION.rad
*BOUNDARY
MIDDLE,3,3,0
CONDUCTION,1,2,0
*DLOAD
*INCLUDE, INPUT=FLUXL.dlo
*INCLUDE, INPUT=FLUXR.dlo
*NODE FILE
RF, U, NT
*EL FILE
S, E
*NODE PRINT,NSET=FRONT
U
*END STEP
```

## Appendix E

# Test Report

### E.1 Thermal Test Report for Standard Tooth

| Test Report | STD |
|---|---|

Thermal Measurements using "Heating System"

Researcher: James Hooton

| Thermal Test Parameter | Value | Units |
|---|---|---|
| Type of Tooth: | STD | - |
| Insert Material: | - | - |
| Temperature Range: | [40; 110] | °C |
| Applied Weight: | 4.6 | kg |
| Point of Contact: | 4.6 | mm |
| Heating Duration: | 45 | min |
| Cooling Duration: | 45 | min |

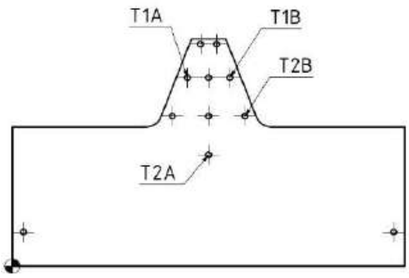


| Thermal Measurments for Heater Temperature | 40 | °C |
|---|---|---|
| Average Room Temperature: | 20.2 | °C |
| Stabilized Temperature for $T_{1A}$: | 19.1 | °C |
| Stabilized Temperature for $T_{2A}$: | 11.8 | °C |
| Stabilized Temperature for $T_{1B}$: | 19.1 | °C |
| Stabilized Temperature for $T_{2B}$: | 15.6 | °C |

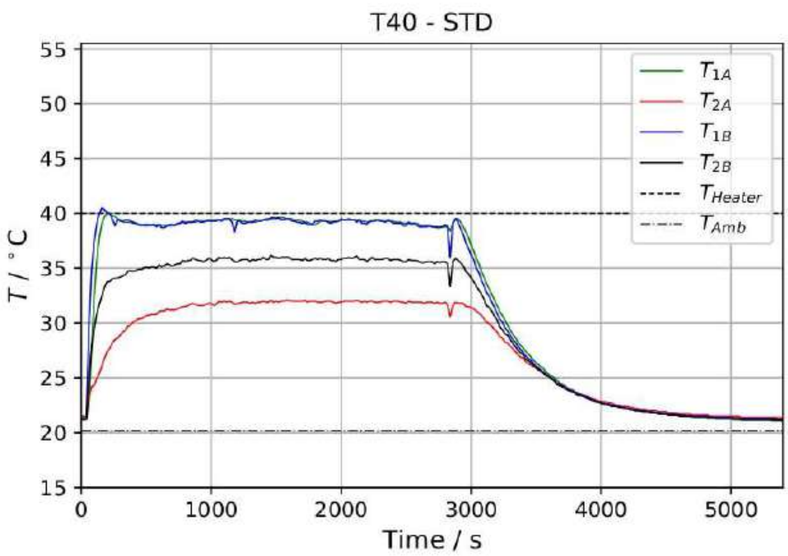

| | | |
|---|---|---|
| Thermal Measurments for Heater Temperature | 50 | °C |
| Average Room Temperature: | 18.6 | °C |
| Stabilized Temperature for $T_{1A}$: | 27.5 | °C |
| Stabilized Temperature for $T_{2A}$: | 15.9 | °C |
| Stabilized Temperature for $T_{1B}$: | 26.6 | °C |
| Stabilized Temperature for $T_{2B}$: | 22.0 | °C |

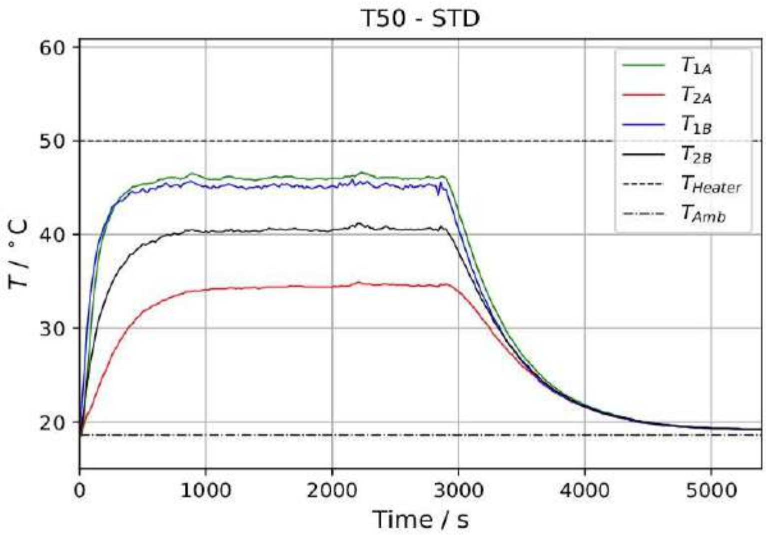


| | | |
|---|---|---|
| Thermal Measurments for Heater Temperature | 60 | °C |
| Average Room Temperature: | 19.0 | °C |
| Stabilized Temperature for $T_{1A}$: | 34.9 | °C |
| Stabilized Temperature for $T_{2A}$: | 20.5 | °C |
| Stabilized Temperature for $T_{1B}$: | 35.1 | °C |
| Stabilized Temperature for $T_{2B}$: | 28.6 | °C |

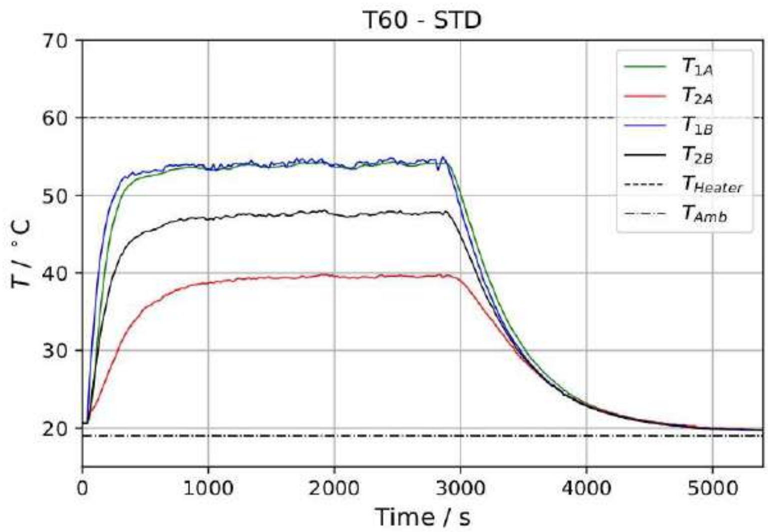

| | | |
|---|---|---|
| Thermal Measurments for Heater Temperature | 70 | °C |
| Average Room Temperature: | 19.8 | °C |
| Stabilized Temperature for $T_{1A}$: | 44.3 | °C |
| Stabilized Temperature for $T_{2A}$: | 26.4 | °C |
| Stabilized Temperature for $T_{1B}$: | 43.7 | °C |
| Stabilized Temperature for $T_{2B}$: | 36.0 | °C |

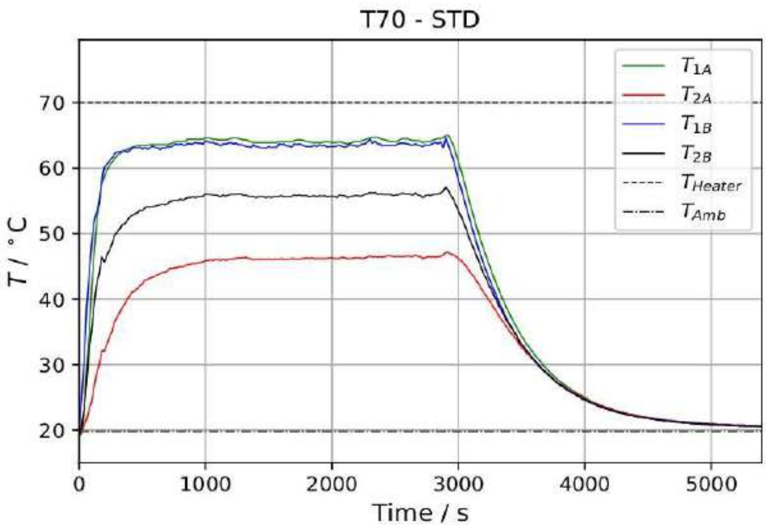


| | | |
|---|---|---|
| Thermal Measurments for Heater Temperature | 80 | °C |
| Average Room Temperature: | 20.0 | °C |
| Stabilized Temperature for $T_{1A}$: | 53.5 | °C |
| Stabilized Temperature for $T_{2A}$: | 32.5 | °C |
| Stabilized Temperature for $T_{1B}$: | 52.5 | °C |
| Stabilized Temperature for $T_{2B}$: | 43.6 | °C |

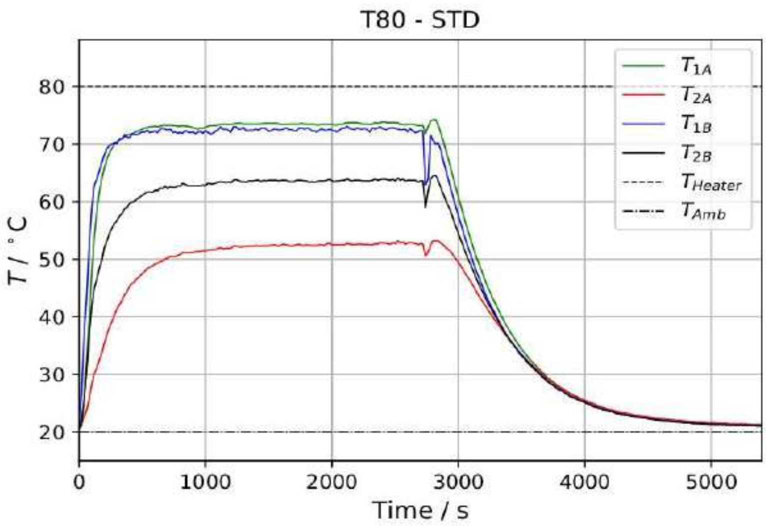

| Thermal Measurments for Heater Temperature | 90 | °C |
|---|---|---|
| Average Room Temperature: | 18.2 | °C |
| Stabilized Temperature for $T_{1A}$: | 61.3 | °C |
| Stabilized Temperature for $T_{2A}$: | 36.7 | °C |
| Stabilized Temperature for $T_{1B}$: | 60.3 | °C |
| Stabilized Temperature for $T_{2B}$: | 50.6 | °C |

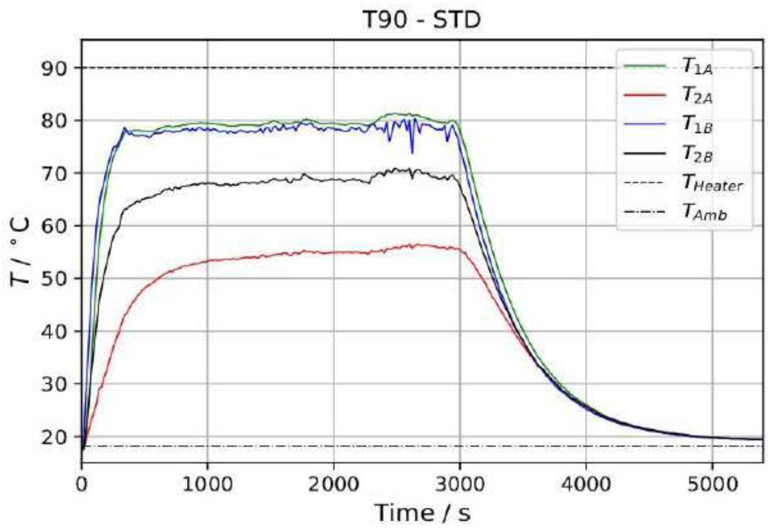


| Thermal Measurments for Heater Temperature | 100 | °C |
|---|---|---|
| Average Room Temperature: | 19.2 | °C |
| Stabilized Temperature for $T_{1A}$: | 70.3 | °C |
| Stabilized Temperature for $T_{2A}$: | 42.4 | °C |
| Stabilized Temperature for $T_{1B}$: | 68.5 | °C |
| Stabilized Temperature for $T_{2B}$: | 57.7 | °C |

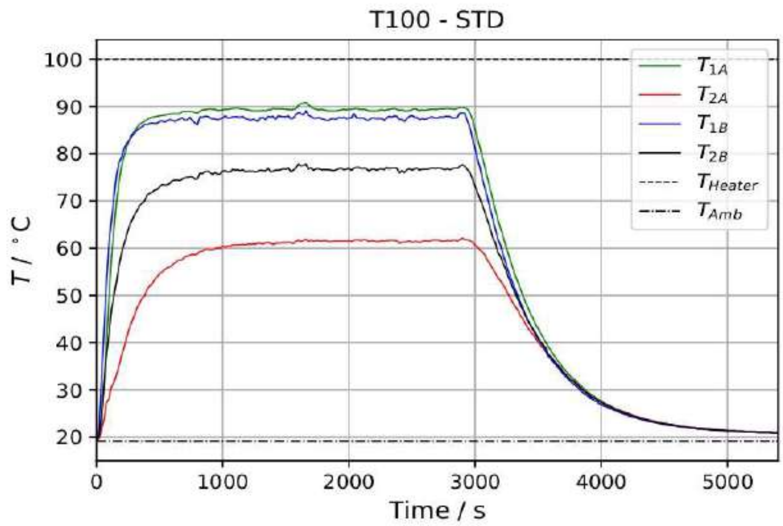

| | | |
|---|---|---|
| Thermal Measurments for Heater Temperature | 110 | °C |
| Average Room Temperature: | 19.9 | °C |
| Stabilized Temperature for $T_{1A}$: | 79.2 | °C |
| Stabilized Temperature for $T_{2A}$: | 48.5 | °C |
| Stabilized Temperature for $T_{1B}$: | 77.4 | °C |
| Stabilized Temperature for $T_{2B}$: | 65.5 | °C |

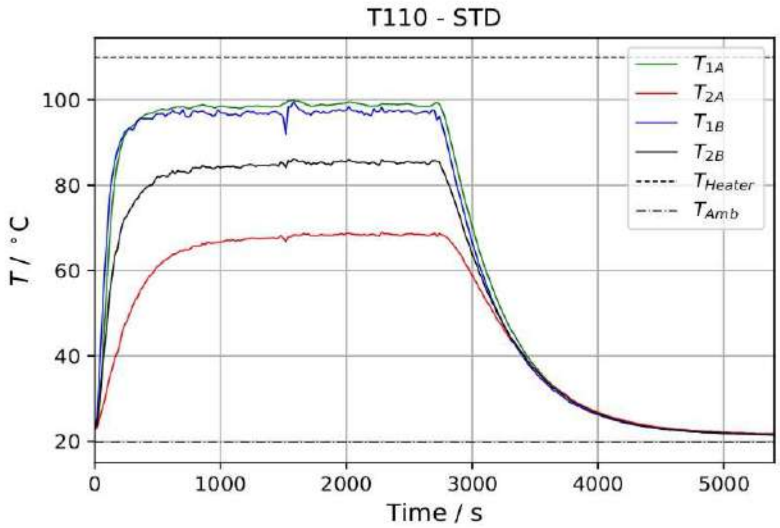

## E.2 Thermal Test Report for Hybrid Tooth (Air)

| Test Report | HT1 |
|---|---|

Thermal Measurements using "Heating System"

Researcher: James Hooton

| Thermal Test Parameter | Value | Units |
|---|---|---|
| Type of Tooth: | HT | - |
| Insert Material: | - | - |
| Temperature Range: | [40; 110] | °C |
| Applied Weight: | 4.6 | kg |
| Point of Contact: | 4.6 | mm |
| Heating Duration: | 45 | min |
| Cooling Duration: | 45 | min |

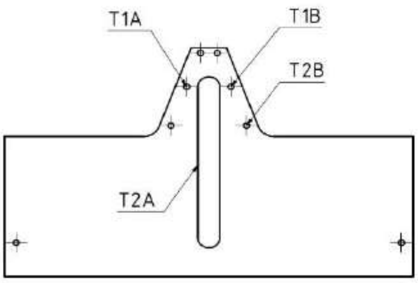


| Thermal Measurments for Heater Temperature | 40 | °C |
|---|---|---|
| Average Room Temperature: | 19.6 | °C |
| Stabilized Temperature for $T_{1A}$: | 19.0 | °C |
| Stabilized Temperature for $T_{2A}$: | 10.5 | °C |
| Stabilized Temperature for $T_{1B}$: | 17.7 | °C |
| Stabilized Temperature for $T_{2B}$: | 17.8 | °C |

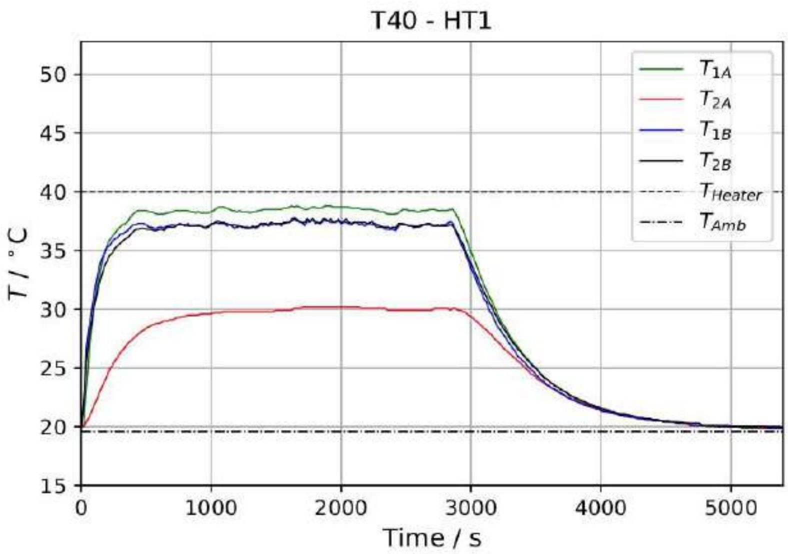

| | | |
|---|---|---|
| Thermal Measurments for Heater Temperature | 50 | °C |
| Average Room Temperature: | 19.9 | °C |
| Stabilized Temperature for $T_{1A}$: | 26.9 | °C |
| Stabilized Temperature for $T_{2A}$: | 15.2 | °C |
| Stabilized Temperature for $T_{1B}$: | 25.4 | °C |
| Stabilized Temperature for $T_{2B}$: | 25.5 | °C |

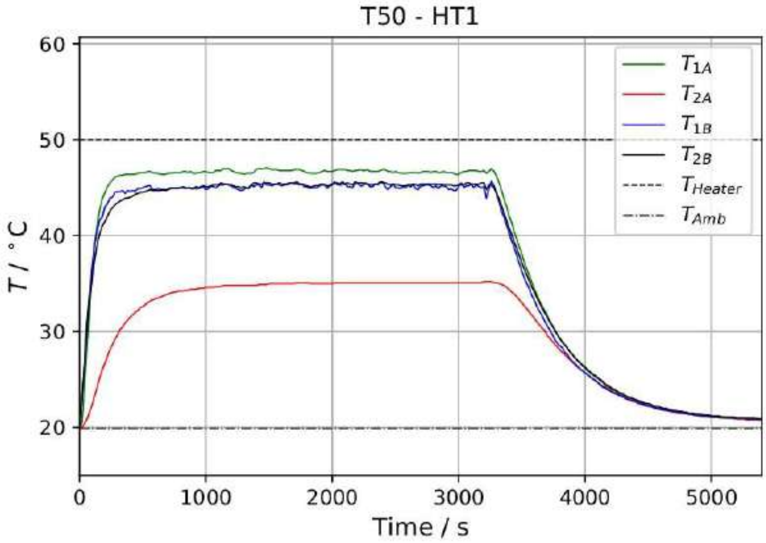


| | | |
|---|---|---|
| Thermal Measurments for Heater Temperature | 60 | °C |
| Average Room Temperature: | 20.6 | °C |
| Stabilized Temperature for $T_{1A}$: | 34.8 | °C |
| Stabilized Temperature for $T_{2A}$: | 19.9 | °C |
| Stabilized Temperature for $T_{1B}$: | 32.8 | °C |
| Stabilized Temperature for $T_{2B}$: | 33.3 | °C |

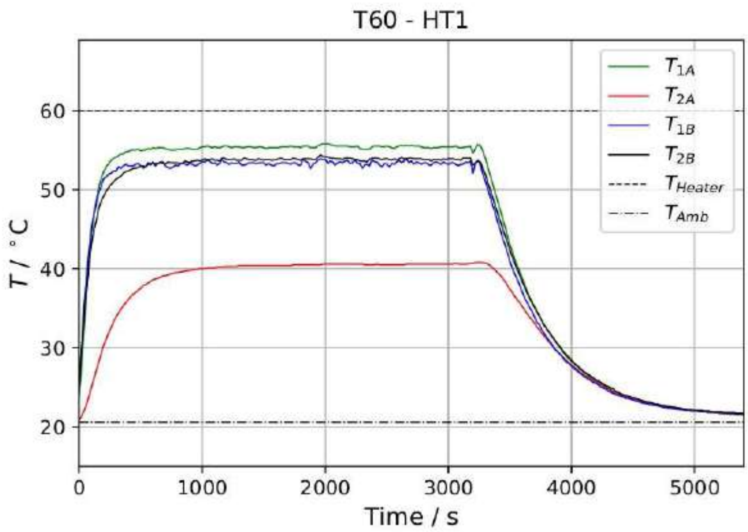

| | | |
|---|---|---|
| Thermal Measurments for Heater Temperature | 70 | °C |
| Average Room Temperature: | 20.9 | °C |
| Stabilized Temperature for $T_{1A}$: | 43.5 | °C |
| Stabilized Temperature for $T_{2A}$: | 25.1 | °C |
| Stabilized Temperature for $T_{1B}$: | 41.1 | °C |
| Stabilized Temperature for $T_{2B}$: | 41.6 | °C |

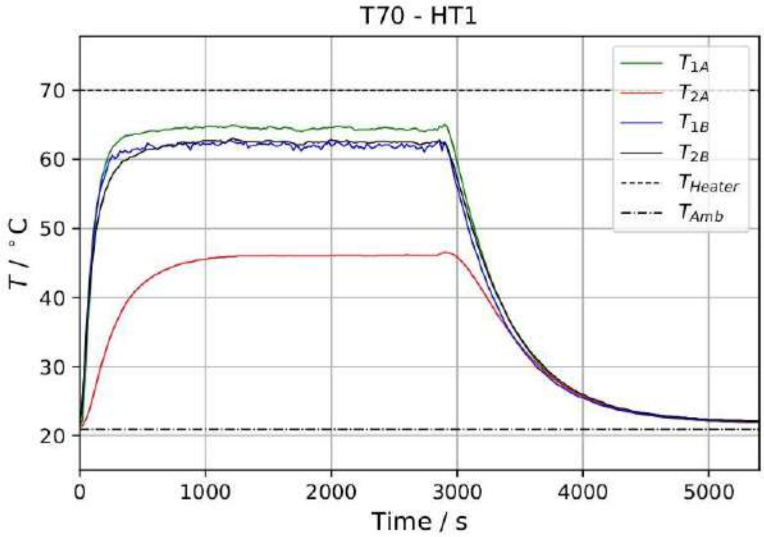


| | | |
|---|---|---|
| Thermal Measurments for Heater Temperature | 80 | °C |
| Average Room Temperature: | 21.3 | °C |
| Stabilized Temperature for $T_{1A}$: | 52.3 | °C |
| Stabilized Temperature for $T_{2A}$: | 30.3 | °C |
| Stabilized Temperature for $T_{1B}$: | 49.7 | °C |
| Stabilized Temperature for $T_{2B}$: | 49.7 | °C |

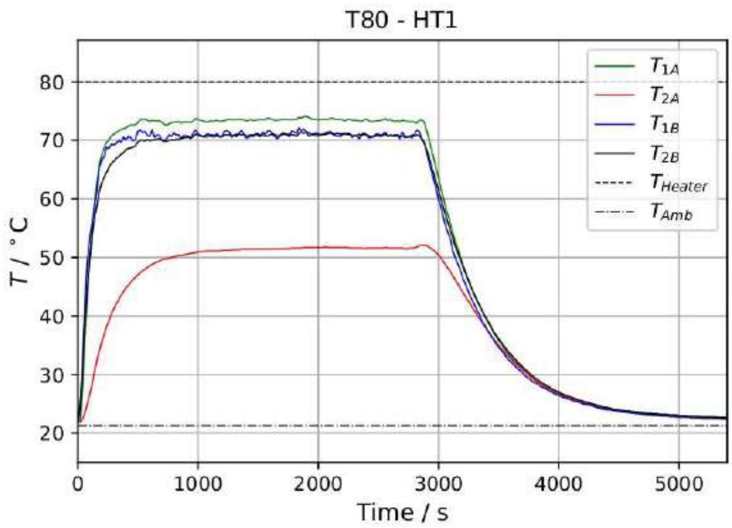

| | | |
|---|---|---|
| Thermal Measurments for Heater Temperature | 90 | °C |
| Average Room Temperature: | 19.8 | °C |
| Stabilized Temperature for $T_{1A}$: | 60.9 | °C |
| Stabilized Temperature for $T_{2A}$: | 35.8 | °C |
| Stabilized Temperature for $T_{1B}$: | 58.7 | °C |
| Stabilized Temperature for $T_{2B}$: | 59.1 | °C |

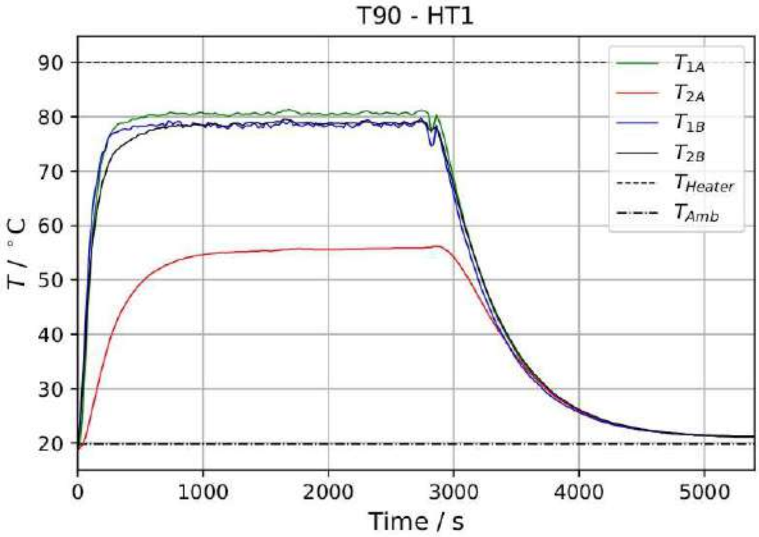


| | | |
|---|---|---|
| Thermal Measurments for Heater Temperature | 100 | °C |
| Average Room Temperature: | 21.5 | °C |
| Stabilized Temperature for $T_{1A}$: | 67.2 | °C |
| Stabilized Temperature for $T_{2A}$: | 41.1 | °C |
| Stabilized Temperature for $T_{1B}$: | 66.0 | °C |
| Stabilized Temperature for $T_{2B}$: | 62.2 | °C |

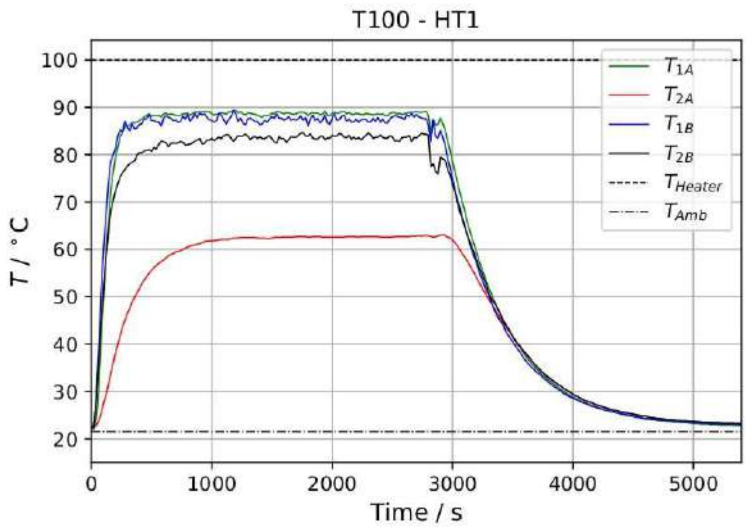

| | | |
|---|---|---|
| Thermal Measurments for Heater Temperature | 110 | °C |
| Average Room Temperature: | 18.5 | °C |
| Stabilized Temperature for $T_{1A}$: | 77.0 | °C |
| Stabilized Temperature for $T_{2A}$: | 48.4 | °C |
| Stabilized Temperature for $T_{1B}$: | 73.5 | °C |
| Stabilized Temperature for $T_{2B}$: | 71.7 | °C |

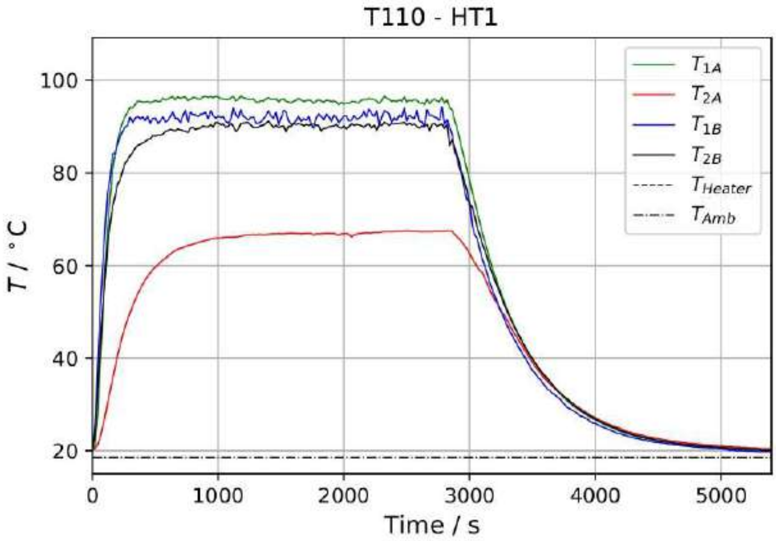

## E.3 Thermal Test Report for Hybrid Tooth (Aluminum)

| Test Report | HT2 |
|---|---|

Thermal Measurements using "Heating System"

Researcher: James Hooton

| Thermal Test Parameter | Value | Units |
|---|---|---|
| Type of Tooth: | HT | - |
| Insert Material: | Aluminum | - |
| Temperature Range: | [40; 110] | °C |
| Applied Weight: | 4.6 | kg |
| Point of Contact: | 4.6 | mm |
| Heating Duration: | 45 | min |
| Cooling Duration: | 45 | min |

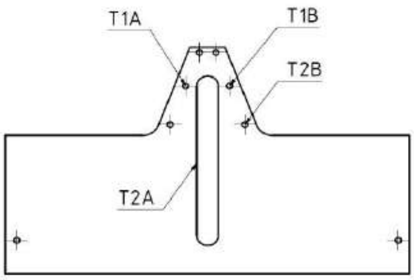


| Thermal Measurments for Heater Temperature | 40 | °C |
|---|---|---|
| Average Room Temperature: | 21.0 | °C |
| Stabilized Temperature for $T_{1A}$: | 20.1 | °C |
| Stabilized Temperature for $T_{2A}$: | 13.4 | °C |
| Stabilized Temperature for $T_{1B}$: | 21.7 | °C |
| Stabilized Temperature for $T_{2B}$: | 18.6 | °C |

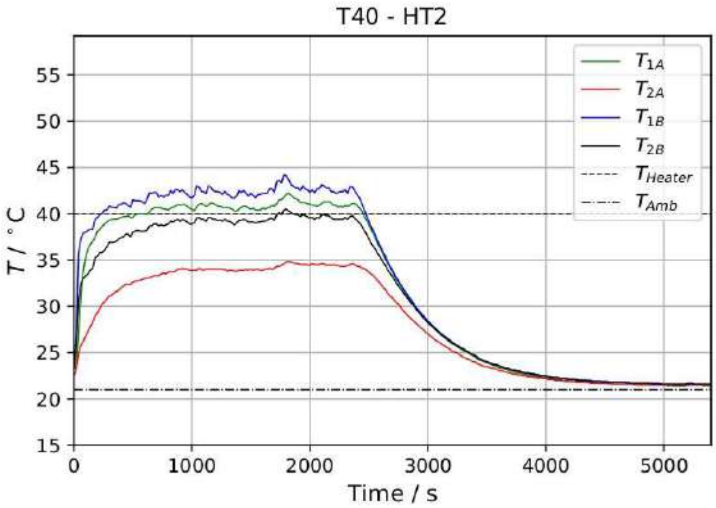

| | | |
|---|---|---|
| Thermal Measurments for Heater Temperature | 50 | °C |
| Average Room Temperature: | 21.0 | °C |
| Stabilized Temperature for $T_{1A}$: | 31.2 | °C |
| Stabilized Temperature for $T_{2A}$: | 21.3 | °C |
| Stabilized Temperature for $T_{1B}$: | 34.1 | °C |
| Stabilized Temperature for $T_{2B}$: | 29.2 | °C |

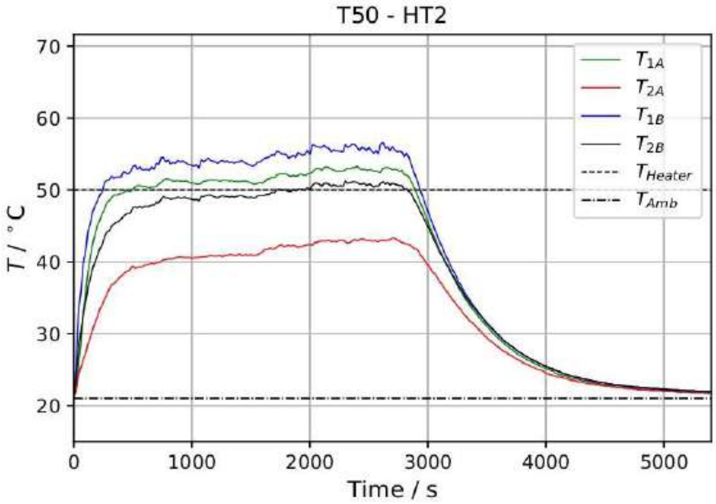


| | | |
|---|---|---|
| Thermal Measurments for Heater Temperature | 60 | °C |
| Average Room Temperature: | 21.2 | °C |
| Stabilized Temperature for $T_{1A}$: | 41.4 | °C |
| Stabilized Temperature for $T_{2A}$: | 28.9 | °C |
| Stabilized Temperature for $T_{1B}$: | 46.0 | °C |
| Stabilized Temperature for $T_{2B}$: | 39.5 | °C |

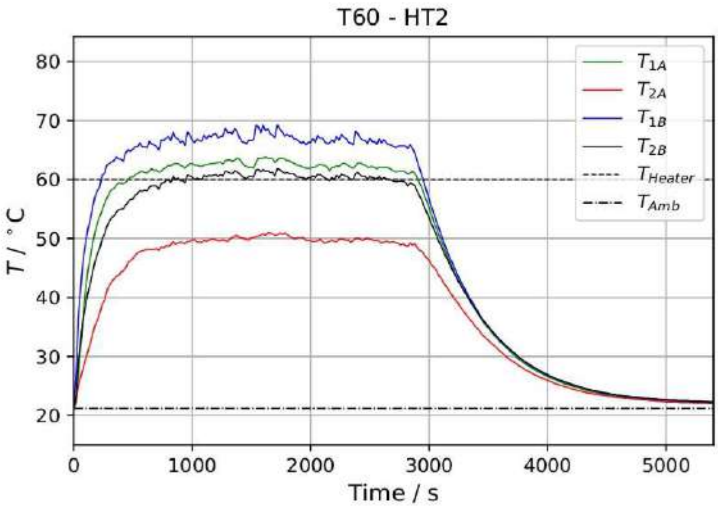

| | | |
|---|---|---|
| Thermal Measurments for Heater Temperature | 70 | °C |
| Average Room Temperature: | 21.6 | °C |
| Stabilized Temperature for $T_{1A}$: | 48.6 | °C |
| Stabilized Temperature for $T_{2A}$: | 32.3 | °C |
| Stabilized Temperature for $T_{1B}$: | 54.5 | °C |
| Stabilized Temperature for $T_{2B}$: | 46.3 | °C |

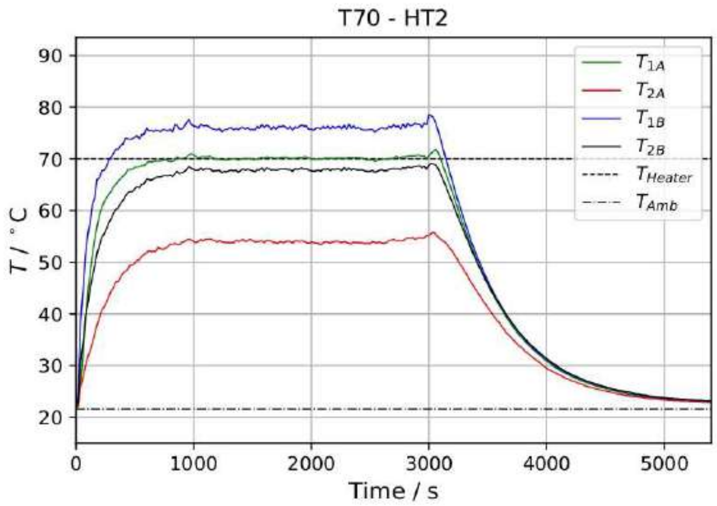


| | | |
|---|---|---|
| Thermal Measurments for Heater Temperature | 80 | °C |
| Average Room Temperature: | 21.1 | °C |
| Stabilized Temperature for $T_{1A}$: | 59.6 | °C |
| Stabilized Temperature for $T_{2A}$: | 40.7 | °C |
| Stabilized Temperature for $T_{1B}$: | 66.3 | °C |
| Stabilized Temperature for $T_{2B}$: | 57.1 | °C |

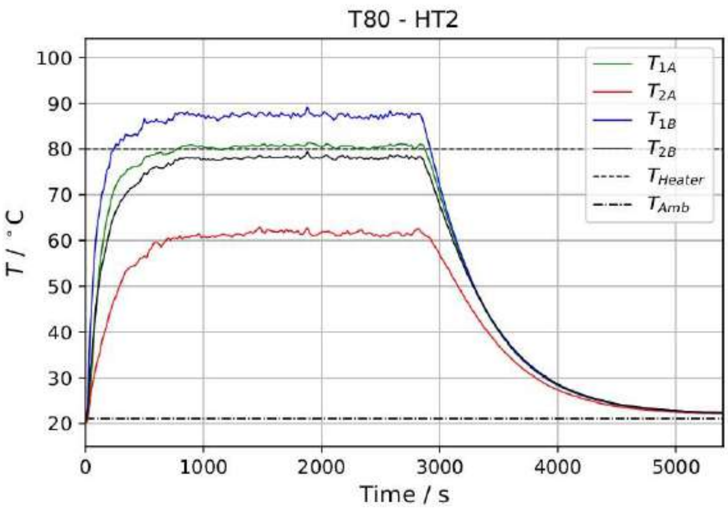

| | | |
|---|---|---|
| Thermal Measurments for Heater Temperature | 90 | °C |
| Average Room Temperature: | 22.0 | °C |
| Stabilized Temperature for $T_{1A}$: | 67.3 | °C |
| Stabilized Temperature for $T_{2A}$: | 45.7 | °C |
| Stabilized Temperature for $T_{1B}$: | 75.7 | °C |
| Stabilized Temperature for $T_{2B}$: | 65.2 | °C |

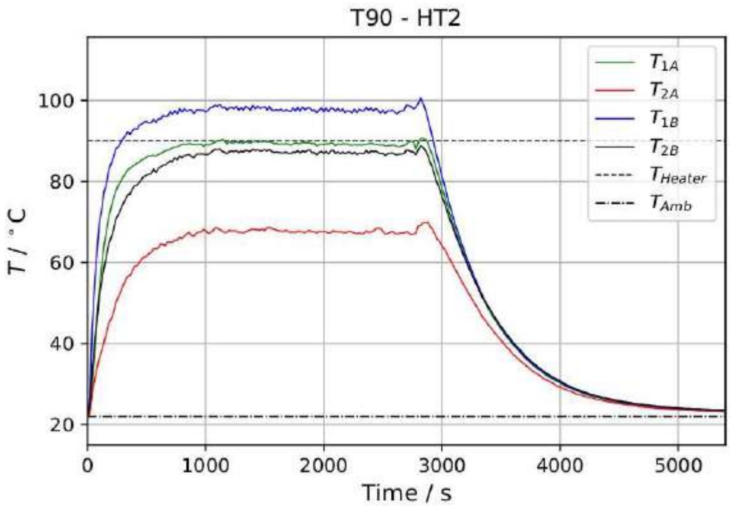


| | | |
|---|---|---|
| Thermal Measurments for Heater Temperature | 100 | °C |
| Average Room Temperature: | 21.0 | °C |
| Stabilized Temperature for $T_{1A}$: | 82.1 | °C |
| Stabilized Temperature for $T_{2A}$: | 60.7 | °C |
| Stabilized Temperature for $T_{1B}$: | 93.2 | °C |
| Stabilized Temperature for $T_{2B}$: | 81.5 | °C |

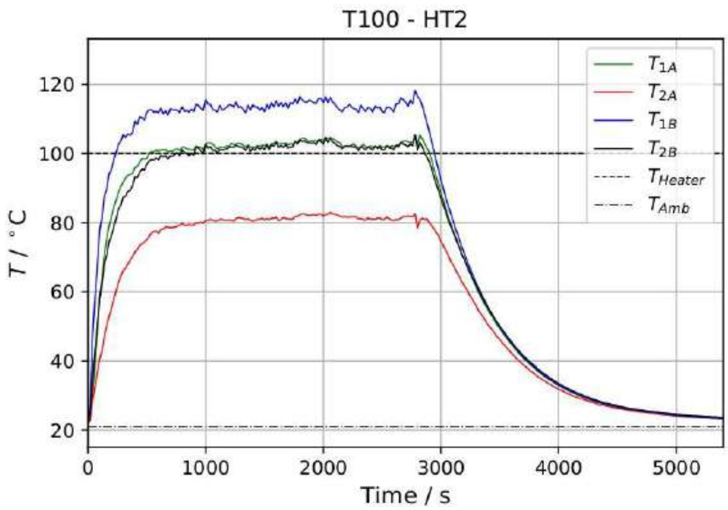

| | | |
|---|---|---|
| Thermal Measurments for Heater Temperature | 110 | °C |
| Average Room Temperature: | 20.6 | °C |
| Stabilized Temperature for $T_{1A}$: | 92.1 | °C |
| Stabilized Temperature for $T_{2A}$: | 67.7 | °C |
| Stabilized Temperature for $T_{1B}$: | 106.9 | °C |
| Stabilized Temperature for $T_{2B}$: | 92.9 | °C |

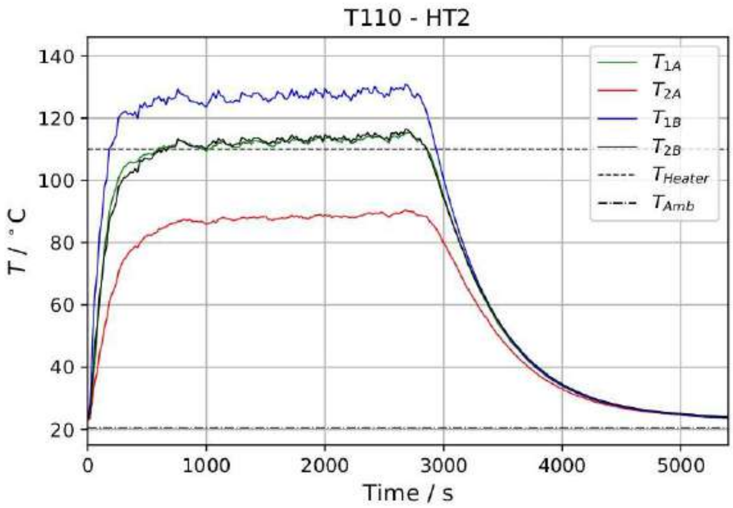

## E.4 Thermal Test Report for Hybrid Tooth (Epoxy)

| Test Report | HT3 |
|---|---|

| Thermal Measurements using "Heating System" |
|---|

| Researcher: James Hooton |
|---|

| Thermal Test Parameter | Value | Units |
|---|---|---|
| Type of Tooth: | HT | - |
| Insert Material: | Epoxy | - |
| Temperature Range: | [40; 110] | °C |
| Applied Weight: | 4.6 | kg |
| Point of Contact: | 4.6 | mm |
| Heating Duration: | 45 | min |
| Cooling Duration: | 45 | min |

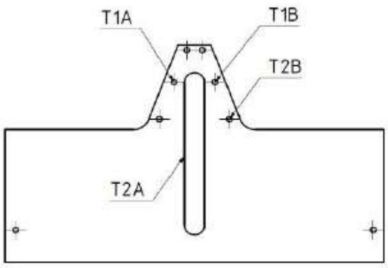


| Thermal Measurments for Heater Temperature | 40 | °C |
|---|---|---|
| Average Ambiente Temperature: | 24.0 | °C |
| Stabilized Temperature for $T_{1A}$: | 15.9 | °C |
| Stabilized Temperature for $T_{2A}$: | 13.4 | °C |
| Stabilized Temperature for $T_{1B}$: | 18.0 | °C |
| Stabilized Temperature for $T_{2B}$: | 15.0 | °C |

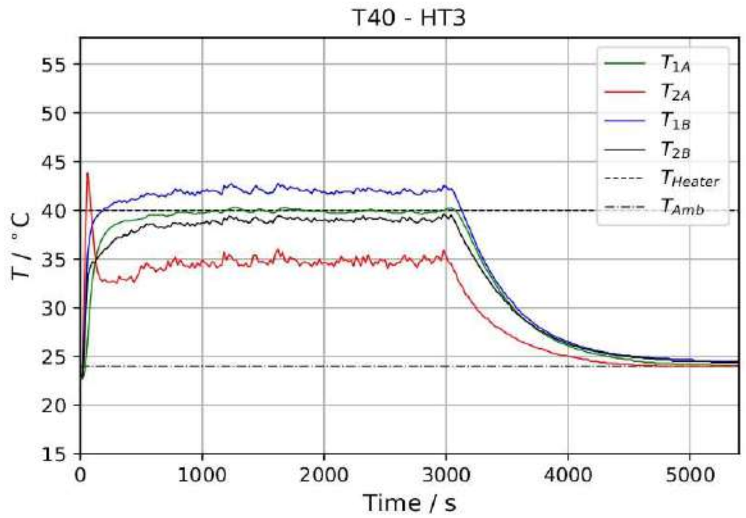

| Thermal Measurments for Heater Temperature | 50 | °C |
|---|---|---|
| Average Ambiente Temperature: | 24.4 | °C |
| Stabilized Temperature for $T_{1A}$: | 26.8 | °C |
| Stabilized Temperature for $T_{2A}$: | 21.3 | °C |
| Stabilized Temperature for $T_{1B}$: | 30.2 | °C |
| Stabilized Temperature for $T_{2B}$: | 25.4 | °C |

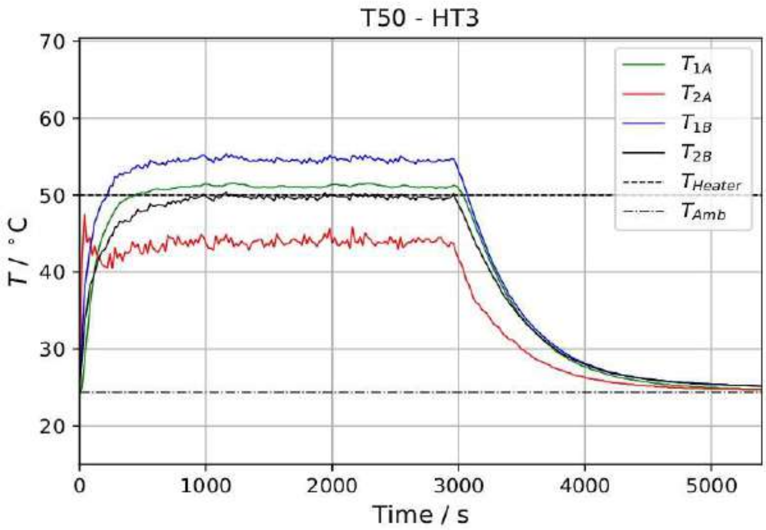


| Thermal Measurments for Heater Temperature | 60 | °C |
|---|---|---|
| Average Ambiente Temperature: | 23.8 | °C |
| Stabilized Temperature for $T_{1A}$: | 38.2 | °C |
| Stabilized Temperature for $T_{2A}$: | 28.9 | °C |
| Stabilized Temperature for $T_{1B}$: | 41.8 | °C |
| Stabilized Temperature for $T_{2B}$: | 34.6 | °C |

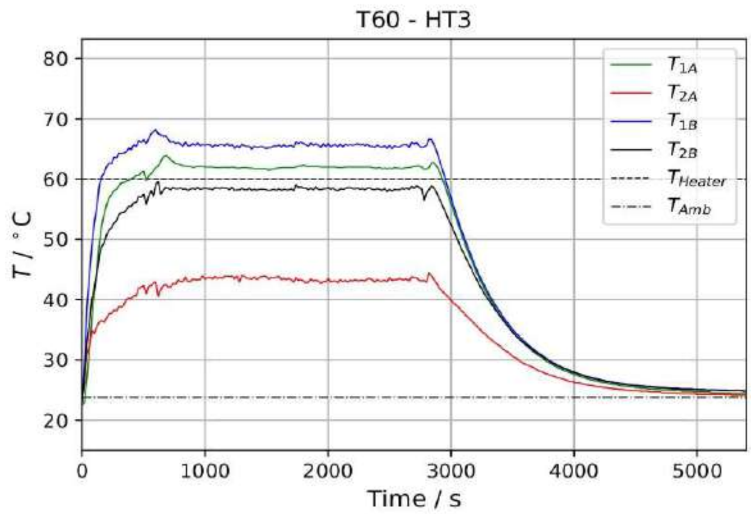

| | | |
|---|---|---|
| Thermal Measurments for Heater Temperature | 70 | °C |
| Average Ambiente Temperature: | 24.2 | °C |
| Stabilized Temperature for $T_{1A}$: | 48.2 | °C |
| Stabilized Temperature for $T_{2A}$: | 32.3 | °C |
| Stabilized Temperature for $T_{1B}$: | 53.3 | °C |
| Stabilized Temperature for $T_{2B}$: | 43.6 | °C |

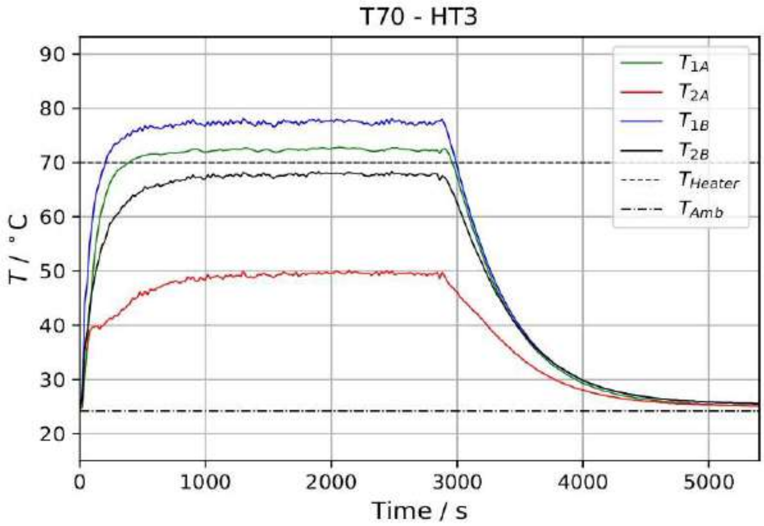


| | | |
|---|---|---|
| Thermal Measurments for Heater Temperature | 80 | °C |
| Average Ambiente Temperature: | 21.8 | °C |
| Stabilized Temperature for $T_{1A}$: | 61.7 | °C |
| Stabilized Temperature for $T_{2A}$: | 40.7 | °C |
| Stabilized Temperature for $T_{1B}$: | 67.9 | °C |
| Stabilized Temperature for $T_{2B}$: | 55.5 | °C |

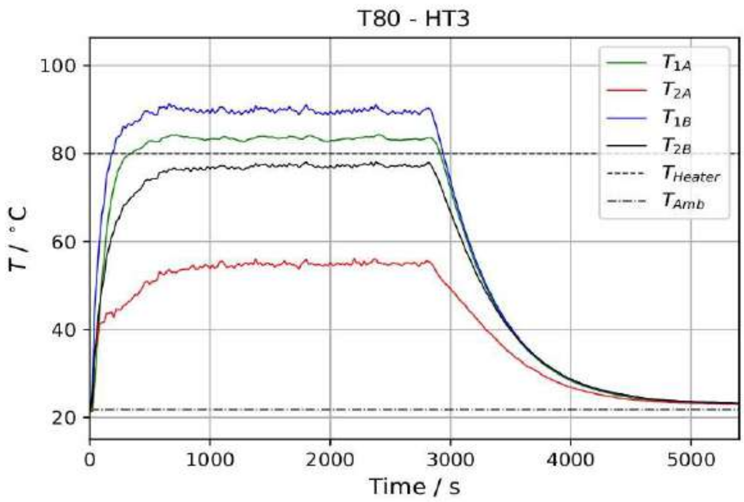

| | | |
|---|---|---|
| Thermal Measurments for Heater Temperature | 90 | °C |
| Average Ambiente Temperature: | 23.0 | °C |
| Stabilized Temperature for $T_{1A}$: | 70.1 | °C |
| Stabilized Temperature for $T_{2A}$: | 45.7 | °C |
| Stabilized Temperature for $T_{1B}$: | 76.8 | °C |
| Stabilized Temperature for $T_{2B}$: | 63.3 | °C |

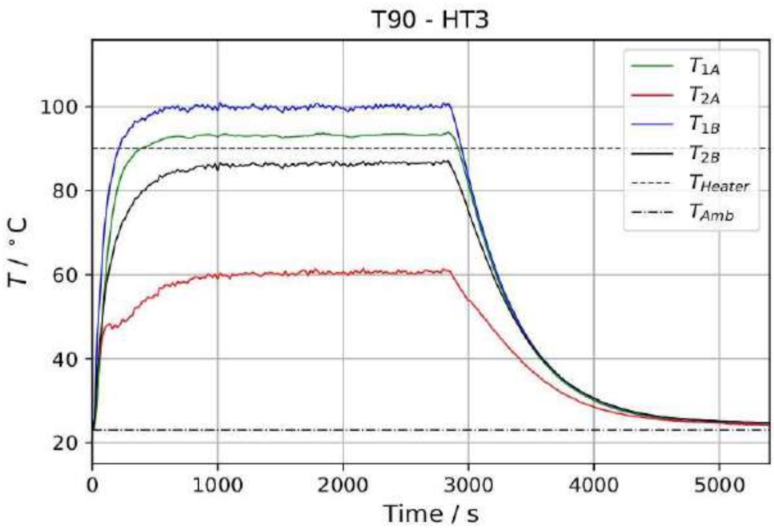


| | | |
|---|---|---|
| Thermal Measurments for Heater Temperature | 100 | °C |
| Average Ambiente Temperature: | 24.2 | °C |
| Stabilized Temperature for $T_{1A}$: | 79.6 | °C |
| Stabilized Temperature for $T_{2A}$: | 60.7 | °C |
| Stabilized Temperature for $T_{1B}$: | 86.7 | °C |
| Stabilized Temperature for $T_{2B}$: | 72.0 | °C |

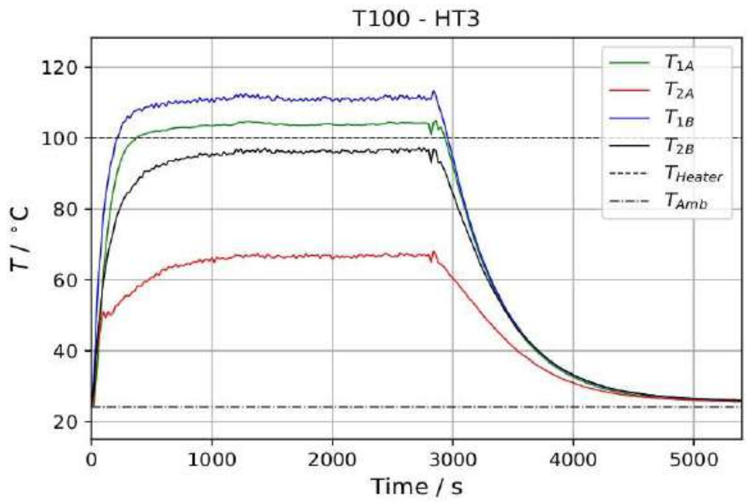

| | | |
|---|---|---|
| Thermal Measurments for Heater Temperature | 110 | °C |
| Average Ambiente Temperature: | 25.0 | °C |
| Stabilized Temperature for $T_{1A}$: | 88.9 | °C |
| Stabilized Temperature for $T_{2A}$: | 67.7 | °C |
| Stabilized Temperature for $T_{1B}$: | 96.8 | °C |
| Stabilized Temperature for $T_{2B}$: | 80.5 | °C |

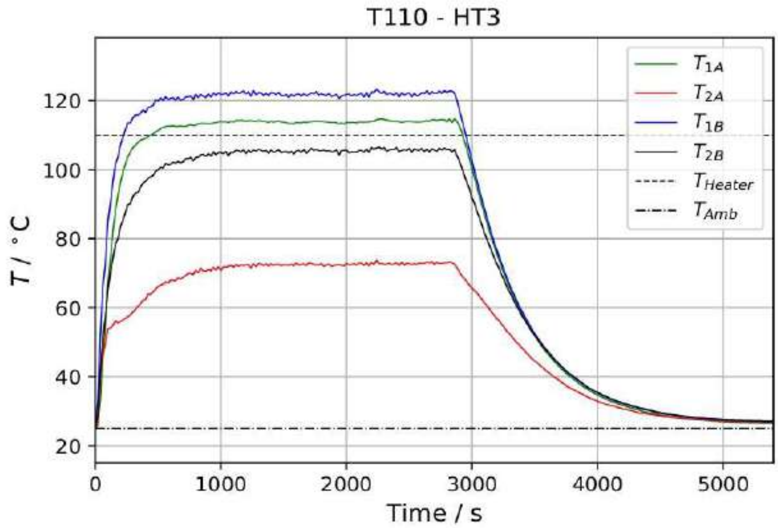

## E.5 DIC Test Report for Standard Tooth

**Test Report**

DIC Measurements using "Heating System"

Researcher: James Hooton

| Thermal Test Parameter | Value | Units |
|---|---|---|
| Type of Tooth: | STD | - |
| Insert Material: | - | - |
| Temperature Range: | [40;70;100] | ºC |
| Applied Weight: | 4.6 | kg |
| Point of Contact: | 4.6 | mm |
| Heating Duration: | 30 | min |
| Total Heating Duration: | 90 | min |
| Cooling Duration: | 45 | min |

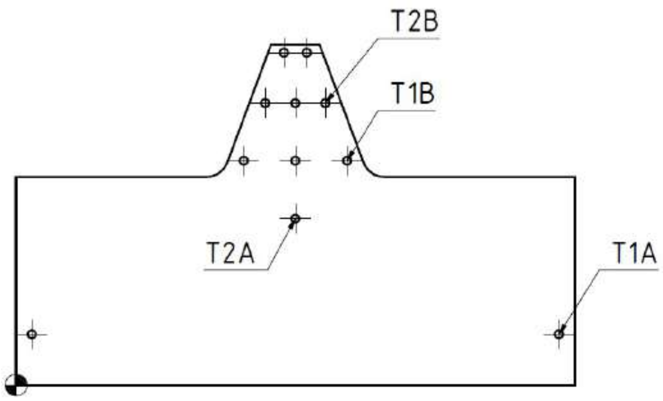


| Thermal Measurments for Heater Temperature | 40 | ºC |
|---|---|---|
| Stabilized Temperature for $T_{1A}$: | 5.8 | ºC |
| Stabilized Temperature for $T_{2A}$: | 13.1 | ºC |
| Stabilized Temperature for $T_{2B}$: | 22.7 | ºC |
| Thermal Measurments for Heater Temperature | 70 | ºC |
| Stabilized Temperature for $T_{1A}$: | 15.5 | ºC |
| Stabilized Temperature for $T_{2A}$: | 29.2 | ºC |
| Stabilized Temperature for $T_{2B}$: | 50.2 | ºC |
| Thermal Measurments for Heater Temperature | 100 | ºC |
| Stabilized Temperature for $T_{1A}$: | 24.1 | ºC |
| Stabilized Temperature for $T_{2A}$: | 46.7 | ºC |
| Stabilized Temperature for $T_{2B}$: | 73.4 | ºC |
| Average Ambiente Temperature: | 20.1 | ºC |

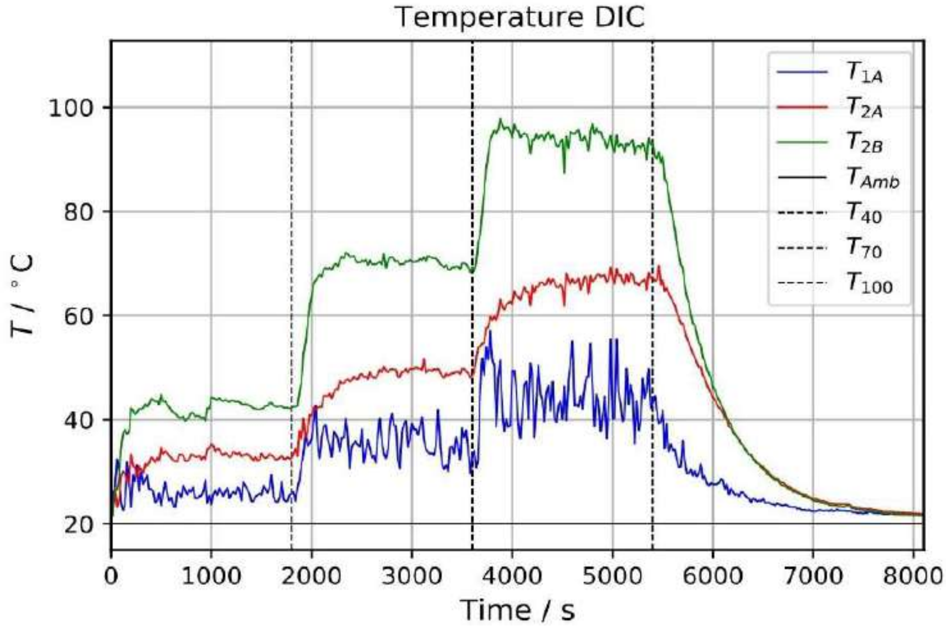
Temperature DIC
T / °C
Time / s
0
1000
2000
3000
4000
5000
6000
7000
8000
20
40
60
80
100
$T_{1A}$
$T_{2A}$
$T_{2B}$
$T_{Amb}$
$T_{40}$
$T_{70}$
$T_{100}$

## E.6 DIC Test Report for Hybrid Tooth (Air)

**Test Report**

DIC Measurements using "Heating System"

Researcher: James Hooton

| Thermal Test Parameter | Value | Units |
|---|---|---|
| Type of Tooth: | HT | - |
| Insert Material: | - | - |
| Temperature Range: | [40;70;100] | °C |
| Applied Weight: | 4.6 | kg |
| Point of Contact: | 4.6 | mm |
| Heating Duration: | 30 | min |
| Total Heating Duration: | 90 | min |
| Cooling Duration: | 45 | min |

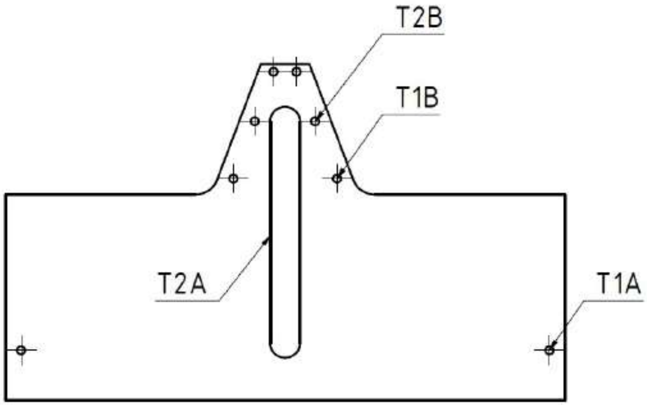


| | | |
|---|---|---|
| Thermal Measurments for Heater Temperature | 40 | °C |
| Stabilized Temperature for $T_{1A}$: | 4.8 | °C |
| Stabilized Temperature for $T_{2A}$: | 9.6 | °C |
| Stabilized Temperature for $T_{1B}$: | 14.4 | °C |
| Stabilized Temperature for $T_{1B}$: | 17.1 | °C |
| Thermal Measurments for Heater Temperature | 70 | °C |
| Stabilized Temperature for $T_{1A}$: | 15.6 | °C |
| Stabilized Temperature for $T_{2A}$: | 26.2 | °C |
| Stabilized Temperature for $T_{1B}$: | 38.6 | °C |
| Stabilized Temperature for $T_{1B}$: | 45.8 | °C |
| Thermal Measurments for Heater Temperature | 100 | °C |
| Stabilized Temperature for $T_{1A}$: | 30.3 | °C |
| Stabilized Temperature for $T_{2A}$: | 46.9 | °C |
| Stabilized Temperature for $T_{1B}$: | 64.7 | °C |
| Stabilized Temperature for $T_{1B}$: | 75.9 | °C |
| Average Ambiente Temperature: | 21.7 | °C |

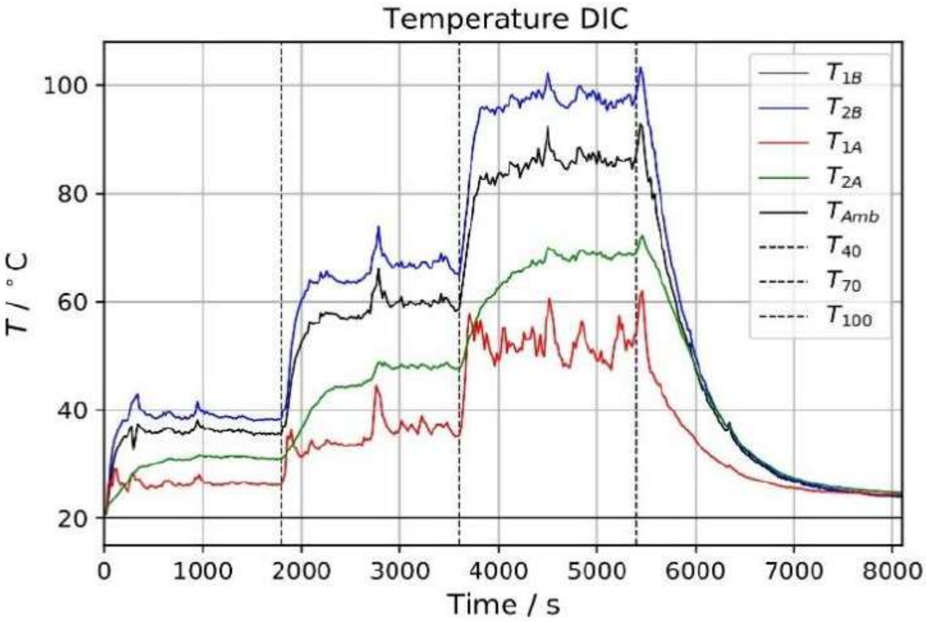
Temperature DIC
$T$ / °C
Time / s
$T_{1B}$
$T_{2B}$
$T_{1A}$
$T_{2A}$
$T_{Amb}$
$T_{40}$
$T_{70}$
$T_{100}$
20
40
60
80
100
0
1000
2000
3000
4000
5000
6000
7000
8000